PhD-FSTM-2024-011
The Faculty of Science, Technology and Medicine

DISSERTATION

Defence held on 21/02/2024 in Esch-sur-Alzette, Luxembourg

to obtain the degree of

DOCTEUR DE L'UNIVERSITÉ DU LUXEMBOURG

EN *Biologie*

by

Ali Mohamed Ali Ali KISHK
Born on 02 June 1992 in Gharbeya, Egypt

TOWARDS EFFECTIVE PREDICTION OF REPURPOSABLE DRUGS THROUGH METABOLIC MODELING: EVALUATION AGAINST APPROVED DRUGS USING PRECLINICAL AND CLINICAL DATA

Dissertation defence committee

Dr Thomas Sauter, dissertation supervisor
Professor, Université du Luxembourg

Dr Evan Williams, Chairman
Associate Professor, Université du Luxembourg

Dr Jun Pang
Assistant Professor, Université du Luxembourg

Dr Mattia Zampieri
Professor, University of Basel

Dr Ujjwal Neogi
Associate professor, Karolinska Institute

Towards Effective Prediction of Repurposable Drugs Through Metabolic Modeling: Evaluation Against Approved Drugs Using Preclinical and Clinical Data

UNIVERSITY OF LUXEMBOURG

by Ali Mohamed Ali Ali Kishk

Born on the 2nd of June 1992 in Egypt

Dissertation Defence Committee:

Prof. Dr.-Ing. Thomas Sauter, dissertation supervisor
Professor, University of Luxembourg

Prof. Dr. Evan Williams
Associate professor, University of Luxembourg

Prof. Dr. Jun Pang
Assistant professor, University of Luxembourg

Prof. Dr. Mattia Zampieri
Professor, University of Basel

Prof. Dr. Ujjwal Neogi
Associate professor, Karolinska Institute

This doctoral thesis has been performed at the Systems Biology Group, Department of Life Sciences and Medicine, University of Luxembourg, Luxembourg

under the guidance of

Prof. Dr. Ing. Thomas Sauter, Systems Biology Group, Department of Life Sciences and Medicine, University of Luxembourg, Luxembourg

Affidavit

I hereby confirm that the PhD thesis entitled **"Towards Effective Prediction of Repurposable Drugs Through Metabolic Modeling: Evaluation Against Approved Drugs Using Preclinical and Clinical Data"** has been written independently and without any other sources than cited.

Luxembourg, _____

_____

Ali Kishk

List of Publications

Reviews:

Review of Current Human Genome-Scale Metabolic Models for Brain Cancer and Neurodegenerative Diseases
A Kishk*, M.P. Pacheco*, T Heurtaux, L Sinkkonen, J Pang, S Fritah, S.P. Niclou, and T Sauter,
Cells, Volume 20 (Issue 11), 2022, Page 2486
https://www.mdpi.com/2073-4409/11/16/2486

Original work:

DCcov: Repositioning of drugs and drug combinations for SARS-CoV-2 infected lung through constraint-based modeling
A Kishk, M.P. Pacheco, and T Sauter,
iScience, Volume 24 (Issue 11), 2021, https://doi.org/10.1016/j.isci.2021.103331

Bruceine D Identified as a Drug Candidate against Breast Cancer by a Novel Drug Selection Pipeline and Cell Viability Assay
C Cipriani, M.P. Pacheco, **A Kishk**, M Wachich, D Abankwa, E Schaffner-Reckinger, and T Sauter,
Pharmaceuticals, Volume 15, 2022, https://doi.org/10.3390/ph15020179

In silico drug target prediction using metabolic modelling identifies six novel repurposable drugs for melanoma
T Bintener*, M.P. Pacheco*, D Philippidou, C Margue, **A Kishk**, G Del Mistro, L Di Leo, Maria Moscardó Garcia, Halder, L Sinkkonen, D De Zio, S Kreis, D Kulms, and T Sauter,
Cell Death and Disease, Volume 14, 468, 2023,
https://www.nature.com/articles/s41419-023-05955-1

Metabolic models predict fotemustine and the combination of eflornithine/rifamycin and adapalene/cannabidiol for the treatment of gliomas
A Kishk, M.P. Pacheco, T Heurtaux, and T Sauter
Briefings in Bioinformatics, Volume 25, Issue 3, May 2024, bbae199, https://doi.org/10.1093/bib/bbae199

Other contributions:

Project-based learning course on metabolic network modelling in computational systems biology
T Sauter, T Bintener, **A Kishk**, L Presta, T Prohaska, D Guignard, N Zeng, C Cipriani, S Arshad, T Pfau, P.M. Conde, and M.P. Pacheco
PLoS Computational Biology, Volume 18, e1009711
https://doi.org/10.1371/journal.pcbi.1009711

Drug Target Prediction Using Context-Specific Metabolic Models Reconstructed from rFASTCORMICS

T Bintener, M.P. Pacheco, **A Kishk**, J Didier, T Sauter,

Cancer Drug Resistance: Methods and Protocols 2535, 221–240

https://link.springer.com/protocol/10.1007/978-1-0716-2513-2_17

AMBRA1 predicts melanoma response to MAPK inhibitors [SUBMITTED]

L Di Leo, C Pagliuca, **A Kishk**, S Rizza, C Tsiavou, C Pecorari, C Dahl, M.P. Pacheco, R Tholstrup, J.R. Brewer, P Berico, E Hernando, F Cecconi, R Ballotti, C Bertolotto, G Filomeni, M.F. Gjerstorff, T Sauter, P Lovat, P Guldberg, D De Zio

Sex-Specific Frailty Classification Outshines Mixed Models and Reveals Latent Differences of the Respective Frailty Profiles – Data from the Berlin Aging Study II (BASE-II) [UNDER PREPARATION]

J Didier, S De Landtsheer, M.P. Pacheco, **A Kishk**, J.G. Schneider, I Demuth, E Steinhagen-Thiessen, T Siedler, D Spira, T Sauter

General Abstract

Living organisms, from Archaea to Bacteria and Eukarya, are primarily composed of a fixed set of small molecules known as metabolites. Metabolism encompasses the biochemical interactions of these metabolites to maintain cellular functions of producing energy and synthesizing new molecules. The rise of genome sequencing in the 90s revolutionized molecular biology research from investigating individual disconnected entities such as enzymes into studying biology at a systems level of interconnected entities. This systems approach, called Systems Biology, aims to integrate entities at different scales, including networks of metabolites, genes, cells, tissues, and even networks of organisms in an ecosystem. Due to the well-annotation of the enzymatic biochemical interactions, metabolic networks were the first reconstructed biological networks representing the collective interactions of metabolites, genes, and reactions.

Metabolic network modeling is one of the Systems Biology tools with many applications, such as improving industrial metabolite yield, analysis of interspecies interactions, biomarker discovery, and drug repurposing. Metabolic network modeling extends to discovering new hypotheses by analyzing inconsistencies between experimental results and predictions. Like other Systems Biology approaches, metabolic network modeling is scalable from core-metabolism networks into genome-scale metabolic models (GEMs), multi-cellular GEMs, and whole-body multi-tissue GEMs. Regardless of the GEMs' scalability, they are built using generic reconstructions that are species-specific, disease-agnostic GEMs that compromise all possible reactions in this species. Generic reconstructions are routinely used to construct disease-specific GEMs, known as context GEMs, with model-building tools such as (r)FASTCORMICS. These context GEMs allow target identification and drug repurposing, redirecting approved drugs to new diseases. Drug repurposing is a cost and time-effective alternative to traditional drug discovery to escape phase I toxicity clinical trials. In addition to computational drug repurposing, experimental drug repurposing usually involves high-throughput screenings (HTS) of approved drugs *in vitro* or *in vivo*. While many computational drug repurposing approaches have been developed, metabolic modeling-based drug repurposing stands out for its interpretation and holistic method.

In this thesis, we showed the applications of metabolic modeling for drug repurposing in glioma, melanoma, breast cancer, and COVID-19. With a focus on glioma, we started with a review of GEMs in the brain that define valuable resources for our work in glioma metabolic modeling. The rationale for focusing on glioma is the limited preclinical models for low-grade glioma and the extremely poor survival in glioblastoma. Continuing the work in our department by Tamara Bintener for melanoma metabolic modeling, we benchmarked the predicted drugs against the approved and other preclinical drugs in nitric oxide metabolism under various metastasis, drug resistance, and BRAF/NRAS mutation conditions. In the four studied diseases, we evaluated the predicted drugs to approved drugs in the respective diseases using *in vitro* HTSs, xenografts HTSs, and clinical trials. Aside from drug repurposing, metabolic modeling identified different metabolic exchanges in the glioma subtypes and Covid19 consistent with metabolomics studies and radiotracers uptake.

At least a third of the predicted drugs in glioma, melanoma, and Covid19 tested in clinical trials showed comparable or improved survival compared to the approved drugs. Notably, predicted TXNRD1 vulnerability by fotemustine in melanoma and glioma was found to be approved in some countries for melanoma and showed comparable survival to an approved drug in glioma. Exceeding the largest combination HTS by more than 20 folds, combination prediction for glioma predicted 17 combinations out of $>$ 124,000 possible combinations, of which two combinations matched known vulnerabilities in the respective glioma subtypes.

Overall, this thesis provides an overview of how metabolic modeling can be used to detect biomarkers and repurpose drugs, where metabolic modeling was competitive with preclinical methods and could predict new drugs.

Acknowledgements

Never mind Publish or Perish .. Continue even if you feel sluggish
Negative results are not a blemish .. Patience is a virtue you can cherish
Science is not racing to the finish .. It's a marathon of who can replenish

The best lessons I learned from my supervisors, Prof. Dr. Thomas Sauter and Dr. Maria Pires Pacheco, with whom I am indebted for their mountainous efforts, patience, and support. Completing this thesis was a journey, and with the metabolic modeling team, I found my safe ship. Slowly to be harbored. Once part of its crew, I belonged; now, for their harbour will be longed. Starting my Ph.D. two weeks after the COVID-19 pandemic showed me the huge support from my supervisors in helping me remotely to the minute details.

I would also like to thank the CET committee members, Prof. Dr. Simone Niclou, for her continuous feedback on the glioma modeling and Prof. Jun Pang for his constructive questions that allowed me to simplify my work.

Especial thanks to Dr. Lasse Sinkkonen and Dr. Tony Heurteux for their assistance in the review of the brain metabolic models. Many thanks for Jeff Diddier's support in teaching and HPC tips, Apurva Badkas's wonderful Indian desserts, and Evelyn Gonzalez's infinite stack of chocolates.

Finally, I would like to thank my family, my wife Aya, and two kids, Mariam and Abdur-Rahman, for their patience and continuous support.

Contents

List of Figures

List of Tables

Abbreviations

1p/19q co-deletion: short arm of chromosome 1 (1p) and the long arm of chromosome 19 (19q)

2HG: 2-Hydroxy-glutarate

ABC: ATP-binding cassette

ACE2: Angiotensin I-converting enzyme 2

ACEIs: Angiotensin-converting enzyme inhibitors

AD: Alzheimer's disease

AG: Automatically generated

ANLS: Astrocyte–neuron lactate shuttle theory

AntiBC: Anti-brain tumor chemotherapies

ARDS: Acute respiratory distress syndrome

ARSA: Arylsulphatase A

AST: Astrocytoma

ATIC: 5-Aminoimidazole-4-carboxamide ribonucleotide formyltransferase

ATP: Adenosine triphosphate

AT-1,7: Angiotensin-(1,7)

AT-II: Angiotensin II

AUC: Area under the curve

BBB: Brain–blood barrier

BRC: Breast cancer

BzCl: Benzethonium chloride

CAi: Carbonic anhydrase inhibitor

CA: Carbonic anhydrase

CBM: Constraint-based modeling

CCLE: Cancer cell line encyclopedia

CDK: Cyclin-dependent kinase

CNS: Central nervous system

COPD: Chronic obstructive pulmonary disease

COVID-19: Coronavirus disease 2019

CPE: Cytopathic effect

CRISPR: Clustered regularly interspaced short palindromic repeats

CRLS1: Cardiolipin synthase 1

CSF: Cerebrospinal fluid

DDI: Drug-drug interaction

DEG: Differentially expressed gene

DepMap: Cancer Dependency Map

DERs: Differentially expressed reactions

DHFR: Dihydrofolate reductase

DHODH: Dihydroorotate dehydrogenase

DKO: Double gene knockout

DMSO: Dimethyl sulfoxide

DSS: Drug Sensitivity Score

DTP: Drug-tolerant persister

ER: Estrogen receptor

ERα: Estrogen receptor α

ERβ: Estrogen receptor β

FAO: Fatty acid oxidation

FBA: Flux balance analysis

FDA: Food and Drug Administration

FPKM: Fragments per kilobase per million mapped fragments

fRMA: Frozen robust multiarray analysis

FVA: Flux Variability Analysis

GABA: Gamma-aminobutyric acid

GAG: Glycosaminoglycan

GBM: Glioblastoma Multiforme

GEM: Genome-scale metabolic model

GEO: Gene Expression Omnibus

GPR: Gene–protein-reaction

grRatio: Growth rate ratio

GSH: Glutathione

GSR: Glutathione reductase

GSSG: Oxidized glutathione

GUK1: Guanylate kinase

HER2: human epidermal growth factor receptor 2

HIF1A: Hypoxia-inducible factor 1 subunit alpha

HMA: Human Metabolic Atlas

HPA: Human Protein Atlas

HR: Hormone receptor

HTS: High-throughput screening

IAG: Investigational anti-glioma drug

IBD: Inflammatory bowel disease

IC_{50}: Half maximal inhibitory concentration

ICIs: immune checkpoint inhibitors

IDH: Isocitrate dehydrogenase

ISYNA1: Inositol-3-phosphate synthase 1

KD: Knock-down

KO: Knock-out

KRAS: KRAS proto-oncogene, GTPase

LGG: Lower-grade glioma

MAGeCK: Model-based Analysis of Genome-wide CRISPR/Cas9 Knockout

MAOA/B: Monoamine oxidase A/B

MAP2K1: Mitogen-activated protein kinase kinase 1

MOA: Mode-of-action

MOI: Multiplicity of infection

mOS: Median OS

mTOR: Mechanistic target of rapamycin kinase

MYC: MYC proto-oncogene, bHLH transcription factor

NADP: Nicotinamide adenine dinucleotide phosphate

NAD: Nicotinamide adenine dinucleotide

nGBM: Newly diagnosed GBM

NDD: Neurodegenerative disease

NHBE: Normal human bronchial epithelial

NO: Nitric oxide

NO-drugs: Nitric oxide-based drugs

NP: Natural product

NRAS: NRAS Proto-Oncogene, GTPase

ODG: Oligodendroglioma

OF: Objective function

ORF3a: Open reading frame 3 A

OS: Overall survival

OXPHOS: Oxidative phosphorylation

PCA: Principal component analysis

PCV: Procarbazine/lomustine[CCNU]/vincristine combination

PD: Parkinson's

PDX: Patient-derived xenograft

PFS: Progression-free survival

PI3K: Phosphoinositide 3-kinase

PK: Pharmacokinetics

PPP: Pentose phosphate pathways

PR: Progesterone receptor

PUFAs: Free polyunsaturated fatty acids

RAF: Serine/Threonine Kinase

RCT: Randomized controlled trial

RNS: Reactive nitrogen species

ROS: Reactive oxygen species

RPKM: Reads Per Kilobase of transcript

RRM2B: Ribonucleotide reductase regulatory TP53 inducible subunit

rxnGeneMat: Reaction–gene matrix

SARS-CoV-2: Severe acute respiratory syndrome coronavirus 2

SGMS1: Sphingomyelin synthase 1

SI: Similarity score

SKO: Single gene deletion

SOC: Standard-of-care

TBK1: TANK binding kinase 1

TCGA: The Cancer Genome Atlas Program

TMZ: Temozolomide

TXNRD1: Thioredoxin Reductase 1

TYMS: Thymidylate synthase

U.S.: United States

VBOF: Viral biomass objective function

VEGF: Vascular endothelial growth factor

WHO: World Health Organization

αKG: Alpha-ketoglutarate

Chapter 1

Synopsis

1.1 Introduction

Besides the various historical pharmacopeias, the rigorous search for treatments has evolved steadily from compound isolation from natural products (NPs) and chemical synthesis in the 19th century to biotechnologically-derived drugs since 1935 [1]. In the latter phase, also known as the Golden Age of drug discovery, many antibiotics and cardiovascular drugs, among others, were discovered, transforming the top deadliest diseases of the early 20th century into preventable or treatable rare diseases [1]. Preclinical models have been the gold drug discovery standard, including cell lines, animal models, xenografts, and organoids [2]. Despite their importance, preclinical models face many challenges that reduce the candidate drugs' success in clinical trials [2]. For instance, preclinical models fail to capture the complexity of human patients [3], some disease models are hard to culture, such as oligodendroglioma (ODG) [4], and infection disease models may require extensive biosafety measures [5]. Consequently, half of phase II clinical trials between 2005 and 2015 failed to exceed the predetermined primary outcomes [6]. Similarly, the overall probability of success to pass from phase I to approval is 13.8%, with oncology drugs having the lowest 3.4% probability of success [6]. These challenges lead to a time-consuming and costly drug discovery process [7] that is less efficient in multi-factorial diseases such as neurodegeneration and cancer [8] and rare diseases with a small population [9].

While drug discovery is still increasing the arsenal of approved drugs with new mode-of-actions and improved affinity, the plateau of newly approved drugs in the last three decades is forcing the drug industry to utilize these previously approved drugs [10]. Drug repurposing, redirecting approved drugs to other target diseases, contributes increasingly to drug approvals,

escaping years of phase I safety trials [11]. Once preclinical efficacy is established for the new target disease, drug repurposing redirects approved drugs to phase II trials [11]. Besides approved chemotherapies, repurposing non-cancer drugs to cancer is gaining more momentum, either as combined with chemotherapies or as monotherapy preventive drugs to reduce cancer incidence [12]. Among the most successful repurposed non-cancer drugs is the immunosuppressant rapamycin, approved for a kidney transplant, which was later repurposed and approved for renal cancer [13]. Most preclinical drug discovery and repurposing approaches utilize small compounds to reverse the disease phenotype or inhibit the disease target. Meanwhile, experimental high-throughput drug screening (HTS) allowed automated screening of thousands of approved and investigational drugs on the preclinical models using robotics [14]. Various types of HTS assays evolved both drug discovery and repurposing, such as target inhibition, cellular viability reduction [14], and reversing pathogen-host molecular hijacking [15]. Still, the preclinical model's limitations constrain experimental drug repurposing, and exhaustive drug combination screening is infeasible.

Complementary to preclinical models, computational drug discovery advanced the approval of new drugs through two phases: structure-based drug design and genome sequencing. In 1981, captopril became the first drug to be approved employing a computer-aided drug design based on the angiotensin-converting enzyme (ACE) protein structure [16]. In 2003, the first human reference genome and the subsequent commercially available next-generation sequencing advanced drug discovery through a systematic association between genotype and phenotype [17]. Notably, two-thirds (n=33) of the 50 Food and Drug Administration (FDA)-approved drugs in 2021 were supported by human genetic evidence using structure and genome data [18]. Unlike previous associations of single genes to the target disease, Systems Biology integrates the complex interactions of the different genomic levels [17], [19]. Systems Biology application in medicine, or Systems Pharmacology, allowed associating drug response with genetic biomarkers or transcriptomic signatures, changed clinical trial randomization, and introduced new targeted therapies and diagnoses [20]. For example, finerenone was approved in 2021 based on a Systems Biology analysis linking an NR3C2 variant to chronic kidney disease using genome-wide associations and functional genomics [21]. Still, signature- and genome-based drug discovery lacks mechanistic interpretation [22]; meanwhile, structure-based drug discovery fails with multi-factorial complex diseases [23]. While the annotation quality is lacking or non-existent for non-metabolic genes and their interactions, metabolic genes and their biochemical reactions are by far the most well-annotated [24].

Of the computational drug discovery approaches, metabolic network modeling is a qualitative method that simulates the physiological cellular metabolism or the pathological metabolic rewiring [25]. The publication of the human genome reference allowed the building of the first human generic reconstruction facilitating metabolic network modeling for human diseases [26]. A generic reconstruction is a species-specific, phenotype-agnostic, mathematical representation of the biochemical network that incorporates metabolites, reactions, and genes on a genome-scale [26]. Each reaction is defined by a Boolean rule (gene-protein-reaction rules, GPR rules) of gene isoforms, using "AND" or "OR" rules [26]. The mathematical representation of metabolic modeling depends on constraints distinguishing it from kinetic models [27]. The constraints of metabolic modeling consist of linear equalities of mass balance and inequalities of upper and lower boundaries. The equalities come from the metabolic network's representation as a sparse stoichiometric matrix $\boldsymbol{S}$ of m metabolites in rows and n reactions in columns [25]. The values of the $\boldsymbol{S}$ matrix are the stoichiometric coefficients of the interacting metabolites in each reaction, while the sign of these stoichiometric coefficients represents the directionality of the metabolites in each reaction [25]. Most of the $\boldsymbol{S}$ matrix contains zero coefficients that represent no reactions of the related metabolites [25]. In addition to the S matrix, the rates of the reaction turnover are represented by a flux vector v that has n length. Under the steady-state assumption, the metabolic production and consumption are balanced in mass and charge, and thus, the multiplication of $\boldsymbol{S}$ matrix and v equals zero.

$$S * v = 0 \tag{1.1}$$

To simulate the metabolic process of interest, an objective function (OF) is assigned based on the biological question and set to be maximized, such as ATP production or biomass growth, or minimized, such as in unneeded byproducts [25]. The allowable flux search space for the OF is reduced using the constraints of balances and boundaries. Among the permissible flux distributions, the most optimal solution is determined by the Flux Balance Analysis (FBA) to achieve the selected OF [28]. Meanwhile, the flux range of specific reactions is defined by the Flux Variability Analysis (FVA) to achieve the OF, for example, determining if a metabolic exchange is an uptake, efflux, or both [29]. Since the different metabolic reactions vary across phenotypes, tissues, and diseases, building genome-scale metabolic models (GEMs) out of the generic reconstruction is crucial for drug repurposing. FASTCORMICS [30] and rFASTCORMICS [31] are for context model-building workflows using microarray and RNA-Seq, respectively, in addition to a generic reconstruction. Both workflows utilize the FASTCORE

algorithm that takes a set of core reactions as input and searches for the minimal set of non-core reactions to obtain a flux-consistent subnewtork [32]. FASTCORMICS was benchmarked against other model-building algorithms, where it retrieved the highest fraction of core reactions and the lowest fraction of non-core reactions [33].

The interpretability and the scalability of metabolic modeling advanced many industrial applications, such as improving microbial metabolite yield [34] and *ex vivo* tissue generation for cultivated meat [35]. In human health, metabolic modeling's applications extend to disease target identification [31], drug repurposing [36], biomarker prediction [37], modeling in-born metabolism errors [38], and understanding microbiome-host interactions [39]. Similar to genome-scale CRISPR gene knock-out (KO), *in silico* gene deletion can predict disease-specific essential genes of the context GEMs whose KO would reduce the OF but on only metabolic genes [40]. Moreover, the drug deletion pipeline simulates the multi-gene KO by the drug targets similar to the HTS [31]. While metabolic modeling applications in microbial engineering are enormous, few drugs predicted by metabolic modeling went into clinical trials [41], [42]. Similar to finerenone approval that was supported by functional genomics [21], drug repurposing using metabolic modeling could advance drug approval with improved interpretation, especially for multi-factorial diseases such as cancer and newly emerging infections.

In the United States (U.S.) between 2013 and 2019, five-year relative survival for melanoma and breast cancer (BRC) were 93.5% and 90.8% [43]. Meanwhile, the five-year relative survival of glioma patients — a type of brain cancer that originates from the glial cell— varies among the glioma subtypes (6.2% for glioblastoma multiforme (GBM) and 45.9% for astrocytoma (AST)) [43]. On the other hand, by using the five-year incidence rate per 100,000, breast cancer has a much higher incidence rate (127) than melanoma (21) and glioma (0.8-3.2) [43]. Despite the variations in survival and incidence, the discovery of many cancer type-specific oncogenes and biomarkers transformed cancer diagnosis and treatment, such as estrogen receptor (ER), HER2, and BRCA1/2 in BRC [44], BRAF and NRAS mutation in melanoma [45], and IDH1/2 mutation and 1p/19q co-deletion in glioma [46]. Generally, approved chemotherapies by the U.S. FDA for these cancer types are either cell cycle inhibitors (CCIs) or targeted therapy inhibiting signaling pathways. Among the targeted therapies, immune checkpoint inhibitors (ICIs) were the first drug class to enhance advanced melanoma survival and are currently approved in melanoma and BRC, especially for BRAF-wiltype and non-V600E mutants [47]. Meanwhile, more than half of melanoma patients, 3% GBM and 2-5% low-grade glioma (LGG), possess BRAF V600E mutation [45]. Consequently, the RAF/MEK inhibitor combination was

approved by the FDA for BRAF-mutant cancers firstly for melanoma [48] and recently in June 2023 for LGG [49]. Still, BRAF-mutant melanoma shows resistance to RAF/MEK inhibitor combination and high relapse rate [50].

Similarly, the PI3K/AKT/mTOR signaling pathway is dysregulated in the three cancers [51], which is targeted by approved drugs in BRC and glioma. Despite these advances, alkylating agents of the CCIs, such as temozolomide (TMZ) and dacarbazine, are the most commonly prescribed drug class in melanoma patients lacking BRAF V600E mutation and glioma patients, with low efficacy and high resistance. Additionally, only a fraction of melanoma and BRC patients respond to ICIs with unclear response biomarkers, unlike the well-defined RAF/MEK inhibitors for the BRAF V600E mutant [52]. Additionally, approved combinations inhibit redundant targets for the same pathway, leading to preventable toxicity [53]. The high incidence of BRC, the low survival rate and approved drugs for glioma, and the high relapse of melanoma encourage the search for new preventive drugs for BRC and the repurposing of previously approved drugs for glioma and melanoma.

Unlike cancer, emerging infections usually lack any approved treatment, and the incidence rate increases dramatically if they develop into a pandemic like COVID-19. COVID-19 is a highly proliferating viral infection of the human respiratory system that hijacks the host molecular pathways [54] to enhance viral replication and infectivity rising to the 2020 global pandemic. The host hijacking starts with viral entry via ACE2, an essential protein for oxidative stress, then initiates RNA synthesis, mRNA translation, viral assembly, and exocytosis [55]. While cancer showed prolonged immune evasion that requires ICIs to reactivate the immune system, COVID-19 is often characterized by an acute immune response leading to an inflammatory cytokine storm [54]. In 2020, searching for new effective treatments against COVID-19 was pivotal but slow due to the biosafety requirements for viral experiments. In 2023, in addition to vaccination, approved treatments for COVID-19 are either immunomodulators targeting host immune response or antivirals targeting viral entry or replication mechanisms [55]. Acknowledging the host metabolic hijacking by COVID-19 in the early pandemic, many approved drugs have been tested in clinical trials for COVID-19 to modulate the host metabolism [56]. Still, none of the metabolic-modulating drugs have passed the phase IV clinical trials [56].

Besides the dysregulated ACE2 system in COVID-19, metabolic rewiring plays a crucial role in cancer, from dysregulation of oxidative stress in LGG [57], ER in BRC, and

lipid metabolism in melanoma. Additionally, few approved drugs in GBM, drug resistance in melanoma, and high incidence in BRC and COVID-19 motivate the repurposing of new drugs and combinations to address the disease-induced metabolic rewiring. Despite the scale of HTS, combination HTS requires brute-force the squared number of drug experiments that limit the options of tested drugs [58]. Meanwhile, computational drug repurposing allows faster drug prioritization, especially with the prediction of drug combinations [23] and hard-to-cultivate cell lines such as ODG [4]. Similarly, computational drug repurposing of infectious diseases is crucial due to the *in vitro* biosafety restrictions and the urgency to cope with new emerging variants [59]. Thus, the need for computational drug repurposing through metabolic modeling for these diseases with proper interpretation as quality control is pivotal.

In this synopsis, we cover four papers on metabolic modeling applications in drug repurposing and evaluate the strengths and limitations given the proposed aim. These aims are:

- Prediction of essential genes and FDA-approved repurposable drugs for COVID-19 [60] and glioma [61].
- Ranking NPs with potential anti-BRCs effect [62].
- Evaluating predicted drugs for melanoma under metastasis, drug resistance, and BRAF/N-RAS mutation. [63].

Post-publication evaluation includes ranking predicted to approved drugs in xenografts, cross-study comparison of the predicted essential genes and drugs, and how the variations in predicted genes and drugs are consistent with literature and clinical trials. Finally, we will discuss the limitations in each paper and perspectives on drug repurposing in pan-cancer stratification and multi-organ infectious diseases. These perspectives could enhance drug repurposing for cancer or new COVID-19 variants into clinical application.

1.2 Methods

1.2.1 Data and model building

rFASTCORMICS [31] was fed with RNA-Seq from glioma subtypes' patients [64], melanoma cell lines and tissues, and SARS-CoV-2 infected lung cells [65], [66] to build consensus GEMs for every disease with various ReconX generic reconstructions and medium constraining (see Table 1.1 for details). Meanwhile, FASTCORMICS [30] was fed with NP- and DMSO-treated BRC microarray data [67] with Recon3D [68] as input reconstruction. The ReconX generic

reconstructions used from the COVID-19 model building were curated with the viral biomass objective function (VBOF) of SARS-CoV-2-infected alveolar macrophage model (BioModels: MODEL2003020001) [69]. Unlike the *in vitro* medium of melanoma and BRC models, glioma models were built with a biofluid medium (cerebrospinal fluid, CSF [70], [71]) because our previous review defined CSF as the commonly used medium for brain GEMs [72]. The default growth function (biomass_reaction) in ReconX was used as an OF for the three cancers. Meanwhile, the VBOF was set as OF for COVID-19 GEMs while ensuring the host OF and VBOF carry flux simultaneously by setting the host OF's upper bounds to 10% of its maximal flux.

Table 1.1: Summary of the aim, data, model building algorithm, and generic reconstruction used for the four studied diseases.

Disease	**Motivation**	**Input expression data**	**Model building algorithm**	**Generic reconstruction**	**Medium data**
Glioma	• Our review on brain GEMs indicated the absence of LGG GEMs and GBM GEMs are either built non-genome scale or lack manual curation [72]. • IDH-mutation in LGG induces metabolic rewiring [57]. • GBM patients suffer from poor survival, which increases clinical trial failure [73]. • Preclinical models in LGG are limited [57], [74]. • Few drugs are approved for glioma.	Patient RNA-Seq data for glioblastoma (TCGA-GBM) and LGG (TCGA-LGG) [64]	rFASTCORMICS [31]	Recon3D [68]	CSF [70], [71]
Melanoma	• RAF/MEK inhibitors are ineffective for melanoma patients lacking BRAF V600E mutation and show resistance in BRAF mutant patients [47]. • Approved immune-checkpoint inhibitors are only effective in a sub-population with poorly defined biomarkers [52]. • Resistant melanoma shifts to oxidative phosphorylation and deregulated lipid biosynthesis [75].	Various RNA-Seq data from melanoma patients and cell lines.	rFASTCORMICS	Recon2 [76]	RPMI

Breast cancer	• Many natural products (NPs), some of which are part of the daily diet, have a phytoestrogen effect that could modulate the hormone response in BRC [77]. • More than 60% of approved anti-cancers and 23.8% of all approved drugs originate from NPs [78], [79].	Microarray data of NP-treated BRC cell line [67]	FASTC-ORMICS [30]	Recon3D	MEM/-EBSS
COVID-19	• ACE2 is the viral entry receptor into the host cell and is crucial in oxidative stress [55]. • The required biosafety laboratories for handling infected cell lines emphasize the need for *in silico* drug repurposing [5]. • SARS-CoV-2 infected lung is a highly proliferating cell with an active glycolysis profile as cancer [80].	RNA-Seq data from lung cell lines infected with SARS-CoV-2. [65], [66]	rFASTC-ORMICS	Recon2 and Recon3D	No medium

1.2.2 Prediction of essential genes and drugs

Single gene deletion from the COBRA Toolbox v.3.0 [40] was used to predict essential genes in glioma, melanoma, and COVID-19, whose KO would reduce the viral/cancer proliferation. Due to the small number of samples in DMSO BRC GEM, single-gene deletion was excluded for BRC. Genes whose KO is predicted to reduce the OF by at least 50% were considered essential genes.

To predict single drugs, the drug deletion pipeline [81] was run with FDA-approved drugs (>2300 drugs) for glioma, melanoma, and COVID-19 GEMs. Meanwhile, the NPs and approved anti-BRCs were used for BRC GEMs. Drug-target interactions were extracted from databases such as DrugBank [82] in the drug deletion pipeline. Due to the small number of approved combinations and their redundant target pathways in glioma, drug deletion was applied to the glioma GEMs to predict new combinations using FDA-approved drugs combined with investigational anti-glioma drugs (IAGs). Similar to essential genes, drugs, and combinations whose multi-gene KO are predicted to reduce the OF by at least 50% were considered candidate single drugs and combinations, and due to the absence of target information for 56% of the NPs, drug prioritization in NP GEMs (n=102) employed various steps to define potential anti-BRC even without target information. The drug prioritization in NP consisted of four steps: 1) drug deletion with NP targets, 2) dissimilarity to the DMSO GEM, 3) similarity to approved anti-BRC GEMs, and 4) metabolic pathway alternation. This multi-step approach

ensured ranking for NPs without target information.

1.2.3 Drug prioritization and essential genes evaluation

Predicted drugs, their targets, and essential genes were evaluated against approved drugs and their targets *in vitro*, in xenografts and clinical trials in melanoma and glioma. This analysis was extended to melanoma to identify if the predicted drugs and their targets would maintain their efficacy in resistance, metastasis, and BRAF/NRAS mutation.

1.2.3.1 Evaluation of metabolic exchanges from literature

Differences between the glioma subtype GEMs in metabolic exchanges can help to evaluate the model quality using known metabolic exchanges from the literature. The minimum and maximum fluxes for the uptake and export reactions for the three glioma GEMs were computed using FVA in the COBRA Toolbox v.3.0 [40]. Metabolic exchanges with narrow bounds were selected as mandatory uptake or export reactions and were compared to known metabolic variations in the glioma subtypes in literature. Due to the lack of metabolic exchange studies on COVID-19 in 2020, predicted essential genes and their pathways in COVID-19 were compared to a metabolomics [83] and a multi-omics [84] studies.

1.2.3.2 *In vitro* drug HTS

To evaluate predicted drugs in glioma and melanoma against approved, *in vitro* pan-cancer and glioma-specific HTS databases were used. Viability reduction from two databases [85], [86], IC_{50} measures from four databases [86]–[88] and literature allowed retrieving these two measures for predicted and approved drugs. Median viability reduction and IC_{50} measures were calculated for each drug across the cancer cell lines. Due to the high relapse rate in melanoma patients treated with RAF/MEK inhibitors' resistance, predicted drugs for melanoma were compared to approved drugs using three analyses: metastatic, anti-melanoma resistant, and BRAF/NRAS mutant cell lines.

1.2.3.3 Pan-cancer CRISPR dependency data

To evaluate the predicted essential genes and drug targets of glioma and melanoma against approved drug targets' performance in reducing cancer cell growth, a genome-scale pan-cancer CRISPR-Cas9 dependency data (Cancer Dependency Map, DepMap) [89] was used. The dependency probabilities (the likelihood that the KO of a gene reduces cell growth or induces cell death) were retrieved for essential genes, predicted, and approved drug targets from DepMap 22Q1. The median dependency probabilities were calculated for each gene across the respective cancer cell lines.

1.2.3.4 Xenograft data

Three GBM patient-derived xenograft (PDX) HTS [90], [91] allowed ranking predicted drugs for glioma against approved drugs. Median growth reduction was calculated across the GBM PDXs for each drug.

1.2.3.5 Clinical trial data

Predicted drugs in glioma and melanoma were searched for phase I/II or higher clinical trials in `beta.clinicaltrials.gov` [92] and Cochrane Library [93] in their respective cancer indication. If available, priority was given in order of network meta-analysis, systematic reviews, and two-arm randomized controlled trials (RCT) where one arm is an approved drug and the 2nd arm is a predicted drug. Due to the limited clinical trials in melanoma for the predicted drugs, the search was expanded to skin cancer.

1.2.4 Post-publication drug prioritization

Previous evaluations of predicted drugs and essential genes were limited in BRC and COVID-19 due to the scarcity of HTS screening for NPs and SARS-CoV-2-infected human cells in 2020. In this section, we extend the published evaluations to include more HTS screening databases, xenograft data for melanoma and BRC, and clinical trial data for COVID-19, BRC, and melanoma. Moreover, we compare the predicted NPs from the microarray to the

remaining NPs excluded from our analysis (hereafter will be referred to as "Excluded").

1.2.4.1 In vitro drug HTS

In addition to IC_{50} measures from literature, *PharmacoGx* R package [94] was used to retrieve IC_{50} measures for predicted and approved drugs across the three cancers from 14 pan-cancer and cancer-specific HTS databases [86]–[88], [95]–[103]. Additionally, the median viability reduction from 23Q2 PRISM database [86] was retrieved for the predicted and approved drugs in the respective cancer indication. Meanwhile, most *in vitro* HTS in COVID-19 are limited due to the required biosafety laboratories and mainly applied to non-human cell lines [104]. Among the various HTS against COVID-19, cytopathic effect (CPE) reduction assay indirectly monitors the ability of drugs (or genes in case of knock-down/CRISPR) to decrease live viral replication and infection through reversing the hijacked host molecular mechanisms [105]. Most *in vitro* CPE HTS in COVID-19 are tested using the non-human primate kidney Vero/Vero E6 cell lines that have metabolic profiles from human cells [106]. Across 15 *in vitro* CPE HTS in COVID-19, none was tested on human lung cells, so we choose Ellinger *et al.* 2021 [107] as it was tested on human Caco-2 cell line. Predicted and approved (including FDA/EMA-authorized for approval by Oct 2023) [55] drugs in COVID-19 were ranked based on their CPE scores.

1.2.4.2 Pan-cancer CRISPR dependency data

Similar to drug target ranking in melanoma and glioma, predicted essential genes for COVID-19 were compared against approved drug targets using a CRISPR screen on five SARS-CoV-2-infected cells (four human cells and Vero E6 cell) [108].

1.2.4.3 Xenograft data

To identify the candidate drugs with potential *in vivo* cytotoxicity, *in vivo* PDX reduction effect was extended from glioma to melanoma and BRC. Predicted and approved drugs for melanoma and BRC were ranked using two PDX screening for melanoma [109] and BRC [110], respectively. Across the three cancers, median IC_{50} for each drug was compared to the median PDX score (growth reduction in glioma, DSS in melanoma, and AUC in BRC) to define which

predicted drug maintained *in vivo* efficacy.

1.2.4.4 Clinical trial data

In addition to the collected clinical trial data in melanoma and glioma, `beta.clinicaltrials.gov` was searched for the predicted drugs in BRC and COVID-19. Other retrospective studies were included due to the scarcity of clinical data for NPs.

1.3 Results

In this synopsis, the predicted essential genes of three diseases (glioma, melanoma, and COVID-19) were compared to disease-specific vulnerabilities in literature and evaluated against approved drug targets in CRISPR screen dependency. The drug deletion pipeline results were further assessed for the four studies (glioma, melanoma, BRC, and COVID-19), precisely over three drug development phases *in vitro*, in xenografts, and clinical trials. This evaluation was extended in melanoma into metastatic, drug-resistant, BRAF/NRAS mutant cell lines. In BRC, predicted NPs were compared to both approved BRC drugs and NPS excluded from the 101 NPs.

1.3.1 Disease-specific essential genes match literature-retrieved dependencies in glioma, melanoma, and COVID-19

Before drug repurposing, model quality was evaluated to verify the predicted essential genes' consistency with known vulnerabilities in the literature. Single gene analysis predicted 25, 35, and 23 essential genes (whose single KO reduced viral/cancer proliferation to at least 50%) for glioma, melanoma, and COVID-19 (see Table 1.2). Pathway analysis of the three gene sets identified similar essential genes, especially between melanoma and glioma, and differences indicative of disease-specific dependencies (see Figure 1.1). Six essential genes were shared between the three diseases participating in nucleotide interconversion (CMPK1 and GUK1), fatty acid uptake (SLC27A4), amino acid uptake (SLC7A5), sphingomyelin synthesis (SGMS1), and cardiolipin synthesis (CRLS1). Lipid and cholesterol synthesis essential genes were unique for melanoma. Meanwhile, cholesterol esterification was shared between glioma

and melanoma. These differences agree with the role of lipid and cholesterol synthesis in resistant melanoma cell lines [75]. On the other hand, glioma, especially GBM, bypass cholesterol synthesis through CSF uptake, and cholesterol can be only targeted via uptake inhibition, efflux activation [111] or esterification [112]. Additionally, six of the 25 glioma essential genes have been previously tested *in vitro* KO or KD studies glioma, where five genes (TXNRD1, RRM1-2, SPLTC1, and SLC27A4) decreased proliferation, and only one gene (PCYT2) increased proliferation (see Figure 3.2).

Despite the shared metabolic essential genes, COVID-19 showed distinct vulnerabilities in cysteine synthesis (CTH and SLC7A11), glycine synthesis (AGXT and PEPD), one-carbon cycle by folate (OCCF: TYMS and DHFR), and sphingolipid salvage (GLTP). SAR-CoV-2 hijacking of OCCF has been validated *in vitro* [113]. Cysteine and glycine synthesis are crucial for glutathione (GSH) synthesis and biomarkers for ferroptosis, an iron-dependent programmed cell death that selenium can inhibit. Unlike the *de novo* sphingolipid synthesis predicted essential in glioma and melanoma, COVID-19 is predicted to utilize sphingolipid via the salvage pathway. All in all, predicted essential genes accurately matched literature-identified vulnerabilities such as ribonucleoside interconversion, cholesterol/lipid synthesis, and OCCF in glioma, melanoma, and COVID-19, respectively.

1.3.2 Glioma and COVID-19 GEMs correctly captured biomarkers consistent with patient data

The model quality was further evaluated based on consistency with literature in metabolic exchanges. The three glioma subtype GEMs showed differential metabolic exchanges, of which six out of seven reactions agreed with the literature (see Figure 3.1). Notably, high glutamate uptake predicted by the LGG models was consistent with the LGG-specific glutamate depletion in cell lines [114] due to IDH mutation-induced metabolic rewiring. Meanwhile, high thymidine uptake predicted by the GBM GEM was consistent with GBM-specific thymidine uptake in patients compared to AST [115] and ODG [116] patients.
Due to the lack of such metabolic uptake studies in COVID-19 in 2020, a metabolomics study of SARS-CoV-2-positive and negative patients [83] was compared to the enriched pathways of the predicted essential genes for COVID-19. Significant high serum ferroptosis biomarkers were found in SARS-CoV-2-positive patients of the metabolomics study [83] such as kynurenines, methionine sulfoxide, cystine, and free polyunsaturated fatty acids. Similarly, a cross-sectional

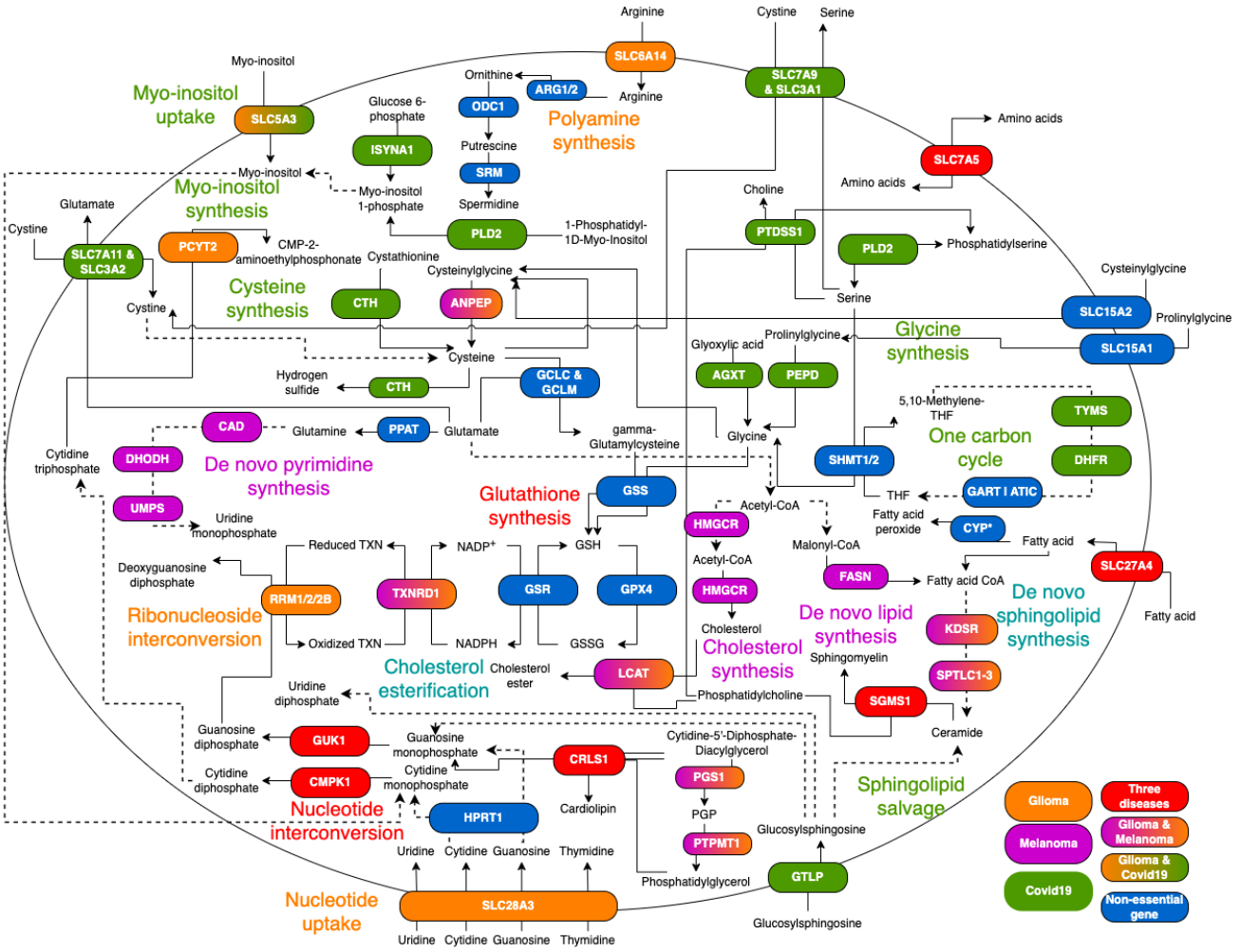

FIGURE 1.1: **Predicted essential genes in glioma, melanoma, and COVID-19 showed variations in nucleotide uptake/synthesis, lipid synthesis, sphingolipid salvage/synthesis, and one-carbon cycle, respectively.**

Single gene deletion was applied to glioma, melanoma, and COVID-19 to predict genes whose KO would reduce viral/cancer proliferation. 25, 35, and 23 essential genes were predicted for glioma, melanoma, and COVID-19. Six essential genes were shared between the three diseases in five pathways: nucleotide interconversion (CMPK1 and GUK1), uptake of fatty acids (SLC27A4) and amino acids (SLC7A5), and synthesis of sphingomyelin (SGMS1) and cardiolipin (CRLS1). Notable disease-specific dependencies were ribonucleoside interconversion and nucleotide uptake for glioma, *de novo* lipid synthesis and pyrimidine synthesis for melanoma, and one-carbon cycle and cysteine synthesis for COVID-19. Six of 25 glioma essential genes have been previously tested for *in vitro* KO or KD, where five genes of ribonucleoside interconversion (RRM1 and RRM2), sphingolipid synthesis (SPLTC1) and fatty acid uptake (SLC27A4) reduced glioma proliferation, meanwhile PCYT2 increased proliferation. Similarly, one-carbon cycle and lipid synthesis were dysregulated in COVID-19 and melanoma, respectively. In summary, predicted essential genes accurately captured disease-specific glioma, melanoma, and COVID-19 vulnerabilities. Abbreviations: THF: tetrahydrofolate; TXN: thioredoxin; GSH: reduced glutathione; GSSG: oxidized glutathione.

Table 1.2: Summary of the model statistics and model predictions in essential genes and drugs in the four studied diseases.

Disease	Number of consensus models	Number of samples per model	Median number of reactions	Number of predicted drugs	Number of predicted essential genes
Glioma	• Cancer: 3 • Control: 1	• Cancer: 117-140 • Control: 4	3269	• Single drugs: 33 • Combinations: 17	25
Melanoma	• Cancer: 33 • Control: 24	• Cancer: 28-8792 • Control: 3-740	1773	• Single drugs: 28	35
Breast cancer	• NP-treated MCF-7: 102 • DMSO-treated MCF-7: 1	• NP-treated MCF-7: 2-4 • DMSO-treated MCF-7: 6	1895	• Single drugs: 23	Not predicted
COVID-19	• Infected: 28 • Control: 22	• Infected: 2-4 • Control: 2-4	2456	• Single drugs: 85 • Combinations: 52	23

study compared COVID-19 survivors to non-survivors, where selenium level was found higher in tissue samples from COVID-19 survivors [117], which was further confirmed later in a meta-analysis [118]. These serum COVID-19-specific biomarkers are consistent with the ferroptosis-based predicted essential glycine and cysteine synthesis genes. Predicted GEMs in glioma and COVID-19 accurately predicted metabolic exchanges in glioma patients and SARS-CoV-2-positive high serum metabolites, respectively.

1.3.3 Predicted drugs in melanoma and glioma target cholesterol/pyrimidine synthesis and oxidative stress/cell cycle, respectively

While predicted essential genes represent single-gene KO, drug deletion simulates the simultaneous multi-gene KO of the drug targets. The mode-of-action (MOA) of the predicted single drugs varied between glioma and melanoma, indicative of the dysregulated pathways in each cancer (see Figure 1.2.A-B). Antimetabolites and lipid-lowering were the most predicted MOAs among glioma and melanoma, respectively. Among the four predicted antimetabolites for melanoma, two targeted nucleotide interconversion (gemcitabine and cladribine) similar to glioma: meanwhile, teriflunomide and leflunomide *de novo* pyrimidine synthesis. Additionally, predicted melanoma-specific antifungals target lipid synthesis, while glioma-specific antivirals

and TXNRD1-inhibitors target cell cycle, respectively. This increases the predicted drugs targeting cell cycle in glioma to 23 and drugs targeting lipid synthesis in melanoma to 19.
Due to the small number of approved combinations in glioma, drug deletion was applied to predict new synergistic combinations targeting alternative reactions. Seventeen predicted combinations for glioma consisting of 19 individual drugs (see Figure 1.2.C) were found to target hypoxia (12 carbonic anhydrase inhibitors, CAi), GSH exchange (rifamycin), cell cycle (fluorouracil and zidovudine), synthesis of polyamine (eflornithine), glutamate (adapalene), and GSH (cannabidiol and resveratrol). Fifteen combinations were predicted for all glioma subtypes. Meanwhile, eflornithine/rifamycin and cannabidiol/adapalene were predicted combinations for GBM and LGG, respectively (see Figure 3.3). Targeting glutamate and GSH synthesis in LGG with cannabidiol/adapalene is consistent with glutamate depletion due to IDH-mutant-induced rewiring [114]. Among the eflornithine/rifamycin targets, an ABC transporter (ABCG2) is responsible for heme byproducts efflux [119]. A literature search found heme synthesis to be impaired to LGG compared to GBM, which is consistent with the predicted specificity of eflornithine/rifamycin. Targets of the predicted single drugs and combinations for glioma are summarized in Figure 3.7.

Unlike the approved drugs predicted for glioma and melanoma, Most NPs in BRC are preclinical compounds with multiple MOAs or undefined targets. The 23 predicted NPs consisted of seven antioxidants, six ER inhibitors, and three toxins, among others (see Figure 1.2.D). The predicted ER inhibitors among NPs are consistent with MCF-7 BRC cell line dependency on estrogen activation [120]. Meanwhile, predicted drugs for COVID-19 targeted once carbon cycle (DHFR, TYMS, ATIC, and TYMP), nucleotide interconversion (GUK1 and CMPK1), cysteine synthesis (SLC7A11 and ANPEP), glycine synthesis (SLC15A1 and SLC15A2), and lactate efflux (SLC16A1). Unlike lipid-lowering predicted for melanoma that targeted cholesterol synthesis, rosuvastatin, and pravastatin were predicted for COVID-19 to target cysteine synthesis (SLC7A11) and lactate efflux (SLC16A1), respectively. Similarly, glycine synthesis was targeted by ACE inhibitors of the viral entry protein.
In summary, predicted single drugs favored cell cycle, *de novo* pyrimidine/lipid synthesis, ER, and glycine/cysteine synthesis for glioma, melanoma, BRC, and COVID-19, respectively, that agree with dysregulated pathways or known vulnerabilities in the corresponding diseases. Additionally, GBM and LGG-specific combinations are consistent with upregulated heme synthesis and glutamate depletion, respectively.

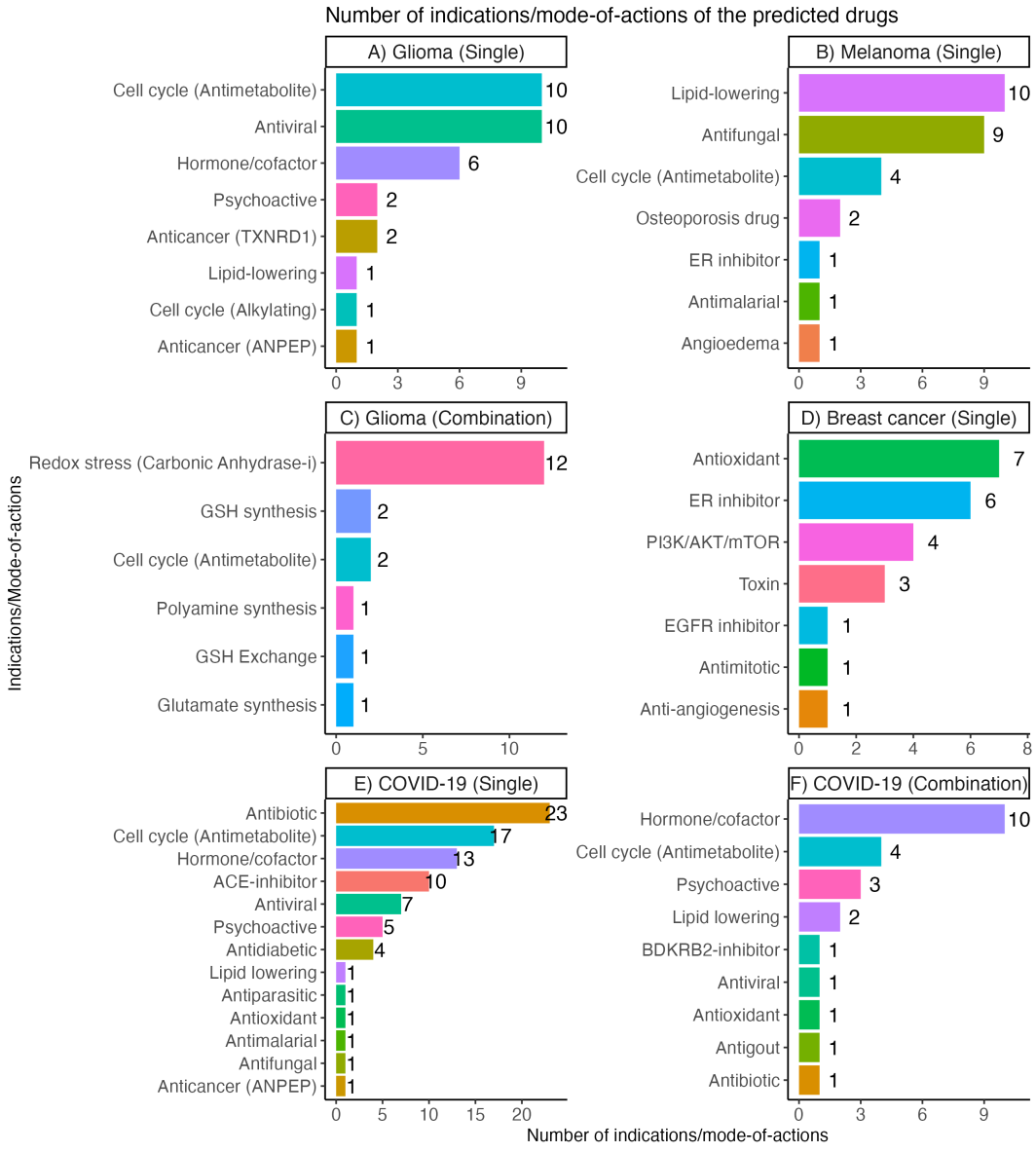

FIGURE 1.2: **Antimetabolites and lipid-lowering drugs are the most repurposed single drugs to glioma melanoma, respectively.**

1.3.4 Predicted drugs in glioma, melanoma, and BRC showed improved, comparable, and reduced IC_{50} than approved drugs, respectively

To rank candidate drugs for testing, predicted drugs in the three cancers were compared to approved drugs using viability reduction in PRISM 23Q2 and IC_{50} across 14 HTS databases in their respective cancer cell lines (see Figure 1.3). Predicted antimetabolites (red triangles) in glioma and melanoma showed improved and comparable potency to approved antimitotics (blue triangles) and RAF/MEK inhibitors (green squares), respectively. Unlike low potency and viability reduction of the RAF/MEK inhibitors in glioma, RAF/MEK inhibitors showed stronger viability reduction in melanoma in agreement with the small prevalence of RAF/MEK mutations in glioma. In melanoma, in-depth drug ranking showed three drugs (gemcitabine,

cladribine, and fluvastatin) exceeding approved drugs in potency and viability reduction, regardless of metastasis, drug resistance, and BRAF/NRAS-mutant status [63] (see Chapter 4). Variations in drug rank between viability reduction and IC_{50}, such as CDK inhibitors (magenta triangles), indicate non-linear dose response. Despite three predicted NPs in BRC (hypaconitine, daidzin, and narciclasine) showing high potency below 1 μM, overall predicted NPs in BRC showed comparable potency to the excluded NPs and reduced potency to approved drugs. Four excluded NPs showed IC_{50} below 1 μM (arenobufagin, bufalin, bufotaline, and isoalantolactone), of which the first three belong to cardiotoxins called bufanolides. Similarly, the top excluded NP (cinobufatolin) belongs to bufanolides with 100% viability reduction exceeding all approved drugs. None of the submicromolar excluded NPs have a metabolic target in the Recon3D model, which could explain their absence from drug ranking. Among others, bufanolides possess anti-cancer action through apoptosis and epigenetics modulation that could be missed with metabolic modeling [121], [122]. In summary, compared to approved drugs, predicted antimetabolites in glioma and melanoma showed improved and comparable potency, respectively. While predicted NPs showed lower potency than approved drugs, predicted toxin and ESR1-inhibitor NPs showed submicromolar potency.

1.3.5 Predicted essential genes in glioma and melanoma showed higher dependency than approved targets in a CRISPR screening

While drug HTSs allowed ranking candidate drugs for further testing, these drugs usually act by multi-gene KO, and drug HTSs are unable to identify which gene has a higher dependency. Pan-cancer, genome-scale CRISPR screens such as DepMap identify vulnerability genes whose individual KO will reduce cell growth or induce cell death. DepMap was used to rank essential genes and drug targets in the three cancers to identify highly dependent genes. In melanoma and glioma, predicted essential genes (in purple) showed higher dependency than predicted drug targets (in green) and approved drug targets (in blue), as the latter usually depends on multi-gene KO. Similarly, in glioma, predicted single drug targets (in green) had higher dependency than combination targets (in orange). In melanoma, further ranking of the targets of predicted and approved drugs found that predicted RMM1 and RRM2 have higher dependency probability than approved targets in both metastatic and drug-resistant cell lines (see Figure 4.4- 4.5). Moreover, 42% and 43% of the predicted essential genes in glioma and melanoma showed more than 50% dependency, respectively (see Figure 1.4). High dependency of HMGCR in glioma cell lines could be attributed to differences between *in*

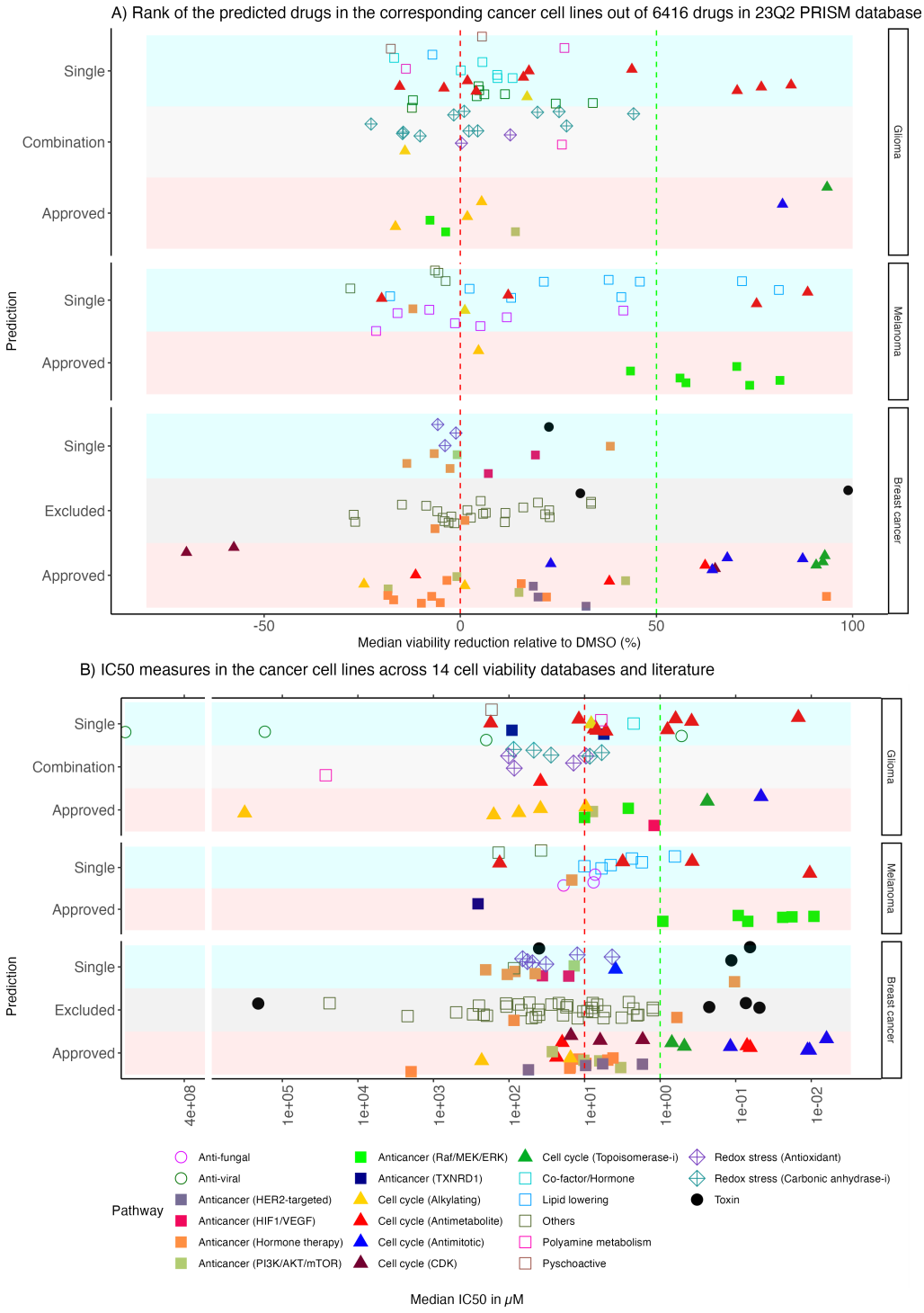

FIGURE 1.3: **Predicted antimetabolites in melanoma and glioma showed strong viability reduction and IC_{50} comparable to approved drugs.**
To rank the predicted drugs in the three cancer types, viability reduction and IC_{50} measures were retrieved from the PRISM database and 14 HTS databases, respectively. Each drug set was ranked in their respective cancer cell lines. Excluded NPs from the BRC drug ranking were added to compare predicted versus excluded. Across the three cancers, alkylating agents (yellow triangles) showed small viability reduction, matching their high clinical dosage. Meanwhile, predicted antimetabolites and approved topoisomerase inhibitors showed the strongest viability reduction and IC_{50}. Due to the prevalence of BRAF mutation in melanoma, RAF/MEK inhibitors showed strong IC_{50} and viability reduction in melanoma. Being mostly preclinical compounds, only half of the predicted NPs were found in the PRISM database, with emodin having the highest viability reduction of 38%. Three predicted NPs and four excluded NPs belonging to cardiotoxic bufanolide showed submicromolar potency in BRC. Overall, predicted drugs in glioma and melanoma showed improved and comparable potency to approved drugs, respectively, while predicted NPs in BRC failed to show improvement to excluded NPs and approved drugs.

vitro medium and *in vivo* CSF that shifts glioma cell lines to cholesterol synthesis. Overall, in glioma and melanoma, predicted essential genes and drug targets showed improved and comparable gene dependencies to approved targets, respectively.

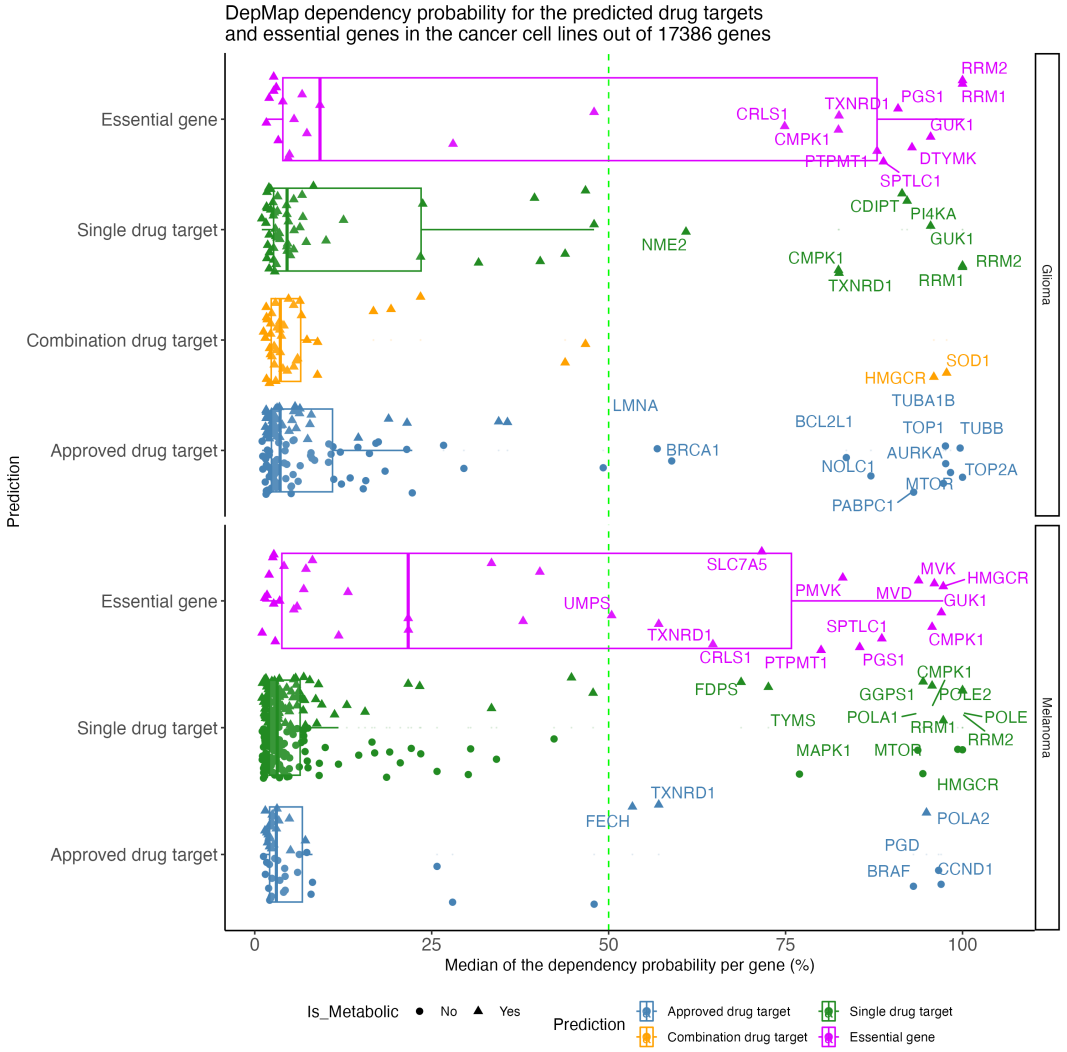

FIGURE 1.4: **42% of predicted essential genes in melanoma and glioma showed at least 50% gene dependency probability in high-throughput CRISPR screening.**
Predicted essential genes and targets of approved and predicted drugs were ranked by their dependency probability (the likelihood that the KO of a gene reduces cell growth or induces cell death) in DepMap pan-cancer genome-scale CRISPR screen. Predicted essential genes showed higher dependency probability than approved and predicted drug targets, as predicted drugs depend on multi-gene KO. Predicted drug targets with high dependency involve nucleotide biosynthesis and lipid metabolism in glioma and melanoma, respectively.

1.3.6 Predicted antimetabolites in melanoma and glioma showed comparable growth reduction to approved drugs in xenografts

To assess if any of the predicted drugs in the three cancers would maintain their efficacy *in vivo*, PDX HTS were retrieved for the three cancers to compare predicted versus

approved drugs. Unlike the well-established pan-cancer *in vitro* HTS, PDX HTS are mostly cancer-specific, or even sub-population-specific, with smaller drug panels. Three PDX HTS studies on GBM [90], [91], a PDX HTS on NRAS-mutant melanoma [109] and BRC [110] were retrieved where the median growth reduction score was calculated for each drug (growth reduction% in GBM, DSS in melanoma, and AUC in BRC). Among the available tested drugs, predicted antimetabolites in melanoma (gemcitabine) and glioma (gemcitabine, clofarabine, and cladribine) showed comparable growth reduction to approved drugs (blue dots) (see Figure 1.5.A-B). A clear separation is observed between alkylating agents and other approved drugs in melanoma and glioma, where alkylating agents had the lowest growth reduction. Interestingly, trametinib (MEK-inhibitor) showed high growth reduction in GBM PDXs despite the low prevalence of BRAF mutation in GBM (3%) [45]. In BRC, only one predicted NP (narciclasine) was retrieved, and none of the excluded NPs. Narciclasine exceeded all approved BRC drugs in growth reduction while showing moderate potency (see Figure 1.5.C). Other *in vivo* animal screening that screened NPs, such as "DTP NCI In Vivo Antitumor Assays" (`https://wiki.nci.nih.gov/display/NCIDTPdata/In+Vivo+Antitumor+Assays`) included only narciclasine of the 101 NPs in BRC models. In summary, in FDA-approved drug repurposing, predicted antimetabolites with comparable growth reduction to approved reduction affirm the comparability metabolic modeling ability to *in vivo* cancer models.

1.3.7 Predicted drugs for COVID-19 targeting one-carbon cycle have higher cytopathic effect reduction than approved drugs

Similar to cancer HTS and DepMap, predicted drugs for COVID-19 were ranked against approved drugs using a CPE reduction assay in Cacao-2 cell [107]; meanwhile, predicted essential genes were ranked using a CRISPR screen in five cells [108] against approved drug targets. The CPE reduction screen retrieved five approved drugs (hydrocortisone, ritonavir, tofacitinib, dexamethasone, and baricitinib) for COVID-19 (see Figure 1.6.A). Meanwhile, the CRISPR screen retrieved the targets of five approved immunomodulators (hydrocortisone, dexamethasone, baricitinib, tofacitinib, tocilizumab, and anakinra) (see Figure 1.6.B). Six predicted drugs exceeded 50% CPE reduction, outperforming all approved drugs. These six drugs are predicted to target OCCF (gemcitabine, tioguanine, and pyrimethamine), cystine uptake (thimerosal), nucleotide uptake and interconversion (azathioprine), and lactate efflux (salicylic acid). On the other hand, eight essential genes involved in nucleotide interconversion (GUK1, CMPK1, and CRLS1), sphingolipid salvage (GLTP), OCCF (DHFR), cystine

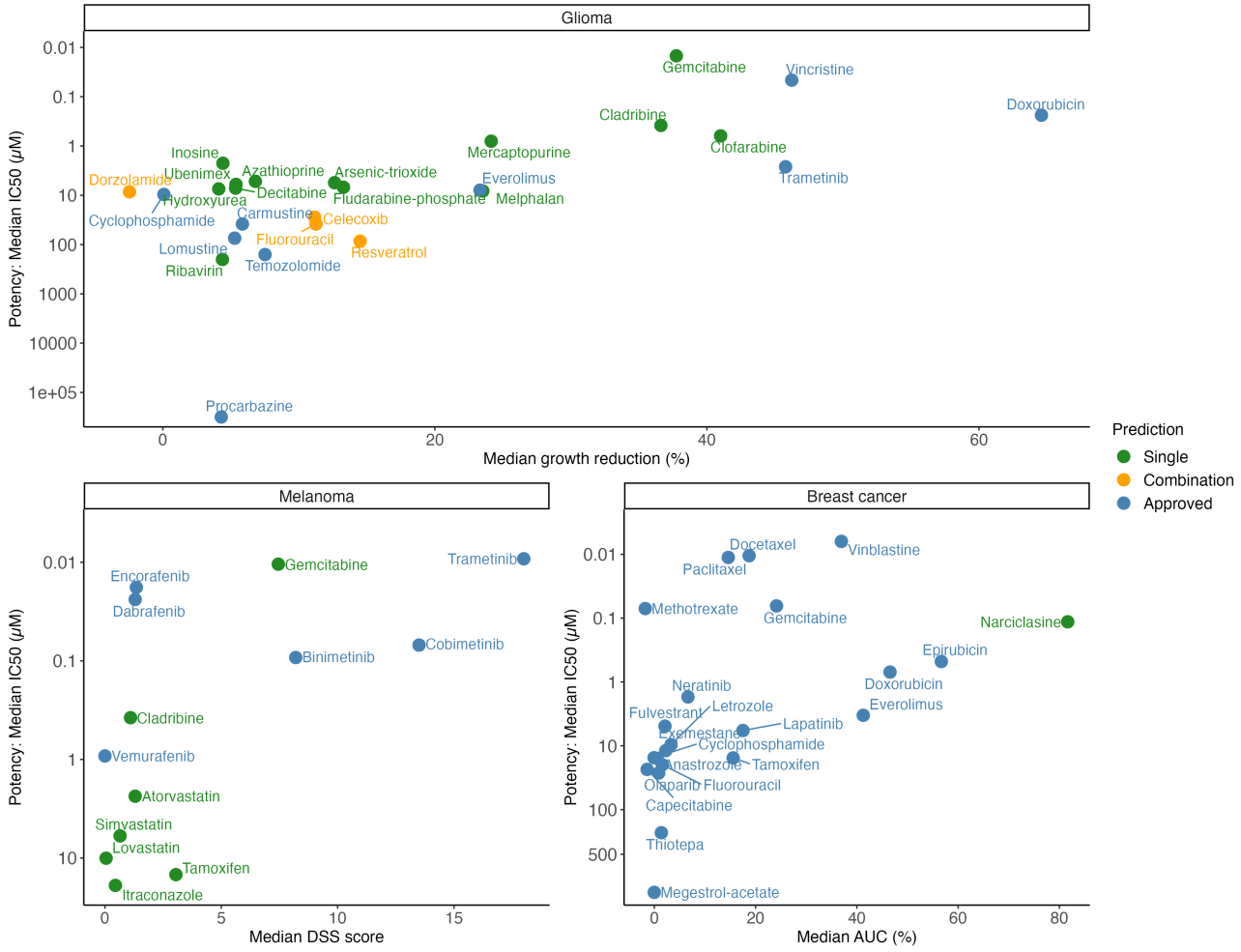

FIGURE 1.5: **Predicted antimetabolites in glioma and melanoma showed comparable *in vivo*-to-in vitro potency to approved drugs, while the predicted NP narciclasine exceeded approved drugs in breast cancer xenografts.**

To evaluate if *in vitro* potent predicted drugs would maintain their *in vivo* efficacy, xenograft data across the three cancers (x-axis) [90], [91], [109], [110] were used against the median IC_{50} from 1.3.B (y-axis). The predicted antimetabolite gemcitabine showed comparable growth reduction in glioma and melanoma to approved drugs. Interestingly, the predicted NP narciclasine exceeded the approved BRC drugs in growth reduction. Approved alkylating agents showed the lowest growth reduction across the three cancer types. Meanwhile, MEK inhibitors and doxorubicin (topoisomerase inhibitor) showed the strongest growth reduction in melanoma and glioma, respectively.

uptake (SLC3A2), and myo-inositol synthesis (ISYNA), showed higher dependency than all approved immunomodulators' targets in the CRISPR screen. Except for nucleotide interconversion genes, the remaining five essential genes are predicted exclusively for COVID-19. Similarly, CTH involved in cysteine synthesis showed moderate dependency higher than nine approved immunomodulatory targets. In summary, predicted drugs and essential genes involved in OCCF and cysteine synthesis surpassed the approved drugs and their targets in the SARS-CoV-2-infected CPE reduction assay and CRISPR screen, respectively.

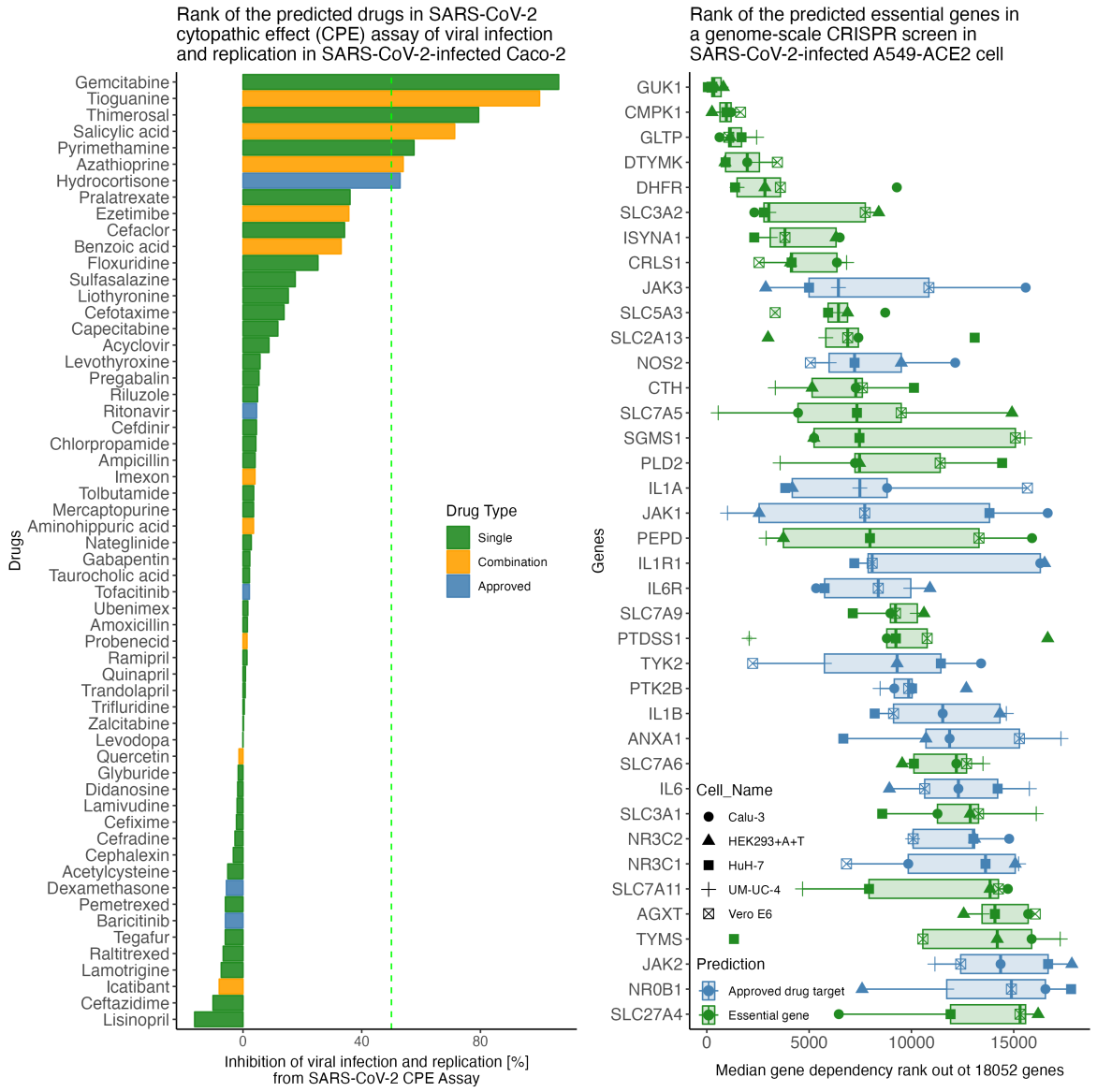

FIGURE 1.6: **Predicted drugs and essential genes for COVID-19 involved in the one-carbon cycle and cysteine synthesis exceeded approved drugs and their targets in SARS-CoV-2-infected CPE reduction assay and CRISPR screen, respectively.**

To benchmark predicted drugs for COVID-19 against approved drugs, a drug cytopathic effect (CPE) assay of SARS-CoV-2 infected human Caco-2 was used. Similarly, essential genes were compared to approved drug targets using a CRISPR screening of five SARS-CoV-2 infected cells. CPE assays measure the effect of a drug (or gene KO) on host genes to reduce viral infection and replication. Five approved drugs and the targets of six approved drugs were retrieved from the drug CPE assay and the CRISPR screening, respectively. Six predicted drugs outperformed approved drugs with 50% CPE inhibition that target one-carbon cycle (gemcitabine, tioguanine, and pyrimethamine), cystine uptake (thimerosal), nucleotide uptake and interconversion (azathioprine) and lactate efflux (salicylic acid). Meanwhile, eight essential genes showed higher dependency on approved drug targets that involve, among others, the one-carbon cycle (DHFR) and cystine uptake (SLC3A2).

1.3.8 Targeting TXNRD1 in glioma and melanoma, glioma-specific polyamine metabolism and melanoma-specific cholesterol synthesis improved patient survival in clinical trials

Translation of preclinical drug experiments to clinical trials mostly shows high failure rates, especially in phase II and III, due to differences in drug toxicity and efficacy for the target disease. To identify which of the predicted drugs had positive or adverse clinical outcomes, clinical data (meta-analysis, phase I/II clinical trials, and retrospective studies) were collected for the predicted drugs from PubMed, `beta.clinicaltrials.gov` [92], and Cochrane Library [93]. Overall clinical data results are summarized in Table 1.3.8 while detailed survival data for glioma's predicted drugs are detailed in Figure 3.6.

Two predicted drugs targeting polyamine metabolism in glioma, valganciclovir [123]–[125] and eflornithine [126], improved median overall survival (mOS) combined with the standard-of-care (SOC) compared to the SOC arm. Fotemustine, a predicted drug for glioma's TXNRD1 target, ranked best in effectiveness as mOS in a network meta-analysis of eleven approved and investigational drugs in recurrent GBM (rGBM) [127]. Although TXNRD1 was the predicted essential gene in melanoma, fotemustine was missed from the predicted drugs due to the absence of the target information in the DrugBank v5.1.3 compared to DrugBank v5.1.9 used for glioma. Nevertheless, fotemustine is approved in some countries for melanoma brain metastasis, the most aggressive form of melanoma [128]. In skin cancer clinical trials, drugs targeting cholesterol synthesis (statins in two retrospective studies [129], [130]) and both cholesterol synthesis and lipid peroxidation (tamoxifen in a meta-analysis of nine clinical trials [131]) improved survival when combined with the SOC. Meanwhile, in two non-melanoma skin cancer clinical trials, itraconazole targeting lipid peroxidation only showed stable disease in a sub-population.

Four antimetabolites (gemcitabine [132], cladribine [133], mercaptopurine [134] and fluorouracil [135]), and an alkylating agent (melphalan [136]) failed in clinical trials in glioma. Despite two predicted antimetabolites for melanoma (leflunomide and gemcitabine) failing in skin cancer clinical trials, gemcitabine [137] showed stable disease in 35% of non-melanoma skin cancer patients. All clinically failed antimetabolites and alkylating agent in glioma and melanoma are ABC transporter substrates, which could induce their drug resistance and efflux. All in all, metabolic modeling predicted vulnerabilities that improved glioma and melanoma patient survival in clinical trials, such as glioma-specific polyamine metabolism, melanoma-specific cholesterol synthesis, and targeting TXNRD1 with fotemustine in glioma and melanoma. On

the other hand, targeting melanoma-specific pyrimidine synthesis with leflunomide and targeting cell cycle with antimetabolites in glioma and melanoma failed in clinical trials.

Table 1.3: Summary of positive and negative clinical outcomes of the predicted drugs in the four diseases.

Disease	Positive clinical trial outcomes	Negative clinical trial outcomes
Glioma	• In a network meta-analysis of eleven approved and investigational drugs in recurrent GBM, fotemustine ranked best in effectiveness as mOS [127]. • In two-arm, phase I/II trials, two single drugs (fotemustine [138] and valganciclovir [123]–[125]) and two combination drugs (eflornithine [126] and celecoxib [139]) improved the primary survival outcome compared to the control arm.	• Gemcitabine [132], melphalan [136] and cladribine [133] failed in single-arm phase II glioma trials. • When combined with carmustine, both mercaptopurine and fluorouracil showed an antagonistic [134] and a non-additional [135] effect, respectively.
Melanoma	• Fotemustine, an inhibitor for the predicted essential gene TXNRD1, is approved in some countries against melanoma brain metastasis [128]. • Tamoxifen in a meta-analysis of nine clinical trials [131] in advanced melanoma in combination with chemotherapies showed improved overall complete and partial response without improvement in 1-year survival. • A case-control retrospective study identified statins use is linked to reduced melanoma incidence [129]. • A retrospective study of concomitant medications on ICIs' response in melanoma identified statins to improve ICIs' objective response rate significantly [130].	• Gemcitabine and itraconazole showed no response in non-melanoma skin cancer phase II trials, but as stable disease in a subset of the treated patients (35% [137] in gemcitabine and 21% [140] to 91% [141] in itraconazole). • Leflunomide combined with vemurafenib in phase I/II clinical trial in BRAF-mutant metastatic melanoma failed due to adverse effects (NCT01611675) [142].
Breast cancer	• A case-control study found dietary resveratrol intake from grapes, not wine, to reduce breast cancer risk [143] significantly.	
COVID-19	• Two meta-analysis of eight RCTs in sofosbuvir (CMPK1-inhibitor) [144] and three RCTs in acetylcysteine (SLC7A11-inhibitor) [145] found both drugs to significantly reduce mortality and severity in COVID-19 patients compared to control arm. • Three predicted drugs (icatibant (ANPEP-inhibitor) [146], quercetin (SLC16A1-inhibitor) [147] and probenecid (SLC16A1-inhibitor) [148] were tested in three phase II RCTs, where they enhanced severity/survival in COVID-19 outpatients compared to placebo/SOC. • Sulfasalazine (SLC7A11-inducer), a ferroptosis-inducer, showed increased risk COVID-19 severity and death in three cohorts with autoimmune diseases [149]. • A retrospective study of 3.9 million COVID-19 outpatients identified rosuvastatin (SLC7A11-inhibitor) to decrease COVID-19 hospitalization rate [150].	• A phase II RCT in hospitalized COVID-19 patients found ACE-inhibitors (ten predicted SLC15A1-2 inhibitors) [151] showed no improvement in survival and likely worsened.

1.3.9 In COVID-19 clinical trials, drugs targeting cysteine synthesis combined with SOC reduced mortality/severity, unlike glycine synthesis

Clinical trial data in COVID-19 (Table 1.3.8) covered mostly GSH synthesis genes through cysteine synthesis (ANPEP and SLC7A11) and glycine synthesis (SLC15A1-2). All predicted drugs tested in clinical trials were combined with the SOC except for probenecid, which was tested as monotherapy. Additionally, targeting nucleotide interconversion with sofosbuvir in a meta-analysis of eight RCTs [144] and lactate efflux with quercetin [147] and probenecid [148] in RCTs enhanced severity/survival in COVID-19 patients compared to SOC. SLC7A11 inhibitors, acetylcysteine in a meta-analysis, and rosuvastatin in a retrospective study decreased mortality and hospitalization rates, respectively. Similarly, icatibant, an ANPEP inhibitor, enhanced severity and survival in COVID-19 outpatients compared to SOC. On the other hand, sulfasalazine, a SLC7A11-inducer, increased the risk of COVID-19 severity and death in three cohorts [149]. These results highlight the importance of ferroptosis in COVID-19 severity. In summary, predicted vulnerabilities of cysteine synthesis and lactate efflux in COVID-19 consistently reduced patients' mortality or severity. Meanwhile, targeting glycine synthesis increased COVID-19 hospitalized mortality.

All in all, metabolic modeling predicted drug candidates in clinical trials with an effective-to-ineffective ratio of 33% in melanoma and COVID-19 and 44% in glioma. Moreover, metabolic modeling allowed interpretation of the target genes consistent with literature on the disease-specific vulnerabilities.

1.4 Discussion

Metabolic rewiring is a hallmark of cancer and COVID-19-specific host hijacking. Glioma, melanoma, and BRC patients suffer from low survival, high relapse, and high incidence, respectively, which motivate the repurposing of new drugs and combinations. Similarly, the COVID-19 pandemic and its needed biosafety laboratories forced researchers to repurpose effective drugs computationally. In this work, we summarized the predicted drugs and essential genes from metabolic modeling in three cancers and COVID-19. We compared the results to *in vitro* HTS, xenografts, and clinical data. In addition to biomarker identification, metabolic modeling allowed the repurposing of approved drugs for glioma, melanoma, and COVID-19, the prediction of new combinations for glioma, and the repositioning of preclinical compounds in BRC. Metabolic modeling showed consistency between the predicted essential genes and

disease-specific vulnerabilities in the literature, such as TXNRD1 for glioma and melanoma, ER in BRC, and cysteine synthesis in COVID-19. These vulnerabilities were consistent with clinical data from meta-analyses, clinical trials, and retrospective studies. Notably, TXNRD1 was predicted in glioma and melanoma, which is inhibited by fotemustine, approved in some countries for melanoma brain metastasis and showed comparable survival as monotherapy to approved bevacizumab in glioma. Metabolic modeling extends beyond single drugs into combination prediction in glioma with glioma-subtype specific combinations matching vulnerabilities in LGG and GBM. Moreover, metabolic modeling of the post-treatment expression data of NPs ranked NPs in BRC, which showed comparable *in vitro* efficacy to approved drugs. Similarly, the predicted NP narciclasine exceeded approved drugs in xenografts, and resveratrol dietary intake reduced BRC risk in a retrospective study. Nevertheless, of the clinically tested drugs, a third of predicted drugs in melanoma and COVID-19 and 44% of predicted drugs in glioma enhanced patients' survival. The clinically failed drugs may be attributed to ABC transporter resistance in glioma and the absence of an *in vivo* interstitial fluid medium for lung and melanoma cells.

1.4.1 Target identification via metabolic modeling correctly predicted essential genes with reaction precision in the glioma subtypes and melanoma

Beyond shared essential genes, a comparison between predicted essential genes in glioma, melanoma, and COVID-19 identified disease-specific dependencies such as polyamine synthesis in glioma, pyrimidine, cholesterol, and lipid synthesis in melanoma, and OCCF, glycine and cysteine synthesis in COVID-19. Additionally, both glioma and melanoma shared sphingolipid synthesis, cholesterol esterification, and TXNRD1. Despite the consistency between disease-specific vulnerabilities and literature, less than half of the essential genes are druggable due to the limited targets of the approved drugs. Metabolic modeling allowed the prediction of metabolic biomarkers for the glioma subtypes and COVID-19, consistent with the literature (see Table 1.4). Compared to approved drugs, targeting some of the disease-specific pathways showed stronger or comparable *in vitro* efficacy, such as antimetabolites in glioma, statins in melanoma, and inhibitors of OCCF and cysteine synthesis in COVID-19. Similarly, the specificity of cholesterol esterification, not synthesis, in glioma dependencies precisely agrees with the literature [111], [112]. Additionally, the predicted drug targets RRM1 and RRM2 show stronger dependency probability in DepMap than approved targets in melanoma and glioma cell lines (see Figure 1.5). Even in drug-induced resistance and metastatic melanoma cell lines,

RMM1 and RRM2 exceeded all approved targets (see Figures 4.4- 4.5 [81]). RMM1, RRM2, and TXNRD1 are predicted in glioma and melanoma drug targets and are the crosslink between GTH detoxification and nucleotide interconversion. All in all, despite the undruggable essential genes, metabolic modeling accurately predicted disease-specific essential genes.

TABLE 1.4: **Clinical trial data showed three out of the five predicted disease-specific dependencies have positive clinical outcomes.**

Disease	Target pathway	Clinical evidence	Repurposed drugs	Clinical outcome	References
Glioma	Polyamine synthesis	Phase II and III RCT	Eflornithine and valganciclovir	Improved survival combined with approved drugs.	[123]–[126]
Melanoma	Cholesterol /lipid synthesis	Retrospective study	Statins	Improved survival combined with immune therapy.	[129], [130]
Melanoma	Pyrimidine synthesis	Phase I/II RCT	Leflunomide	Failed combined with immune therapy.	[142]
COVID-19	Cysteine synthesis	Meta-analysis, Retrospective study	Acetylcysteine and rosuvastatin	Reduced mortality and severity combined with standard of care.	[145], [150]
COVID-19	Glycine synthesis	Phase II RCT	ACE-inhibitors	Showed no improvement in survival and likely worsened.	[151]
Glioma and melanoma	Oxidative stress through TXNRD1	Approved/ Meta-analysis	Fotemustine	Ranked best in effectiveness among eleven approved and investigational drugs in recurrent GBM. Approved in some countries for melanoma brain metastasis.	[127], [128], [138]

1.4.2 Clinically efficacy of predicted drugs in glioma and melanoma is linked to ABC transporter affinity

Inspection of the commonality between clinically ineffective drugs in melanoma and glioma identified all of the clinically ineffective drugs, except itraconazole, are ABC transporter substrates or inducers. ReconX reconstructions have 28 ABC transporter genes that participate in the efflux of toxic byproducts, but none is curated for drug efflux. The efflux of lipid peroxidation byproducts (with ABCC1 and ABCC11) is predicted as a vulnerability in all glioma subtypes and melanoma; meanwhile, the efflux of heme synthesis byproducts (with ABCG2) is only predicted in GBM. These variations are in line with the literature signature of melanoma-specific [152] and pan-glioma [153] lipid peroxidation and GBM-specific heme synthesis [119]. Further analysis of the clinically effective drugs found that celecoxib in glioma and tamoxifen

in melanoma are ABC transporter inhibitors. In addition to drug efflux and resistance, ABC transporters in glioma control drug BBB permeability and diffusion to the core tumor[154]. In summary, metabolic modeling was able to predict drugs for ABC transporters' role in byproduct efflux, but the lack of drug efflux role in the GEMs resulted in clinical trial inactivity.

1.4.3 Clinical data of targeting lipid synthesis support predicted its efficacy in melanoma compared to GBM

In addition to targeting cholesterol esterification and lipid peroxidation, targeting lipid synthesis was predicted by single drugs in melanoma and only by cannabidiol/eflornithine combination in glioma. While our review [72] highlighted the debated effect of lipid-lowering drugs such as statins on glioma cell lines, more in-depth investigation into the clinical data found their inefficacy in GBM. More recently, cholesterol was found to be targeted in glioma via uptake inhibition, efflux activation [111], or esterification inhibition [112]. A meta-analysis of five prospective observational studies found no statistically significant benefit of statins on prolonging GBM survival [155]. Similarly, a phase II clinical trial of atorvastatin combined with RT and TMZ (NCT02029573) in GBM failed to achieve the primary outcome compared to the historical control with 80% of patients discontinued because of disease progression [156]. On the other hand, in two retrospective studies, statin use is linked to reduced melanoma risk [129] and enhanced melanoma survival combined with approved ICIs [130]. All in all, predicted melanoma-specific lipid synthesis is supported by statins efficacy in melanoma and no improvement in GBM.

1.4.4 Metabolic modeling allows drug combination prediction on a larger scale than HTS, and on difficult-to-culture ODG

While HTS can screen thousands of drugs and predict cancer-type-specific drugs, their scalability for drug combinations is limited. Drug combination prediction in glioma screened 124,762 possible combinations (53 investigational anti-glioma and approved anti-brain cancer against 2354 FDA-approved) over three models to predict 17 combinations. Computationally, the drug combination prediction took under 8.5 hours using an average laptop (MacBook Pro, 2.4 GHz Quad-Core Intel Core i5, 16 GB RAM). Meanwhile, NCI ALMANAC, the largest primary combination HTS in cancer, has 5,232 screened combinations over 60 cancer cell lines,

mostly anti-cancers [157]. While experimental combination HTSs could define combination hits beyond metabolism, the staggering variation and scalability of metabolic modeling-based combination prediction and the number of screening combinations allow testing more diverse targets to enhance potential synergism. Similarly, due to high oxidative stress, ODG cancer cell lines are hard to culture [4], and LGG has limited animal models [74]. Meanwhile, metabolic modeling enabled drug prediction on LGG and accurate prediction of metabolic exchanges in LGG patients. To summarize, metabolic modeling allowed scale combination prediction and predicting biomarkers in hard-to-culture cell lines.

1.4.5 Clinical drug repurposing depends on defining interstitial fluid rather than *in vitro* medium

Across the four studies, *in vitro* medium was used for melanoma and BRC, while *in vivo* CSF was used in glioma, and no medium was used for COVID-19. Variations in drug response between *in vitro* and *vivo* were more noticeable in melanoma than glioma, possibly due to using *in vitro* medium in melanoma model building. Similar observations were found for RAF inhibitors in melanoma. *In vivo* mediums such as the CSF are better defined and allow avoiding synthesis pathways that only exist *in vitro* as vulnerabilities, such as cholesterol synthesis in glioma. A challenge in *in vivo* medium defined from metabolomics studies is their inability to distinguish between tissue export metabolites or true biofluid composition. Nevertheless, the medium constraining, in turn, improved the prediction of single drugs and synergistic combinations acting on alternative pathways. While other biofluid mediums might be poorly defined compared to the CSF, using clinically defined radiotracers [158], metabolite concentration from metabolomics studies, and exo-metabolomic data [159] could help fine-tune the model building. In summary, comparing *in vitro*-to-*in vivo* drug responses in HTSs provides a quality assessment of the used medium in the translational application.

1.4.6 Metabolic modeling of post-treatment expression data predicts new investigational drugs with comparable potency to approved drugs

While diseased expression data is the most widely used for model building, cell line post-treatment expression data becomes a cornerstone in repositioning new investigational drugs such as the LINCS database. Post-treatment expression data of the MCF-7 cell line allowed

the ranking of 23 NPs among 101 NPs. While the predicted NPs showed no improvement to excluded NPs, the predicted NPs showed comparable *in vitro* drug efficacy. The highly potent excluded NPs belong to a cardiotoxin with non-metabolic MOA, such as apoptosis and epigenetic modulation. Moreover, two NPs- narciclasine and resveratrol- exceeded approved drugs in PDXs and reduced BRC risk in a retrospective study, respectively. Generally, post-treatment expression data of patients have been increasingly used to predict disease response and define biomarkers for responders.

1.4.7 Lack of clinical trial database with survival information hinders developing or repurposing new drugs

Unlike *in vitro* and *in vivo* HTS databases, clinical trials are poorly curated, and few publish their results [160], [161]. In this work, we collected two-arm phase I/II clinical trials, if available, and retrospective studies of drug relationship to disease incidence/survival. Clinical trial registries such as ClinicalTrials.gov only record clinical trials' metadata, such as phase and recruitment, but they mostly miss survival outcomes and reasons for trial failure. The absence of survival outcomes challenges the systematic search of predicted drugs for possible survival data and requires a literature search for published results [161]. Additionally, adverse clinical outcomes such as failed trials due to toxicity or no improvement in the treatment arm are routinely unreported. Despite these challenges in clinical trial data, the collected clinical data provided enough validation for some of the disease-specific vulnerabilities, such as lipid synthesis and TXNRD1 in melanoma and glioma and cysteine synthesis in COVID-19.

1.5 Conclusion

Metabolism is the part of the cellular system responsible for generating energy and synthesizing new molecules needed for cell growth or maintaining normal functions. Cancers and viral infections hijack the healthy metabolism for high proliferation and increasing replication, respectively, which can be simulated by metabolic modeling. This work aimed to evaluate the extent of metabolic modeling compared to preclinical and clinical approaches in three cancers and COVID-19 by benchmarking predicted drugs and essential genes. Metabolic modeling correctly predicted biomarkers in glioma and COVID-19 in agreement with patients' serum metabolome and radiotracers' uptake, respectively. Moreover, predicted essential genes

and drugs showed disease-specific differences coherent with preclinical and clinical data. Notably, targeting TXNRD1 in melanoma and glioma, polyamine metabolism in glioma, and cysteine synthesis in COVID-19 have shown enhanced survival. Despite the lack of distinction between predicted and excluded NPs, the predicted narciclasine surpassed approved drugs in xenografts' growth reduction, and resveratrol dietary intake reduced BRC incidence in a retrospective study. These results affirm metabolic modeling as a precise and effective tool for biomarker prediction and drug repurposing fitting for clinical trials. This work warrants fotemustine as both pan-glioma and melanoma monotherapy and eflornithine/rifamycin and cannabidiol/adapalene as promising new combinations for GBM and LGG, respectively.

1.6 Contribution

I carried out the work and wrote the manuscripts for COVID-19, glioma, and the review of brain GEMs. In addition to collecting clinical data, I carried out and wrote only *in silico* drug evaluation in metastatic, drug-resistant, and mutant melanoma cell lines. I helped plan, carry out, and write the manuscript for NP drug ranking in breast cancer.
Following from the motivation and outline, the specific aims of this thesis are:

Aim 1: Defining the published works for metabolic modeling in the brain and advancing on it for drug repurposing of the glioma subtypes.
Here, we start with a review of metabolic models in the brain to identify their strengths and limitations. Using resources and lessons from the review, we built three glioma subtype GEMs to repurpose single and combination drugs. The study included identifying subtype-specific biomarkers and benchmarking of predicted drugs *in vitro*, in xenografts, and clinical trials.

Aim 2: Evaluation of previously predicted drugs in melanoma compared to approved anti-melanoma drugs under metastasis a, drug resistance, and BRAF/NRAF mutation conditions.
A previous study in our department repurposed drugs for melanoma using metabolic modeling. We expanded on this study by benchmarking the repurposed drugs against approved anti-melanoma drugs and drugs targeting the nitric oxide pathway under three conditions: metastasis a, drug resistance, and BRAF/NRAF mutation.

Aim 3: Drug prioritization of natural products for anti-breast cancer activity using drug-treated expression data.
To rank candidate natural products (NPs), many are part of the diets for anti-breast cancer activity using drug-treated expression data. As drug-treated expression data is increasingly

crucial in personalized medicine, this work employed various metabolic modeling techniques to define candidate NPs without target information.

Aim 4: Drug repurposing for a newly-discovered COVID-19.

To repurpose candidate drugs and predict essential genes for a newly discovered infection disease, COVID-19, whose needed biosafety measures for drug screening are limited globally. This work was based on expression data from COVID-19-infected lung cell lines. The pathways of predicted essential genes were compared to a metabolomics study of severe COVID-19 patients.

Chapter 2

Review of Current Human Genome-Scale Metabolic Models for Brain Cancer and Neurodegenerative Diseases

Ali Kishk[1†], Maria Pires Pacheco[1†], Tony Heurtaux[1,2], Lasse Sinkkonen[1], Jun Pang[3], Sabrina Fritah[4], Simone P. Niclou[4], and Thomas Sauter[1,*]

[1] Department of Life Sciences and Medicine, University of Luxembourg, Belval Campus, 2, avenue de l'Université L-4365 Esch-sur-Alzette, Luxembourg

[1] Department of Life Sciences and Medicine, University of Luxembourg, L-4367 Belvaux, Luxembourg

[2] Luxembourg Center of Neuropathology, L-3555 Dudelange, Luxembourg

[3] Department of Computer Science, University of Luxembourg, L-4364 Esch-sur-Alzette, Luxembourg

[4] NORLUX Neuro-Oncology Laboratory, Luxembourg Institute of Health, Department of Cancer Research, L-1526 Luxembourg, Luxembourg

* Correspondence: thomas.sauter@uni.lu

† These authors contributed equally to the manuscript

This review has been published in:

Cells, Volume 20 (Issue 11), 2022, Page 2486

, https://doi.org/10.3390/cells11162486

Introduction to the paper

The cost of brain disorders rose to 800 billion euros by 2010 and affected 169 million Europeans by 2019. Of these brain disorders, neurodegeneration disease incidence is rapidly growing due to the increase in the aging population. Neurodegeneration has no cure and approved drugs mostly treat symptoms despite decades of research. Similarly, there are multiple poorly defined subtypes of central nervous system cancers, with only a handful of approved drugs. In this work, we aim to define the established studies for genome-scale metabolic models in the brain, focusing mainly on neurodegeneration diseases and brain cancer to define their strengths and limitations. We also compare the various studies based on the multi-cellular interactions, curation of the biomass, and used experimental validations.

Contribution: I carried out the literature review, co-wrote the manuscript, and prepared the figures.

Abstract

Brain disorders represent 32% of the global disease burden, with 169 million Europeans affected. Constraint-based metabolic modeling and other approaches have been applied to predict new treatments for these and other diseases. Many recent studies focused on enhancing, among others, drug predictions by generating generic metabolic models of brain cells and on the contextualization of the genome-scale metabolic models with expression data. Experimental flux rates were primarily used to constrain or validate the model inputs. Bi-cellular models were reconstructed to study the interaction between different cell types. This review highlights the evolution of genome-scale models for neurodegenerative diseases and glioma. We discuss the advantages and drawbacks of each approach and propose improvements, such as building bi-cellular models, tailoring the biomass formulations for glioma, and refining the cerebrospinal fluid composition.

2.1 Introduction

In Europe, 169 new million cases of brain disorders were reported in 2019 [1]. Neurological disorders, brain and central nervous system (CNS) cancer, strokes, and mental disorders are all examples of brain disorders [2]. The high toll on the life quality of patients suffering from neurodegenerative diseases (NDD) and the societal burden that are increasing with the aging

of the Western population. Alongside cardiovascular diseases and cancer, NDD are a major health care challenge, with dementia being the most expensive disease to manage [3]. While the annual cost of dementia is 1.5 times more than cancer in the UK, research funding for dementia is only 30% of cancer [4]. Brain cancers can be considered rare diseases with an estimated 308,000 new cases and 251,000 new deaths worldwide in 2020 [5] of which glioblastoma (GBM) accounts for more than half of malignant CNS cancers [6]. However, unlike NDD, which develops over decades, the life expectancy of GBM patients is 5% survival over five years [7]. However, both NDD and GBM are incurable, age-related (the median age of diagnosis for GBM is 65 years old [6]), and show metabolic deficiencies or rewiring that could be exploited as potential drug targets [8].

Lower grade gliomas (LGG), a less aggressive glioma form than GBM, is more heterogeneous in prognosis and response to treatment and is characterized by lower proliferation speed [9]. More than 80% of LGG have mutations in isocitrate dehydrogenases that play a central role in metabolism as catalyzing reaction in the Krebs cycle, redox homeostasis, biosynthesis of lipids, and glutamine metabolism [9] [10]. These LGG are classified into astrocytoma (AST) and oligodendroglioma (ODG) based on the glial cell type they originated from. GBM and LGG also have different preferred energy sources. Glucose, the main fuel of neurons [11], and glutamine, required for the biosynthesis of neurotransmitters [12], are abundant in the brain microenvironment and have been linked to GBM invasion [13], [14]. The Warburg effect is a hallmark of GBM with a shift from oxidative phosphorylation (OXPHOS) and TCA cycle to glycolysis for energy production [15]. The upregulation of glycolysis and downregulation of OXPHOS and TCA is linked to poor survival in GBM [16]. This increased glycolysis rate, even under hyperoxia, increases GBM chemoresistance [17]. Furthermore, this metabolic shift allows the channeling carbon and nitrogen fluxes into the biosynthesis of nucleotides via the pentose phosphate pathways (PPP) [18]. The PPP also permits reducing NADP+ to NADPH and hence maintains oxidative homeostasis [18]. A lesser-known GBM subtype, mitochondrial GBM, was identified by multi-omics analysis with decreased glycolysis and increased OXPHOS (reverse Warburg effect) [19]. This reverse Warburg effect occurs in late tumor formation and is characterized by sensitivity to OXPHOS inhibitors [19]. Neuron-glioma metabolic interactions through neurotransmitters can change glioma progression [20]. Mainly, dysregulation in neurotransmitter exchange, such as of glutamine and gamma-aminobutyric acid (GABA), emerges as part of the GBM metabolic remodelling [20]. Glutamine, a neurotransmitter precursor, is required in glycolytic cells to fuel the TCA cycle and the biosynthesis pathways. Unlike GBM, LGG shows low glycolysis [21], which may explain their relatively decreased proliferation, and ODG growth is robust to glutamine starvation [22]. Similarly, GABA may

be linked to increased GBM stemness [23] where the pharmacological inhibition of GABA release of the GBM cells reduced GBM growth [24]. The main astrocyte-neuron metabolic interactions under healthy conditions in addition to glioma and NDD are summarised in Figure 2.1.

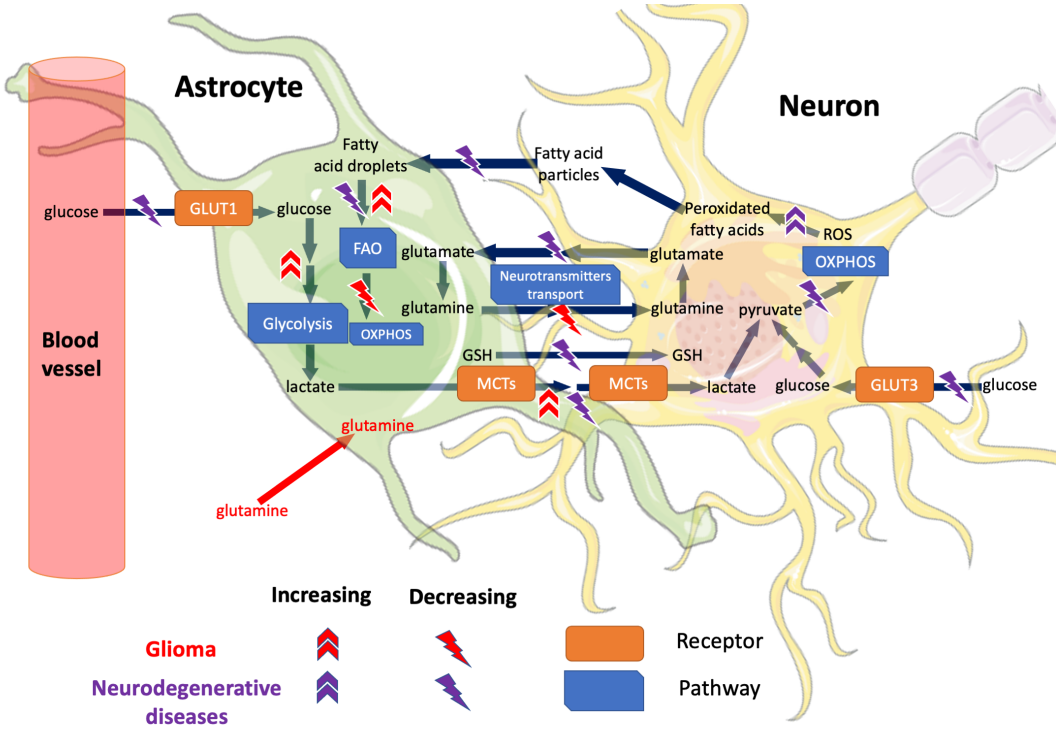

FIGURE 2.1: **Dysregulated metabolic reactions between astrocytes and neurons in healthy conditions, NDD, and glioma.**
Under healthy conditions, astrocytes provide metabolic support with nutrients to neurons and carry out neurotransmitter and ROS detoxification [25]. As glial cells are becoming malignant in glioma, they shift from OXPHOS to glycolysis [16] and FAO [26] for energy generation. Moreover, astrocytic glutamine transport to the neuron is disrupted [27] in glioma, and glutamine uptake by the glial cell is increased [12]. Meanwhile, in NDD, neurons shift to reduced glycolysis and OXPHOS to decrease the produced energy [25]. In some NDD, the bi-cellular transport from astrocytes to neurons of both GSH and glutamate are decreased [25], with the former accumulating ROS and peroxidized fatty acids from the neuronal activity [28]. The peroxidized fatty acids are exacerbated by the deceased astrocytic FAO. Because of the difference in astrocytic glycolysis between glioma and NDD, astrocytic lactate transport to the neuron is increased in glioma [29]; meanwhile, it is decreased in NDD [25]. Other cellular interactions were excluded for simplification, such as astrocyte–glioma cell interactions [30], oligodendrocytes, microglia, and the different neuron cell types. FAO: fatty acid oxidation, GLUT1/3: glucose transporter 1/3, GSH: glutathione, MCT: monocarboxylate transporters, OXPHOS: oxidative phosphorylation, ROS: reactive oxygen species. Parts of the figure were drawn by using pictures from Servier Medical Art. Servier Medical Art by Servier is licensed under a Creative Commons Attribution 3.0 Unported License (https://creativecommons.org/licenses/by/3.0/).

Besides glycolysis and neurotransmitter metabolism, deregulation of the lipid metabolism, notably cholesterol metabolism, was shown to accumulate in GBM due to an increase in uptake

and a downregulation of the efflux pathway. Cholesterol accumulation is a hallmark of cancer [31]. Due to the role of cholesterol in signaling and membrane plasticity, the deregulation of cholesterol pathways often leads to uncontrolled proliferation, cell invasion, and migration. Cholesterol can scarcely pass through the brain–blood barrier (BBB) [32]. This limits the pool of cholesterol in the brain, which is synthesized mainly by the astrocytes. The effect of cholesterol biosynthesis on GBM is debated, and the results are not consistent between studies. Cholesterol biosynthesis was found upregulated in GBM neurospheres, tumor-initiating cells, cell lines, and patient samples, and a factor related to decreased patient survival and tumor growth [33]–[36]. This upregulation allowed statins (cholesterol biosynthesis inhibitors) to reduce the growth of GBM tumor-initiating cells [35]İn another study, cholesterol biosynthesis has reduced expression in GBM cell lines [37]. The reduced cholesterol biosynthesis in GBM cell lines is supported by GBM resistance to statins [38]. On the other hand, AST cells with an upregulation in this pathway are sensitive to atorvastatin [39]. Besides cholesterol deregulation, an upregulation of fatty acid synthesis, and beta-oxidation has been described in GBM [26]. In a nutrient-rich microenvironment, beta-oxidation channels fatty acids to cancer cell proliferation. Meanwhile, in lower nutrient levels, fatty acids are diverted to OXPHOS to produce ATP and precursors for amino acids and nucleotide synthesis. Inhibition of fatty acid oxidation (FAO) and carnitine transport show synergistic effects in GBM cell lines' survival [40]. Moreover, the transporter of very long fatty acids SLC27A3 is upregulated in glioma but not in the healthy brain and are linked to patient survival. Genetic knockout of SLC27A3 decreased stearic acid uptake and reduced the GBM cell line U87MG growth [41]. Recently, some GBM xenografts were found to be resistant to glycolysis inhibitors with upregulation of OXPHOS and dependency on FAO [42]. The combination of glycolysis and FAO inhibitors synergistically decreased the growth of these resistant xenografts [42]. These studies show GBM's ability to shift energy dependency from glycolysis to FAO and the potential of FAO pathway that could be exploited for drug repurposing [41].

Besides neurons and astrocytes that play a central role in gliomas, other glial cell types, oligodendrocytes, and microglia, were described to play a role in tumor progression [43]. Oligodendrocytes are cells engulfing the neuron axon with the myelin sheath to maintain neuronal signal [44]. Similar to astrocytes, oligodendrocytes provide metabolic support of nutrients to neurons such as lactate and pyruvate [44]. In addition to ODG and mixed glioma originating from oligodendrocytes, oligodendrocytes increase the invasiveness of GBM [45]. Microglial cells are the resident immune cells of the CNS, dedicated to the maintenance of CNS homeostasis. These cells are implicated in numerous processes essential for tissue development and maintenance, remodeling, and repair of the neural environment [46]. Microglia play important roles

in the adult brain but also earlier during brain development [47]. These cells are able to eliminate extra synapses (synaptic pruning) but also to eliminate dying neurons by phagocytosis. Microglia are also devoted to rapidly reacting to any kind of pathological insults (pathogens, debris, dying cells, aberrant proteins) [48]. Similar to macrophages, microglia generate an immune response to pathogens or any insults [49]. An excessive microglial reactivity can play a critical role in the development and progression of brain diseases.Microglia can switch from a quiescent state to pro-inflammatory or anti-inflammatory phenotypes and vice-versa [50]. This change of phenotype is often accompanied by metabolic shifts [51]. Pro-inflammatory microglia are known to quickly release a large panel of pro-inflammatory compounds such as cytokines, chemokines but also reactive oxygen and nitrogen species (ROS/RNS) [51]. Anti-inflammatory microglia will be important in order to calm down the inflammation and to favour tissue repair [51]. For this purpose, anti-inflammatory microglia produce high levels of anti-inflammatory cytokines. The expression of anti-inflammatory phenotype biomarkers can be used to differentiate between grade 2 and 4 astrocytoma [52]. In addition, GBM subtypes show significant percentages of microglia cells in the microenvironment, with the mesenchymal subtype having the highest percentage and lowest survival [53]. Microglia, monocytes, and macrophages make up nearly 30–50% of the GBM tumor weight [54]. Little is known about the exact metabolic role of the two microglia phenotypes in GBM [29]. While both phenotypes are expressed in the different stages of GBM, more pro-inflammatory microglia are activated in early glioma development using glycolysis and OXPHOS for energy [29]. In a second stage, the pro-inflammatory microglia depend on glycolysis mainly due to inflammation-induced hypoxia. This second stage is characterized by nitric oxide formation and lactate production [29]. Lastly, the high concentration of lactate in the microenvironment and lack of oxygen favor the anti-inflammatory phenotype. The overrepresentation of anti-inflammatory macrophages in glioma induces immunosuppression, increasing glutamine uptake and angiogenesis through vascular endothelial growth factor (VEGF) expression [29].

Despite the diversity of NDD pathologies, including Parkinson's (PD), Alzheimer's (AD), Huntington's and amyotrophic lateral sclerosis, they share several metabolic hallmarks. Cell death of neurons in many NDD has been observed due to protein misfolding and accumulation [55]. Aging, oxidative stress, and mutations are the main factors for protein misfolding [56]. The pathological protein accumulation can be either intra- or extracellular depending on the disease [57]. This in turn causes malfunctions with membrane receptors and further distribution in the neural signalling [57]. Moreover, protein accumulation increases lipid oxidation and mitochondrial dysfunction [28]. Glial cells such as astrocytes and oligodendrocytes show a supportive rule in alleviating the cellular damage and redistributing metabolites to

neurons in NDD [58]. Similar to neurons, cellular damage in astrocytes and oligodendrocytes occurs due to protein accumulation that causes loss of normal functions such as the distribution of neuronal lactate uptake from glial cells and gain of toxic functions [59], [60]. Hypomyelination of oligodendrocytes induced by protein accumulation is further accelerating neuron damage [60]. Microglia protect from neurodegeneration by maintaining synaptic remodelling and phagocytosis of dead cells. Similar to neuron cells, intracellular protein accumulation may cause loss of the astrocytes and microglia normal functions that may aggravate NDD [59], [61]. An increase in microglial phagocytic activity has been shown concomitant to an increase in the production of anti-inflammatory mediators and a decrease of pro-inflammatory mediators [62]. Balance between pro-inflammatory/anti-inflammatory microglia activation shows improved prognosis and treatment of NDD [63]. Mainly, shifting from pro-inflammatory to anti-inflammatory activation decreased neuroinflammation in some NDD [64]. In most NDD, neuronal glucose uptake is downregulated and glucose metabolism is impaired [65]. The alteration in glucose metabolism and the downregulation of GLUT transporters lead, together with the mitochondria dysfunction, to lower energy levels that aggravate the pathologies. Mitochondrial dysfunction does not only impair cellular energy, but as mitochondria play a key role in calcium and redox homeostasis, they also contribute to redox stress. Furthermore, dysfunction in OXPHOS increases the production of ROS that will further increase mitochondrial damage and eventually initiate apoptosis [66]. Lipid peroxidation is another hallmark of many NDDs in early development due to mitochondrial damage and increased ROS [28]. Some by-product metabolites of lipid peroxidation are potential biomarkers for different NDDs such as isoprostanes in AD and malondialdehyde in PD [66]. Lastly, metabolism of polyamines such as spermidine and spermine is also deregulated in NDD. Both metabolites are antioxidants and have antiapoptotic properties with expression in neurons and glial cells. Deregulated polyamine metabolism was detected in AD, and PD and was accompanied with mitochondrial damage and apoptosis [67].

Constraint-based metabolic modelling (CBM) and genome-scale metabolic models (GEM) are commonly applied to study metabolism and, notably in cancer, where it was used to understand rewiring strategies and predict repurposable drugs [68] and drug off-targets [69]. GEM is an *in silico* representation of the metabolism where the interactions between metabolites and the biochemical reactions are formulated in a sparse stoichiometric matrix and the relationship between genes and reactions by Boolean rules (GPR rules). Moreover, GEM is used to simulate the role of the microbiome in the development of PD [70], [71] or to study psychiatric diseases [72] and AD [73] in humans and PD-like phenotypes in mice [74]. However, brain metabolism has specific properties that must be considered before applying CBM. The brain

is protected by the BBB that controls the exchange of metabolites between cerebrospinal fluid (CSF) and the blood [75]. The permeability of the BBB can be altered in numerous diseases, which also impacts the CSF composition and the brain microenvironment [76], a feature that can be further used to constrain metabolic models. Furthermore, the metabolism of neurons and glial cells is interconnected and numerous exchanges between glial cells, notably astrocytes that are part of the BBB, have been described. For instance, glial cells store glucose in the form of glycogen, and, when required, glycogen fuels glycolysis [77]. The produced lactate can then be taken up by surrounding neurons [78]. Hence, for the study of some diseases, a bi-cellular or multicellular model is more suitable than an averaged brain model that lacks the required resolution.

In this review paper, we survey brain GEMs that could be used to study brain cancer, NDD or other brain disorders. We focus mainly on the modeled cell type, the type of model (single versus bi-cellular models), the curation level and the overall quality of the model in terms of the gene, metabolite and reaction annotations. We further consider the type and quality of data used to support the inclusion of reactions in the models as well as the validation used in the different studies. The model size, the inclusion of cell type-specific pathways and the optimisation function were also used to assess the models' completeness and specificity. We further compare the metabolite composition in models with a biomass function to assess their specificity in the investigated system. Finally, we highlight the strengths of the different GEMs, in terms of applied constraints, data utilized for model-building and validation that could be incorporated in future models and suggest some improvements.

2.2 Materials and Methods

2.2.1 Literature Search for Manually Curated Brain GEMs

An extensive literature review was performed to gather brain GEMs. To distinguish between the different curation levels, we classified the metabolic models into three classes: curated, semi-curated, and automatically generated (AG). In this review, we focused mostly on curated and semi-curated models. Curated: models built starting from a list of biochemical reactions collected from literature or databases to which reactions were then added to fill the gaps or add the missing information. Alternatively, the starting point can also be an automatically generated GEM. However, most pathways have been carefully checked to eliminate reactions with no or low support from the literature that is not required for modelling purposes and to add missing reactions but are known to be present in the studied system. Semi-curated:

models built using a generic reconstruction or an automatically generated model that was curated via the addition of constraints, modifications (addition and removal of reactions) in key pathways or required to combine two models in a bi-cellular model.

Automatically generated: models built automatically using a model-building algorithm such as FASTCORE [79], FASTCORMICS [80], rFASTCORMICS [68], GIMME [81], mCADRE [82], PRIME [83], iMAT [84], RegrEX [85], and tINIT [86] from a GEM, and expression data (transcriptomic or proteomic) without or with limited manual curation.

2.2.2 Inclusion and Exclusion Criteria of Publications

Publications focusing on building curated and semi-curated GEMs for the human brain and using CBM were included. In addition to curated and semi-curated models, only one AG GEM was included for relevance to GBM. Five types of brain GEMs were excluded from this review: (1) AG GEM without validation, (2) curated GEM with a follow-up included in the present review, (3) dynamic metabolic models in the brain, (4) publications with no publicly available model files in the supplementary files or BioModels, and (5) Non-human GEM. Dynamic metabolic models were excluded as they are out of the scope of the current review, and they were already covered in a previous review [87]. We also focused on human GEM as being more relevant for personalised medicine. Due to missing abbreviated names for some GEM, we referred to each model by the last name of the first author and the date of the publication.

2.2.3 Metadata Gathering for Determining the Extensiveness of the Manual Curation

After selecting brain GEM publications, basic information was retrieved from each publication regarding the model used as template, cell type, diseases, and data used during model building or validation. Moreover, the detailed types of the different omics and experimental data were collected with the number of samples to identify the extensiveness of the manual curation of the model.

2.2.4 Determining Model Sizes and Common Genes

The model files were imported using the COBRA Toolbox V3 [88], and the number of reactions, genes and metabolites were determined. The median, minimum and maximum numbers were

computed for publications with more than two GEM. Since some reactions may not be able to carry a flux at all, the number of flux-consistent reactions were identified using FASTCC [79]. Moreover, the brain GEMs' model genes were mapped to ENTREZ IDs to compare the overlap between the different models using the UpSet plot in R. Two generic models, Recon3D and Human1, were used in the gene overlap analysis. The intersection and the union of the model genes were retrieved for publications with more than two GEM.

2.2.5 Determining the Level of Completeness and Specificity of the Brain GEM

To evaluate the specificity and the completeness of the human brain GEM, tissue gene categories were retrieved from the Brain Atlas [89] of the Human Protein Atlas (HPA) [90]. HPA classifies the protein-coding genes into five categories according to the expression level in a target tissue compared to other tissues. These categories were retrieved for the human brain and mapped to the ENTREZ identifiers. The five categories were grouped for simplification into two types: Supported (which includes "Elevated in brain", "Elevated in other but expressed in brain" and "Low tissue specificity but expressed in brain"), and unsupported (which includes "Not detected in brain" and "Not detected in any tissue"). The different HPA data were mapped to the genes of the brain GEM, and to two generic models, Recon3D and Human1, to assess the fraction of genes of each model that are supported or unsupported in the brain by the HPA protein data. Two scores were calculated for each brain GEM, specificity and completeness. Model specificity (indicated as two numbers) is the number of supported or unsupported genes in each GEM. In contrast, model completeness is the ratio of the model-supported or unsupported genes to the total count of genes in each category.

2.2.6 Evaluation of Objective Function and Validation Used in the Brain GEM

The brain GEMs were further evaluated by their objective function (OF) and used validation data to determine the strengths and limitations of these GEMs. Different brain GEMs include different OFs depending on the diseases of interest. These OFs were categorized into tailored or generic based on the manual curation. In addition, the rationale for choosing a specific OF according to the research question was summarised. The OFs of the GBM GEMs were compared using their metabolite composition. Moreover, the data used for validation in the brain GEMs were outlined and their importance for the research question was discussed.

Finally, the limitations and the strengths of the brain GEMs were summarised based on the choice of the template model, model-building technique, study design, use of constraints data, presence of sink reactions, heuristic thresholds in the discretization of the expression data, and applying standard identifiers.

2.3 Results

In this review, we discuss nine publications that focus on reconstructing GEMs that could be employed for NDD, brain cancer, and other brain diseases. The selection of these models was based on their public availability (see Supplementary File S1 Table S1), the curation level, and/or the pertinence to GBM. By curation, we understand the contextualization of the models with constraints retrieved from literature or published experimental data, the addition of reactions specific to the cell type of interest, the choice of the OF, and if the OF was tailored to the cell type of interest. Finally, we discussed the validations used in the different publications and the strengths and limitations of these GEMs.

2.3.1 *Selected Brain Metabolic Models Could Be Potentially Reused for NDD and Glioma*

The main difference between the curated and semi-curated is the extension of the curation. For example, *Thiele2020*, considered curated, defines 578 core reactions (reactions supported by literature in the brain) and added 43 metabolites to the list of metabolites passing BBB. While *Baloni2020* completed the list of BBB metabolites with an additional 372, no core reactions were added. Five curated, three semi-curated and one AG GBM GEM were selected. Most of these GEMs integrated transcriptomic and proteomic data for model-building, while only two GEMs used metabolomics data to define exchange reactions (see Supplementary File S1 Table S2).

2.3.2 *Lewis2010 (iNL403)*

Lewis2010 [91] is a bi-cellular GEM of a neuron and an astrocyte with 1073 reactions and 987 metabolites [91]. This GEM was built by extracting the reactions of glycolytic, mitochondrial, and transport pathways from the generic reconstruction Recon 1 [92]. The presence of each of these reactions in the brain was determined based on expression from different sources. *Lewis2010* was curated by adding brain cell type-specific (astrocyte and neuron) biochemical

reactions [91]. The models were then contextualised using manually selected neuron cell type-specific reactions to build glutamatergic, GABAergic, and cholinergic neurons. In addition, the model bounds were constrained using uptake rates obtained from the literature.

2.3.3 *Sertbaş2014 (iMS570) from Tunahan Çakır Lab*

Sertbaş *et al.*, 2014 [93] expanded the brain reconstruction of Çakır *et al.*, 2007 to obtain a bi-cellular astrocyte and neuron model with 630 reactions and 530 metabolites from the literature [93]. ATP production and glutamineglutamate exchange were added as OF, whereas GABA exchange was included to ensure the coupling of the exchange reactions between the astrocyte and the neuron model.

2.3.4 *Özcan2016 (iMS570g) from Tunahan Çakır Lab*

Since the curated *Sertbaş2014* only includes non-cancerous OFs, Özcan *et al.*, 2016 [94] added 29 reactions to integrate a tailored growth OF [94]. Among the 29 reactions, 25 are biomass-related and four reactions are linked to glutamine metabolism in GBM. The tailored OF was formulated based on the contribution of both the astrocyte and the neuron to the dry weight of the white matter.

2.3.5 *MartínJiménez2017*

A curated astrocyte GEM [95] was reconstructed using the Human Metabolic Atlas (HMA) [96] and microarray data of foetal cortical astrocytes. The completeness of the model was assessed by identifying gaps that were filled by adding astrocyte-specific reactions based on enzymes present in the HPA [90]. Lastly, experimental constraints specific to hypoxia were used to compare the activated reactions under normal and hypoxic conditions.

2.3.6 *Thiele2020*

Thiele *et al.*, 2020 [97], built two sex-specific multi-tissue models (Harvey and Harvetta for male and female, respectively) of 26 organs with $>$ 80,000 reactions [97]. Reactions for the protein and drug metabolism pathways were removed initially from the Recon3D model [98], before assembling according to the connections of the different organs. The two multi-tissue models were built using FASTCORE [79] from the assembled reconstructions and organ-specific core

reactions from omics data and literature. Exchange reactions of the organs and extracellular fluid such as the CSF were constrained by metabolomics data from the Human Metabolome Database [99]. Meanwhile, the exchange reactions between the extracellular fluid of the different organs and the systemic blood circulation were obtained from the literature. Moreover, organ-specific models were further extracted from the two multi-tissue models as standalone consistent GEMs. The man and woman brain GEMs will be referred to as *Thiele2020_Harvey* and *Thiele2020_Harvetta*.

2.3.7 *Baloni2020*

Baloni *et al.*, 2020 [100] built seven brain region-specific GEMs using the Recon3D model [98] and transcriptomic data from different brain regions of healthy and AD patients with the mCADRE algorithm [82]. The reactions of the drug metabolism pathway were removed from the Recon3D model. Then, the transcriptomic data were discretized using the top 25th percentile cut-off to obtain a set of reactions used as input for mCADRE. After the building, the model was constrained using metabolites passing the BBB from *Thiele2020*, bile acid metabolites from targeted metabolomics of brain samples, uptake rates obtained from *Lewis2010* and other literature sources were integrated. Furthermore, gap filling was performed using HPA expression [90] to determine gene presence. Finally, the OF of *Sertbaş2014* was integrated into the GEM.

2.3.8 *EcheverriPeña2021* $Neuro-Glia\_GEM$

EcheverriPeña *et al.*, 2021 [101] integrated two AG GEMs [102], to build a bi-cellular neuron-glia metabolic model. These models were obtained using Recon 2 [102] and HPA [90] as input for the MinMax algorithm [103]. To identify the metabolic pathways changes related to Arylsulphatase A (ARSA) deficiency, EcheverriPeña *et al.*, 2021 added reactions of sulfatide degradation from the myelin band. The added reactions made the glial cellular compartment more specific for oligodendrocytes.

2.3.9 *Lam2021*

Lam *et al.* [104] analysed telomeric ageing in AD and PD compared to healthy controls by aggregating gene expression data from six sources via batch correction. The combined AD and PD samples were stratified into three subclasses using unsupervised clustering. Four semi-curated GEMs were built from the expression of the three clusters in addition to the control

samples using tINIT [86] from the RAVEN Toolbox [105]. The template model for model-building was an adipocyte GEM, iAdipocytes1850 [106], after mapping the *gprRules* from the generic reconstruction HMR3 [107] and constraints from *Baloni2020* [100]. Flux balance analysis and reporter metabolite analysis were applied to define the different pathways and metabolites between the three combined AD-PD GEMs and the control GEM. These pathways and metabolites were validated using semi-curated zebrafish GEMs built from normal and enhanced aging. The zebrafish GEMs were built from zebrafish expression data of wildtype and mutant TERT gene responsible for telomere maintenance.

2.3.10 *Larsson2020*

Larsson2020 [108] merged 139 patient-derived AG GEMs to build a GBM model using tINIT [86]. These 139 AG GEMs were built by Uhlén *et al.* [109] using the generic reconstruction HMR2 [107] and the RNA-Seq data of GBM from the TCGA-GBM dataset [110]. Furthermore, single-gene deletion was performed on both the patients and the generic GBM models using FastGeneSL [111]. Then, the genes whose *in silico* knockout might affect healthy tissues were excluded by evaluating the effect of a knock-out on 77 pre-defined metabolic tasks (defined as metabolites that must be produced from a defined minimal media or a set of metabolites) on an AG healthy brain model from the HMA [96]. The different data used by the brain GEMs, their curation status, and cell types are summarised in Table 2.1.

Table 2.1: Curated, semi-curated, and automatically generated human GEMs in the brain and their associated phenotypes.
The list of metabolic models in the human brain was classified as curated, semi-curated, or AG according to the level of manual curation after model-building. The detailed omic types for the "Data" column and the number of samples are summarised in Supplementary File S1 Table S2.

Model	Goal	Model used as template	Curation status	Cell type	Diseases	Data

Lewis2010 (*iNL403*) [91]	Building a curated bi-cellular human brain metabolic model to study AD	Recon 1 [92]	Curated	Astrocyte-Neuron	AD	• Human Protein Reference Database [112] • HINV [113] • HUPO brain proteome project [114] • Literature information for transport reactions between compartments • Constraints for neuron cell types • Microarray data of AD
Sertbaş2014 (*iMS570*) [93]	Identifying biomarker metabolites for six NDD	Çakır *et al.*, 2007 [115]	Curated	Astrocyte-Neuron	Six NDD	• Microarray of the six NDD • Literature-derived constraints for a healthy brain
Özcan2016 (*iMS570g*) [94]	Metabolic rewiring pathways in three GBM subtypes	*Sertbaş2014*	Curated	Astrocyte-Neuron (glutamatergic, GABAergic, cholinergic)	Three GBM subtypes	• Curated growth objective function • Literature-derived constraints for 26 reactions for GBM • Microarray data of the three GBM cell lines
MartínJiménez 2017 [95]	Building an astrocyte model reconstruction	HMA [96]	Curated	Astrocyte	Hypoxia	• Microarray data of foetal cortical astrocytes • Literature-derived constraints for healthy astrocyte exchange reactions
Thiele2020 [97]	Building sex-specific, multi-organ, whole-body model	Recon3D Model [98]	Curated	Whole-brain		• Human Proteome Map [116] • HPA [90] • CSF metabolites from Human Metabolome Database [99] and other resources • Organ-specific reactions from literature

Baloni2020 [100]	Analyzing the effect of bile acid synthesis in AD in different brain regions	Recon3D Model [98]	Semi-curated	Seven brain regions	AD	• RNA-Seq data for brain regions from post-mortem of normal and AD patients • Metabolomics of primary and secondary bile acids from the post-mortem brain samples • BBB reactions from *Thiele2020* • Constraints from *Lewis2010* • Human Protein Atlas
EcheverriPeña-2021 (*NeuroGlia_GEM*) [101]	Building a bi-cellular neuron-glial model to identify pathways linked to ARSA deficiency	Two tissue AG models from Recon 2 [102] (Glia: MODEL1310-110064, neuron: MODEL1310-110033)	Semi-curated	Neuron-Glia	Metachromatic leukodystrophy	• Reactions of the sulfatide degradation from the myelin band
Lam2021 [104]	Analyzing telomeric aging in AD and PD	iAdipocytes-1850 [106] with gprRules from HMR3 [107]	Semi-curated	Whole-brain	AD, BD	• RNA-Seq of healthy brain from HPA [90] & GTEx [117] • CAGE expression of healthy brain samples from FANTOM5 [118] • RNA-Seq of AD and PD brain samples from Rajkumar dataset [119] and Zhang/Zheng dataset [120], [121] • Single-cell RNA-Seq of AD and PD brain samples from ROSMAP [122] • Constraints from *Baloni2020* [100]
Larsson2020 [108]	Predicting non-toxic essential genes for GBM & identifying metabolic pathways for GBM low & high overall survival	139 AG patient-derived models [109] using HMR2 generic reconstruction [107]	AG		GBM	• RNAseq of TCGA-GBM [110] • Healthy brain GEM from HMA [96] • CRISPR-Cas9 data for GBM [123]

2.3.11 *Manual Curation Included Tissue-Specific Constraints, Added Reactions, and Compartments*

A curation can either be a refinement of a curated or an AG GEM by the addition or removal of reactions, metabolites, and flux rates. Four models incorporated experimental flux rates to contextualize their models to represent healthy brain cell models (*Sertbaş2014*, *Lewis2010* and *MartínJiménez2017*), and GBM (*Özcan2016*). Most experimental flux rates are specific to a cell type (mostly glial or neuronal), while others, such as glucose uptake, are measured at the BBB. While *Sertbaş2014* assumed equal glucose consumption for the glial and neuron model, *Özcan2016* divided the overall brain glucose, oxygen, and glutamine uptakes based on the neuron and glial proportion in the white matter mass.

Four models included a compartment to simulate the exchange between the models and the BBB, *Lewis2010*, *MartínJiménez2017*, *Thiele2020*, and *Baloni2020*. Furthermore, metabolites that cannot cross the BBB were defined in *Thiele2020*, and the respective transporters were removed. Overall, to better model the physiology of the studied diseases, the models have to be adapted by adding or removing reactions or by applying the constraints based on experimental measurements obtained from diseased patients or cell lines. Besides whether there is binary information if a metabolite passes or not passes the BBB, or what metabolites can be uptaken by a specific cell type, experimental rates can be used to validate and constrain the model prior to the reconstruction. *Sertbaş2014* and *MartínJiménez2017* collected 14 and 23 flux rates corresponding to hypoxia in astrocyte and healthy astrocyte–neuron models, respectively (see Supplementary File S2 Tables S6–S8).

The second type of manual curation of brain GEMs consists of the addition of new brain-specific reactions. For example, *Lewis2010* added manually-curated reactions for the acetylcholine synthesis, which is decreased in the neurons of AD patients. These reactions were identified by flux balance analysis on the generic reconstruction Recon 1. Meanwhile, reactions linked to the ARSA gene, which is responsible for the degradation of the sulfatides in the myelin sheath, were added in *EcheverriPeña2021*.

2.3.12 *The Completeness Is Highly Variable between the Models While Having a Similar Specificity*

The size of the models in terms of the number of reactions, metabolites, and genes varies greatly between the models and ranges from 639 to a median of 5942 reactions for *Baloni2020* (see Table 2.2), and only 35 genes were shared among the models after the conversion of

the model gene identifiers to ENTREZ gene identifiers (Supplementary File S1 Figure S1). This low overlap results to some extent from the comparison between bi-cellular glial-neuron, astrocyte, and whole-brain models. However, the low overlap also results from the strategy used during the model building. Two bottom-up models (*Sertbaş2014* and *Özcan2016*) were smaller and focused mainly on the central brain metabolism. The size of the remaining seven models correlated with the size of the reconstruction used as a template for the building process that varies between 2469 consistent reactions for Recon 1 to 10,600 for Recon3D.

Table 2.2: Model statistics for the brain GEMs.

The curated and semi-curated models were retrieved as explained in Supplementary File S1 Table S1. For studies with more than two models (*Larsson2020*, *Baloni2020*, and *Lam2021*), the median sizes and range were computed. The number of reactions was determined for consistent models of these studies using FASTCC [79]. Since the models used different gene identifiers, the identifiers were mapped to ENTREZ genes.
∗ Brain GEMs with more than two models per study.

Model	Reactions	Consistent Reactions	Metabolites	Genes	Gene Field Format	Number of ENTREZ Genes
Lewis2010	1073	727	987	403	ENTREZ Gene	403
Sertbaş2014	630	589	523	570	Gene Symbol	532
Özcan2016	659	644	548	569	ENTREZ Gene	569
MartínJiménez2017	5659	4848	5007	3765	Ensembl Gene	3674
Thiele2020_ Harvey	3602	3510	2201	1836	ENTREZ Transcript	1548
Thiele2020_ - Harvetta	3602	3508	2203	1843	ENTREZ Transcript	1551
Baloni2020∗	5942 (5341–6328)	5327 (4870–5696)	3784 (2808–3926)	1684 (1524–1846)	ENTREZ Transcript	1409 (1292–1559)
EcheverriPeña2021	3831	3622	2473	1375	ENTREZ Transcript	1148
Lam2021∗	3283 (3274–3334)	2774 (2658–2815)	2122 (2118–2138)	1523 (1478–1572)	Ensembl Gene	1516 (1478–1572)
Larsson2020∗	3917 (2226–4877)	2951 (1382–3276)	1649 (1178–2086)	1840 (1103–2034)	Ensembl Gene	1838 (1102–2031)

MartínJiménez2017 has 948 genes that were not included in any of the other brain models (Supplementary File S1 Figure S1) but also has the highest number of supported and unsupported genes by the HPA protein data in the brain according to the HPA (Figure 2.2). Similarly, *Thiele2020* and *Baloni2020* share 2762 (26.1%) and a median of 5110 (48.2%) reactions, respectively, with the Recon3D model. The ratio between the supported and unsupported genes in the brain is rather conserved across the brain models and generic GEMs (Figure 2.2A), showing that, to include more supported genes in the brain, inactive reactions in the

brain had to be included. In terms of completeness, *MartínJiménez2017* included a higher percentage of the supported and unsupported genes in the brain. Taken together, two strategies were used, bottom-up (*Sertbaş2014* and *Özcan2016*) and top-down (*MartínJiménez2017*, *Thiele2020*, *Baloni2020*, *EcheverriPeña2021*, *Lam2021*, *Larsson2020*), that do not dictate the quality of the model but rather have an impact on their size. *Lewis2010* used a compromise between the two approaches by reconstructing a subnetwork using GIMME and expression data. While focusing mainly on three pathways and the fulfillment of metabolic tasks associated with the synthesis and metabolism of acetylcholine, the inclusion of transcriptomic data allowed us to obtain a larger model than the ones using the bottom-up approach. Regarding specificity and completeness, increasing the number of brainspecific reactions causes the inclusion of genes that are considered unsupported by the HPA [90].

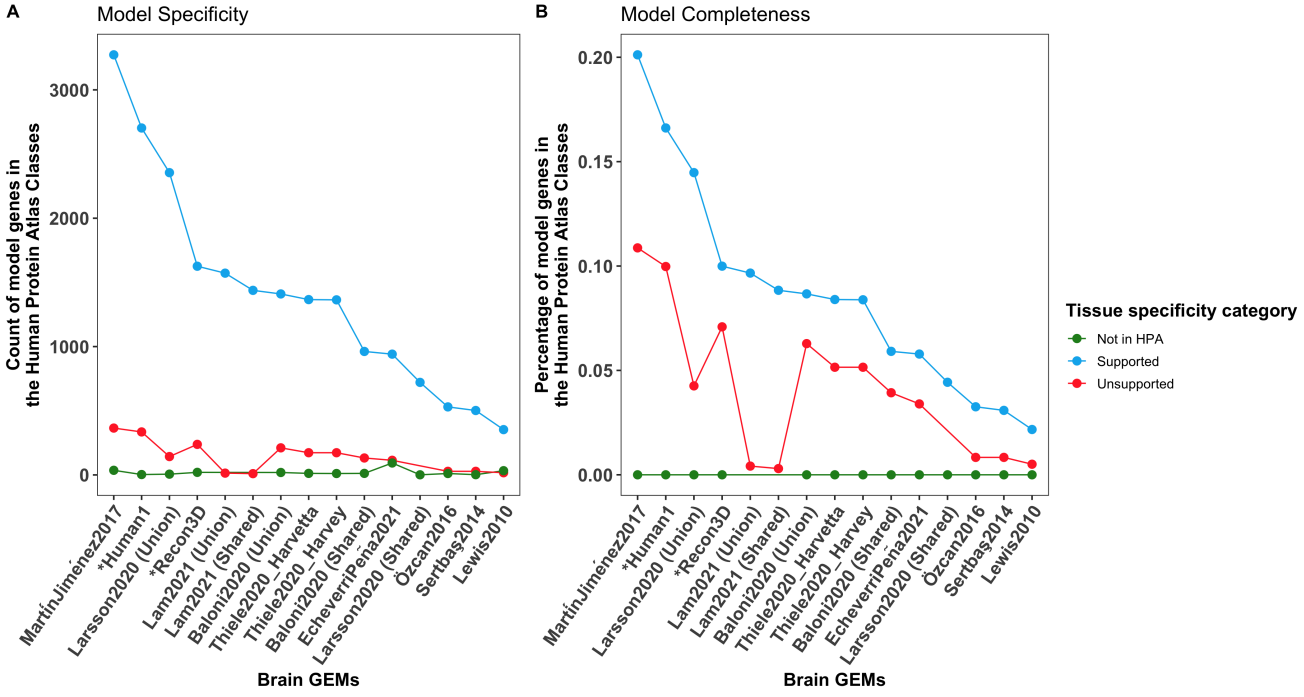

FIGURE 2.2: **Completeness of the human brain metabolic reconstructions is linked to less specificity according to the Human Protein Atlas brain-specific category.**
A) The genes of the brain reconstructions in addition to the Recon3D model and Human1 were classified into five categories based on differential tissue expression of the brain. These five categories were grouped into supported (in blue) and unsupported (in red). Model genes outside the HPA coding genes were coloured in blue. B) Since the total number of genes in each category differs, completeness was computed as the ratio of model genes in a category and the total number of genes in that category. The number and completeness of supported and unsupported genes are higher in *MartínJiménez2017* than in Human1, which indicates the loss of brain specificity by increasing the completeness of the model.

2.3.13 *Glutamine/Glutamate/GABA Exchange Is a Brain-Specific Objective Function for Non-Glioma Models*

The choice of the OF and its formulation should be tailored to the modeled cell type and condition. Thus, we compared the OFs used for non-glioma and glioma models to evaluate their relevance to brain functions (see Table 2.3). The OF is a reaction with the set of metabolites needed for a cell to carry out a specific task. The main task of the neuron cells is resetting the action potential by Na+/K+ ATPase, which is costly in energy [124]. This energy generated as ATP comes from either glycolysis or tricarboxylic acid cycle and OXPHOS. Many hypotheses have been proposed for the specific roles of glial and neuronal cells in the transport of energy substrates, such as the astrocyte–neuron lactate shuttle theory (ANLS) [78]. The ANLS theory states that the glucose is transported from the blood vessels to the astrocyte and then metabolized through glycolysis to produce lactate supplied to neurons. Hence, lactate production could be used as OF. However, for non-glioma, like for other healthy tissues, ATP production or maintenance is more commonly chosen. In the whole-brain *Thiele2020*, two maintenance OFs were used: biomass_maintenance and biomass_maintenance_noTrTr in normal and fasting conditions, respectively. In the brain bi-cellular models, glutamate, glutamine, and GABA cycles are used as an additional OF to ensure a coupling between the two models. Furthermore, *MartínJiménez2017* used only glutamate uptake and glutamine release for their role in the detoxification of neurotransmitters from the CSF. In summary, ATP production, biomass maintenance, glutamate, glutamine, GABA cycles, and neurotransmitter exchange reactions can be used as OFs for non-glioma brain models depending on the cell type.

2.3.14 *GABA and Ornithine Were Included in the Biomass Formulation of a GBM-Specific Biomass Function*

Only *Özcan2016* and *Larsson2020* are modeling high proliferative cells, and, accordingly, they used the biomass reaction as an OF. While *Larsson2020* used the generic biomass function included in all HMR reconstructions, *Özcan2016* built a tailored biomass function for glioma that could be adapted to future GBM models. *Özcan2016* added to the healthy *Sertbaş2014* 24 pseudo reactions and a final biomass reaction for which the coefficients were adjusted in function of the contribution of each cell type of the white matter (94% in glial and 6% in neuron). By comparing the metabolite composition of the two OFs, we identified some differences between the two models, notably, GABA and ornithine present uniquely in *Özcan2016*

Table 2.3: Objective Functions for Various Models.

Objective functions used in the brain-specific models and the rationales for using these objective functions. [m]: mitochondria, [x]: extracellular, [c]: cytosol.

Model	Objective Function(s)	Rationale for choosing the OF
Lewis2010	ATP demand for both astrocyte and neuron cell: $DM_{atp}(c) : atp[c] + h2o[c] \rightarrow adp[c] + h[c] + pi[c]$	Production of the cholinergic neurotransmitter is ATP-dependent.
Sertbaş2014	1- Maximization of the sum of glutamate/glutamine/GABA cycles. 2- Setting the value of the sum of the three-cycle fluxes to the optimal solution, then minimizing the Euclidean norm of fluxes.	The 1st OF ensures compact coupling of the intercellular exchange between the astrocyte and neuron. The 2nd OF ensures fluxes with minimal utilization of metabolic enzymes.
Özcan2016	Curated biomass growth reactions: $2.9404protein + 0.9074lipid_{WM} + 0.1091RNA + 24ATP \rightarrow biomass + 24ADP$	Adjusting the contribution of neurons and astrocytes of macromolecules based on their percentage in the white matter and the macromolecule composition of the white matter.
MartínJiménez2017	(A) ATP production: $ADP[m] + 4\,H + [c] + Pi[m] \rightarrow ATP[m] + 3\,H + [m] + H2O[m]$ (B) Glutamate uptake and glutamine release: $Glutamate[x] + Glutamine[c] \rightarrow Glutamate[c] + Glutamine[x]$	The 1st OF ensures the consumption of different metabolites for energy production. The 2nd OF resembles the astrocyte's role in detoxification of the extracellular glutamate produced by neurons and secretion of glutamine needed by the neuron.
Thiele2020	The brain model didn't have a default OF; rather, the model included different OFs for different scenarios: 1- Biomass maintenance 2- Biomass maintenance with no transcription and translation	Biomass maintenance didn't include DNA molecules (dgtp[n], dctp[n], datp[n], dttp[n]) as the brain cells don't replicate. The 2nd OF resembles a fasting condition.
Baloni2020	Equal to *MartínJiménez2017*	
EcheverriPeña2021	ATP synthesis	Modeling the highly oxidative state of the excited neuron releasing neurotransmitters
Lam2021	ATP synthesis	
Larsson2020	Growth OF of the generic reconstruction HMR2	

and, glycogen, cysteine, proline, and tryptophan (included in the generic biomass function of *Larsson2020*) (Figure 2.3). In addition, *Larsson2020*'s OF shows a higher diversity of phospholipids than *Özcan2016*, as the former is reconstructed from the generic HMR2 that covers the lipid metabolism exhaustively [107]. The neurotransmitter GABA, which is missing in the *Larsson2020*'s OF, was shown to control the proliferation and growth of glioma [24]. Meanwhile, glycogen, which is absent in *Özcan2016*'s OF, 16 of 28 is required for cancer cell survival [125] and optimal glucose utilisation under hypoxia conditions [126]. As a result, GABA and glycogen should be potentially added to future GBM OFs.

2.4 Figure 3

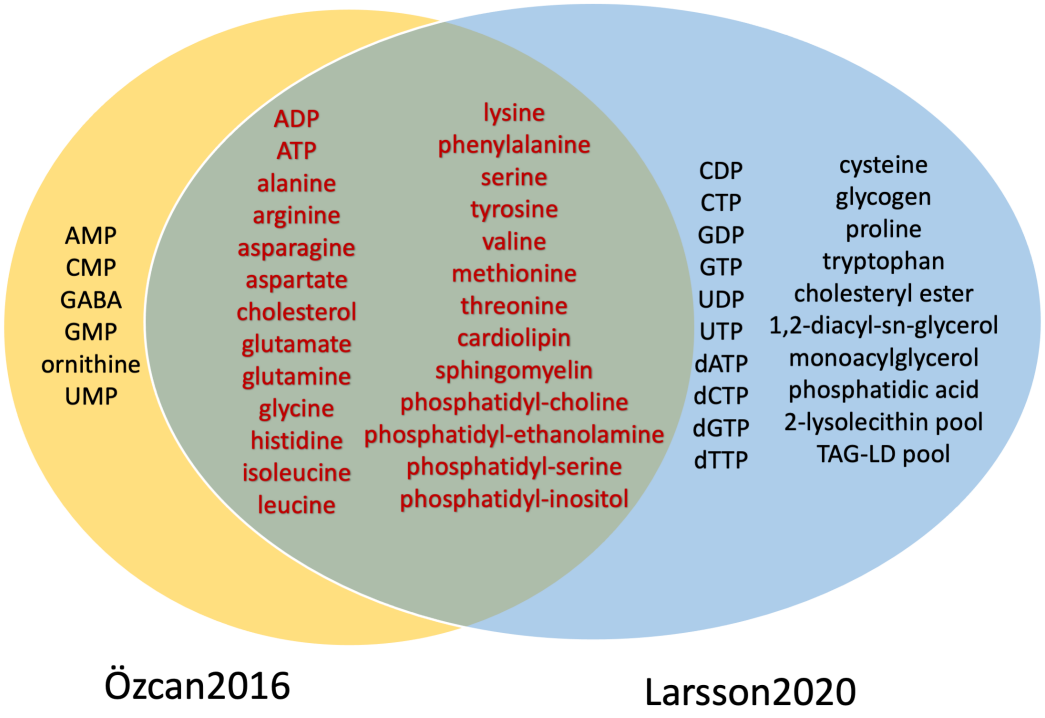

FIGURE 2.3: **GABA, ornithine, and some phospholipids are different between the tailored glioblastoma and the generic OFs.**
Two brain GEMs have a biomass function: *Özcan2016* and *Larsson2020*. Both models' OFs share 26 metabolites, mostly amino acids, cholesterol, and phospholipids. While *Özcan2016*'s OF has six unique metabolites, notably GABA and ornithine, *Larsson2020*'s OF has 20 unique metabolites such as cysteine, glycogen, proline, tryptophan, nucleotides, and fatty acids.

2.4.1 *CRISPR-Cas9 screens, experimental fluxes and simulating metabolic dysregulation are used as validation*

Validation of the various *in silico* predictions produced with the metabolic models is crucial for ensuring the quality of the curated, semi-curated, or AG models. Validation methods applied in the different publications are summarised in Table 2.4. *Sertbaş2014* and *Özcan2016* compared the predicted and measured flux rates for healthy and GBM, respectively. Also, *Lewis2010* validated the predicted cholinergic neurotransmission and ATP production rates with experimental data. *Larsson2020* compared the predicted essential genes for GBM, against high-throughput CRISPR-Cas9 data [123]. While *MartínJiménez2017* collected the dysregulated metabolic reactions (up- or down-regulations) in metachromatic leukodystrophy from literature to compare the predicted dysregulated reactions. Flux rates can thus be employed for either model contextualization or validation, as long as the same data is not used for both. Furthermore, in the absence of experimental data, information on the up- and down-regulation of metabolic pathways of a disease retrieved from different literature can be used as an alternative for validation.

Table 2.4: Some advantages and drawbacks in the brain GEMs.

Model	Strengths	Drawbacks
Lewis2010	• Inclusion of a compartment for BBB (EndotheliumAndBlood) with 55 metabolites that can bypass through it (Supplementary File 2, Table S3) • Adding brain cell type-specific reactions from literature (Lewis *et al.*, 2010, Supplementary Table 1) • Comparison with experimental data of cholinergic neurotransmission rate	• The generic reconstruction used as input is outdated and has lots of shortcomings
Sertbaş2014	• Constraining with literature-derived constraints. • Comparison with experimental flux ratios for healthy brain cells (Supplementary File 2, Table S6-S7).	• Using non-standard reaction identifiers in the model • Missing metFormula field that prevents evaluating the stoichiometric consistency
Özcan2016	• Constraining with literature-derived constraints. • Comparison with experimental flux ratios for GBM (Supplementary File 2, Table S9).	• Using non-standard reaction identifiers in the model • Missing metFormula field that prevents evaluating the stoichiometric consistency

MartínJiménez2017	• Constraining with literature-derived constraints (Supplementary File 2, Table S8) • Validation with dysregulated reactions in ischemia (MartínJiménez *et al.*, 2017 [95], Table 4)	• High rate of included genes that are unsupported in brains • The discretization method used for the expression data is not explained • Missing metFormula field that prevents evaluating the stoichiometric consistency
Thiele2020	• Extracting core reactions from literature and other expression data (Supplementary File 2, Table S5) • Defining permeable and impermeable metabolites across the BBB (Supplementary File 2, Table S3) • Defining CSF metabolic composition from different metabolomics data (Supplementary File 2, Table S4)	• Discretization of the Human Proteome Map using a heuristic threshold
Baloni2020	• Updating the list of *Thiele2020* for metabolites passing the BBB (Supplementary File 2, Table S3) • Inclusion of constraints from *Lewis2010* and OF from *MartínJiménez2017*	• Discretization of the expression data using a heuristic threshold • Manual curation on the AG models after model-building with mCADRE. • Gap filling with 389 sink reactions
EcheverriPeña2021	• Adding reactions of myelin sheath degradation in oligodendrocyte	• Individual AG models [102] used for integrating into a neuron-glial model, were built using the outdated MinMax algorithm • Manual curation by adding reactions after integrating the two AG models • Missing metFormula field that prevents evaluating the stoichiometric consistency
Lam2021		Using an adipocyte GEM with *gprRules* of the generic HMR3 instead of using the genetic reconstruction itself
Larsson2020	• Removing essential toxic genes using predefined tasks for a healthy cell. • Validation of the predicted GBM essential genes against CRISPR-Cas9 data.	• AG reconstruction only

2.5 Discussion

2.5.1 *Limitations in the brain models include non-standard reaction identifiers and the use of outdated model-building algorithms*

This review focused on human brain metabolic models summarising the different resources used for building better brain models. These models resembled differences in cell type from uni- and bi-cellular models, whole-brain, and region-specific models. While the previous nine models gather information and data which can be employed for reconstructing future brain-specific models, the models themselves have some limitations that restrict their future use (see the summary of the strengths and drawbacks in Table 2.4). *EcheverriPeña2021* only used the unchanged flux of neurotransmitters after ARSA knockout as a quality check and would require a more thorough validation before any future use. Because the link between TERT mutation and AD is still debated [127], using TERT mutation of zebrafish in *Lam2021* as a validation of telomeric ageing in AD and PD may be insufficient. The two curated models (*Sertbaş2014* and *Özcan2016*) use non-standard reaction identifiers, making modifications or comparisons to databases or other models more difficult [128], [129]. Moreover, *EcheverriPeña2021* integrated two AG models built by MinMax [103], an algorithm published in 2008 and no longer considered to conform to the state-of-the-art, from tissue-specific expression data and Recon2 [102]. While *Baloni2020* was built using the Recon3D model, a heuristic threshold of the top 25-percentile was used to discretise the transcriptomic data, which strongly affects the quality of the models as shown by Opdam *et al.*, 2017 [130]. Further, unlike *Thiele2020*, manual curation with constraints and added reactions in *Baloni2020* were applied after the building by mCADRE. This resulted in blocked reactions in *Baloni2020* that were solved using 398 sink reactions. Likewise, in *EcheverriPeña2021*, manual curation was mostly applied to combine two AG models. Instead of using the generic model HMR3 itself, *Lam2021* was built from an adipocyte-specific GEM after mapping the *gprRules* from HMR3, which may not be directly relevant to brain function. *Lewis2010* was based on Recon1 (2007) [92], which has numerous shortcomings. The metFormulas field, which determines the chemical elements of each metabolite, was missing in four models (*Sertbaş2014*, *Özcan2016*, *MartínJiménez2017*, *EcheverriPeña2021*). This missing field prevented evaluating the mass balance of these models with MEMOTE [131]. Some brain GEMs incorporated boundary constraints from previous GEMs, without the required recalculation due to the use of different input reconstructions and biomass formulations. Despite the drawbacks of these reconstructions, the resources employed by these models can be reused (see Table 2.4). Finally, among the nine brain models, *Thiele2020* and

MartínJiménez2017 are the most curated models and, unlike *Sertbaş2014* and *Özcan2016*, use standard annotations and are larger. *Thiele2020* was built using state-of-art context-specific algorithms and reconstructions [88]. Furthermore, constraints and brain-specific reactions obtained from literature were fed to FASTCORE [79] already as input, allowing for building of higher quality models. *MartínJiménez2017*, in the pursuit of completeness, might have also lost specificity. Generally, using AG or semi-curated models with only a few refinements built by older algorithms and input reconstruction should be avoided. Instead, it would be advisable to rebuild the models using Recon3D [98] or Human1 [132] and more recently published building algorithms, while integrating the resources of the previous models as input for the algorithms (Table 2.4).

2.5.2 *A high completeness is obtained at the cost of the specificity*

The selected models presented in this review follow two different approaches. The first is a bottom-up approach that aims to build a model around a few brain-specific pathways. The second is a top-down approach that aims to remove inactive pathways in the brain from a generic reconstruction, a database or an expression data. While bottom-up approaches were less comprehensive and often not genome-scale, the top-down strategies were lacking in the review paper in specificity, with the ratio of highly versus unsupported in brain models comparable to the generic GEM used as input. An enrichment of tissue-specific genes and reactions is expected in context-specific models compared to their input reconstruction [133]. This lack of specificity could have resulted from the choice of the low expression threshold and/or the use of data from different brain regions with different metabolisms that blurred the specificities of each area. Thus the balance between completeness and specificity should be observed during building brain models.

2.5.3 *Using standard identifiers and confidence scores are required for model comparison and improvement*

Furthermore, using non-standardized identifiers for reactions and metabolites renders the reuse of *Sertbaş2014* and *Özcan2016* more difficult. In general, GEMs should be built with Ensembl transcript identifiers over ENTREZ gene identifiers as different transcripts might code for different isoforms that are not all functional [128], [134]. Added reactions should highlight the number of supporting literature. They should preferably have at least two supporting publications that prove experimentally that a reaction occurs in the tissue of interest. For

semi-curated and AG models, it is advisable to use the gathered information from these studies, and reconstruct new models with a state-of-the-art model-building algorithm [133] and a recent generic reconstruction such as Recon3D and Human1, rather than using the models directly. Moreover, heuristic thresholds for discretization during model-building should be avoided. These thresholds affect the quality of the output models [130], as the number of included genes, and by extension, reactions, is highly dependent on these thresholds. Confidence scores and supporting literature identifiers for manually added reactions are absent for some models. Therefore, confidence scores and supporting PubMed identifiers should be clarified and included as fields in the model file as SBML XML or MAT files. This confidence field should highlight if the manually added reactions are from literature, expression data, or for modeling purposes (i.e. gap-filling). Also, several models could not be included in these studies, as being not available or in a non-standard format such as excel files renders their use more difficult.

2.5.4 *The application of constraints to the generic model prior to the context-specific model reconstruction increases predictability*

The quality and extensiveness of the manual curation of these brain models varied strongly among the studies. Generally, the tailoring and inclusion of OF, adding core reactions from literature, and medium constraint exchange reactions to the BBB should be applied to the generic input model before the reconstruction with an algorithm and forced to be included in the output model. This tailoring might require some adjustment in the code of some algorithms but would avoid extensive post-reconstruction curation. After reconstruction, some refinement will still be required to include some reactions or pathways lacking support from the input transcriptomic and literature data. GEMs should be flux consistent or include the number of non-blocked reactions in the main text, as blocked reactions and reactions that can only carry a flux due to sink reactions, would need to be removed for most modeling purposes. Reporting these blocked reactions would help any future manual curation replace these sink reactions based on recent biochemical evidence.

2.5.5 *Constraining with flux rates should be adjusted to the generic model*

Medium constraints can either be binary, such as adding a BBB compartment or continuous such as flux rates or exo-metabolomics data. While the most updated list of metabolites that can bypass the BBB is used in *Baloni2020*, *Thiele2020* also compiled a list that cannot pass this

barrier, which can filter drugs and metabolites and predict blood biomarkers for brain diseases. Due to various diseases' alterations in the BBB function, metabolites bypassing the BBB may need to be updated in the models according to the diseases under study by either metabolomics data of the CSF or based on literature search. For instance, metabolomics of the LGG identified dysregulated metabolites in the CSF [135], that can be used to update the healthy CSF composition from *Thiele2020* for medium constraining of LGG. In GBM, tumor cells infiltrate and disrupt the BBB. Infiltrating GBM cells produce VEGF, downregulating the tight-junction proteins, and promoting angiogenesis and hypoxia [136]. Similarly, metabolomic analysis of NDD identified increased metabolites in the CSF such as kynurenine, ceramide, nitric oxide, neopterin, and other dysregulated metabolites that differ between NDDs [137]. Exo-metabolite data can be used to fine-tune medium constraining. The uptake and production rates of 213 metabolites of 60 cancer cell lines of NCI-60 [138] include two GBM and three astrocytoma cell lines. These flux rates were used to calculate the fluxes using a core cancer reconstruction from Recon 2, and the boundaries were then adjusted to Recon 2 (Zielinski *et al.*, 2017 [139], Supplementary Data, "FBA constraints" sheet). $>$ 99% of the carbon demand of the cancer cells is met by these 23 metabolites. The calculated boundaries would need to be recalculated but could allow refining the boundaries of future models. Similarly, differences in the generic models and the units of flux rates should be considered while employing constraints from one model to another.

2.5.6 *Metabolic tasks of brain cell functions could be employed in addition to tailoring the OF*

The previous brain models' OFs are condition-specific, either for a healthy brain or glioma. Instead of applying the same OF for both neuronal and glial cells, the OF should be tailored to the cell type. In addition to neurotransmitter detoxification and ATP production, the OFs of glial cells could include lactate production and glutamate uptake. The OFs of the neurons may include the production of the various neurotransmitters and the uptake of lactate, glutamine, and pyruvate [140]. Rather than using optimization functions, defining tasks that should be fulfilled at a given flux rate would often make more sense. Additionally, enforcing the biomass maintenance, lactate secretion and others to have a non-zero baseline reaction could be used to model the low proliferation of healthy glial cells compared to gliomas. Even with the above-mentioned brain GEM, manually curated GEMs for LGG, microglia and other relevant cell types are still missing, and only an AG GEM for LGG has been built so far [133]. Microglia GEM can be built from expression data of microglia with the OFs taken from a

curated macrophage GEM (ATP production, redox maintenance, NO production, production of extracellular matrix precursors, and polyamines production) [141]. Microglia GEM may then be further integrated into a multicellular GEM of GBM in order to understand cellular interactions between the microglia, astrocytes, neurons and GBM cells. Dendritic cells are another immune cell resident in the brain that increases tumor proliferation upon activation via glycolysis shift [142]. Other peripheral immune cells such as macrophages, monocytes, regulatory T cells, and cytotoxic T lymphocytes penetrate the BBB after damage of tumor growth [142], [143]. Modeling these immune cellular interactions, especially the resident cells, with glioma GEM can help in understanding the metabolic modeling of the immune microenvironment. In general, generic biomass OF forces the addition of pathways that might not be active in some brain cells. Therefore, tailoring at least the metabolite composition of the biomass OF with the biochemical knowledge of the glioma would improve the predictions and, notably, the prediction of essential genes that are not predicted due to the inclusion of alternative pathways that are inactive in the brain.

2.5.7 *Bulk regional expression data of the brain may serve as an alternative for capturing cellular heterogeneity*

Despite the recent developments of single-cell expression in capturing intercellular heterogeneity, robust and rigorously benchmarked tools for integrating single-cell expression into the metabolic model-building at genome-scale are non-existent for now. In the future these tools might help in building accurate multicellular brain GEMs without the need for intensive manual curation. Besides, brain disorders being influenced by many cells of a specific region, they can also be affected by the impairment of other regions, e.g. cellular damage in NDD and conditioning in glioma extends to the nearby regions [144]. Regional expression profiling of the brain outweighs conventional bulk expression in capturing the regional vulnerability for different diseases [145]. Previous brain reconstructions tried to simulate brain heterogeneity through multicellular models (*Özcan2016*), independent regional brain models (*Baloni2020*), or multicellular, independent regional models (*Lewis2010*). The connection information (i.e. exchange reactions) of the different brain regions can help in building an interconnecting multi-regional model similar to multi-tissue models [97], [146]. Similarly, a multi-regional model can be extended from the healthy brain to GBM. Regional expressional profiling using isolated GBM samples based on histomorphological features identified regional heterogeneity in five regions (infiltrating tumor, cellular tumor, pseudo-palisading cells around necrosis, leading-edge, and microvascular proliferation) [147]. These five regions were mapped recently to a

proteomic model of three pathways (KRAS-, MYC-, and hypoxia). The KRAS-, MYC-, and hypoxia pathways were identified with three main phenotypes: migration, proliferation, and altered metabolism, respectively [148]. Consequently, building a multi-regional reconstruction for GBM could identify the metabolic regional heterogeneity and vulnerability.

Taken together the choice of the brain model depends on the focus of the study. To study the NDD a bi-cellular model might be more suitable than a whole-brain model that would be more relevant for the interplay between different organs and the brain. The brain models *Thiele2020* and *MartínJiménez2017* can be further contextualized using a context-specific algorithm, expression data, and additional constraints to obtain more specific models. Finally, the data collected in these studies can be included in the reconstruction process of new models.

2.6 Summary and Outlook

Previous GEMs of the brain suffer from many drawbacks that would limit their applications. Nevertheless, the brain tissue GEMs of the whole-body model (*Thiele2020_Harvey* and *Thiele2020_Harvetta*) can be used for building other brain disorder models [97]. While the review covered two works on GBM (*Larsson2020* and Özcan201), GEMs of the LGG are still to be built. Other GEMs for GBM were published after the submission of our review, such as *Tomi-Andrino2022* [149] and *Shen2023* [150]. While *Tomi-Andrino2022* [149] aimed at repositioning preclinical drugs by defining essential reactions, *Shen2023* [150] aimed at defining essential genes correlated with GBM survival. Future GEMs built from temporal or single-cell RNA-Seq could avoid manually defining the various glial and neuron cells, but still, manual curation of the OFs is crucial.

Supplementary Figure and Table Legends

Supplementary File 1 Table S1: Public availability of brain genome-scale metabolic models Supplementary File 1 Table S2: Detailed type of OMICs for the data used in the brain metabolic models and the number of samples. Supplementary File 1 Figure S1: Low overlap between the genes included in the brain genome-scale metabolic models. To evaluate the overlap between the genes of the brain models, the intersection of these genes was counted in an UpSet plot. Brain models were retrieved as explained in Supplementary 1, Table S1, in addition to two consistent generic models (Human1 and Recon3D). For studies that have more than two models (*Baloni2020*, *Larsson2020* and *Lam2021*), the intersection and the union of all the model's genes were appended into two gene lists. The y-axis represents the number of intersected genes between different sets on the x-axis, and the "Set Size" represents

the total number of genes in that set. Supplementary File 2 Table S3: Identified metabolites bypassing the blood-brain barrier in four brain reconstructions from Thiele *et al.,* 2020, Table EV9 and Baloni *et al.*, 2020, Table S12 Supplementary File 2 Table S4: The metabolic composition of the cerebrospinal fluid used in *Thiele2020* model from Thiele *et al.*, 2020, Table EV8 Supplementary File 2 Table S5: Brain-specific core and absent reactions used to build *Thiele2020* model with FASTCORE from Thiele *et al.*, 2020, Table EV1 Supplementary File 2 Table S6: Experimental flux rates used in the astrocyte of *Sertbaş2014* model from Sertbaş et., al 2014, Table 1 Supplementary File 2 Table S7: Experimental flux rates used in the neuron of *Sertbaş2014* model from Sertbaş et., al 2014, Table 1 Supplementary File 2 Table S8: Experimental flux rates used in the *MartínJiménez2017* hypoxic astrocyte model from MartinJimenez *et al.*, 2017, Table 1 Supplementary File 2 Table S9: Constraints used in the *Özcan2016* glioblastoma model from Ozcan *et al.*, 2016, Table 1

Author Contributions:

Conceptualization, A.K., M.P.P. and T.S.; Methodology, A.K. and M.P.P.; Formal Analysis, A.K.; Investigation, A.K., M.P.P. and T.S.; Resources, A.K.; Data Curation, A.K.; Writing—Original Draft Preparation, A.K., M.P.P. and T.S.; Writing—Review Editing, A.K., M.P.P., T.H., L.S., J.P., S.F., S.P.N., T.S.; Visualization, A.K., M.P.P., T.H., and T.S. All authors have read and agreed to the published version of the manuscript.

Declarations of interest:

None

References

[1] I. f. H. Metrics and E. (IHME), *GBDCompareDataVisualization*, Publication Title: IHME, University of Washington (Seattle, WA), 2016.

[2] V. L. Feigin, E. Nichols, T. Alam, *et al.*, "Global, regional, and national burden of neurological disorders, 1990–2016: A systematic analysis for the Global Burden of Disease Study 2016," *The Lancet Neurology*, vol. 18, no. 5, pp. 459–480, May 2019, Publisher: Lancet Publishing Group. DOI: 10.1016/S1474-4422(18)30499-X.

[3] A. S. Kelley, K. McGarry, R. Gorges, and J. S. Skinner, "The burden of health care costs for patients with dementia in the last 5 years of life," *Annals of Internal Medicine*, vol. 163, no. 10, pp. 729–736, Nov. 2015, Publisher: American College of Physicians. DOI: 10.7326/M15-0381.

[4] A. R. UK, *Government's missed opportunity on research funding leaves dementia community disappointed*, Publication Title: Alzheimer's Research UK Blog, 2021.

[5] "World Health Organization. Fact Sheet Cancer. Available online: Https://www.who.int/news-room/fact-sheets/detail/cancer (accessed on 28/02/2022).,"

[6] Q. T. Ostrom, N. Patil, G. Cioffi, K. Waite, C. Kruchko, and J. S. Barnholtz-Sloan, "CBTRUS statistical report: Primary brain and other central nervous system tumors diagnosed in the United States in 2013-2017," *Neuro-Oncology*, vol. 22, no. Supplement_1, pp. IV1–IV96, Oct. 2020, Publisher: Oxford University Press. DOI: 10.1093/NEUONC/NOAA200.

[7] A. F. Tamimi and M. Juweid, "Epidemiology and Outcome of Glioblastoma," in *Glioblastoma*, S. D. Vleeschouwer, Ed., Codon Publications, 2017.

[8] J. H. Garcia, S. Jain, and M. K. Aghi, "Metabolic Drivers of Invasion in Glioblastoma," *Frontiers in Cell and Developmental Biology*, vol. 9, Jul. 2021, Publisher: Frontiers Media S.A. DOI: 10.3389/FCELL.2021.683276.

[9] D. N. Louis, A. Perry, P. Wesseling, *et al.*, "The 2021 WHO classification of tumors of the central nervous system: A summary," *Neuro-Oncology*, vol. 23, no. 8, pp. 1231–1251, Aug. 2021, Publisher: Oxford University Press. DOI: 10.1093/NEUONC/NOAB106.

[10] S. Han, Y. Liu, S. J. Cai, *et al.*, "IDH mutation in glioma: Molecular mechanisms and potential therapeutic targets," *British Journal of Cancer*, vol. 122, no. 11, pp. 1580–1589, May 2020, Publisher: Springer Nature. DOI: 10.1038/S41416-020-0814-X.

[11] K. J. Martin-McGill, A. G. Marson, C. T. Smith, and M. D. Jenkinson, "The Modified Ketogenic Diet in Adults with Glioblastoma: An Evaluation of Feasibility and Deliverability within the National Health Service," *Nutrition and Cancer*, vol. 70, no. 4, pp. 643–649, May 2018, Publisher: Routledge. DOI: 10.1080/01635581.2018.1460677.

[12] S. K. Natarajan and S. Venneti, "Glutamine metabolism in brain tumors," *Cancers*, vol. 11, no. 11, Nov. 2019, Publisher: MDPI AG. DOI: 10.3390/CANCERS11111628.

[13] Z. Bao, K. Chen, S. Krepel, *et al.*, "High Glucose Promotes Human Glioblastoma Cell Growth by Increasing the Expression and Function of Chemoattractant and Growth Factor Receptors," *Translational Oncology*, vol. 12, no. 9, pp. 1155–1163, Sep. 2019, Publisher: Neoplasia Press, Inc. DOI: 10.1016/J.TRANON.2019.04.016.

[14] P. S. Yao, D. Z. Kang, R. Y. Lin, B. Ye, W. Wang, and Z. C. Ye, "Glutamate/glutamine metabolism coupling between astrocytes and glioma cells: Neuroprotection and inhibition of glioma growth," *Biochemical and Biophysical Research Communications*, vol. 450, no. 1, pp. 295–299, Jul. 2014, Publisher: Academic Press Inc. DOI: 10.1016/J.BBRC.2014.05.120.

[15] T. Duraj, N. García-romero, J. Carrión-navarro, *et al.*, "Beyond the warburg effect: Oxidative and glycolytic phenotypes coexist within the metabolic heterogeneity of glioblastoma," *Cells*, vol. 10, no. 2, pp. 1–23, Feb. 2021, Publisher: MDPI. DOI: 10.3390/CELLS10020202.

[16] K. M. Stanke, C. Wilson, and S. Kidambi, "High Expression of Glycolytic Genes in Clinical Glioblastoma Patients Correlates With Lower Survival," *Frontiers in Molecular Biosciences*, vol. 8, Dec. 2021, Publisher: Frontiers Media S.A. DOI: 10.3389/FMOLB.2021.752404.

[17] Y. Qian, P. Ding, J. Xu, X. Nie, and B. Lu, "CCL2 activates AKT signaling to promote glycolysis and chemoresistance in glioma cells," *Cell Biology International*, vol. 46, no. 5, pp. 819–828, May 2022, Publisher: John Wiley and Sons Inc. DOI: 10.1002/CBIN.11778.

[18] L. Jin and Y. Zhou, "Crucial role of the pentose phosphate pathway in malignant tumors (review)," *Oncology Letters*, vol. 17, no. 5, pp. 4213–4221, May 2019, Publisher: Spandidos Publications. DOI: 10.3892/OL.2019.10112/DOWNLOAD.

[19] L. Garofano, S. Migliozzi, Y. T. Oh, *et al.*, "Pathway-based classification of glioblastoma uncovers a mitochondrial subtype with therapeutic vulnerabilities," *Nature Cancer*, vol. 2, no. 2, pp. 141–156, Feb. 2021, Publisher: Nature Research. DOI: 10.1038/S43018-020-00159-4.

[20] T. Johung and M. Monje, "Neuronal activity in the glioma microenvironment," *Current Opinion in Neurobiology*, vol. 47, pp. 156–161, Dec. 2017, Publisher: Elsevier Ltd. DOI: 10.1016/J.CONB.2017.10.009.

[21] F. Fack, S. Tardito, G. Hochart, *et al.*, "Altered metabolic landscape in IDH -mutant gliomas affects phospholipid, energy, and oxidative stress pathways," *EMBO Molecular Medicine*, vol. 9, no. 12, pp. 1681–1695, Dec. 2017, Publisher: EMBO. DOI: 10.15252/EMMM.201707729.

[22] M. Chiu, G. Taurino, M. G. Bianchi, *et al.*, "Oligodendroglioma cells lack glutamine synthetase and are auxotrophic for glutamine, but do not depend on glutamine anaplerosis for growth," *International Journal of Molecular Sciences*, vol. 19, no. 4, Apr. 2018, Publisher: MDPI AG. DOI: 10.3390/IJMS19041099.

[23] E. A. El-Habr, L. G. Dubois, F. Burel-Vandenbos, *et al.*, "A driver role for GABA metabolism in controlling stem and proliferative cell state through GHB production in glioma," *Acta Neuropathologica*, vol. 133, no. 4, pp. 645–660, Apr. 2017, Publisher: Springer Verlag. DOI: 10.1007/S00401-016-1659-5.

[24] A. Blanchart, R. Fernando, M. Häring, *et al.*, "Endogenous GAB AA receptor activity suppresses glioma growth," *Oncogene*, vol. 36, no. 6, pp. 777–786, Feb. 2017, Publisher: Nature Publishing Group. DOI: 10.1038/ONC.2016.245.

[25] P. Mulica, A. Grünewald, and S. L. Pereira, "Astrocyte-Neuron Metabolic Crosstalk in Neurodegeneration: A Mitochondrial Perspective," *Frontiers in Endocrinology*, vol. 12, May 2021, Publisher: Frontiers Media S.A. DOI: 10.3389/FENDO.2021.668517.

[26] B. Taïb, A. M. Aboussalah, M. Moniruzzaman, *et al.*, "Lipid accumulation and oxidation in glioblastoma multiforme," *Scientific Reports*, vol. 9, no. 1, Dec. 2019, Publisher: Nature Research. DOI: 10.1038/S41598-019-55985-Z.

[27] I. Marin-Valencia, C. Yang, T. Mashimo, *et al.*, "Analysis of tumor metabolism reveals mitochondrial glucose oxidation in genetically diverse human glioblastomas in the mouse brain in vivo," *Cell Metabolism*, vol. 15, no. 6, pp. 827–837, Jun. 2012. DOI: 10.1016/J.CMET.2012.05.001.

[28] C. Peña-Bautista, M. Vento, M. Baquero, and C. Cháfer-Pericás, "Lipid peroxidation in neurodegeneration," *Clinica Chimica Acta*, vol. 497, pp. 178–188, Oct. 2019, Publisher: Elsevier B.V. DOI: 10.1016/J.CCA.2019.07.037.

[29] A. Virtuoso, R. Giovannoni, C. D. Luca, *et al.*, "The glioblastoma microenvironment: Morphology, metabolism, and molecular signature of glial dynamics to discover metabolic rewiring sequence," *International Journal of Molecular Sciences*, vol. 22, no. 7, Apr. 2021, Publisher: MDPI AG. DOI: 10.3390/IJMS22073301.

[30] D. H. Heiland, V. M. Ravi, S. P. Behringer, *et al.*, "Tumor-associated reactive astrocytes aid the evolution of immunosuppressive environment in glioblastoma," *Nature Communications*, vol. 10, no. 1, Dec. 2019, Publisher: Nature Publishing Group. DOI: 10.1038/S41467-019-10493-6.

[31] F. Ahmad, Q. Sun, D. Patel, and J. M. Stommel, "Cholesterol metabolism: A potential therapeutic target in glioblastoma," *Cancers*, vol. 11, no. 2, Jan. 2019, Publisher: MDPI AG. DOI: 10.3390/CANCERS11020146.

[32] J. M. Dietschy and S. D. Turley, "Cholesterol metabolism in the central nervous system during early development and in the mature animal," *Journal of Lipid Research*, vol. 45, no. 8, pp. 1375–1397, 2004, Publisher: Lipid Research Inc. DOI: 10.1194/JLR.R400004-JLR200.

[33] Z. Qiu, W. Yuan, T. Chen, *et al.*, "HMGCR positively regulated the growth and migration of glioblastoma cells," *Gene*, vol. 576, no. 1, pp. 22–27, Jan. 2016, Publisher: Elsevier B.V. DOI: 10.1016/J.GENE.2015.09.067.

[34] D. M. Kambach, A. S. Halim, A. G. Cauer, *et al.*, "Disabled cell density sensing leads to dysregulated cholesterol synthesis in glioblastoma," *Oncotarget*, vol. 8, no. 9, pp. 14 860–14 875, 2017, Publisher: Impact Journals LLC. DOI: 10.18632/ONCOTARGET.14740.

[35] X. Wang, Z. Huang, Q. Wu, *et al.*, "MYC-regulated mevalonate metabolism maintains brain tumor–initiating cells," *Cancer Research*, vol. 77, no. 18, pp. 4947–4960, Sep. 2017, Publisher: American Association for Cancer Research Inc. DOI: 10.1158/0008-5472.CAN-17-0114.

[36] H. Y. Kim, D. K. Kim, S. H. Bae, *et al.*, "Farnesyl diphosphate synthase is important for the maintenance of glioblastoma stemness," *Experimental and Molecular Medicine*, vol. 50, no. 10, Oct. 2018, Publisher: Nature Publishing Group. DOI: 10.1038/S12276-018-0166-2.

[37] L. Pirmoradi, N. Seyfizadeh, S. Ghavami, A. A. Zeki, and S. Shojaei, "Targeting cholesterol metabolism in glioblastoma: A new therapeutic approach in cancer therapy," *Journal of Investigative Medicine*, vol. 67, no. 4, pp. 715–719, Apr. 2019, Publisher: BMJ Publishing Group. DOI: 10.1136/JIM-2018-000962.

[38] G. R. Villa, J. J. Hulce, C. Zanca, *et al.*, "An LXR-Cholesterol Axis Creates a Metabolic Co-Dependency for Brain Cancers," *Cancer Cell*, vol. 30, no. 5, pp. 683–693, Nov. 2016, Publisher: Cell Press. DOI: 10.1016/J.CCELL.2016.09.008.

[39] R. Yang, Y. Zhao, Y. Gu, *et al.*, "Isocitrate dehydrogenase 1 mutation enhances 24(S)-hydroxycholesterol production and alters cholesterol homeostasis in glioma," *Oncogene*, vol. 39, no. 40, pp. 6340–6353, Oct. 2020, Publisher: Springer Nature. DOI: 10.1038/S41388-020-01439-0.

[40] B. Juraszek, J. Czarnecka-Herok, and K. A. Nałęcz, "Glioma cells survival depends both on fatty acid oxidation and on functional carnitine transport by SLC22A5," *Journal of Neurochemistry*, vol. 156, no. 5, pp. 642–657, Mar. 2021, Publisher: John Wiley and Sons Inc. DOI: 10.1111/JNC.15124.

[41] E. Kolar, X. Shi, E. Clay, *et al.*, "Very long-chain acyl-CoA synthetase 3 mediates onco-sphingolipid metabolism in malignant glioma," *Medical Research Archives*, vol. 9, no. 5, 2021, Publisher: Knowledge Enterprise Journals. DOI: 10.18103/MRA.V9I5.2433.

[42] T. T. T. Nguyen, E. Shang, C. Shu, *et al.*, "Aurora kinase A inhibition reverses the Warburg effect and elicits unique metabolic vulnerabilities in glioblastoma," *Nature Communications*, vol. 12, no. 1, Dec. 2021, Publisher: Nature Research. DOI: 10.1038/S41467-021-25501-X.

[43] G. Menna, P. P. Mattogno, C. M. Donzelli, L. Lisi, A. Olivi, and G. M. D. Pepa, "Glioma-Associated Microglia Characterization in the Glioblastoma Microenvironment through A 'Seed-and Soil' Approach: A Systematic Review," *Brain Sciences*, vol. 12, no. 6, Jun. 2022, Publisher: MDPI. DOI: 10.3390/BRAINSCI12060718.

[44] A. S. Saab, I. D. Tzvetanova, and K. A. Nave, "The role of myelin and oligodendrocytes in axonal energy metabolism," *Current Opinion in Neurobiology*, vol. 23, no. 6, pp. 1065–1072, Dec. 2013. DOI: 10.1016/J.CONB.2013.09.008.

[45] T. Kawashima, M. Yashiro, H. Kasashima, *et al.*, "Oligodendrocytes up-regulate the invasive activity of glioblastoma cells via the angiopoietin-2 signaling pathway," *Anticancer Research*, vol. 39, no. 2, pp. 577–584, Feb. 2019, Publisher: International Institute of Anticancer Research. DOI: 10.21873/ANTICANRES.13150.

[46] S. A. Wolf, H. W. G. M. Boddeke, and H. Kettenmann, "Microglia in Physiology and Disease," *Annual Review of Physiology*, vol. 79, pp. 619–643, Feb. 2017, Publisher: Annual Reviews Inc. DOI: 10.1146/ANNUREV-PHYSIOL-022516-034406.

[47] D. A. Menassa and D. Gomez-Nicola, "Microglial dynamics during human brain development," *Frontiers in Immunology*, vol. 9, no. MAY, May 2018, Publisher: Frontiers Media S.A. DOI: 10.3389/FIMMU.2018.01014/PDF.

[48] N. Lannes, E. Eppler, S. Etemad, P. Yotovski, and L. Filgueira, "Microglia at center stage: A comprehensive review about the versatile and unique residential macrophages of the central nervous system," *Oncotarget*, vol. 8, no. 69, pp. 114 393–114 413, 2017, Publisher: Impact Journals LLC. DOI: 10.18632/ONCOTARGET.23106.

[49] J. Yin, K. L. Valin, M. L. Dixon, and J. W. Leavenworth, "The Role of Microglia and Macrophages in CNS Homeostasis, Autoimmunity, and Cancer," *Journal of Immunology Research*, vol. 2017, 2017, Publisher: Hindawi Limited. DOI: 10.1155/2017/5150678.

[50] D. G. Walker and L. F. Lue, "Immune phenotypes of microglia in human neurodegenerative disease: Challenges to detecting microglial polarization in human brains," *Alzheimer's Research and Therapy*, vol. 7, no. 1, Aug. 2015, Publisher: BioMed Central Ltd. DOI: 10.1186/S13195-015-0139-9.

[51] R. Orihuela, C. A. McPherson, and G. J. Harry, "Microglial M1/M2 polarization and metabolic states," *British Journal of Pharmacology*, vol. 173, no. 4, pp. 649–665, Feb. 2016, Publisher: John Wiley and Sons Inc. DOI: 10.1111/BPH.13139.

[52] M. Prosniak, L. A. Harshyne, D. W. Andrews, *et al.*, "Glioma grade is associated with the accumulation and activity of cells bearing M2 monocyte markers," *Clinical Cancer Research*, vol. 19, no. 14, pp. 3776–3786, Jul. 2013. DOI: 10.1158/1078-0432.CCR-12-1940.

[53] M. Martinez-Lage, T. M. Lynch, Y. Bi, *et al.*, "Immune landscapes associated with different glioblastoma molecular subtypes," *Acta Neuropathologica Communications*, vol. 7, no. 1, Nov. 2019, Publisher: BioMed Central Ltd. DOI: 10.1186/S40478-019-0803-6.

[54] M. Sielska, P. Przanowski, B. Wylot, *et al.*, "Distinct roles of CSF family cytokines in macrophage infiltration and activation in glioma progression and injury response," *Journal of Pathology*, vol. 230, no. 3, pp. 310–321, Jul. 2013. DOI: 10.1002/PATH.4192.

[55] V. Kumar, N. Sami, T. Kashav, A. Islam, F. Ahmad, and M. I. Hassan, "Protein aggregation and neurodegenerative diseases: From theory to therapy," *European Journal of Medicinal Chemistry*, vol. 124, pp. 1105–1120, 2016, Publisher: Elsevier Masson SAS. DOI: 10.1016/J.EJMECH.2016.07.054.

[56] S. Grimm, A. Hoehn, K. J. Davies, and T. Grune, "Protein oxidative modifications in the ageing brain: Consequence for the onset of neurodegenerative disease," *Free Radical Research*, vol. 45, no. 1, pp. 73–88, Jan. 2011. DOI: 10.3109/10715762.2010.512040.

[57] T. L. Spires-Jones, J. Attems, and D. R. Thal, "Interactions of pathological proteins in neurodegenerative diseases," *Acta Neuropathologica*, vol. 134, no. 2, pp. 187–205, Aug. 2017, Publisher: Springer Verlag. DOI: 10.1007/S00401-017-1709-7.

[58] M. L. Cooper, S. Pasini, W. S. Lambert, *et al.*, "Redistribution of metabolic resources through astrocyte networks mitigates neurodegenerative stress," *Proceedings of the National Academy of Sciences of the United States of America*, vol. 117, no. 31, pp. 18 810–18 821, Aug. 2020, Publisher: National Academy of Sciences. DOI: 10.1073/PNAS.2009425117.

[59] H. Phatnani and T. Maniatis, "Astrocytes in neurodegenerative disease," *Cold Spring Harbor Perspectives in Biology*, vol. 7, no. 6, pp. 1–18, 2015, Publisher: Cold Spring Harbor Laboratory Press. DOI: 10.1101/CSHPERSPECT.A020628.

[60] G. J. Duncan, T. J. Simkins, and B. Emery, "Neuron-Oligodendrocyte Interactions in the Structure and Integrity of Axons," *Frontiers in Cell and Developmental Biology*, vol. 9, Mar. 2021, Publisher: Frontiers Media S.A. DOI: 10.3389/FCELL.2021.653101.

[61] S. Hickman, S. Izzy, P. Sen, L. Morsett, and J. E. Khoury, "Microglia in neurodegeneration," *Nature Neuroscience*, vol. 21, no. 10, pp. 1359–1369, Oct. 2018, Publisher: Nature Publishing Group. DOI: 10.1038/S41593-018-0242-X.

[62] E. Janda, L. Boi, and A. R. Carta, "Microglial phagocytosis and its regulation: A therapeutic target in parkinson's disease?" *Frontiers in Molecular Neuroscience*, vol. 11, Apr. 2018, Publisher: Frontiers Media S.A. DOI: 10.3389/FNMOL.2018.00144/PDF.

[63] G. J. Song and K. Suk, "Pharmacological modulation of functional phenotypes of microglia in neurodegenerative diseases," *Frontiers in Aging Neuroscience*, vol. 9, no. MAY, May 2017, Publisher: Frontiers Media S.A. DOI: 10.3389/FNAGI.2017.00139/PDF.

[64] B. Zhang, Y. Z. Wei, G. Q. Wang, D. D. Li, J. S. Shi, and F. Zhang, "Targeting MAPK pathways by naringenin modulates microglia M1/M2 polarization in lipopolysaccharide-stimulated cultures," *Frontiers in Cellular Neuroscience*, vol. 12, Jan. 2019, Publisher: Frontiers Media S.A. DOI: 10.3389/FNCEL.2018.00531/PDF.

[65] R. Han, J. Liang, and B. Zhou, "Glucose metabolic dysfunction in neurodegenerative diseases—new mechanistic insights and the potential of hypoxia as a prospective therapy targeting metabolic reprogramming," *International Journal of Molecular Sciences*, vol. 22, no. 11, Jun. 2021, Publisher: MDPI. DOI: 10.3390/IJMS22115887.

[66] L. G. d. Oliveira, Y. d. S. Angelo, A. H. Iglesias, and J. P. S. Peron, "Unraveling the Link Between Mitochondrial Dynamics and Neuroinflammation," *Frontiers in Immunology*, vol. 12, Mar. 2021, Publisher: Frontiers Media S.A. DOI: 10.3389/FIMMU.2021.624919.

[67] J. M. Bourgognon and J. R. Steinert, "The metabolome identity: Basis for discovery of biomarkers in neurodegeneration," *Neural Regeneration Research*, vol. 14, no. 3, pp. 387–390, Mar. 2019, Publisher: Wolters Kluwer Medknow Publications. DOI: 10.4103/1673-5374.245464.

[68] M. P. Pacheco, T. Bintener, D. Ternes, *et al.*, "Identifying and targeting cancer-specific metabolism with network-based drug target prediction," *EBioMedicine*, vol. 43, pp. 98–106, May 2019, Publisher: Elsevier B.V. DOI: 10.1016/J.EBIOM.2019.04.046.

[69] B. Turanli, C. Zhang, W. Kim, *et al.*, "Discovery of therapeutic agents for prostate cancer using genome-scale metabolic modeling and drug repositioning," *EBioMedicine*, vol. 42, pp. 386–396, Apr. 2019, Publisher: Elsevier B.V. DOI: 10.1016/J.EBIOM.2019.03.009.

[70] J. Hertel, A. C. Harms, A. Heinken, *et al.*, "Integrated Analyses of Microbiome and Longitudinal Metabolome Data Reveal Microbial-Host Interactions on Sulfur Metabolism in Parkinson's Disease," *Cell Reports*, vol. 29, no. 7, 1767–1777.e8, Nov. 2019, Publisher: Elsevier B.V. DOI: 10.1016/J.CELREP.2019.10.035.

[71] F. Baldini, J. Hertel, E. Sandt, *et al.*, "Parkinson's disease-associated alterations of the gut microbiome predict disease-relevant changes in metabolic functions," *BMC Biology*, vol. 18, no. 1, Jun. 2020, Publisher: BioMed Central Ltd. DOI: 10.1186/S12915-020-00775-7.

[72] S. T. R. Moolamalla and P. K. Vinod, "Genome-scale metabolic modelling predicts biomarkers and therapeutic targets for neuropsychiatric disorders," *Computers in Biology and Medicine*, vol. 125, Oct. 2020, Publisher: Elsevier Ltd. DOI: 10.1016/J.COMPBIOMED.2020.103994.

[73] A. Bayraktar, S. Lam, O. Altay, *et al.*, "Revealing the molecular mechanisms of alzheimer's disease based on network analysis," *International Journal of Molecular Sciences*, vol. 22, no. 21, Nov. 2021, Publisher: MDPI. DOI: 10.3390/IJMS222111556.

[74] T. Cakir, C. S. Tacer, and K. O. Ulgen, "Metabolic pathway analysis of enzyme-deficient human red blood cells.," *Bio Systems*, vol. 78, no. 1-3, pp. 49–67, Dec. 2004. DOI: 10.1016/j.biosystems.2004.06.004.

[75] M. D. Sweeney, Z. Zhao, A. Montagne, A. R. Nelson, and B. V. Zlokovic, "Blood-brain barrier: From physiology to disease and back," *Physiological Reviews*, vol. 99, no. 1, pp. 21–78, Jan. 2019, Publisher: American Physiological Society. DOI: 10.1152/PHYSREV.00050.2017.

[76] Y. Pan and J. A. Nicolazzo, "Impact of aging, Alzheimer's disease and Parkinson's disease on the blood-brain barrier transport of therapeutics," *Advanced Drug Delivery Reviews*, vol. 135, pp. 62–74, Oct. 2018, Publisher: Elsevier B.V. DOI: 10.1016/J.ADDR.2018.04.009.

[77] L. R. Rich, W. Harris, and A. M. Brown, "The Role of Brain Glycogen in Supporting Physiological Function," *Frontiers in Neuroscience*, vol. 13, Nov. 2019, Publisher: Frontiers Media S.A. DOI: 10.3389/FNINS.2019.01176.

[78] P. J. Magistretti and I. Allaman, "Lactate in the brain: From metabolic end-product to signalling molecule," *Nature Reviews Neuroscience*, vol. 19, no. 4, pp. 235–249, Apr. 2018, Publisher: Nature Publishing Group. DOI: 10.1038/NRN.2018.19.

[79] N. Vlassis, M. P. Pacheco, and T. Sauter, "Fast Reconstruction of Compact Context-Specific Metabolic Network Models," *PLoS Computational Biology*, vol. 10, no. 1, 2014, Publisher: Public Library of Science. DOI: 10.1371/JOURNAL.PCBI.1003424.

[80] M. P. Pacheco, E. John, T. Kaoma, *et al.*, "Integrated metabolic modelling reveals cell-type specific epigenetic control points of the macrophage metabolic network," *BMC Genomics*, vol. 16, no. 1, Oct. 2015, Publisher: BioMed Central Ltd. DOI: 10.1186/S12864-015-1984-4.

[81] S. A. Becker and B. O. Palsson, "Context-specific metabolic networks are consistent with experiments," *PLoS Computational Biology*, vol. 4, no. 5, 2008, Publisher: Public Library of Science. DOI: 10.1371/JOURNAL.PCBI.1000082.

[82] Y. Wang, J. A. Eddy, and N. D. Price, "Reconstruction of genome-scale metabolic models for 126 human tissues using mCADRE," *BMC Systems Biology*, vol. 6, Dec. 2012. DOI: 10.1186/1752-0509-6-153.

[83] K. Yizhak, E. Gaude, S. L. Dévédec, *et al.*, "Phenotype-based cell-specific metabolic modeling reveals metabolic liabilities of cancer," *eLife*, vol. 3, no. November, pp. 1–23, Nov. 2014, Publisher: eLife Sciences Publications Ltd. DOI: 10.7554/ELIFE.03641.

[84] H. Zur, E. Ruppin, and T. Shlomi, "iMAT: An integrative metabolic analysis tool," *Bioinformatics*, vol. 26, no. 24, pp. 3140–3142, Dec. 2010. DOI: 10.1093/BIOINFORMATICS/BTQ602.

[85] S. Robaina-Estévez and Z. Nikoloski, "On the effects of alternative optima in context-specific metabolic model predictions," *PLoS Computational Biology*, vol. 13, no. 5, C. A. Ouzounis, Ed., e1005568, May 2017, ISBN: 1111111111. DOI: 10.1371/journal.pcbi.1005568.

[86] R. Agren, A. Mardinoglu, A. Asplund, C. Kampf, M. Uhlen, and J. Nielsen, "Identification of anticancer drugs for hepatocellular carcinoma through personalized genome-scale metabolic modeling," *Molecular Systems Biology*, vol. 10, no. 3, 2014, Publisher: Blackwell Publishing Ltd. DOI: 10.1002/MSB.145122.

[87] R. Jolivet, I. Allaman, L. Pellerin, P. J. Magistretti, and B. Weber, "Comment on recent modeling studies of astrocyte-neuron metabolic interactions," *Journal of Cerebral Blood Flow and Metabolism*, vol. 30, no. 12, pp. 1982–1986, Dec. 2010. DOI: 10.1038/JCBFM.2010.132.

[88] L. Heirendt, S. Arreckx, T. Pfau, *et al.*, "Creation and analysis of biochemical constraint-based models using the COBRA Toolbox v.3.0," *Nature Protocols*, vol. 14, no. 3, pp. 639–702, Mar. 2019, Publisher: Nature Publishing Group. DOI: 10.1038/S41596-018-0098-2.

[89] E. Sjöstedt, W. Zhong, L. Fagerberg, *et al.*, "An atlas of the protein-coding genes in the human, pig, and mouse brain," *Science*, vol. 367, no. 6482, eaay5947, 2020.

[90] M. Uhlén, L. Fagerberg, B. M. Hallström, *et al.*, "Tissue-based map of the human proteome," *Science*, vol. 347, no. 6220, Jan. 2015, Publisher: American Association for the Advancement of Science. DOI: 10.1126/SCIENCE.1260419.

[91] N. E. Lewis, G. Schramm, A. Bordbar, *et al.*, "Large-scale in silico modeling of metabolic interactions between cell types in the human brain," *Nature Biotechnology*, vol. 28, no. 12, pp. 1279–1285, Dec. 2010. DOI: 10.1038/NBT.1711.

[92] N. C. Duarte, S. A. Becker, N. Jamshidi, *et al.*, "Global reconstruction of the human metabolic network based on genomic and bibliomic data," *Proceedings of the National Academy of Sciences of the United States of America*, vol. 104, no. 6, pp. 1777–1782, Feb. 2007. DOI: 10.1073/PNAS.0610772104.

[93] M. Sertbaş, K. Ülgen, and T. Çakir, "Systematic analysis of transcription-level effects of neurodegenerative diseases on human brain metabolism by a newly reconstructed brain-specific metabolic network," *FEBS Open Bio*, vol. 4, pp. 542–553, 2014, Publisher: Elsevier. DOI: 10.1016/J.FOB.2014.05.006.

[94] E. Özcan and T. Çakir, "Reconstructed metabolic network models predict flux-level metabolic reprogramming in glioblastoma," *Frontiers in Neuroscience*, vol. 10, no. APR, Apr. 2016, Publisher: Frontiers Media S.A. DOI: 10.3389/FNINS.2016.00156/PDF.

[95] C. A. Martín-Jiménez, D. Salazar-Barreto, G. E. Barreto, and J. González, "Genome-scale reconstruction of the human astrocyte metabolic network," *Frontiers in Aging Neuroscience*, vol. 9, no. FEB, Feb. 2017, Publisher: Frontiers Research Foundation. DOI: 10.3389/FNAGI.2017.00023.

[96] N. Pornputtapong, I. Nookaew, and J. Nielsen, "Human metabolic atlas: An online resource for human metabolism," *Database*, vol. 2015, 2015, Publisher: Oxford University Press. DOI: 10.1093/DATABASE/BAV068.

[97] I. Thiele, S. Sahoo, A. Heinken, *et al.*, "Personalized whole-body models integrate metabolism, physiology, and the gut microbiome," *Molecular Systems Biology*, vol. 16, no. 5, May 2020, Publisher: EMBO. DOI: 10.15252/MSB.20198982.

[98] E. Brunk, S. Sahoo, D. C. Zielinski, *et al.*, "Recon3D enables a three-dimensional view of gene variation in human metabolism," *Nature Biotechnology*, vol. 36, no. 3, pp. 272–281, Mar. 2018, Publisher: Nature Publishing Group. DOI: 10.1038/NBT.4072.

[99] D. S. Wishart, Y. D. Feunang, A. Marcu, *et al.*, "HMDB 4.0: The human metabolome database for 2018," *Nucleic Acids Research*, vol. 46, no. D1, pp. D608–D617, Jan. 2018, Publisher: Oxford University Press. DOI: 10.1093/NAR/GKX1089.

[100] P. Baloni, C. C. Funk, J. Yan, *et al.*, "Metabolic Network Analysis Reveals Altered Bile Acid Synthesis and Metabolism in Alzheimer's Disease," *Cell Reports Medicine*, vol. 1, no. 8, Nov. 2020, Publisher: Cell Press. DOI: 10.1016/J.XCRM.2020.100138.

[101] O. Y. Echeverri-Peña, D. A. Salazar-Barreto, A. Rodríguez-Lopez, *et al.*, "Use of a neuron-glia genome-scale metabolic reconstruction to model the metabolic consequences of the Arylsulphatase a deficiency through a systems biology approach," *Heliyon*, vol. 7, no. 7, Jul. 2021, Publisher: Elsevier Ltd. DOI: 10.1016/J.HELIYON.2021.E07671.

[102] I. Thiele, N. Swainston, R. M. T. Fleming, *et al.*, "A community-driven global reconstruction of human metabolism," *Nature Biotechnology*, vol. 31, no. 5, pp. 419–425, May 2013. DOI: 10.1038/NBT.2488.

[103] T. Shlomi, M. N. Cabili, M. J. Herrgård, B. Ø. Palsson, E. Ruppin, and E. P. B. Ø. Ruppin, "Network-based prediction of human tissue-specific metabolism," *Nature Biotechnology*, vol. 26, no. 9, pp. 1003–1010, Sep. 2008, ISBN: 1546169610870156. DOI: 10.1038/nbt.1487.

[104] S. Lam, N. Hartmann, R. Benfeitas, *et al.*, "Systems Analysis Reveals Ageing-Related Perturbations in Retinoids and Sex Hormones in Alzheimer's and Parkinson's Diseases," *Biomedicines*, vol. 9, no. 10, p. 1310, 2021. DOI: 10.3390/biomedicines9101310.

[105] H. Wang, S. Marcišauskas, B. J. Sánchez, *et al.*, "RAVEN 2.0: A versatile toolbox for metabolic network reconstruction and a case study on Streptomyces coelicolor," *PLOS Computational Biology*, vol. 14, no. 10, e1006541, 2018. DOI: 10.1371/journal.pcbi.1006541.

[106] A. Mardinoglu, R. Agren, C. Kampf, *et al.*, "Integration of clinical data with a genome-scale metabolic model of the human adipocyte," *Molecular systems biology*, vol. 9, no. 1, p. 649, Apr. 2013, ISBN: 1744-4292 (Electronic)\r1744-4292 (Linking) Publisher: EMBO Press. DOI: 10.1038/msb.2013.5.

[107] A. Mardinoglu, R. Agren, C. Kampf, A. Asplund, M. Uhlen, and J. Nielsen, "Genome-scale metabolic modelling of hepatocytes reveals serine deficiency in patients with non-alcoholic fatty liver disease," *Nature Communications*, vol. 5, Jan. 2014, Publisher: Nature Publishing Group. DOI: 10.1038/NCOMMS4083.

[108] I. Larsson, M. Uhlén, C. Zhang, and A. Mardinoglu, "Genome-Scale Metabolic Modeling of Glioblastoma Reveals Promising Targets for Drug Development," *Frontiers in Genetics*, vol. 11, Apr. 2020, Publisher: Frontiers Media S.A. DOI: 10.3389/FGENE.2020.00381.

[109] M. Uhlen, C. Zhang, S. Lee, *et al.*, "A pathology atlas of the human cancer transcriptome," *Science*, vol. 357, no. 6352, eaan2507, Aug. 2017, ISBN: 1095-9203 (Electronic) 0036-8075 (Linking). DOI: 10.1126/science.aan2507.

[110] C. W. Brennan, R. G. W. Verhaak, A. McKenna, *et al.*, "The Somatic Genomic Landscape of Glioblastoma," *Cell*, vol. 155, no. 2, pp. 462–477, 2013. DOI: 10.1016/j.cell.2013.09.034.

[111] C. Zhang, B. Ji, A. Mardinoglu, J. Nielsen, and Q. Hua, "Logical transformation of genome-scale metabolic models for gene level applications and analysis," *Bioinformatics (Oxford, England)*, vol. 31, no. 14, pp. 2324–2331, 2015. DOI: 10.1093/bioinformatics/btv134.

[112] T. S. K. Prasad, R. Goel, K. Kandasamy, *et al.*, "Human Protein Reference Database—2009 update," *Nucleic Acids Research*, vol. 37, no. Database issue, pp. D767–D772, 2009. DOI: 10.1093/nar/gkn892.

[113] Y. Fujii, T. Imanishi, and T. Gojobori, "[H-Invitational Database: Integrated database of human genes]," *Tanpakushitsu Kakusan Koso. Protein, Nucleic Acid, Enzyme*, vol. 49, no. 11 Suppl, pp. 1937–1943, 2004.

[114] K. A. Reidegeld, M. Müller, C. Stephan, *et al.*, "The power of cooperative investigation: Summary and comparison of the HUPO Brain Proteome Project pilot study results," *Proteomics*, vol. 6, no. 18, pp. 4997–5014, 2006. DOI: 10.1002/pmic.200600305.

[115] T. Çakır, S. Alsan, H. Saybaşılı, A. Akın, and K. Ö. Ülgen, "Reconstruction and flux analysis of coupling between metabolic pathways of astrocytes and neurons: Application to cerebral hypoxia," *Theoretical Biology and Medical Modelling*, vol. 4, no. 1, pp. 1–18, 2007.

[116] M.-S. Kim, S. M. Pinto, D. Getnet, *et al.*, "A draft map of the human proteome," *Nature*, vol. 509, no. 7502, pp. 575–581, 2014. DOI: 10.1038/nature13302.

[117] K. G. Ardlie, D. S. DeLuca, A. V. Segrè, *et al.*, "The Genotype-Tissue Expression (GTEx) pilot analysis: Multitissue gene regulation in humans," *Science*, vol. 348, no. 6235, pp. 648–660, May 2015, ISBN: 0036-8075. DOI: 10.1126/science.1262110.

[118] M. Lizio, I. Abugessaisa, S. Noguchi, *et al.*, "Update of the FANTOM web resource: Expansion to provide additional transcriptome atlases," *Nucleic Acids Research*, vol. 47, no. D1, pp. D752–D758, Jan. 2019. DOI: 10.1093/nar/gky1099.

[119] A. P. Rajkumar, G. Bidkhori, S. Shoaie, *et al.*, "Postmortem Cortical Transcriptomics of Lewy Body Dementia Reveal Mitochondrial Dysfunction and Lack of Neuroinflammation," *The American Journal of Geriatric Psychiatry: Official Journal of the American Association for Geriatric Psychiatry*, vol. 28, no. 1, pp. 75–86, 2020. DOI: 10.1016/j.jagp.2019.06.007.

[120] Y. Zhang, M. James, F. A. Middleton, and R. L. Davis, "Transcriptional analysis of multiple brain regions in Parkinson's disease supports the involvement of specific protein processing, energy metabolism, and signaling pathways, and suggests novel disease mechanisms," *American Journal of Medical Genetics. Part B, Neuropsychiatric Genetics: The Official Publication of the International Society of Psychiatric Genetics*, vol. 137B, no. 1, pp. 5–16, 2005. DOI: 10.1002/ajmg.b.30195.

[121] B. Zheng, Z. Liao, J. J. Locascio, *et al.*, "PGC-1, A Potential Therapeutic Target for Early Intervention in Parkinson's Disease," *Science translational medicine*, vol. 2, no. 52, 52ra73, 2010. DOI: 10.1126/scitranslmed.3001059.

[122] S. Mostafavi, C. Gaiteri, S. E. Sullivan, *et al.*, "A molecular network of the aging human brain provides insights into the pathology and cognitive decline of Alzheimer's disease," *Nature Neuroscience*, vol. 21, no. 6, pp. 811–819, Jun. 2018. DOI: 10.1038/s41593-018-0154-9.

[123] R. M. Meyers, J. G. Bryan, J. M. McFarland, *et al.*, "Computational correction of copy-number effect improves specificity of CRISPR-Cas9 essentiality screens in cancer cells," *Nature genetics*, vol. 49, no. 12, pp. 1779–1784, 2017. DOI: 10.1038/ng.3984.

[124] Y. Pirahanchi, R. Jessu, and N. R. Aeddula, "Physiology, Sodium Potassium Pump," in *StatPearls*, StatPearls Publishing, 2022.

[125] R. Baumeister, C. T. Murphy, and T. Heimbucher, "Metabolic adaptation to hypoxia: Do worms and cancer cells share common metabolic responses to hypoxic stress?" *Cell Death and Differentiation*, vol. 28, no. 4, pp. 1434–1436, 2021. DOI: 10.1038/s41418-021-00741-y.

[126] E. Favaro, K. Bensaad, M. G. Chong, *et al.*, "Glucose utilization via glycogen phosphorylase sustains proliferation and prevents premature senescence in cancer cells," *Cell Metabolism*, vol. 16, no. 6, pp. 751–764, 2012. DOI: 10.1016/j.cmet.2012.10.017.

[127] Y. Fu, G. Bu, T. Kanekiyo, and J. Zhao, "Counteracting Alzheimer's disease via somatic TERT activation," *Nature Aging*, vol. 1, no. 12, pp. 1081–1082, 2021. DOI: 10.1038/s43587-021-00145-0.

[128] T. Pfau, M. P. Pacheco, and T. Sauter, "Towards improved genome-scale metabolic network reconstructions: Unification, transcript specificity and beyond," *Briefings in Bioinformatics*, vol. 17, no. 6, pp. 1060–1069, Nov. 2016, ISBN: 1477-4054 (Electronic) 1467-5463 (Linking). DOI: 10.1093/bib/bbv100.

[129] N. Pham, R. G. A. v. Heck, J. C. J. v. Dam, P. J. Schaap, E. Saccenti, and M. Suarez-Diez, "Consistency, Inconsistency, and Ambiguity of Metabolite Names in Biochemical Databases Used for Genome-Scale Metabolic Modelling," *Metabolites*, vol. 9, no. 2, p. 28, 2019. DOI: 10.3390/metabo9020028.

[130] S. Opdam, A. Richelle, B. Kellman, S. Li, D. C. Zielinski, and N. E. Lewis, "A Systematic Evaluation of Methods for Tailoring Genome-Scale Metabolic Models," *Cell Systems*, pp. 1–12, Feb. 2017, Publisher: Elsevier Inc. DOI: 10.1016/j.cels.2017.01.010.

[131] C. Lieven, M. E. Beber, B. G. Olivier, *et al.*, "MEMOTE for standardized genome-scale metabolic model testing," *Nature Biotechnology*, vol. 38, no. 3, pp. 272–276, Mar. 2020. DOI: 10.1038/s41587-020-0446-y.

[132] J. L. Robinson, P. Kocabaş, H. Wang, *et al.*, "An atlas of human metabolism," *Science Signaling*, vol. 13, no. 624, Mar. 2020, Publisher: American Association for the Advancement of Science. DOI: 10.1126/SCISIGNAL.AAZ1482.

[133] M. P. Pacheco, T. Pfau, and T. Sauter, "Benchmarking Procedures for High-Throughput Context Specific Reconstruction Algorithms," *Frontiers in Physiology*, vol. 6, p. 410, 2016. DOI: 10.3389/fphys.2015.00410.

[134] J. Y. Ryu, H. U. Kim, and S. Y. Lee, "Framework and resource for more than 11,000 gene-transcript-protein-reaction associations in human metabolism," *Proceedings of the National Academy of Sciences*, vol. 114, no. 45, E9740–E9749, Nov. 2017. DOI: 10.1073/pnas.1713050114.

[135] S. Feng and Y. Liu, "Metabolomics of Glioma," in *Cancer Metabolomics: Methods and Applications*, S. Hu, Ed., Springer International Publishing, 2021, pp. 261–276.

[136] E. Belykh, K. V. Shaffer, C. Lin, V. A. Byvaltsev, M. C. Preul, and L. Chen, "Blood-Brain Barrier, Blood-Brain Tumor Barrier, and Fluorescence-Guided Neurosurgical Oncology: Delivering Optical Labels to Brain Tumors," *Frontiers in Oncology*, vol. 10, 2020.

[137] J. Yan, U. Kuzhiumparambil, S. Bandodkar, R. C. Dale, and S. Fu, "Cerebrospinal fluid metabolomics: Detection of neuroinflammation in human central nervous system disease," *Clinical & Translational Immunology*, vol. 10, no. 8, e1318, 2021. DOI: 10.1002/cti2.1318.

[138] M. Jain, R. Nilsson, S. Sharma, *et al.*, "Metabolite Profiling Identifies a Key Role for Glycine in Rapid Cancer Cell Proliferation," *Science*, vol. 336, no. 6084, pp. 1040–1044, May 2012. DOI: 10.1126/science.1218595.

[139] D. C. Zielinski, N. Jamshidi, A. J. Corbett, A. Bordbar, A. Thomas, and B. O. Palsson, "Systems biology analysis of drivers underlying hallmarks of cancer cell metabolism," *Scientific Reports*, vol. 7, p. 41 241, Jan. 2017, Publisher: Nature Publishing Group. DOI: 10.1038/srep41241.

[140] D. A. Turner and D. C. Adamson, "Neuronal-Astrocyte Metabolic Interactions: Understanding the Transition into Abnormal Astrocytoma Metabolism," *Journal of neuropathology and experimental neurology*, vol. 70, no. 3, pp. 167–176, Mar. 2011. DOI: 10.1097/NEN.0b013e31820e1152.

[141] A. Bordbar, M. L. Mo, E. S. Nakayasu, *et al.*, "Model-driven multi-omic data analysis elucidates metabolic immunomodulators of macrophage activation," *Molecular Systems Biology*, vol. 8, no. 1, p. 558, Jun. 2012, ISBN: 1744-4292 (Electronic)\backslash{\}r1744-4292 (Linking) Publisher: Nature Publishing Group. DOI: 10.1038/msb.2012.21.

[142] R. Qiu, Y. Zhong, Q. Li, Y. Li, and H. Fan, "Metabolic Remodeling in Glioma Immune Microenvironment: Intercellular Interactions Distinct From Peripheral Tumors," *Frontiers in Cell and Developmental Biology*, vol. 9, p. 693 215, Jun. 2021. DOI: 10.3389/fcell.2021.693215.

[143] R. D. Leone and J. D. Powell, "Metabolism of immune cells in cancer," *Nature reviews. Cancer*, vol. 20, no. 9, pp. 516–531, 2020. DOI: 10.1038/s41568-020-0273-y.

[144] A. A. Moustafa, J. Phillips, S. Kéri, B. Misiak, and D. Frydecka, "On the Complexity of Brain Disorders: A Symptom-Based Approach," *Frontiers in Computational Neuroscience*, vol. 10, p. 16, 2016. DOI: 10.3389/fncom.2016.00016.

[145] J. Seidlitz, A. Nadig, S. Liu, *et al.*, "Transcriptomic and cellular decoding of regional brain vulnerability to neurogenetic disorders," *Nature Communications*, vol. 11, p. 3358, 2020. DOI: 10.1038/s41467-020-17051-5.

[146] A. Bordbar, A. M. Feist, R. Usaite-Black, J. Woodcock, B. O. Palsson, and I. Famili, "A multi-tissue type genome-scale metabolic network for analysis of whole-body systems physiology," *BMC Systems Biology*, vol. 5, no. 1, p. 180, 2011, ISBN: 1752050917520509. DOI: 10.1186/1752-0509-5-180.

[147] R. B. Puchalski, N. Shah, J. Miller, *et al.*, "An anatomic transcriptional atlas of human glioblastoma," *Science (New York, N.Y.)*, vol. 360, no. 6389, pp. 660–663, 2018. DOI: 10.1126/science.aaf2666.

[148] K. H. B. Lam, A. J. Leon, W. Hui, *et al.*, "Topographic mapping of the glioblastoma proteome reveals a triple-axis model of intra-tumoral heterogeneity," *Nature Communications*, vol. 13, p. 116, 2022. DOI: 10.1038/s41467-021-27667-w.

[149] C. Tomi-Andrino, A. Pandele, K. Winzer, J. King, R. Rahman, and D.-H. Kim, "Metabolic modeling-based drug repurposing in glioblastoma," *Scientific Reports*, vol. 12, no. 1, p. 11 189, 2022.

[150] Q. Shen, H. Yang, Q.-P. Kong, G.-H. Li, and L. Li, "Metabolic modeling identifies a novel molecular type of glioblastoma associated with good prognosis," *Metabolites*, vol. 13, no. 2, p. 172, 2023.

Chapter 3

Metabolic models predict fotemustine and the combination of eflornithine/rifamycin and adapalene/cannabidiol for the treatment of gliomas

Ali Kishk[1], Maria Pires Pacheco[1], Tony Heurtaux[1,2], and Thomas Sauter[1], *

[1] Department of Life Sciences and Medicine, University of Luxembourg, L-4367 Belvaux, Luxembourg

[2] Luxembourg Centre of Neuropathology, L-3555 Dudelange, Luxembourg

* Correspondence: thomas.sauter@uni.lu

This article has been published in:

Briefings in Bioinformatics, Volume 25, Issue 3, May 2024, bbae199, https://doi.org/10.1093/bib/bbae199\

Introduction to the paper

The lack of animal models in low-grade glioma (LGG) and the aggressiveness of glioblastomas call for alternate approaches that allow integrating patient data to identify metabolic vulnerabilities and suggest drug candidates. Approved anti-brain cancer chemotherapies target mostly hypoxia and angiogenesis with targeted therapies or cell cycle with alkylating agents, among others. Moreover, the two approved combinations inhibit redundant pathways, limiting any potential synergism. We present genome-scale metabolic models (GEMs) of the

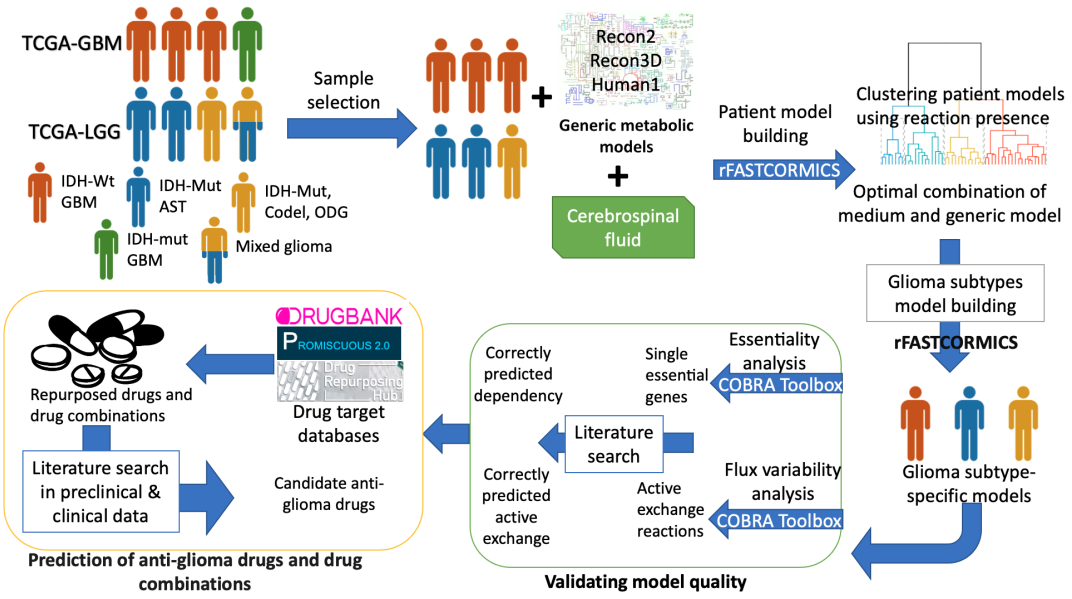

Graphical abstract

three well-defined glioma subtypes that predicted repurposable FDA-approved single drugs and combinations for gliomas. We confirmed our predicted drugs using published *in vitro* and xenograft drug screenings and found that antimetabolites and TXNRD1-inhibitors induced a growth reduction comparable to anti-brain chemotherapies *in vitro* and in xenografts. Furthermore, fotemustine, showed a higher effectiveness in glioblastoma clinical trials than AntiBCs. Additionally, we predicted 17 drug combinations mostly to be efficient on all three subtypes, with eflornithine/rifamycin and cannabidiol/adapalene being glioblastoma- and LGG-specific, which is coherent with the known LGG-specific glutamate and glutathione depletion. This work presents the first GEMs that go beyond glioblastoma into the glioma subtypes, accurately capture the intra-heterogeneity, and further predict repurposable combinations.

Contribution: I carried out the literature review, wrote the manuscript, and prepared the figures.

Abstract

Gliomas are the most common type of malignant brain tumors, with glioblastoma (GBM) having a median survival of 15 months due to drug resistance and relapse. The treatment of gliomas relies on surgery, radiotherapy, and chemotherapy. Only 12 anti-brain tumor chemotherapies (AntiBCs), mostly alkylating agents, have been approved so far. Glioma subtype-specific metabolic models were reconstructed to simulate metabolite exchanges, *in silico* knockouts, and the prediction of drug and drug combinations for all three subtypes. The

simulations were confronted with literature, high-throughput screenings (HTS), xenograft, and clinical trial data to validate the workflow and further prioritize the drug candidates. The three subtype models accurately displayed different degrees of dependencies toward glutamine and glutamate. Furthermore, 33 single drugs, mainly antimetabolites and TXNRD1-inhibitors, as well as 17 drug combinations were predicted as potential candidates for gliomas. Half of these drug candidates have been previously tested in HTSs. Half of the tested drug candidates reduce proliferation in cell lines and two-thirds in xenografts. Most combinations were predicted to be efficient for all three glioma types. However, eflornithine/rifamycin and cannabidiol/adapalene were predicted specifically for GBM and low-grade glioma (LGG), respectively. Most drug candidates had comparable efficiency in preclinical tests, cerebrospinal fluid bioavailability, and MOA to AntiBCs. However, fotemustine and valganciclovir alone and eflornithine and celecoxib in combination with AntiBCs improved the survival compared to AntiBCs in two-arms, phase I/II and higher glioma clinical trials. Our work highlights the potential of metabolic modeling in advancing glioma drug discovery, which accurately predicted metabolic vulnerabilities, repurposable drugs, and combinations for the glioma subtypes.

Keywords

Glioma, Metabolic modeling, Drug repurposing, Cancer

3.1 Introduction

Gliomas account for 50% of the deaths in cases with primary malignant brain and d central nervous system (CNS) tumors in the United States [1]. The 2021 World Health Organization (WHO) CNS classification [2] stratifies adult gliomas into three subtypes based on the mutation status of the Isocitrate dehydrogenase 1/2 (IDH1/2) and the co-deletion of the short arm of chromosome 1 (1p) and the long arm of chromosome 19 (19q) (1p/19q co-deletion) into: astrocytoma (AST), IDH-mutant; oligodendroglioma (ODG), IDH-mutant and 1p/19q-codeletion; and glioblastoma, IDH-wildtype (glioblastoma multiforme; GBM). GBM shows poor 7% five-year survival that also limits the success rate of clinical trials, compared to 32%-53% in AST and 66%-84% in ODG [1].

The standard of care for GBM treatment is surgery, and radiotherapy, followed mainly by temozolomide (TMZ) chemotherapy [3]. Current approved anti-brain chemotherapies (AntiBCs) consist of eight monotherapies (cell cycle inhibitors and anti-hypoxic agents) and two

combinations: procarbazine/lomustine/vincristine (PCV) and dabrafenib/trametinib [4]. The monotherapy AntiBCs targeting the cell cycle are mostly alkylating agents (TMZ, lomustine, carmustine, and cyclophosphamide) and only doxorubicin targets topoisomerase, meanwhile three anti-hypoxic agents reduce angiogenesis by targeting the mTOR/HIF-1α/VEGF pathway: everolimus (mTOR), belzutifan (HIF-1α), and bevacizumab (VEGF). The recently approved dabrafenib/trametinib combination for BRAF-mutant low-grade glioma (LGG) is the only targeted ABC inhibiting the RAF/MEK pathway. Whether targeting the RAF/MEK by dabrafenib/trametinib or the cell cycle by PCV combination, both combinations show redundancy of the target pathways, which is another potential cause for inefficacy of positive phase II drugs in phase III GBM trials [5]. Despite these treatments, glioma patient survival stays poor, with a high recurrence rate. The need for efficacious drugs and combinations targeting alternative pathways is therefore pivotal.

Drug repurposing, i.e., redirecting approved drugs to other diseases, has been proven as a critical element to shorten the lengthy toxicity trials in cancer drug discovery. However, current preclinical drug repurposing approaches in glioma have been mainly limited to GBM [6], [7], with a high failure rate in clinical trials due to non-efficacy, poor cerebrospinal fluid (CSF) bioavailability, drug resistance, and toxicity [3]. While the exact biological role of 1p/19 co-deletion is still unclear, IDH mutation in most LGG dysregulates the nicotinamide adenine dinucleotide phosphate (NADPH) balance and glutamate biosynthesis, depleting the glutathione, activating oxidative metabolism and increasing the reactive oxygen species (ROS) sensitivity [6].

The role of metabolic rewiring in IDH-mutant glioma encouraged the use of metabolic modelling for the study of gliomas, notably AST and ODG. Metabolic modelling is commonly applied to model the metabolism of cancer cells and to select among all FDA-approved drugs, the ones that target specifically cancer vulnerabilities appearing from metabolic rewiring [8]. Whole-brain and brain cell models were reconstructed to study alterations in the metabolism in neurodegenerative disease and GBM. These published genome-scale brain metabolic models were extensively covered in our previous review [9]. In the present study, we reconstructed three glioma subtype models using patient data from the TCGA, predicted drug and drug combinations, as well as the predicted essential genes in the different subtypes. Extensive literature review and comparison against HTSs, especially against AntiBCs, allowed confirming the model's prediction and further prioritizing the drug candidates.

Importance of the Study

Due to high relapse and drug resistance rates, the three glioma subtypes suffer from poor survival rate, calling for new therapies. We present genome-scale metabolic models (GEMs) of the three well-defined glioma subtypes that predicted repurposable FDA-approved single drugs and combinations for gliomas. We confirmed our predicted drugs using published in vitro and xenograft drug screenings and found that antimetabolites and TXNRD1-inhibitors induced a growth reduction comparable to AntiBCs in vitro and in xenografts. Furthermore, fotemustine, showed a higher effectiveness in GBM clinical trials than AntiBCs. Additionally, we predicted 17 drug combinations mostly to be efficient on all three subtypes, with eflornithine/rifamycin and cannabidiol/adapalene being GBM- and LGG-specific, which is coherent with the known LGG-specific glutamate and glutathione depletion. This work presents the first GEMs that go beyond GBM into the glioma subtypes, accurately capture the intra-heterogeneity, and further predict repurposable combinations.

3.2 Materials and Methods

3.2.1 Model building

Two types of models were built using rFASTCORMICS [10]: sample models to assess the subtype intra- and inter-heterogeneity and consensus models for the three glioma subtypes used for essential gene and drug prediction (see Supplementary Methods for more details). rFASTCORMICS was thereby fed with RNA-Seq data (116 GBM samples and 257 LGG samples) from The Cancer Genome Atlas Program (TCGA) data [11], stratified based on the 2021 WHO CNS classification [2], with the generic model Recon3D [12] as input reconstruction and the composition of CSF [13] as medium constraint. Other models and data formats were tested, but this setting allowed better separation between the sample models of the three glioma subtypes (see Supplementary Methods, Figures S 7.1 7.2 7.3 7.4 and Table S 7.1) matching to literature-retrieved metabolic exchanges (Figure S 7.5), and balanced capturing of common essential genes (Figure S 7.6). To confirm the models' predictions in terms of metabolite exchanges, essential gene, and drug predictions were compared with literature and databases, notably DepMap [14].

3.2.2 Prediction of metabolite exchanges

Different uptake and release reactions in the glioma subtype models allowed for assessing the model quality by comparing the exchange reactions with literature evidence. The minimum and maximum fluxes for the input and output reactions of the three consensus subtype models were computed using the *fluxVariability* function of the COBRA Toolbox v.3.0 [15] while maximizing for biomass production (biomass reaction). Narrow-bounded exchange reactions were selected as any perturbation is predicted to alter the cell growth of the models.

3.2.3 Prediction of essential genes

Single gene deletion from the COBRA Toolbox v.3.0 [15] was used with biomass optimization to predict essential genes. Only genes whose knockout (KO) is predicted to reduce the growth by at least 50% were selected and compared to a list of common essential genes (defined by the Cancer Dependency Map, DepMap, as genes found to be essential in >90% of cell lines in pan-cancer CRISPR-Cas9 screens), retrieved from DepMap 22Q1 [14].

3.2.4 Prediction of anti-glioma drugs and drug combinations

To predict potential single drugs and drug combinations, the drug deletion pipeline [16] was run and hence every target of the FDA-approved drugs and drug combinations was knocked out to assess the predicted effect on cell growth. Single drugs were restricted to FDA-approved drugs (2387 drugs defined by Drug Repurposing Hub [17]) due to the high failure rate in glioma clinical trials of preclinical compounds. For the drug combinations, AntiBCs and investigational anti-glioma drugs (IAGs) were tested in concert with FDA-approved drugs. Only single drugs and combinations that reduced the growth by at least 50% were considered for further analysis. Single drugs predicted to shut down the biomass production completely were not further tested in combination with other drugs. The drug targets were retrieved from DrugBank [18], PROMISCUOUS2 [19], and Drug Repurposing Hub [17]. Information on the IAGs (41 drugs) was gathered from the orpha.net database (ORPHA:182067), and AntiBCs (12 drugs) were retrieved from a review [4] and the NIH website (`https://www.cancer.gov/about-cancer/treatment/drugs/brain`).

Table 3.1: Summary of selected samples and model statistics for the consensus glioma subtype and control models.

Model	Selected samples	Reactions	Metabolites	ENTREZ Genes
`iAST`	116	3269	2460	1273
`iGBM`	140	3526	2621	1302
`iODG`	117	3331	2504	1305
`iCTRL`	4	3407	2585	1603

3.2.5 Drug prioritization and benchmarking

Different clinical, xenograft, *in vitro*, and pharmacokinetics (PK) data in brain cancer were collected to rank the predicted drugs based on their efficacy (see Supplementary Methods for details) and classify them into effective, ineffective, and untested. Most compiled clinical trial data were on phase I/II or higher clinical trials in brain cancer (n = 50) and two-arm trials in glioma (n = 8). Two metrics were considered: overall survival (OS) and progression-free survival (PFS, duration between treatment and symptom worsening). The xenograft data included *in/ex vivo* drug high-throughput screenings (HTSs) in GBM patient-derived xenografts (PDXs) and *in vivo* drug screening from literature. *in vitro* data combined two cellular metrics: IC_{50} and viability reduction, and hence a median IC_{50} across brain cancer cell lines was calculated for each drug as a potency measure. If available, PK data corresponding to CSF bioavailability was prioritized over blood-brain barrier (BBB) permeability as the latter cannot capture the efflux rates of the brain. Single drugs that induced proliferation *in vitro* or cofactors to the target genes were excluded from further ranking. CSF bioavailability data was collected as *logBB*, (logarithm of the drug's CSF-to-plasma concentration ratio).

3.3 Results

Glioma sample models were reconstructed from TCGA-GBM and TCGA-LGG to assess if the metabolism of the 2021 WHO classification glioma subtypes was sufficiently different to be captured by qualitative metabolic models. The subtype models (iGBM, iAST, iODG) include between 32% and 35% of the reactions of the generic metabolic reconstruction Recon3D (Table S 3.1), accurately detected metabolic variations between the IDH-mutant and -wildtype samples and allow for a clear separation between both types (Figure S 7.3).

3.3.1 LGG and GBM models correctly predict high glutamate and thymidine uptake rates

Input and release rates of metabolites were predicted for the three consensus subtype models and compared to the literature (Table S 7.2). Forty metabolites of the predicted 101 metabolite exchanges had narrow-bounded fluxes (with a maximum of 10% of the maximal range) and are predicted to affect cell growth directly. Four of them (Figure S 7.7) matched known differences between the subtypes in cell line uptake, patient biomarkers, and MR radiotracers (Figure 3.1, in cyan). High glutamate uptake was predicted in the LGG models (iAST and iODG), concordant with the known glutamate depletion due to IDH-mutant-induced rewiring [20]. iGBM predicted the highest thymidine uptake, in agreement with an elevated ^{18}F-FLT radiotracer uptake in GBM patients' scans compared to AST [21] and ODG [22]. Finally, the reduced glutamine uptake in iODG conforms to the low ODG-specific glutamine dependency [23]. Together, predicted glutamate and thymidine uptake variations followed known IDH-based differences in the three subtypes. In one instance, the predicted lactate uptake is inconsistent with the literature [24] (Figure 3.1, in magenta). The lactate exchange inconsistency could be attributed to the inactivity of lactate exchange reactions during iGBM model building and their exclusion from the consistent subnetwork. Meanwhile, variations within the subtypes matching metabolomics data in L-phenylalanine and myo-inositol were considered minor validations (Figure 3.1, in gray). For the remaining exchanges, no data could be found in the literature. Notably, octadecenoate and pyruvate could serve as potential biomarkers between the glioma subtypes, but they still require validation (see Figure S 7.7). These experiments were repeated with 90% and 95% of maximation. However, the lowering of the threshold turned most exchanges to become unbounded, due to the high degree of freedom and hence could no longer capture the observations gathered from the literature. For example, glutamine exchange in iGBM was irreversible with 90% maximization, wide uptake range with 95%, and high narrow-bounded with 100% maximization. 100% maximization of glutamine exchange in iGBM was the only setting matching high glutamine uptake in GBM (Figure S 7.8).
Taking together, the metabolic models mostly captured not only metabolic variations between the subtypes but also recapitulated experimental observations.

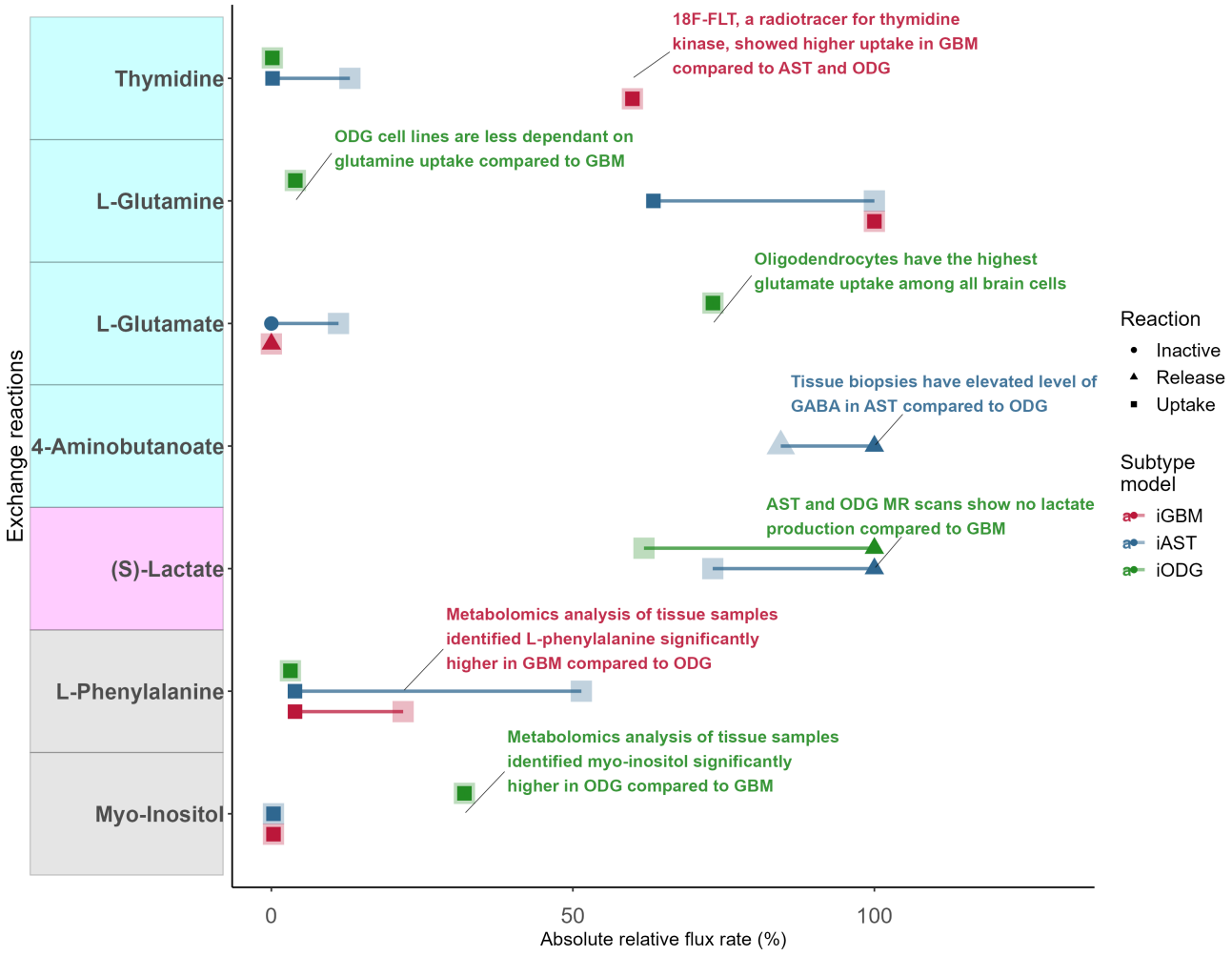

FIGURE 3.1: **The predicted input and release rates of metabolites match the literature and experimental observations.**

Flux Variability Analysis allowed calculating flux ranges that guarantee an optimal growth and hence allowed finding critical metabolite exchanges (narrow-bounded fluxes). Forty out of 101 predicted exchanges were narrow-bounded, and four of the five exchange reactions matched literature and data from radiotracers for three subtypes (see Figure S 7.7 for all reactions). Two exchange reactions matching metabolomics data were considered minor validation due to the unclear metabolic flux. Metabolite names on the y-axis with cyan, magenta and gray correspond to literature matching, contrary to literature and minor validation (Table S 7.2), respectively.

3.3.2 Thioredoxin detoxification and nucleotide interconversion are potential targets for all three subtypes and arginine uptake for GBM

We further predicted vulnerabilities (essential genes) that could be exploited to reduce tumor progression. Twenty-five genes were predicted to be essential (Figure 3.2.A) with 100% growth reduction (Figure S 7.9). iODG yielded the highest number (n=22), matching its known high survival rate and vulnerability [25]. Ten of these genes were identified as common essential genes by DepMap [14], suggesting pan-cancer vulnerabilities. A literature search further found

five genes (TXNRD1, RRM1-2, SPLTC1, SLC27A4) to reduce viability with *in vitro* knockdown (KD) or KO. The KO of thioredoxin reductase (TXNRD1) reduced proliferation and migration in drug-resistant GBM [26]. Moreover, TXNRD1 expression significantly correlated with poorer diagnosis in AST [27] and ODG [28] patients. Due to their radical-scavenging activities, thioredoxin and glutathione (GSH) control oxidative homeostasis and counter mitochondrial oxidative stress. Similarly, KD of SPLTC genes involved in sphingolipid synthesis reduced the viability of GBM cell lines [29]. Likewise, the KD of RRM1 and RRM2, involved in nucleotide interconversion, caused cell death and sensitized GBM to TMZ, respectively (Table S 7.3). However, one predicted essential gene: PYCT2, was described to increase GBM proliferation in a KD experiment [30].

Besides the potential vulnerabilities, 33 FDA-approved drugs could, according to our models, be considered repurposable for glioma (Table S8). The 33 predicted drugs include 14 non-brain anti-cancer drugs (anticancers), 10 antivirals, 6 hormones/cofactors, 2 psychoactive, and 1 lipid-lowering agent. The 14 anticancers are 10 antimetabolites, an ANPEP-inhibitor, 2 TXNRD1-inhibitors (such as fotemustine, also being an alkylating agent) and an alkylating agent. These drugs target 12 essential genes and 48 non-essential genes (Figure 3.2). Among them, TXNRD1 is targeted by arsenic-trioxide and fotemustine (approved in some countries against melanoma brain metastasis [31]), and RRM1–2 by seven antimetabolites. RRM1–2 showed higher dependency probability (the likelihood that the KO of a gene reduces cell growth or induces cell death) than AntiBCs' targets in the glioma cell lines (Figure S 7.10). Furthermore, we predicted valganciclovir that affects arginine transporter SLC6A14 as a GBM-specific single drug. The drug target genes differ among the three subtypes for the same drugs due to differences between the subtype models in gene and reaction compositions during model building. Some of the various targets of several drugs were included in some models and excluded in other based on the expression data. The glioma subtype model genes were compared to other brain metabolic models discussed in our previous review [9] using the Human Protein Atlas [32] brain-specific gene categories. The glioma subtype models showed comparable completeness and specificity to curated and semi-curated brain metabolic models (Figure S 7.11). Taken together, metabolic modeling accurately captured pan-glioma single vulnerabilities, such as thioredoxin detoxification and nucleotide interconversion. Additionally, metabolic modelling proposes arginine uptake as a druggable vulnerability for GBM.

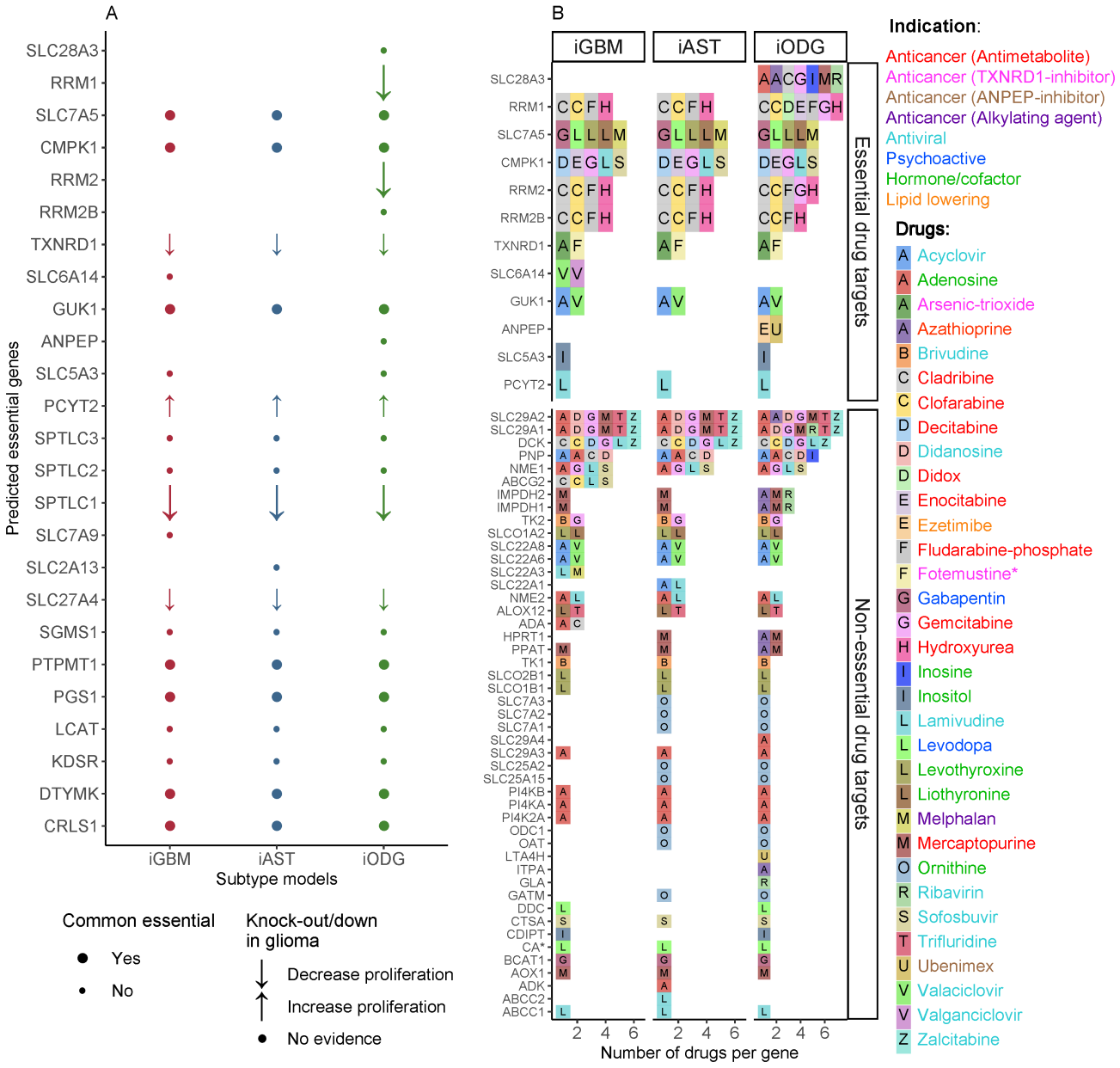

FIGURE 3.2: **Thioredoxin detoxification and nucleotide interconversion are predicted as potential drug targets for glioma. (A) Twenty-five genes were predicted to reduce tumor growth *in silico* knockout KO.**

Six of the 25 essential genes have been previously tested in *in vitro* KO or KD studies glioma (literature, Table S 7.3), where five genes lowered proliferation (down-arrows), and only one (PCYT2) increased proliferation (up arrows). Genes with no support in the literature are marked as dots. Moreover, 10 of the 25 predicted essential genes are common essentials (found essential genes in most cancer cell lines from CRISPR screens) and are marked as a big dot or arrow in (A). (B) Thirty-three FDA-approved drugs were predicted to reduce cell growth and could hence be repurposable for glioma. The 33 single drugs have 60 targets, of which 12 are essential genes ('Essential drug targets'). Classifying the drugs based on approved indication and mode-of-action (MOA) (see color code of the font) showed that nearly a third are antimetabolites and fotemustine (with *) has both TXNRD1-inhibitor and alkylating MOA. For example, in (B), cladribine is marked as 'C' letter in gray box, while its approved indication and MOA is represented in red in the drug name color.

3.3.3 Glutamate and polyamine biosynthesis are predicted suitable target pathways for drug combinations in LGG and GBM, respectively

FDA-approved drugs were tested *in silico* in combination with a set of 53 AntiBCs and IAGs to find meaningful synergistic drug combinations. Seventeen combinations (Figure 3.3.A) composed of 19 drugs (hereafter will be referred to as combination drugs), including one anticancer antimetabolite (fluorouracil), antiviral antimetabolite (zidovudine), 13 carbonic anhydrase inhibitors (CAi) (Table S 7.4 and Tables S9-10), and two herbal antioxidants (cannabidiol and resveratrol) with multi-target actions. As every two drugs in the combinations have independent targets, Bliss combination index was selected to find synergistic, antagonistic, and additive combinations [33] using growth reduction (1-grRatio, see Materials and Methods for details) as drug effect. Fifteen combinations with CAi were predicted to be synergistic in the three subtypes. CA converts CO2 to bicarbonate and is matching the known anti-glioma action of CAi by decreasing extracellular acidosis responsible for drug resistance. Besides CA, zonisamide and resveratrol target MAOA and MOAB genes, which convert oxygen and water into hydrogen peroxide, thereby increasing intracellular hypoxia, with MAOA inhibition found to decrease glioma proliferation and angiogenesis [34]. Two combinations displayed subtype-specific synergism (eflornithine/rifamycin for GBM and cannabidiol/adapalene for LGG), achieved 100% growth reduction in their corresponding subtypes, and did not affect ATP production and biomass maintenance in the healthy model iCTRL (Figure S 7.12). Eflornithine (also known as α-difluoromethylornithine or DFMO) inhibits ornithine decarboxylase (ODC1), coding for an enzyme of the polyamine biosynthesis pathway, while rifamycin targets SLCO genes associated with GSH exchange reduction (Figure 3.3.B). Meanwhile, adapalene inhibits glutamic-oxaloacetic transaminase 1 (GOT1) that governs glutamate biosynthesis from alpha-ketoglutarate, while cannabidiol increases ROS by depleting glutathione production. Both glutamate and GSH biosynthesis depletion align with the known LGG-specific vulnerabilities [20]. Among the combinations drug targets, ABCC1 and ABCG2 of the ATP-binding cassette (ABC) transporters predicted to remove the toxic byproducts of lipid peroxidation (4-hydroxy-2-nonenal) and heme biosynthesis (protoporphyrin), respectively. The predicted GBM-specific protoporphyrin is consistent with impaired heme biosynthesis in LGG cell line [35]. Similarly, 4-hydroxy-2-nonenal was detected in GBM and AST samples affirming the predicted pan-glioma profile of the lipid peroxidation [36]. Altogether, metabolic modeling predicted combinations targeting alternative reactions for potential synergism, many of these reactions match known subtype-specific biosynthesis vulnerabilities. Of these combinations,

the combined targeting of glutamate and GSH biosynthesis is a potentially druggable combination in LGG; meanwhile, targeting polyamine synthesis combined with GSH exchange is a potentially druggable combination in GBM.

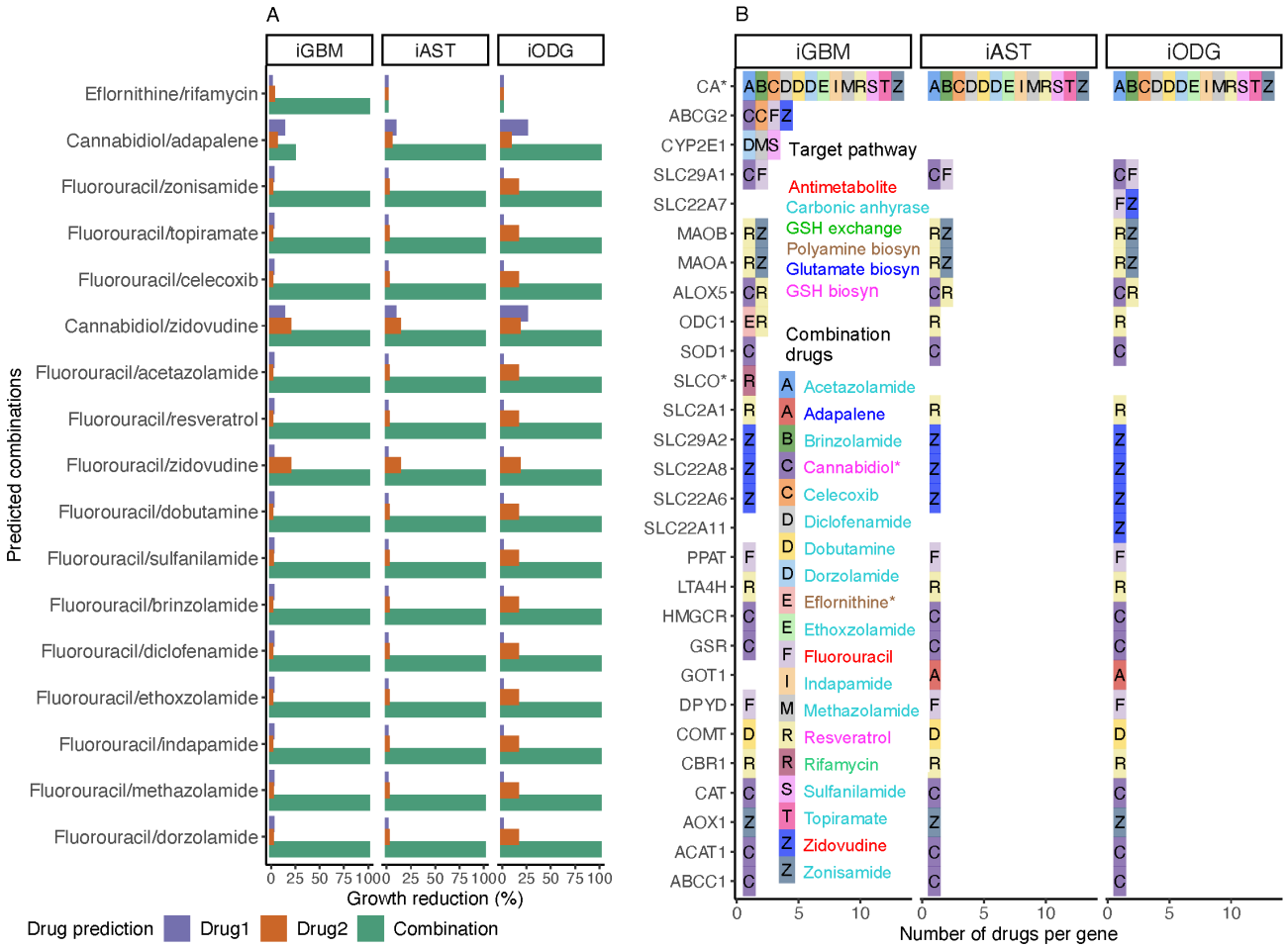

FIGURE 3.3: **Eflornithine/rifamycin and cannabidiol/adapalene are predicted safe synergistic combinations for GBM and LGG, respectively.**

(A) Drug combination predictions were performed between two drug sets: (a) FDA-approved drugs after excluding predicted single drugs with a predicted lethal on the models and (b) approved AntiBCs and IAGs (marked with *). Combinations with growth reduction above 50% are depicted. All combinations, but two, reduce tumor growth across glioma subtypes (top two). (B) Analysis of the targets from the 17 synergistic combinations showed that dual KO of ODC1-SLCO (SLCO1A2, SLCO1B1, SLCO2A1 and SLCO2B1) genes are GBM-specific, while GOT1 and cannabidiol targets are LGG-specific. The drug names are colored based on the targeted pathway. Abbreviations: GSH; glutathione. biosyn, biosynthesis.

3.3.4 Gemcitabine, cladribine, and decitabine have better CSF bioavailability and *in vitro* potency than AntiBCs

To select the most promising drugs and drug combinations, we ranked the drugs from HTS and literature data using IC_{50}, viability reduction, BBB permeability, CSF bioavailability,

ABC transporter affinity, *in/ex vivo* xenograft testing, main MOA, phase I/II clinical trials or higher, and possible drug-drug interactions, aggregated from HTS and the literature (see Supplementary File 2, Tables S8-S16, Supplementary Methods on data gathering and drug ranking and Table S 7.5 for the screening databases). Ten single drugs were excluded for being cofactors to the target genes or induced proliferation *in vitro* (Table S8). As expected, the CSF bioavailability of AntiBCs is inversely correlated with potency (Figure 3.4 and Figure S 7.13). Many single drugs, such as fotemustine, arsenic-trioxide, and hydroxyurea, showed comparable balanced outcomes to AntiBCs. In contrast, three antimetabolites (decitabine, gemcitabine, and cladribine) achieved good potency and bioavailability. These three antimetabolites, especially gemcitabine, notably reduced cell viability compared to most AntiBCs (Figure S 7.14). Some drugs showing high potency, such as clofarabine (predicted) and doxorubicin (AntiBC), however, had poor bioavailability. Taken together, most drug candidates achieved comparable results (TXNRD1-inhibitors) or outperformed (antimetabolites) AntiBCs drugs in terms of potency and bioavailability.

3.3.5 Cladribine and clofarabine reduced growth in GBM PDXs, while fotemustine reduced xenograft growth (data from literature)

Three drug HTS in GBM PDXs [37], [38] (Figure 3.5.A) and PDXs data from the literature (Figure 3.5.B and Table S12) were used to test the drugs in biological contexts closer to *in vivo*. Four non-alkylating AntiBCs (vincristine, trametinib, everolimus and doxorubicin) (Figure 3.4), surpassed 25% PDXs growth reduction. Correspondingly, three antimetabolites (gemcitabine, cladribine, and clofarabine) induced a growth reduction comparable to or higher than these four AntiBCs. However, decitabine showed non-conclusive results between the drug screenings and the literature (Table S12). Fotemustine, which was not tested in HTS PDXs experiments, reduced growth *in vivo* in literature [39]. However, several drugs that showed low growth reductions in the GBM PDXs were predicted only by the LGG subtypes consensus models. Four combination drugs (fluorouracil, celecoxib, resveratrol, and acetazolamide) (Tables S12 and S13) sensitized glioma to TMZ *in vitro* and *in vivo*. Of these, celecoxib caused a moderate *in vivo* growth reduction (with a median of 9%-22%). In summary, the three antimetabolites presented steady *in vitro* potency and *in vivo* growth reduction, and clofarabine outperformed two-thirds of the AntiBCs in PDXs.

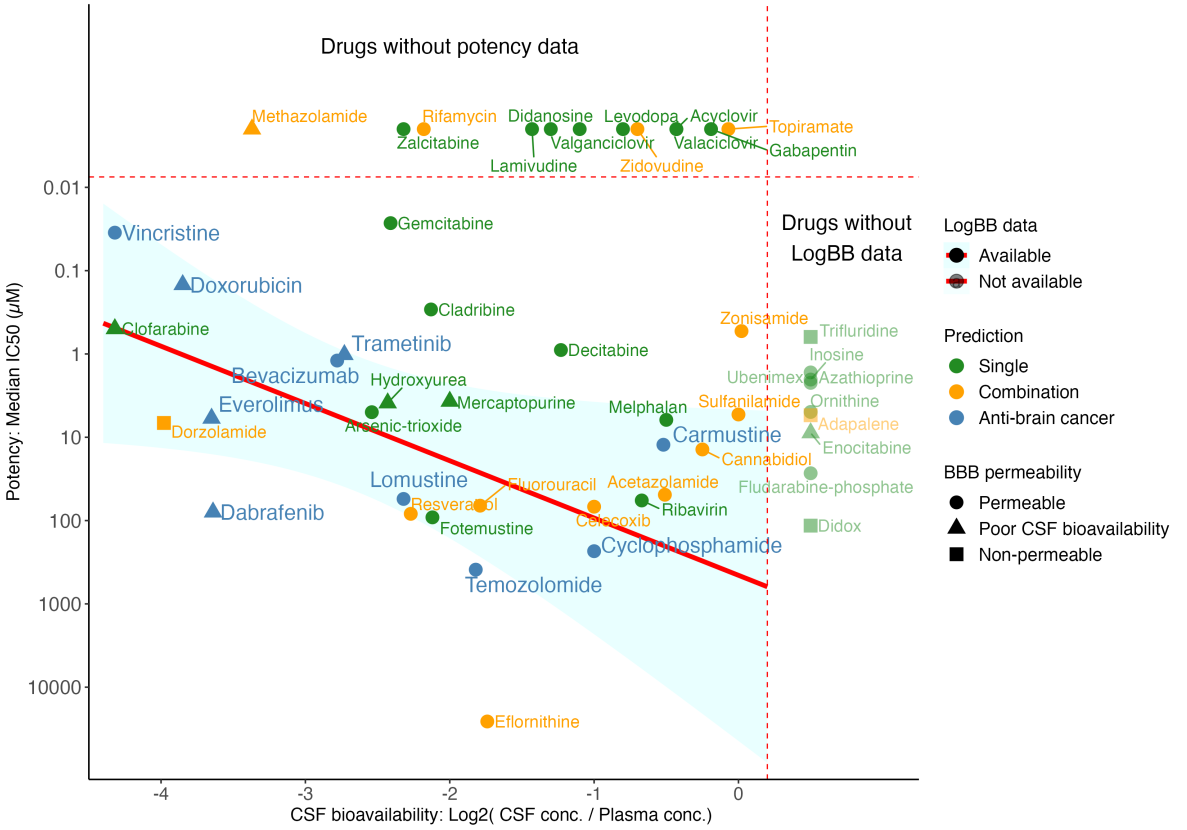

FIGURE 3.4: **Gemcitabine, cladribine, and decitabine showed stronger *in vitro* potency and CSF bioavailability than AntiBCs.**

Potency (y-axis) and CSF bioavailability (x-axis) data were collected from the literature and screening databases (see Figure S 7.13 for detailed potency per database). Potency (median IC_{50} across the brain cancer cell lines) was calculated for single and combination drugs and the AntiBCs. Similarly, CSF bioavailability was collected in *logBB*, which is the logarithm of the CSF-to-plasma concentration ratio. Rightward on the x-axis and upward on the y-axis represent increasing potency and CSF bioavailability, respectively. Drugs without potency or *logBB* data are on the top and right-sides separated by the red dashed lines, respectively.

3.3.6 Fotemustine alone and eflornithine, celecoxib, and valganciclovir in combination improved median OS compared to AntiBCs in phase II glioma trials, while antimetabolites showed no improvement

Drugs were classified into effective, ineffective, and untested for *in vitro* and xenografts using the criteria in Table S 7.6. All single and combination drugs except rifamycin were tested *in vitro*, while only half were tested in xenografts. Of the tested drugs, half and two-thirds were found effective in *in vitro* and xenografts, respectively (Figure 3.6.A). Among the two-arm, phase I/II trials (Table S11), two single drugs (fotemustine and valganciclovir) and two combination drugs (eflornithine and celecoxib) improved the primary survival outcome compared to the ABC arm (Figure 3.6.B). On the other hand, three predicted single drugs show no or minimal activity as monotherapy in single-arm, phase II trials: gemcitabine [40] (AST and

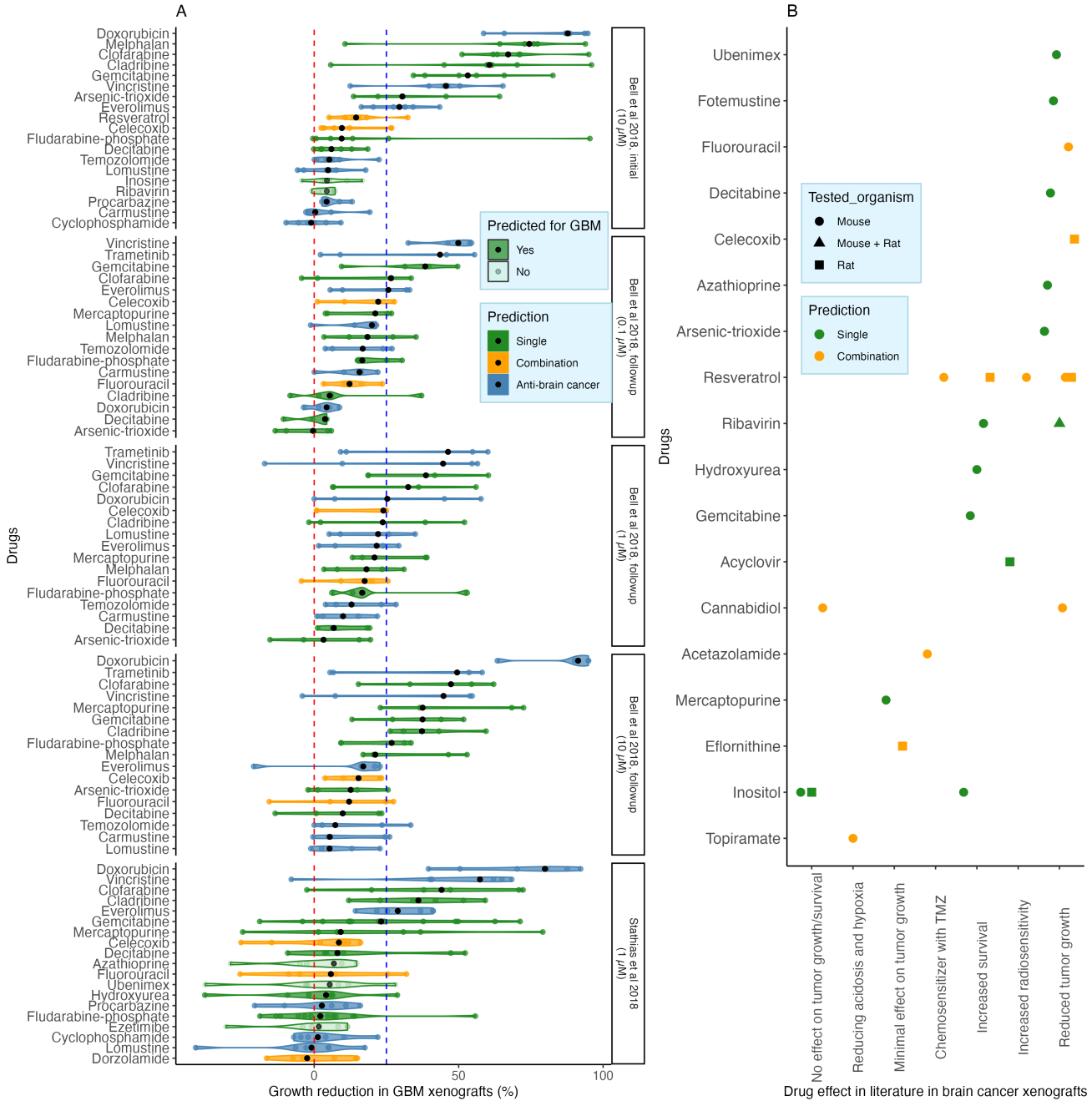

FIGURE 3.5: **Clofarabine has a more robust growth reduction than two-thirds of the AntiBCs in GBM PDXs.**

Xenograft data were collected from HTS tested in GBM PDXs (A) and literature tested in brain cancer generally (B). Clofarabine, gemcitabine and cladribine attained a more robust or comparable growth reduction than half of the AntiBCs in the HTS. Additionally, some drugs not predicted by iGBM (in light green) showed moderate growth reduction in the GBM PDXs.

GBM), cladribine [41] (AST and ODG) and melphalan [42] (AST and GBM). Additionally, when combined with carmustine, mercaptopurine, and fluorouracil showed an antagonistic [43] and a non-additional [44] effect, respectively. The five drugs which failed in phase II trials are either substrate or inducer to the ABC transporters (Table S15), which might cause drug resistance, and all are cell cycle inhibitors.

Beyond cell cycle inhibitors, of the four clinically effective drugs (fotemustine, valganciclovir, eflornithine and celecoxib), only valganciclovir reached statistical significance in the primary outcome in newly diagnosed GBM (nGBM) [45] and recurrent GBM (rGBM) [46], [47]. After the first-line treatment of TMZ and radiotherapy, fotemustine monotherapy slightly exceeded bevacizumab by 1.3 months achieving 8.7 months median OS in a phase II trial in rGBM [48]. Eflornithine added to the PCV combination improved the median OS (mOS) in recurrent LGG with about two and a half years against the PCV combination alone [49]. To a lesser extent, celecoxib combined with TMZ increased median PFS by 3 months in nGBM versus TMZ alone [50] and is the only known ABC transporter inhibitor of the four clinically effective drugs. While none of the 17 predicted combinations had been tested in brain cancer, three combinations (fluorouracil/zidovudine, fluorouracil/celecoxib, and fluorouracil/resveratrol) were found synergistic in non-brain cancer *in vitro*, however, the last two failed as a combination in various clinical trials (Table S 7.7). Eflornithine/rifamycin and cannabidiol/adapalene were ranked first and second for GBM- and LGG-specific subtypes, respectively. Despite the clinical activity of celecoxib in GBM, fluorouracil/celecoxib was ranked fourth due to predicted major drug-drug interaction (DDI) by DrugBank (Table S16) and the absence of an additional effect of the combination in phase III colon cancer trial [51]. Meanwhile, zonisamide showed the strongest *in vitro* potency among the combination drugs, and the fluorouracil/zonisamide was predicted with minor DDI of increased arrhythmia; hence, this combination was ranked third. All in all, metabolic modeling predicted drug candidates with a steady effective-to-ineffective ratio in *in vitro* (49%), in xenografts (64%) and in clinical trials (44%). Unlike the redundancy of the AntiBCs combinations' target pathways, predicted combinations covered multiple alternative pathways, increasing potential synergism, of which three combinations were tested in non-brain cancer.

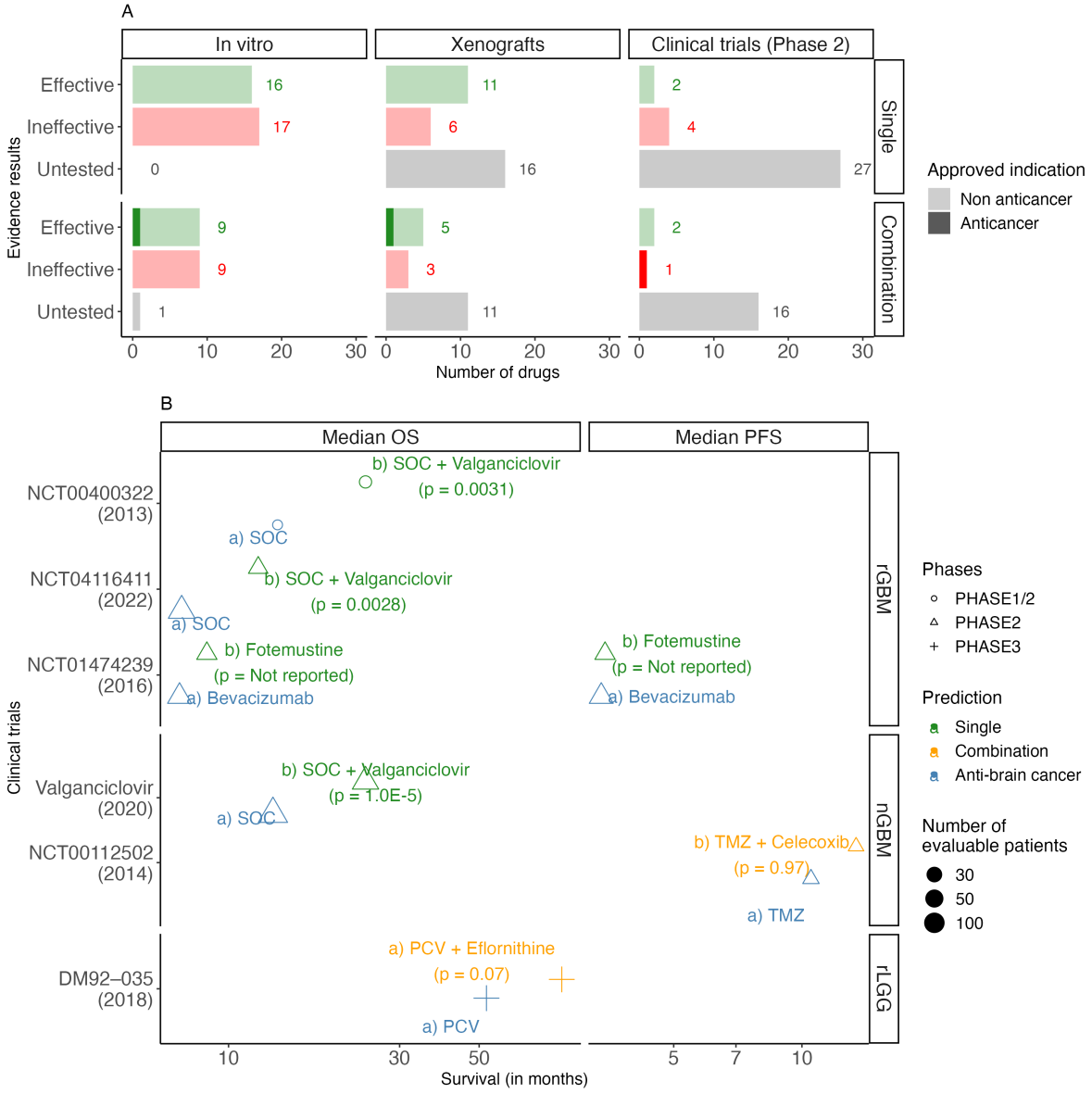

FIGURE 3.6: **Among the tested predicted drugs, half and two-thirds were effective *in vitro* and xenografts, respectively, with four drugs showing comparable survival to AntiBCs in two-arm, phase II clinical trials.**

(A) Predicted single and combination drugs were classified into effective, ineffective, and untested against AntiBCs using the criteria in Table S 7.5. (B) Two-arm, phase II clinical trials in gliomas were selected to compare the predicted drugs to the ABC arm as monotherapy or in combination. Among the single drugs, fotemustine monotherapy and valganciclovir in combination improved median OS. Likewise, eflornithine and celecoxib improved mOS and median PFS, respectively. Only valganciclovir achieved statistical significance versus the ABC arm. On the other hand, two antimetabolites (gemcitabine and cladribine) and melphalan failed in single-arm trials with no reported survival, while mercaptopurine and fluorouracil reduced and kept mOS when combined with carmustine, respectively. Statistical significance of the predicted drug arm versus the AntiBCs arm was reported independently for each trial. Abbreviations: rGBM: recurrent GBM, nGBM: newly diagnosed GBM, rLGG: recurrent LGG, TMZ: temozolomide, SOC: standard-of-care, PCV: Procarbazine/lomustine/vincristine combination.

3.4 Discussion

We have built GEMs (iGBM, iAST and iODG) for the three glioma subtypes based on the 2021 WHO classification and have predicted new repurposable, single drugs and combinations. While the sensitivity of essential gene predictions of the metabolic models remains low, the specificity is high [52], [53]. The low sensitivity is often attributed to the fact that in silico single gene KOs only capture essentiality related to metabolism and most specifically to the optimization function and fail capturing essentiality to other processes such as regulatory processes. But also to some extent to limitations of the metabolic models. The large efforts invested in the curation and standardization of genome-scale metabolic reconstruction, notably MEMOTE [54], and MetaNetX [55] as well as the benchmarking of context-specific model algorithms [56]–[58], and the curation of GPR rules [59] and improvement of biomass formulation [53] are likely to further improve the accuracy the predictions [52], [60]. Furthermore, unlike some other computational drug repurposing approaches, metabolic modeling allowed understanding the effect of a KD or KO on a system level and confronting it to the earlier knowledge. Various sanity checks allowed for biologically relevant predictions that included: model selection based on subtype separation, matching metabolic exchanges and gene KD/KO with literature, and evaluation against AntiBCs in vitro, in xenografts and in clinical trials. While model-building used the rFASTCORMICS algorithm [10], a member of the FASTCORE family that were benchmarked by us and other in various studies [57], [58], data collected of gene KD/KO and metabolic exchanges were kept only for validations as recommended in this review [61]. The models recapitulated metabolite exchanges and subtype-specific uptake for radiotracers in patients and medium metabolites measured *in vitro*. Similarly, IDH-mutant models (iAST and iODG) accurately predicted vulnerabilities consistent with the known 2HG-induced NADPH depletion, such as targeting glutamate and GSH biosynthesis [20] with the cannabidiol/adapalene combination, which would aggravate the depletion. Cell cycle and hypoxia are the two common target pathways for glioma chemotherapy, with both AntiBCs combinations targeting redundant pathways, diminishing a potential synergism. However, cell cycle inhibitors are ABC transporter substrates, and hence are transporting the drugs out of the tumor causing drug resistance [62], [63] (Figure 3.7). Meanwhile, all anti-hypoxic AntiBCs, except belzutifan, are ABC transporter inhibitors. Despite poor CSF bioavailability, only non-alkylating AntiBCs surpassed 25% growth reduction in xenograft experiments at 10 μM or lower, which is coherent with the mediocre performance in improving the OS in glioma patients. The subtype models allowed predicting single drugs and drug combinations that could enlarge the panel of therapeutic options in glioma. The single drug candidates predicted

in this study principally target oxidative stress through the KD of TXNRD1, and arginine uptake and nucleotide interconversion (antimetabolites).

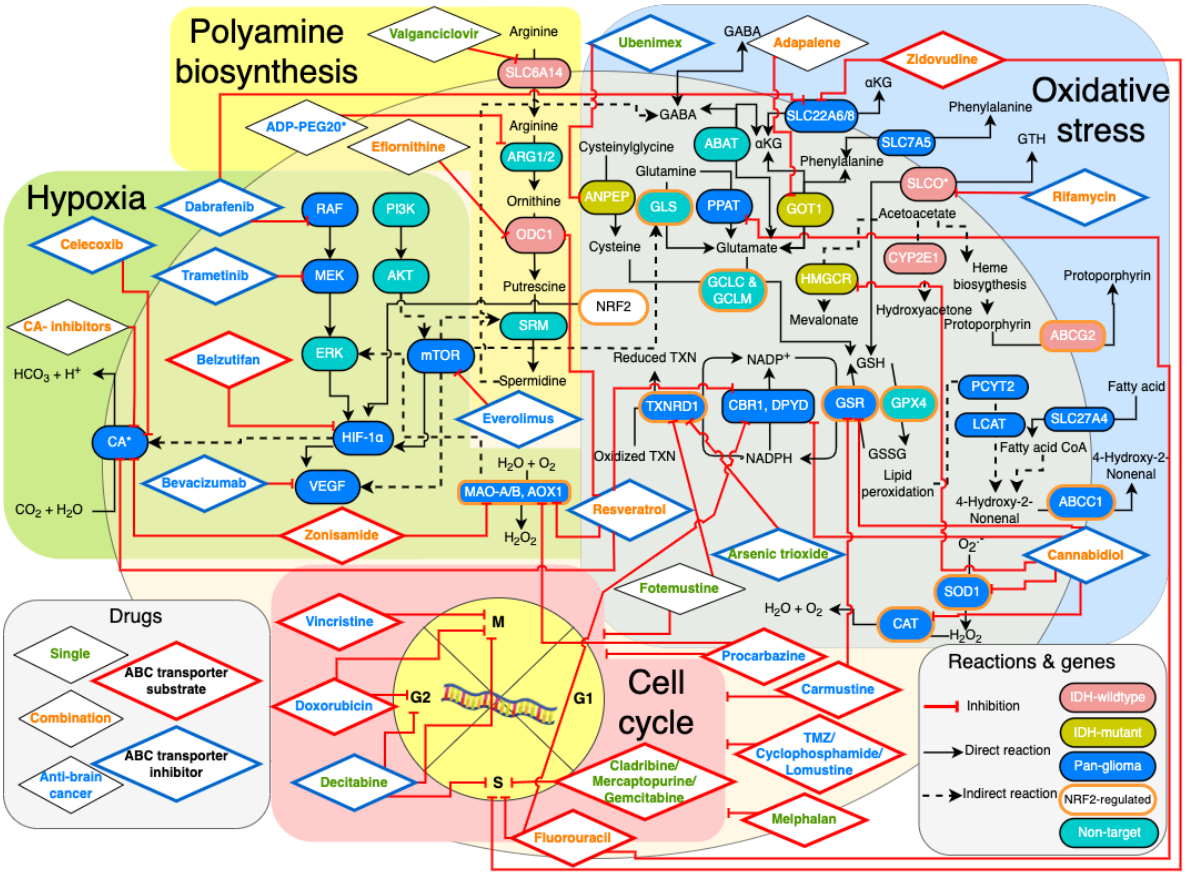

FIGURE 3.7: **Predicted drugs target the same genes as the AntiBCs or downstream genes, mainly covering four biological pathways: hypoxia, oxidative stress, cell cycle and polyamine biosynthesis.**

TXNRD1 is predicted to be a vulnerability present across all glioma subtypes and its expression was shown to highly correlate to AST [27] and ODG [28] patients' survival. Moreover, fotemustine (TXNRD1-inhibitor and alkylating agent) monotherapy displayed comparable survival to bevacizumab in a two-arm, phase II clinical trial in rGBM [48]. In a network meta-analysis of 11 AntiBCs and IAGs in rGBM, fotemustine ranked best in effectiveness as mOS [67]. Another TXNRD1-inhibitor, arsenic-trioxide, was tested as local interstitial monotherapy in a single-arm, phase I/II GBM trial with the first promising results [68], outperformed alkylating AntiBCs *in vivo* and *in vitro*, and an ABC transporter inhibitor. The antiviral valganciclovir, one of our drug candidates, is predicted to target arginine uptake in GBM. *in vitro*, arginine deprivation reduced GBM invasiveness [69] and currently the arginine-degrading agent, ADI-PEG20, has been tested in a phase I GBM trial (NCT04587830) [70]. While valganciclovir

AntiBCs mainly affect hypoxia and cell cycle via growth factors and unselective alkylation, respectively. Meanwhile, the predicted CAis and antimetabolites selectively target DNA biosynthesis and CA, respectively. The transcription factor NRF2, a target of AntiBCs, regulates a third of predicted targets in the oxidative stress pathway (in olive green) [64]–[66]. Furthermore, predicted drugs and AntiBCs share common targets such as glutathione reductase (GSR) between cannabidiol and carmustine, monoamine oxidase A/B (MAO-A/B) are common between procarbazine, zonisamide and resveratrol and SLC22A6/8 between dabrafenib and zidovudine. Most predicted drugs and cell cycle inhibitor AntiBCs that were shown to be clinically inefficient are ABC transporter substrates, while clinically effective predicted drugs are either non-substrate (eflornithine), inhibitor (celecoxib) or have an unknown effect (fotemustine and valganciclovir) on ABC transporter. Unlike clinically ineffective antimetabolites (cladribine, gemcitabine, mercaptopurine and fluorouracil), fotemustine targets both cell cycle and TXNRD1. Meanwhile, polyamine synthesis is targeted uniquely by the clinically effective drugs predicted for GBM (valganciclovir and eflornithine), the phase I/II ADPI-PEG20 IAG. Furthermore, cannabidiol, rifamycin, celecoxib and others inhibit the ABC transporters (ABCC1 and ABCG2) responsible for AntiBCs resistance as well as byproducts detoxification such as the efflux of lipid peroxidation (4-hydroxy-2-nonenal) and heme biosynthesis (protoporphyrin) byproducts. 4-hydroxy-2-nonenal and protoporphyrin predicted for pan-glioma and GBM, respectively, matching the literature in the predicted subtypes. Abbreviations: GSH: reduced glutathione, GSSG: oxidized glutathione, TXN: thioredoxin, αKG: alpha-ketoglutarate.

significantly enhanced mOS when combined with the AntiBCs in both nGBM and rGBM phase II trials, its hypothetical cytotoxic link to arginine uptake inhibition has yet to be proven.

While antimetabolites have been successful in cancer treatment and despite the high *in vitro* potency and viability reduction, four antimetabolites (cladribine, gemcitabine and mercaptopurine from the single drugs and fluorouracil from the combinations drugs) failed in phase II glioma trials. Another predicted antimetabolite, clofarabine showed *in vivo* growth reduction, but has not been tested clinically. While BBB permeability and CSF bioavailability infer drug penetrance, ABC transporter affinity was found to be more crucial for drug diffusion into core tumor regions, even under leaky BBB [71]. Similarly, ABC transporter substrates are more likely to possess low serum concentration due to drug metabolism. Both clinically ineffective predicted drugs and cell cycle inhibitors AntiBCs are ABC transporter substrates which might explain their inefficacy to due to limited drug distribution to the core tumor [71]. Finally, despite having the highest potency, CSF bioavailability and ABC transporter inhibitor affinity, decitabine presented moderate *in vitro* viability and weak xenograft growth reduction. Nevertheless, decitabine prodrugs are currently in two phase II trials for IDH-mutant glioma (NCT03666559 and NCT03922555). Overall, predicted single drugs implicated in oxidative stress and polyamine metabolism pathways are more target-specific than AntiBCs' transcription factors, of which fotemustine, arsenic-trioxide and valganciclovir represent repurposable single drugs for glioma with a clinical profile comparable to AntiBCs.

We further searched for drugs that could increase the potency of AntiBCs and IAGs to predict drug combinations that allow targeting pathways characterized by many isozymes and alternative reactions that must be inhibited simultaneously, avoiding pathway redundancy of

the AntiBCs combinations. The predicted drug combinations allowed targeting CA, GSH exchange, glutamate, polyamine, and GSH biosynthesis. In addition to inhibiting ABC transporters, anti-hypoxic AntiBCs reduce angiogenesis through mTOR/HIF-1α/VEGF or RAF/MEK pathways, while anti-hypoxic combination drugs target their downstream CA and MAO-A/B genes. The relatively high potency and xenograft growth reduction of anti-hypoxic AntiBCs compared to alkylating AntiBCs, is clinically consistent with the superior median overall response rate of anti-angiogenic agents compared to alkylating agents (6.1%) in rGBM phase II trials [72]. CA2, CA9 and CA12 are highly expressed in GBM, especially CA9, which is not expressed in a healthy brain [73] and is significantly correlated with poor survival in GBM [73] and the AST grade [74]. The proposed 17 drug combinations include pairs of a total of 19 drugs. In brain cancer, 18 out of 19 combinations drugs (except rifamycin) have been tested individually. However, none of the 17 proposed combinations has been assessed *in vivo* or *in vitro* for brain cancer, which warrants their testing. Even though three combinations had synergistic effects *in vitro* in non-brain cancer, two failed in clinical trials. Among the 17 predicted combinations, three IAGs: cannabidiol, eflornithine and fluorouracil, were predicted to have a synergistic effect with adapalene (GOT1-inhibitor), rifamycin (SLCO-inhibitor), and zonisamide (CAi), respectively. With cannabidiol and rifamycin being ABC transporter inhibitors, cannabidiol/adapalene and eflornithine/rifamycin combinations present potential combinations for relapsed glioma from AntiBCs resistance. Additionally, iGBM accurately predicted ABCG2 transporter responsible for efflux activity against protoporphyrin, as GBM-specific vulnerability, matching the impaired heme biosynthesis in IDH-mutant glioma [30]. Among the 19 combination drugs, zonisamide (selective CA9-inhibitor, approved for seizures) had the highest potency and CSF bioavailability and target additionally MAOA/B increasing its anti-hypoxic action like procarbazine. While adapalene has poor CSF bioavailability, the recent nanoparticle formulation of adapalene increased its CSF bioavailability [75]. Similarly, the lack of survival of eflornithine monotherapy in GBM but not AST in a phase II clinical trial [49] highlights the importance of testing the eflornithine/rifamycin combination in GBM. Some of the shared genes between Recon3D reconstruction and DepMap's common essential genes are enriched for other functions unrelated to growth (Table S17). As the formulation of the biomass was shown to impact essential gene predictions [53], a tailored biomass formulation should improve accuracy. Besides, curating the biomass growth formulation and updating GPR rules, disease specific reactions could be added before model building to improve essentiality analysis and drug prediction [53]. For example, adding IDH-mutant biochemical reactions would allow more accurate modeling of the LGG. Similarly, formulating evaluation tests of

predicted essential genes on the DepMap scores would allow reproducible predictions and evaluations between studies. Moreover, Flux Variability Analysis of metabolic exchanges could be improved using random sampling especially for reactions with a wide flux range [76]. While the iCTRL model was built from four healthy brain samples from TCGA-GBM, building a healthy brain model from the GTEx expression data [77] with CSF medium or using the brain model from the whole-body model [13] could advance evaluating the safety of the predicted drugs. In summary, metabolic modeling predicted combinations that overcome the target redundancy of the AntiBCs combinations with alternative, accurate glioma subtype-specific targets. The top two combinations present a safety profile and ABC substrate inhibition for one of the two drugs, with variations in subtype-specificity that call for further testing.

3.5 Conclusion

GBM and LGG suffer from poor patient survival and accurate preclinical models, respectively, that hinder new therapies' discovery. Moreover, AntiBCs lack either adequate potency or CSF bioavailability. In addition, two-thirds of AntiBCs are ABC transporter substrates, increasing their drug resistance and core tumor diffusion. In this work, we present glioma subtype-specific GEMs to predict single drugs and combinations that are promising candidates to be translated into clinical trials. Among others, LGG GEMs accurately predicted glutamate and GSH biosynthesis vulnerabilities, while GBM GEM accurately predicted glutamine dependency and heme biosynthesis. Unlike the target redundancy of the combination AntiBCs, predicted combinations target alternative reactions, potentiating their synergism. Of the predicted 33 single drugs (19 combinations drugs), half were effective *in vitro*, and 17 (8) were tested against GBM PDXs, of which 11 (5) were effective. Similarly, predicted drugs show comparable or improved CSF bioavailability to AntiBCs. Despite five cell cycle inhibitors failing in phase II glioma clinical trials due to conceivably being ABC transporter substrates, two single drugs (fotemustine and valganciclovir) and two combination drugs (eflornithine and celecoxib) exceeded the primary survival outcome alone or combined with AntiBCs in phase I/II clinical trials. Our work warrants fotemustine as pan-glioma monotherapy and eflornithine/rifamycin and cannabidiol/adapalene as promising new combinations for GBM and LGG, respectively.

Conflict of Interest

The authors declare no competing interests.

Authorship Contributions

Conceptualization, A.K., M.P.P. and T.S.; Methodology, A.K. and M.P.P.; Formal Analysis, A.K.; Investigation, A.K., M.P.P. and T.S.; Resources, A.K.; Data Curation, A.K.; Writing—Original Draft Preparation, A.K.; Writing—Review Editing, A.K., M.P.P., T.H., T.S.; Visualization, A.K., M.P.P., T.H., and T.S. All authors have read and agreed to the published version of the manuscript.

Key Points

- Glioma metabolic modeling accurately captured inter-subtype metabolic variations
- Fotemustine showed very good performance in a meta-analysis in OS
- Fotemustine alone and eflornithine in combination showed improved survival in glioma trials
- The prediction of glutamate depletion by adapalene in IDH-mutant glioma agrees with literature

Acknowledgments

We would like to thank Simone P. Niclou and Sabrina Fritah for their feedback on the sample stratification. The experiments presented in this paper were carried out using the HPC facilities of the University of Luxembourg [78].

Author Contributions

Declarations of interest: none

Data Availability Statement

All analyzed data are publicly available from the Resources Table in Supplementary Table 1. Analysis code is available under `https://github.com/sysbiolux/GliomaGEM/`

References

[1] Q. T. Ostrom, N. Patil, G. Cioffi, K. Waite, C. Kruchko, and J. S. Barnholtz-Sloan, "CBTRUS statistical report: Primary brain and other central nervous system tumors diagnosed in the United States in 2013-2017," *Neuro-Oncology*, vol. 22, no. Supplement_1, pp. IV1–IV96, Oct. 2020, Publisher: Oxford University Press. DOI: 10.1093/NEUONC/NOAA200.

[2] D. N. Louis, A. Perry, P. Wesseling, *et al.*, "The 2021 WHO classification of tumors of the central nervous system: A summary," *Neuro-Oncology*, vol. 23, no. 8, pp. 1231–1251, Aug. 2021, Publisher: Oxford University Press. DOI: 10.1093/NEUONC/NOAB106.

[3] J. L. King and S. R. Benhabbour, *Glioblastoma multiforme—a look at the past and a glance at the future*, ISSN: 19994923 Issue: 7 Publication Title: Pharmaceutics Volume: 13, 2021. DOI: 10.3390/pharmaceutics13071053.

[4] J. Sun, Q. Wei, Y. Zhou, J. Wang, Q. Liu, and H. Xu, "A systematic analysis of FDA-approved anticancer drugs," *BMC Systems Biology*, vol. 11, no. Suppl 5, Oct. 2017, Publisher: BioMed Central. DOI: 10.1186/S12918-017-0464-7.

[5] J. J. Mandel, S. Yust-Katz, A. J. Patel, *et al.*, "Inability of positive phase II clinical trials of investigational treatments to subsequently predict positive phase III clinical trials in glioblastoma," *Neuro-Oncology*, vol. 20, no. 1, 2018. DOI: 10.1093/neuonc/nox144.

[6] P. Persico, E. Lorenzi, A. Losurdo, *et al.*, "Precision Oncology in Lower-Grade Gliomas: Promises and Pitfalls of Therapeutic Strategies Targeting IDH-Mutations," *Cancers*, vol. 14, no. 5, p. 1125, Mar. 2022, Publisher: Multidisciplinary Digital Publishing Institute (MDPI). DOI: 10.3390/CANCERS14051125.

[7] R. Bjerkvig, S. Bougnaud, and S. P. Niclou, "Animal models for low-grade gliomas," in *Diffuse Low-Grade Gliomas in Adults: Natural History, Interaction with the Brain, and New Individualized Therapeutic Strategies*, vol. 9781447122135, 2013. DOI: 10.1007/978-1-4471-2213-5_11.

[8] M. Moškon and T. Režen, "Context-Specific Genome-Scale Metabolic Modelling and Its Application to the Analysis of COVID-19 Metabolic Signatures," *Metabolites*, vol. 13, no. 1, Jan. 2023, Publisher: MDPI. DOI: 10.3390/METABO13010126.

[9] A. Kishk, M. P. Pacheco, T. Heurtaux, *et al.*, "Review of Current Human Genome-Scale Metabolic Models for Brain Cancer and Neurodegenerative Diseases," en, *Cells*, vol. 11, no. 16, p. 2486, Jan. 2022, Number: 16 Publisher: Multidisciplinary Digital Publishing Institute. DOI: 10.3390/cells11162486.

[10] M. P. Pacheco, T. Bintener, D. Ternes, *et al.*, "Identifying and targeting cancer-specific metabolism with network-based drug target prediction," *EBioMedicine*, vol. 43, pp. 98–106, May 2019, Publisher: Elsevier B.V. DOI: 10.1016/J.EBIOM.2019.04.046.

[11] M. Rahman, L. K. Jackson, W. E. Johnson, D. Y. Li, A. H. Bild, and S. R. Piccolo, "Alternative preprocessing of RNA-Sequencing data in the Cancer Genome Atlas leads to improved analysis results," *Bioinformatics*, vol. 31, no. 22, pp. 3666–3672, May 2015, Publisher: Oxford University Press. DOI: 10.1093/BIOINFORMATICS/BTV377.

[12] E. Brunk, S. Sahoo, D. C. Zielinski, *et al.*, "Recon3D enables a three-dimensional view of gene variation in human metabolism," *Nature Biotechnology*, vol. 36, no. 3, pp. 272–281, Mar. 2018, Publisher: Nature Publishing Group. DOI: 10.1038/NBT.4072.

[13] I. Thiele, S. Sahoo, A. Heinken, *et al.*, "Personalized whole-body models integrate metabolism, physiology, and the gut microbiome," *Molecular Systems Biology*, vol. 16, no. 5, May 2020, Publisher: EMBO. DOI: 10.15252/MSB.20198982.

[14] C. Pacini, J. M. Dempster, I. Boyle, *et al.*, "Integrated cross-study datasets of genetic dependencies in cancer," *Nature Communications*, vol. 12, no. 1, Dec. 2021, Publisher: Nature Research. DOI: 10.1038/S41467-021-21898-7.

[15] L. Heirendt, S. Arreckx, T. Pfau, *et al.*, "Creation and analysis of biochemical constraint-based models using the COBRA Toolbox v.3.0," *Nature Protocols*, vol. 14, no. 3, pp. 639–702, Mar. 2019, Publisher: Nature Publishing Group. DOI: 10.1038/S41596-018-0098-2.

[16] T. Bintener, M. P. Pacheco, A. Kishk, J. Didier, and T. Sauter, "Drug Target Prediction Using Context-Specific Metabolic Models Reconstructed from rFASTCORMICS," in *Methods in Molecular Biology*, vol. 2535, ISSN: 19406029, 2022. DOI: 10.1007/978-1-0716-2513-2_17.

[17] S. M. Corsello, J. A. Bittker, Z. Liu, *et al.*, "The Drug Repurposing Hub: A next-generation drug library and information resource," *Nature Medicine*, vol. 23, no. 4, pp. 405–408, Apr. 2017, Publisher: Nature Publishing Group. DOI: 10.1038/NM.4306.

[18] D. S. Wishart, Y. D. Feunang, A. C. Guo, *et al.*, "DrugBank 5.0: A major update to the DrugBank database for 2018," *Nucleic Acids Research*, vol. 46, no. D1, pp. D1074–D1082, Jan. 2018, Publisher: Oxford University Press. DOI: 10.1093/NAR/GKX1037.

[19] K. Gallo, A. Goede, A. Eckert, B. Moahamed, R. Preissner, and B. O. Gohlke, "PROMISCUOUS 2.0: A resource for drug-repositioning," *Nucleic Acids Research*, vol. 49, no. D1, pp. D1373–D1380, Jan. 2021, Publisher: Oxford University Press. DOI: 10.1093/NAR/GKAA1061.

[20] S. K. McBrayer, J. R. Mayers, G. J. DiNatale, *et al.*, "Transaminase Inhibition by 2-Hydroxyglutarate Impairs Glutamate Biosynthesis and Redox Homeostasis in Glioma," *Cell*, vol. 175, no. 1, 2018. DOI: 10.1016/j.cell.2018.08.038.

[21] A. H. Jacobs, A. Thomas, L. W. Kracht, *et al.*, "18F-Fluoro-l-Thymidine and 11C-Methylmethionine as Markers of Increased Transport and Proliferation in Brain Tumors," *Journal of Nuclear Medicine*, vol. 46, no. 12, 2005.

[22] A. Nikaki, G. Angelidis, R. Efthimiadou, *et al.*, "18F-fluorothymidine PET imaging in gliomas: An update," *Annals of Nuclear Medicine*, vol. 31, no. 7, p. 495, Jun. 2017, Publisher: Springer. DOI: 10.1007/S12149-017-1183-2.

[23] M. Chiu, C. Sabino, G. Taurino, *et al.*, "GPNA inhibits the sodium-independent transport system l for neutral amino acids," *Amino Acids*, vol. 49, no. 8, pp. 1365–1372, Aug. 2017, Publisher: Springer-Verlag Wien. DOI: 10.1007/S00726-017-2436-Z.

[24] M. M. Chaumeil, M. Radoul, C. Najac, *et al.*, "Hyperpolarized 13C MR imaging detects no lactate production in mutant IDH1 gliomas: Implications for diagnosis and response monitoring," *NeuroImage: Clinical*, vol. 12, 2016. DOI: 10.1016/j.nicl.2016.06.018.

[25] I. Simeonova and E. Huillard, *In vivo models of brain tumors: Roles of genetically engineered mouse models in understanding tumor biology and use in preclinical studies.* ISSN: 14209071 Issue: 20 Publication Title: Cellular and molecular life sciences : CMLS Volume: 71, 2014. DOI: 10.1007/s00018-014-1675-3.

[26] V. Pires, I. Bramatti, M. Aschner, V. Branco, and C. Carvalho, "Thioredoxin Reductase Inhibitors as Potential Antitumors: Mercury Compounds Efficacy in Glioma Cells," *Frontiers in Molecular Biosciences*, vol. 9, Jun. 2022, Publisher: Frontiers Media SA. DOI: 10.3389/FMOLB.2022.889971.

[27] H. Haapasalo, M. Kyläniemi, N. Paunu, V. L. Kinnula, and Y. Soini, "Expression of Antioxidant Enzymes in Astrocytic Brain Tumors," *Brain Pathology*, vol. 13, no. 2, pp. 155–164, Apr. 2003, Publisher: John Wiley & Sons, Ltd. DOI: 10.1111/J.1750-3639.2003.TB00015.X.

[28] H. Hannu, B. Helena, P. Niina, *et al.*, "Antioxidant enzymes in oligodendroglial brain tumors: Association with proliferation, apoptotic activity and survival," *Journal of Neuro-Oncology*, vol. 77, no. 2, pp. 131–140, 2006, Publisher: Kluwer Academic Publishers. DOI: 10.1007/S11060-005-9030-Z.

[29] E. Bernhart, S. Damm, A. Wintersperger, *et al.*, "Interference with distinct steps of sphingolipid synthesis and signaling attenuates proliferation of U87MG glioma cells," *Biochemical Pharmacology*, vol. 96, no. 2, pp. 119–130, Jul. 2015, Publisher: Elsevier. DOI: 10.1016/J.BCP.2015.05.007.

[30] T. Osawa, T. Shimamura, K. Saito, *et al.*, "Phosphoethanolamine Accumulation Protects Cancer Cells under Glutamine Starvation through Downregulation of PCYT2," *Cell Reports*, vol. 29, no. 1, 89–103.e7, Oct. 2019, Publisher: Cell Press. DOI: 10.1016/J.CELREP.2019.08.087.

[31] C. Garbe, "Ipilimumab with fotemustine in metastatic melanoma," *The Lancet Oncology*, vol. 13, no. 9, pp. 851–852, Sep. 2012. DOI: 10.1016/S1470-2045(12)70341-8.

[32] E. Sjöstedt, W. Zhong, L. Fagerberg, *et al.*, "An atlas of the protein-coding genes in the human, pig, and mouse brain," *Science*, vol. 367, no. 6482, eaay5947, 2020.

[33] D. Duarte and N. Vale, *Evaluation of synergism in drug combinations and reference models for future orientations in oncology*, ISSN: 25902571 Publication Title: Current Research in Pharmacology and Drug Discovery Volume: 3, 2022. DOI: 10.1016/j.crphar.2022.100110.

[34] S. Kushal, W. Wang, V. P. Vaikari, *et al.*, "Monoamine oxidase A (MAO A) inhibitors decrease glioma progression," *Oncotarget*, vol. 7, no. 12, 2016. DOI: 10.18632/oncotarget.7283.

[35] J. I. Traylor, M. N. Pernik, A. C. Sternisha, S. K. McBrayer, and K. G. Abdullah, *Molecular and metabolic mechanisms underlying selective 5-aminolevulinic acid-induced fluorescence in gliomas*, ISSN: 20726694 Issue: 3 Publication Title: Cancers Volume: 13, 2021. DOI: 10.3390/cancers13030580.

[36] M. Jaganjac, M. Cindrić, A. Jakovčević, K. Žarković, and N. Žarković, *Lipid peroxidation in brain tumors*, ISSN: 18729754 Publication Title: Neurochemistry International Volume: 149, 2021. DOI: 10.1016/j.neuint.2021.105118.

[37] V. Stathias, A. M. Jermakowicz, M. E. Maloof, *et al.*, "Drug and disease signature integration identifies synergistic combinations in glioblastoma," *Nature Communications 2018 9:1*, vol. 9, no. 1, pp. 1–13, Dec. 2018, Publisher: Nature Publishing Group. DOI: 10.1038/s41467-018-07659-z.

[38] J. B. Bell, F. Eckerdt, H. D. Dhruv, *et al.*, "Differential response of glioma stem cells to arsenic trioxide therapy is regulated by MNK1 and mRNA translation," *Molecular Cancer Research*, vol. 16, no. 1, 2018. DOI: 10.1158/1541-7786.MCR-17-0397.

[39] G. Vassal, I. Boland, M. J. Terrier-Lacombe, *et al.*, "Activity of fotemustine in medulloblastoma and malignant glioma xenografts in relation to O6-alkylguanine-DNA alkyltransferase and alkylpurine-DNA N-glycosylase activity," *Clinical Cancer Research*, vol. 4, no. 2, 1998.

[40] S. Z. Gertler, D. MacDonald, M. Goodyear, *et al.*, "NCIC-CTG phase II study of gemcitabine in patients with malignant glioma (IND.94)," *Annals of Oncology*, vol. 11, no. 3, 2000. DOI: 10.1023/A:1008336607135.

[41] S. V. Rajkumar, P. A. Burch, S. Nair, *et al.*, "Phase II North Central Cancer Treatment Group study of 2- chlorodeoxyadenosine in patients with recurrent glioma," *American Journal of Clinical Oncology: Cancer Clinical Trials*, vol. 22, no. 2, 1999. DOI: 10.1097/00000421-199904000-00012.

[42] M. C. Chamberlain, M. D. Prados, P. Silver, and V. A. Levin, "A phase II trial of oral melphalan in recurrent primary brain tumors," *American Journal of Clinical Oncology: Cancer Clinical Trials*, vol. 11, no. 1, 1988. DOI: 10.1097/00000421-198802000-00011.

[43] E. C. Halperin, J. Herndon, S. C. Schold, *et al.*, "A phase III randomized prospective trial of external beam radiotherapy, mitomycin C, carmustine, and 6-mercaptopurine for the treatment of adults with anaplastic glioma of the brain," *International Journal of Radiation Oncology*Biology*Physics*, vol. 34, no. 4, pp. 793–802, Mar. 1996, Publisher: Elsevier. DOI: 10.1016/0360-3016(95)02025-X.

[44] W. R. Shapiro, S. B. Green, P. C. Burger, *et al.*, "A randomized comparison of intra-arterial versus intravenous BCNU, with or without intravenous 5-fluorouracil, for newly diagnosed patients with malignant glioma," *Journal of Neurosurgery*, vol. 76, no. 5, 1992. DOI: 10.3171/jns.1992.76.5.0772.

[45] G. Stragliotto, M. R. Pantalone, A. Rahbar, J. Bartek, and C. Soderberg-Naucler, "Valganciclovir as Add-on to Standard Therapy in Glioblastoma Patients," *Clinical Cancer Research*, vol. 26, no. 15, 2020. DOI: 10.1158/1078-0432.CCR-20-0369.

[46] M. R. Pantalone, A. Rahbar, C. Söderberg-Naucler, and G. Stragliotto, "Valganciclovir as Add-on to Second-Line Therapy in Patients with Recurrent Glioblastoma," *Cancers*, vol. 14, no. 8, 2022. DOI: 10.3390/cancers14081958.

[47] G. Stragliotto, A. Rahbar, N. W. Solberg, *et al.*, "Effects of valganciclovir as an add-on therapy in patients with cytomegalovirus-positive glioblastoma: A randomized, double-blind, hypothesis-generating study," *International Journal of Cancer*, vol. 133, no. 5, 2013. DOI: 10.1002/ijc.28111.

[48] A. A. Brandes, G. Finocchiaro, V. Zagonel, *et al.*, "AVAREG: A phase II, randomized, noncomparative study of fotemustine or bevacizumab for patients with recurrent glioblastoma," *Neuro-Oncology*, vol. 18, no. 9, 2016. DOI: 10.1093/neuonc/now035.

[49] V. A. Levin, S. E. Ictech, and K. R. Hess, "Clinical importance of eflornithine (-difluoromethylornithine) for the treatment of malignant gliomas," *CNS oncology*, vol. 7, no. 2, 2018. DOI: 10.2217/cns-2017-0031.

[50] M. Penas-Prado, o. b. o. t. M. A. C. C. O. Program, t. B. T. T. Collaborative, *et al.*, "Randomized phase II adjuvant factorial study of dose-dense temozolomide alone and in combination with isotretinoin, celecoxib, and/or thalidomide for glioblastoma," *Neuro-Oncology*, vol. 17, no. 2, pp. 266–273, Feb. 2015, Publisher: Oxford Academic. DOI: 10.1093/NEUONC/NOU155.

[51] J. A. Meyerhardt, Q. Shi, C. S. Fuchs, *et al.*, "Effect of Celecoxib vs Placebo Added to Standard Adjuvant Therapy on Disease-Free Survival among Patients with Stage III Colon Cancer: The CALGB/SWOG 80702 (Alliance) Randomized Clinical Trial," *JAMA - Journal of the American Medical Association*, vol. 325, no. 13, 2021. DOI: 10.1001/jama.2021.2454.

[52] B. Strain, J. Morrissey, A. Antonakoudis, and C. Kontoravdi, "How reliable are chinese hamster ovary (cho) cell genome-scale metabolic models?" *Biotechnology and Bioengineering*, vol. 120, no. 9, pp. 2460–2478, 2023.

[53] M. M. García, M. Pacheco, T. Bintener, L. Presta, and T. Sauter, "Importance of the biomass formulation for cancer metabolic modeling and drug prediction," *iScience*, vol. 24, no. 10, Oct. 2021, Publisher: Elsevier Inc. DOI: 10.1016/J.ISCI.2021.103110.

[54] C. Lieven, M. E. Beber, B. G. Olivier, *et al.*, "MEMOTE for standardized genome-scale metabolic model testing," *Nature Biotechnology*, vol. 38, no. 3, pp. 272–276, Mar. 2020. DOI: 10.1038/s41587-020-0446-y.

[55] S. Moretti, V. D. T. Tran, F. Mehl, M. Ibberson, and M. Pagni, "Metanetx/mnxref: Unified namespace for metabolites and biochemical reactions in the context of metabolic models," *Nucleic acids research*, vol. 49, no. D1, pp. D570–D574, 2021.

[56] D. Machado and M. Herrgård, "Systematic Evaluation of Methods for Integration of Transcriptomic Data into Constraint-Based Models of Metabolism," *PLOS Computational Biology*, vol. 10, no. 4, e1003580, 2014. DOI: 10.1371/journal.pcbi.1003580.

[57] M. P. Pacheco, T. Pfau, and T. Sauter, "Benchmarking Procedures for High-Throughput Context Specific Reconstruction Algorithms," *Frontiers in Physiology*, vol. 6, p. 410, 2016. DOI: 10.3389/fphys.2015.00410.

[58] V. Vieira, J. Ferreira, and M. Rocha, "A pipeline for the reconstruction and evaluation of context-specific human metabolic models at a large-scale," *PLoS computational biology*, vol. 18, no. 6, e1009294, 2022.

[59] M. Di Filippo, C. Damiani, and D. Pescini, "Gpruler: Metabolic gene-protein-reaction rules automatic reconstruction," *PLoS computational biology*, vol. 17, no. 11, e1009550, 2021.

[60] D. B. Bernstein, B. Akkas, M. N. Price, and A. P. Arkin, "Evaluating e. coli genome-scale metabolic model accuracy with high-throughput mutant fitness data," *Molecular Systems Biology*, vol. 19, no. 12, e11566, 2023.

[61] J. A. Kaste and Y. Shachar-Hill, "Model validation and selection in metabolic flux analysis and flux balance analysis," *Biotechnology Progress*, vol. 40, no. 1, e3413, 2024.

[62] J. Wijaya, Y. Fukuda, and J. D. Schuetz, *Obstacles to brain tumor therapy: Key ABC transporters*, ISSN: 14220067 Issue: 12 Publication Title: International Journal of Molecular Sciences Volume: 18, 2017. DOI: 10.3390/ijms18122544.

[63] Y. Fukuda and J. D. Schuetz, *ABC transporters and their role in nucleoside and nucleotide drug resistance*, ISSN: 00062952 Issue: 8 Publication Title: Biochemical Pharmacology Volume: 83, 2012. DOI: 10.1016/j.bcp.2011.12.042.

[64] T. Heurtaux, D. S. Bouvier, A. Benani, *et al.*, *Normal and Pathological NRF2 Signalling in the Central Nervous System*, ISSN: 20763921 Issue: 8 Publication Title: Antioxidants Volume: 11, 2022. DOI: 10.3390/antiox11081426.

[65] J. M. DeBlasi and G. M. DeNicola, "Dissecting the crosstalk between nrf2 signaling and metabolic processes in cancer," *Cancers*, vol. 12, no. 10, p. 3023, 2020.

[66] M. Dodson, R. Castro-Portuguez, and D. D. Zhang, "Nrf2 plays a critical role in mitigating lipid peroxidation and ferroptosis," *Redox biology*, vol. 23, p. 101 107, 2019.

[67] C. McBain, T. A. Lawrie, E. Rogozińska, A. Kernohan, T. Robinson, and S. Jefferies, *Treatment options for progression or recurrence of glioblastoma: A network meta-analysis*, ISSN: 14651858 Issue: 12 Publication Title: Cochrane Database of Systematic Reviews Volume: 2020, 2021. DOI: 10.1002/14651858.CD013579.pub2.

[68] D. Han, L. Teng, X. Wang, *et al.*, "Phase I/II trial of local interstitial chemotherapy with arsenic trioxide in patients with newly diagnosed glioma," *Frontiers in Neurology*, vol. 13, 2022. DOI: 10.3389/fneur.2022.1001829.

[69] I. Pavlyk, Y. Rzhepetskyy, A. K. Jagielski, *et al.*, "Arginine deprivation affects glioblastoma cell adhesion, invasiveness and actin cytoskeleton organization by impairment of -actin arginylation," *Amino Acids*, vol. 47, no. 1, 2015. DOI: 10.1007/s00726-014-1857-1.

[70] J. S. Bomalaski, K.-T. Chen, M.-J. Chuang, *et al.*, "Phase IB trial of pegylated arginine deiminase (ADI-PEG 20) plus radiotherapy and temozolomide in patients with newly diagnosed glioblastoma.," *Journal of Clinical Oncology*, vol. 40, no. 16_suppl, 2022. DOI: 10.1200/jco.2022.40.16_suppl.2057.

[71] M. C. d. Gooijer, E. M. Kemper, L. C. M. Buil, *et al.*, "ATP-binding cassette transporters restrict drug delivery and efficacy against brain tumors even when blood-brain barrier integrity is lost," *Cell Reports Medicine*, vol. 2, no. 1, 2021. DOI: 10.1016/j.xcrm.2020.100184.

[72] B. M. Ellingson, P. Y. Wen, S. M. Chang, *et al.*, *Objective response rate targets for recurrent glioblastoma clinical trials based on the historic association between objective response rate and median overall survival*, ISSN: 15235866 Issue: 6 Publication Title: Neuro-Oncology Volume: 25, 2023. DOI: 10.1093/neuonc/noad002.

[73] M. A. Proescholdt, M. J. Merrill, E. M. Stoerr, A. Lohmeier, F. Pohl, and A. Brawanski, "Function of carbonic anhydrase IX in glioblastoma multiforme," *Neuro-Oncology*, vol. 14, no. 11, p. 1357, Nov. 2012, Publisher: Oxford University Press. DOI: 10.1093/NEUONC/NOS216.

[74] H. Yoo, S. Sohn, B. H. Nam, *et al.*, "The expressions of carbonic anhydrase 9 and vascular endothelial growth factor in astrocytic tumors predict a poor prognosis," *International Journal of Molecular Medicine*, vol. 26, no. 1, pp. 3–9, Jul. 2010, Publisher: Spandidos Publications. DOI: 10.3892/IJMM_00000427.

[75] D. X. Medina, E. P. Chung, R. Bowser, and R. W. Sirianni, "Lipid and polymer blended polyester nanoparticles loaded with adapalene for activation of retinoid signaling in the CNS following intravenous administration," *Journal of Drug Delivery Science and Technology*, vol. 52, 2019. DOI: 10.1016/j.jddst.2019.04.013.

[76] H. A. Herrmann, B. C. Dyson, L. Vass, G. N. Johnson, and J.-M. Schwartz, "Flux sampling is a powerful tool to study metabolism under changing environmental conditions," *NPJ systems biology and applications*, vol. 5, no. 1, p. 32, 2019.

[77] J. Lonsdale, J. Thomas, M. Salvatore, *et al.*, "The genotype-tissue expression (gtex) project," *Nature genetics*, vol. 45, no. 6, pp. 580–585, 2013.

[78] S. Varrette, P. Bouvry, H. Cartiaux, and F. Georgatos, "Management of an academic HPC cluster: The UL experience," *Proceedings of the 2014 International Conference on High Performance Computing and Simulation, HPCS 2014*, pp. 959–967, Sep. 2014, ISBN: 9781479953127 Publisher: Institute of Electrical and Electronics Engineers Inc. DOI: 10.1109/HPCSIM.2014.6903792.

Chapter 4

In silico drug target prediction using metabolic modeling identifies six novel repurposable drugs for melanoma

Tamara Bintener[1#], Maria Pires Pacheco[1#], Demetra Philippidou[1], Christiane Margue[1], Ali Kishk[1], Greta Del Mistro[2,3], Luca Di Leo[4], Maria Moscardó Garcia[1], Rashi Halder[5], Lasse Sinkkonen[1], Daniela De Zio[4,6], Stephanie Kreis[1], Dagmar Kulms[2,3], Thomas Sauter[1*]

[1] Department of Life Sciences and Medicine, University of Luxembourg, Belvaux, Luxembourg

[2] Experimental Dermatology, Department of Dermatology, TU-Dresden, Dresden, Germany.

[3] National Center for Tumour Diseases, TU-Dresden, Dresden, Germany.

[4] Melanoma Research Team, Danish Cancer Society Research Center, Copenhagen, Denmark.

[5] Luxembourg Centre for Systems Biomedicine, University of Luxembourg, Belvaux, Luxembourg.

[6] Department of Drug Design and Pharmacology, Faculty of Health and Medical Sciences, University of Copenhagen, Copenhagen, Denmark.

# These authors contributed equally. Tamara Bintener, Maria Pires Pacheco

* Corresponding Author: Thomas Sauter, Department of Life Sciences and Medicine, University of Luxembourg, Esch-Alzette, Luxembourg, Thomas.Sauter@uni.lu

This article has been published in:

Cell Death and Disease, Volume 14, 468, 2023,

https://www.nature.com/articles/s41419-023-05955-1

Introduction to the paper

Melanoma is the most aggressive type of skin cancer that originates from melanocytes due to ultraviolet light exposure. Nearly half and 9% to 29% of melanoma patients possess BRAF and NRAS mutations, respectively, that activate the RAF/MEK pathway, increasing proliferation and metastasis. The other half of melanoma patients have either BRAF-wiltype or other non-hotspot BRAF mutations. The RAF/MEK inhibitors combination of dabrafenib/trametinib was approved in 2018 for BRAF-mutant melanoma patients, while immune-checkpoint inhibitors (ICIs) and alkylating agents are the mainstays for BRAF-wildtype. Despite these approved drugs, melanoma patients taking RAF/MEK inhibitors have a high relapse rate; meanwhile, the biomarkers of ICIs responders are ill-defined. In this paper, we evaluate drugs and essential genes for melanoma that were predicted as part of Tamara Bintener's PhD thesis. Additionally, a group of investigational and approved drugs targeting nitric oxide (NO-based drugs) have been suggested for their anticancer activity. Both approved anti-melanoma and NO-based drugs were compared to the predicted drugs under three conditions: metastasis, drug resistance, and BRAF/NRAS mutation.

Contribution: I carried out the drug evaluation (Supplementary Figures 11-17) and data collection of clinical trials, wrote this section of the manuscript that was revised by co-authors, and prepared the figures.

4.1 Drug prioritisation

The effect of a knock-out of the essential genes, predicted targets, main targets of anti-melanoma drugs, and genes implicated in NO metabolism (NO-related genes) retrieved from the Drug Repurposing Hub [1] and literature [2], [3], were compared based on the median dependency probabilities (the likelihood that the knock-out of a gene reduces cell growth or induce cell death) in the CRISPR-Cas9 Cancer Dependency Map (DepMap) database [4] across melanoma primary, metastatic and uncategorized melanoma cell lines. Likewise, drug-induced resistance melanoma cell lines were used to rank these drug targets and essential genes. The resistance information was extracted from the "depmap_public_comments" column in the cell line metadata.

The viability reduction against DMSO for predicted, anti-melanoma and NO-based drugs was assessed using the Primary PRISM database [5] for primary and metastatic cell lines and resistant versus sensitive. Resistant cell lines were defined as cells with at least 50%

proliferation to anti-melanoma drugs (-50% viability reduction). The anti-melanoma drugs consisted of nine approved anti-melanoma in the Drug Repurposing Hub [1] in addition to the CDK4/6-inhibitor palbociclib that showed modest efficacy in a phase 2 melanoma trial [6]. The NO-based drugs were retrieved from different sources [1] and covered four mode-of-actions (see Supplementary File 2).

While the primary PRISM database covers a wide range of tested drugs (4606), these drugs were tested using a narrow range of concentrations (2.5-5 μM). On the other hand, cell viability databases with more tested concentrations allow determining more precise potency (such as IC_{50}) but on a smaller drug set. The three sets of drugs (predicted, NO-based, and anti-melanoma) were compared using the IC_{50} measures in high-throughput pan-cancer cell viability databases. Four databases with IC_{50} values were merged: Secondary PRISM (19Q4) [5], GDSC1000 (Release 8.4) [7], GDSC2000 (Release 8.4) [7], and Genentech Cell Line Screening Initiative [8]. As fotemustine was the only anti-melanoma missing in the merged IC_{50} database, fotemustine IC_{50} in melanoma cell lines were added manually from the literature. The melanoma cell lines in the secondary database were further classified based on the BRAF and NRAS mutation status to identify sensitive candidate drugs regardless of the cell line mutation profile. Mutation status retrieved from the DepMap website ("Binary Calls for Copy Number and Mutation Data") was used to classify the melanoma cell lines in the secondary PRISM database based on BRAF and NRAS mutations.

4.1.1 Predicted drugs and their targets show higher viability reduction and dependency, respectively, than anti-melanoma drugs and their targets, in both resistant and metastatic melanoma cell lines

The viability reduction was retrieved for 25 predicted, nine anti-melanoma, and 29 NO-based drugs from the primary PRISM database. Aminomethyltransferase enzyme (`https://clue.io/repurposing-app?q=Name:aminomethyltransferase`) was mislabeled as a compound in the Drug Repurposing Hub; thus, it was discarded from the NO-based drugs. Three predicted drugs (cladribine, fluvastatin, and gemcitabine) ranked higher than anti-melanoma drugs in both metastatic (Supplementary Figure S 4.1) and resistant cell lines (Supplementary Figures S 4.2 and S 4.3). Among the 29 NO-based drugs, diphenyleneiodonium is the only drug with a median viability reduction higher than 50% in either metastatic or resistant cell lines. The high ranking of the non-anti-cancer drug, fluvastatin, among the predicted anti-cancers (gemcitabine and cladribine) in both metastatic and resistant cell lines underlines fluvastatin as a potential anti-melanoma drug.

In both metastatic and resistant cell lines, predicted drug main targets have stronger dependency than anti-melanoma targets, with RRM1 and RRM2 scoring the highest; see Supplementary Figures S 4.4 and S 4.5. Main drug targets (anti-melanoma and predicted drugs) were selected from the drug targets using the Drug Repurposing Hub [1] for its highly manual curation. Unlike the primary PRISM database, DepMap offers eight drug-induced resistance cell lines corresponding to four wildtype cell lines. ASS1 was the highest NO-related gene with a 30% dependency probability in metastatic cell lines. As DepMap shows the effect of single gene knock-out in vitro in cell lines, the potential combination effect of NO-related genes with other targets is beyond this database and would need further testing.

4.1.2 Gemcitabine and cladribine show low IC_{50} under 0.4 μM as seven of the ten anti-melanoma drugs in melanoma cell lines from high-throughput drug viability databases.

The merged IC_{50} database included 1804 drugs and 1490 cell lines. The merged IC_{50} database retrieved ten anti-melanoma, 13 predicted, and four NO-based drugs with variant numbers of melanoma cell lines per drug ranging from one to 63. Ranking with the median IC_{50} showed seven of the nine anti-melanoma drugs were below 0.4 μM, see Supplementary Figure S 4.6. Gemcitabine and cladribine of the predicted drugs and only diphenyleneiodonium of the NO-based drugs were below the 0.4 μM threshold. Moreover, two predicted statins (pitavastatin and fluvastatin) were below 1 μM median IC_{50}. Some anti-melanoma drugs, especially BRAF-inhibitors (encorafenib dabrafenib), showed higher resistance in BRAF-wildtype and NRAS-mutant. Meanwhile, for the predicted drugs, especially cladribine, the median IC_{50} remained unaffected regardless of the BRAF or NRAS mutation, see Supplementary Figure S 4.7.

4.1.3 Tamoxifen and lovastatin showed positive clinical outcomes, while gemcitabine and itraconazole showed only stable disease in the sub-population of non-melanoma skin cancer

Furthermore, tamoxifen was found to improve overall complete and partial response in combination with chemotherapies without improving one-year survival in advanced melanoma in a meta-analysis of nine clinical trials [9]. On the contrary, melatonin (NO-based drug) combined with dacarbazine failed to show an additive effect compared to dacarbazine alone in an

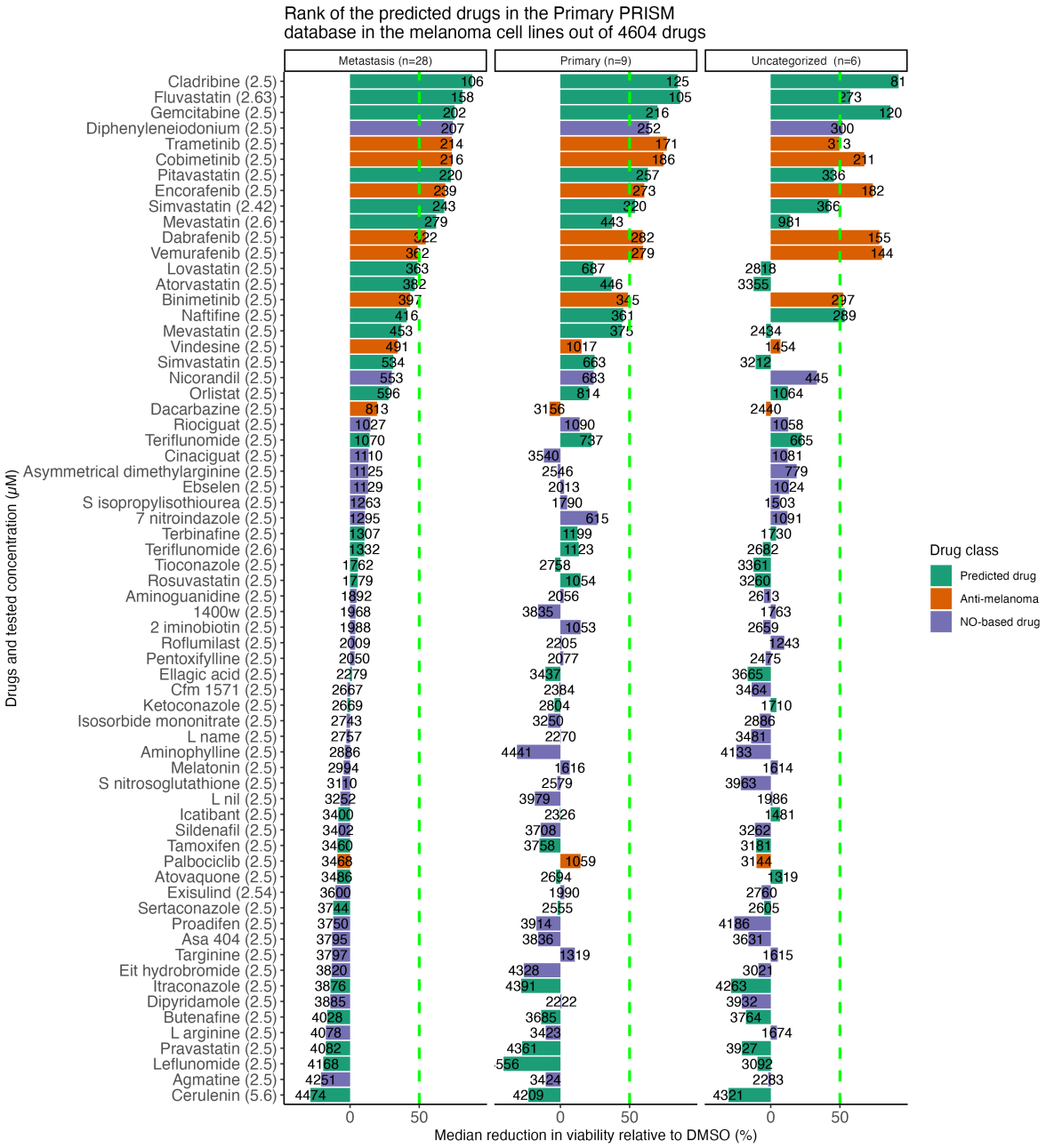

FIGURE 4.1: **Cladribine, fluvastatin, gemcitabine, and the NO-based drug diphenyleneiodonium rank better than anti-melanoma drugs in viability reduction assays.**

The viability reduction relative to DMSO for our 28 predicted, anti-melanoma and NO-based drugs was gathered from the primary PRISM database for metastatic, primary, and uncategorized cell lines. The drugs were ranked by their median viability reduction in metastatic cell lines. The X-axis represents the median viability reduction relative to DMSO (%) for metastatic (left), primary (middle), and uncategorized (right) cell lines. The rank of each drug out of the 4606 tested drugs in the primary PRISM database was printed beside each bar.

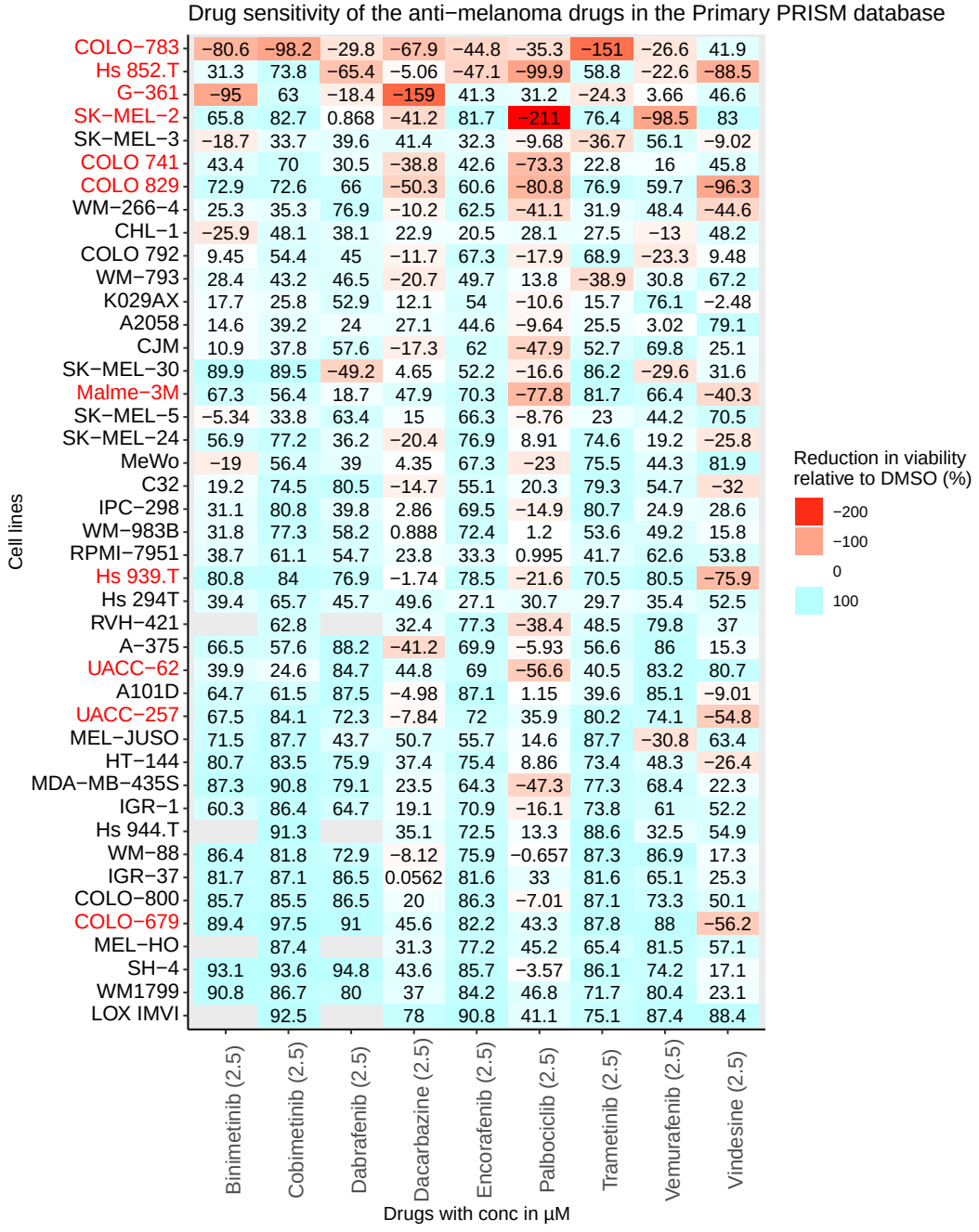

FIGURE 4.2: **Over a quarter of the melanoma cell lines displayed resistance to anti-melanoma drugs in the primary PRISM database.** Effect of drugs ranges from viability reduction (in blue) to increase of proliferation (up to more than 2-fold increase, in red). Cell lines with at least 50% increased proliferation (-50% viability reduction) to any anti-melanoma drug were considered resistant cell lines (names highlighted in red) for visualization in Figure S 4.3. The x-axis represents the anti-melanoma drugs, and the y-axis represents the melanoma cell lines. Missing drug-cell line experiments are marked in grey tiles.

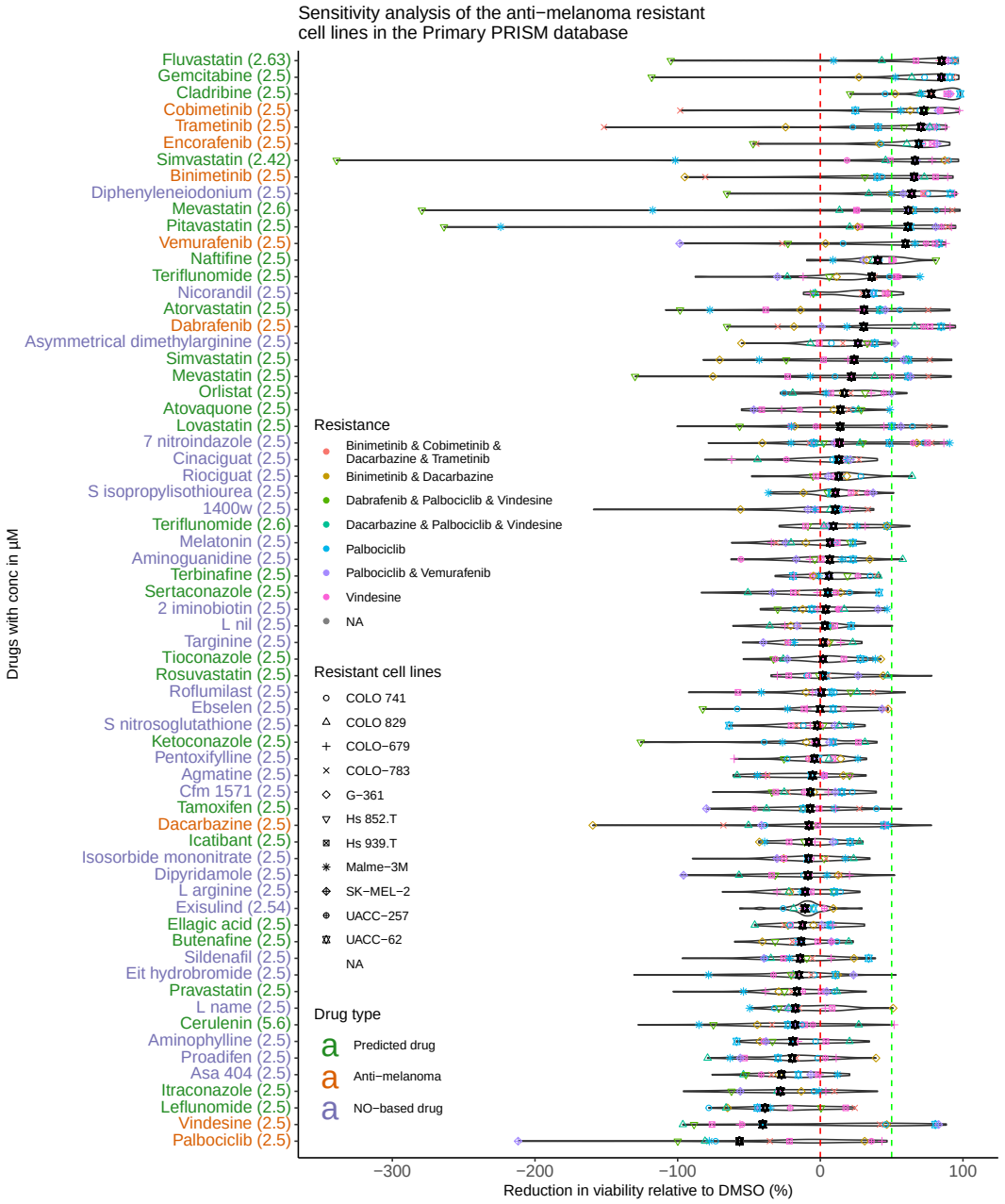

FIGURE 4.3: **Fluvastatin, gemcitabine, and cladribine outperformed anti-melanoma and NO-drugs on anti-melanoma drug-resistant cell lines.** Cell lines annotated as resistant to anti-melanoma drugs in the primary PRISM database (with viability reduction >-50%, names highlighted in red) were used to rank all drugs by their median viability reduction (black dot). The violin plot represents the viability reduction for different drugs across all melanoma cell lines of the primary PRISM database. Predicted, anti-melanoma and NO-based drugs' names on the y-axis have green, orange, and violet colors, respectively. The resistant melanoma cell lines are highlighted by a marker. The marker shape indicates the cell line, and the marker color indicates the drug the cell line is resistant to.

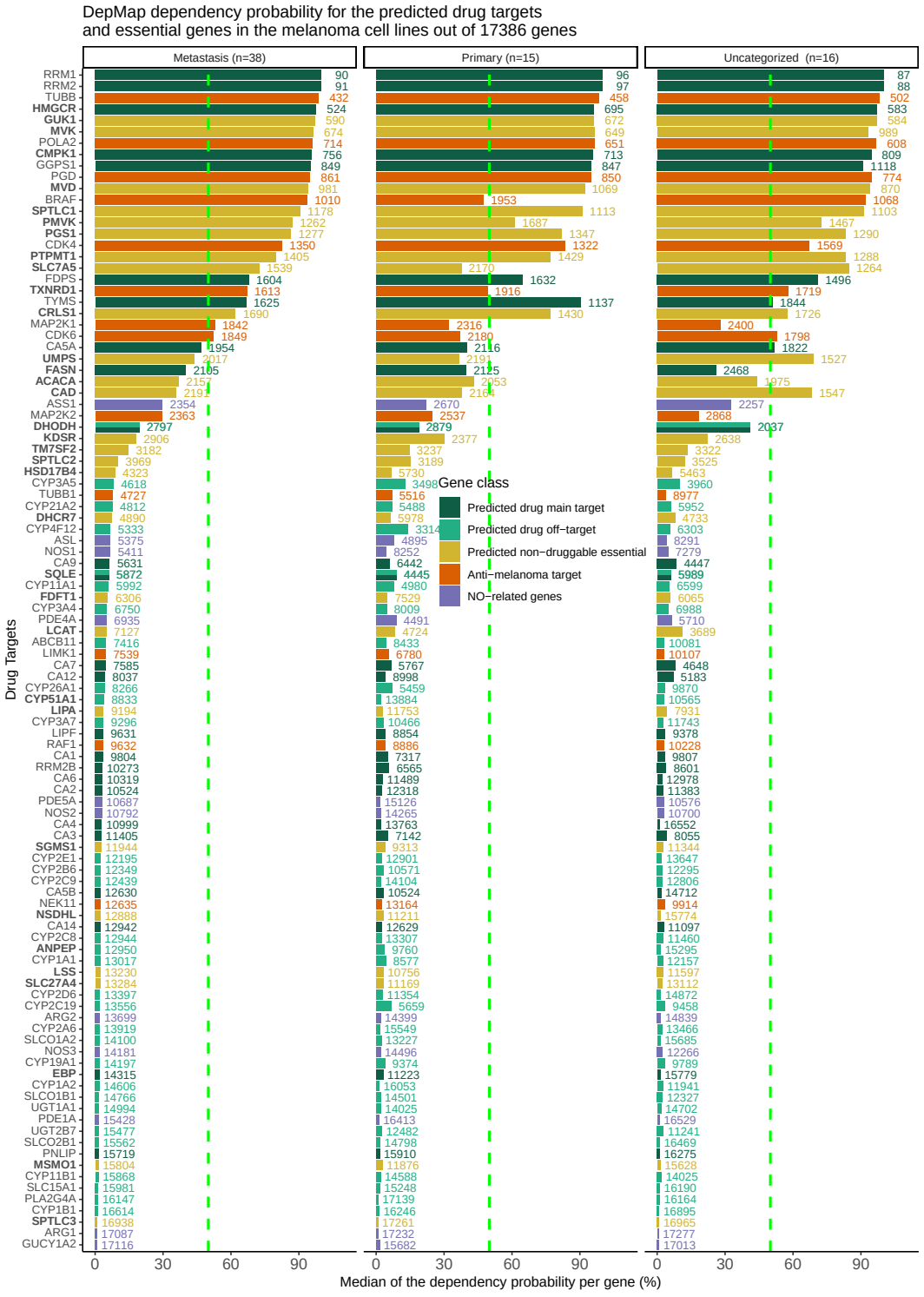

FIGURE 4.4: **The knockout of the predicted drug targets and essential genes induced a stronger viability reduction than the melanoma targets and NO-related genes.** Predicted drug targets and essential genes were compared to both the anti-melanoma targets and NO-related genes based on gene dependency probability scores (probability to induce cell death or stop cell growth upon knock-out) from DepMap in metastatic melanoma cell lines. The X-axis represents the median dependency probability across three types of melanoma cell lines (metastasis, primary, and uncategorized). Essential genes are highlighted in bold, and the non-druggable essential genes (according to DrugBank v5.1.3) have yellow bars. Genes are ranked on the y-axis by the median dependency probability in the metastatic cell lines, with the gene rank displayed on the right of each bar.

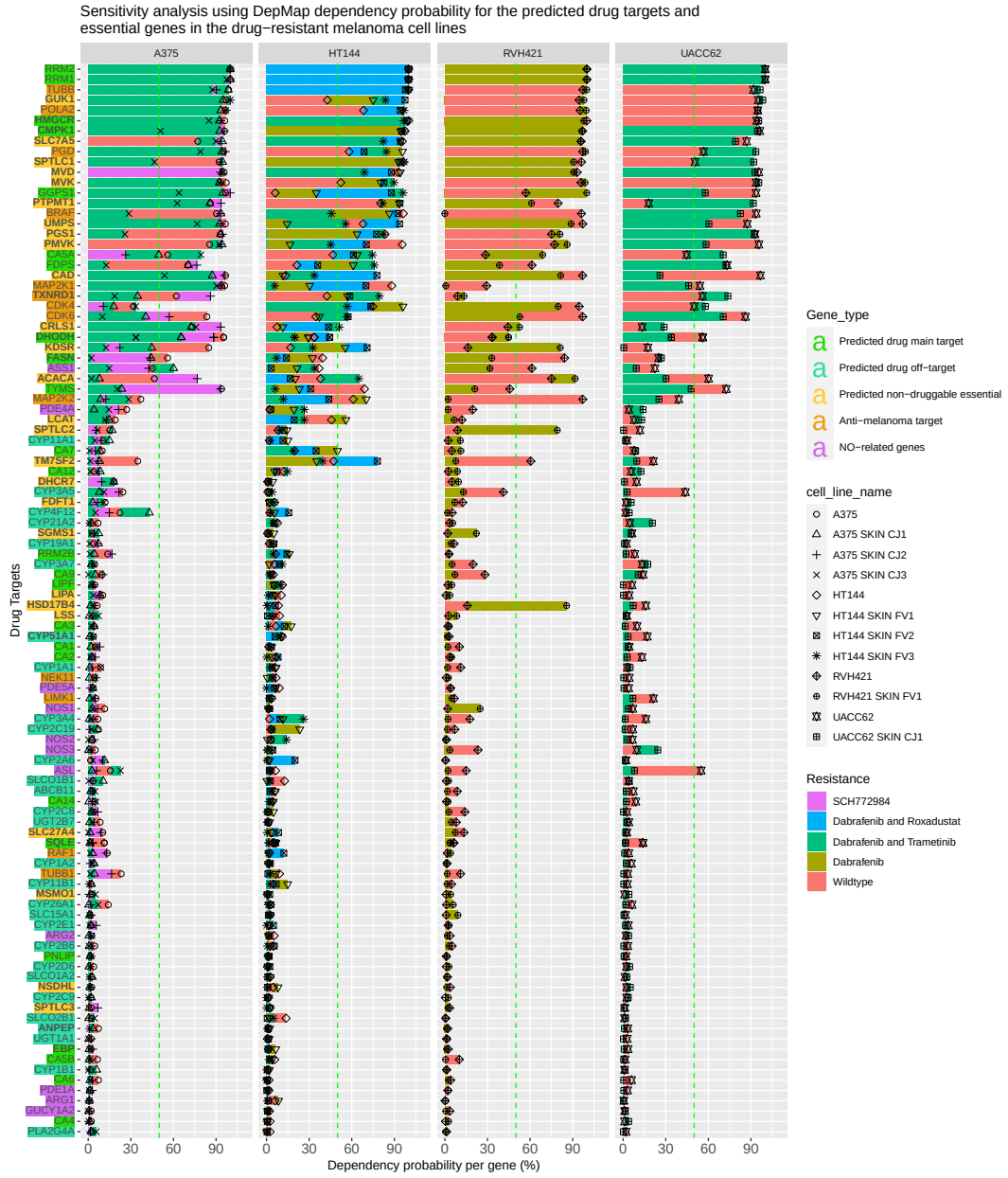

FIGURE 4.5: **The knockout of predicted essential genes induces a higher viability reduction in resistant cell lines.** The dependency probability of the predicted drug targets and essential genes were compared to anti-melanoma targets and NO-related genes using the drug-induced resistance (violet, brown, green, and blue bars) and wildtype (red bars) cell lines from the DepMap database. Genes (predicted drug targets, essential genes, anti-melanoma targets, and NO-related genes) were sorted by the median dependency probability across the eight resistant cell lines.

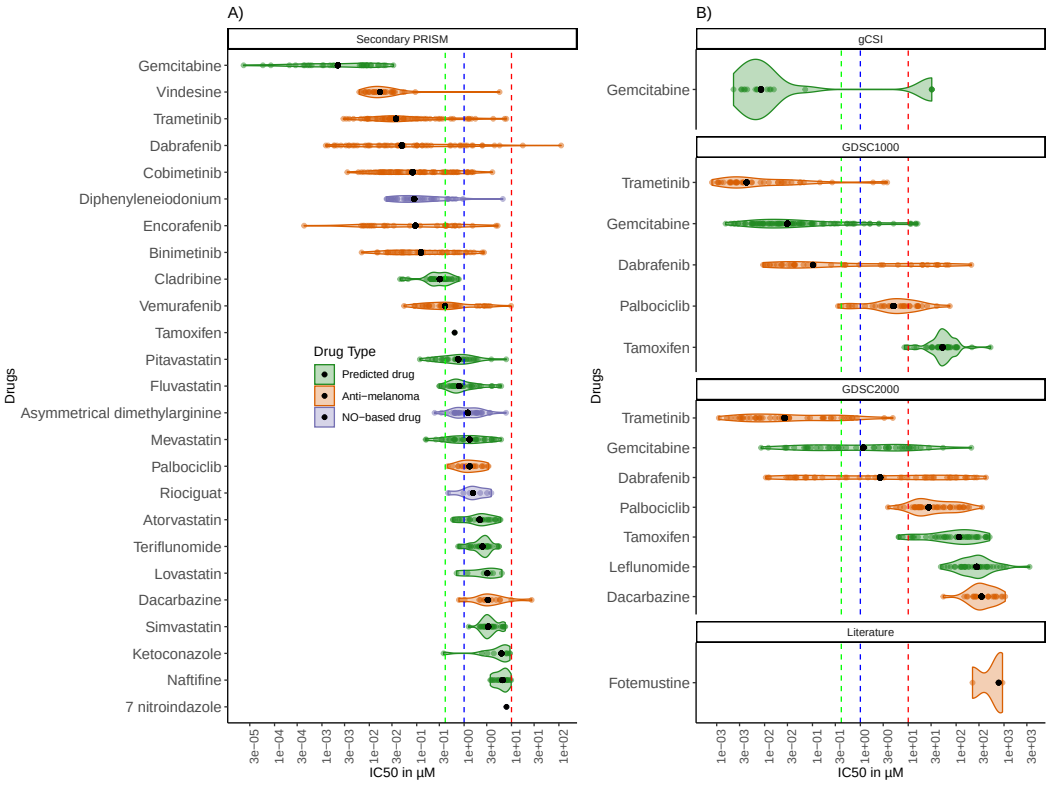

FIGURE 4.6: **Gemcitabine, cladribine and diphenyleneiodonium had comparable IC_{50} value data to known anti-melanoma drugs in melanoma cell lines in the secondary PRISM database.**
Four databases (Secondary PRISM, GDSC1000, GDSC2000, and gSCI) of cell viability in cancer cell lines with IC_{50} values were merged for the tested drugs across melanoma cell lines. Black dots represent the median IC_{50}. Green, blue, and red dashed lines correspond to 0.4, 1, and 10 μM, respectively. Seven of the ten anti-melanoma drugs have median IC_{50} below 0.4 μM (green line), whereas gemcitabine and cladribine have their median IC_{50} below this threshold of 0.4 μM.

early terminated phase II trial of metastatic melanoma [10]. Interestingly, a phase II placebo-controlled preventive trial found that lovastatin may decrease the incidence of melanoma without reducing melanoma biomarkers [11]. Gemcitabine and itraconazole in non-melanoma skin cancer phase II trials show no response but stable disease in a subset of the treated patients (35% in gemcitabine [12] and 21% [13] to 91% [14] in itraconazole the disease remained stable) (see Supplementary File 2). While cladribine is still untested in a clinical trial for melanoma, it can be administered subcutaneously for cancer [15]. Using IC_{50} values and prior knowledge as criteria, we selected 12 out of the 28 predicted drugs (three FDA-approved non-melanoma anticancer and nine FDA-approved for other diseases) for experimental validation. Two predicted drugs (gemcitabine and cladribine) and one NO-based drug (diphenyleneiodonium) have a reported median IC_{50} below 0.4 μM in melanoma cell lines, this being comparable to known anti-melanoma drugs (Supplementary Figure S 4.6.A). Unlike targeted anti-melanoma drugs

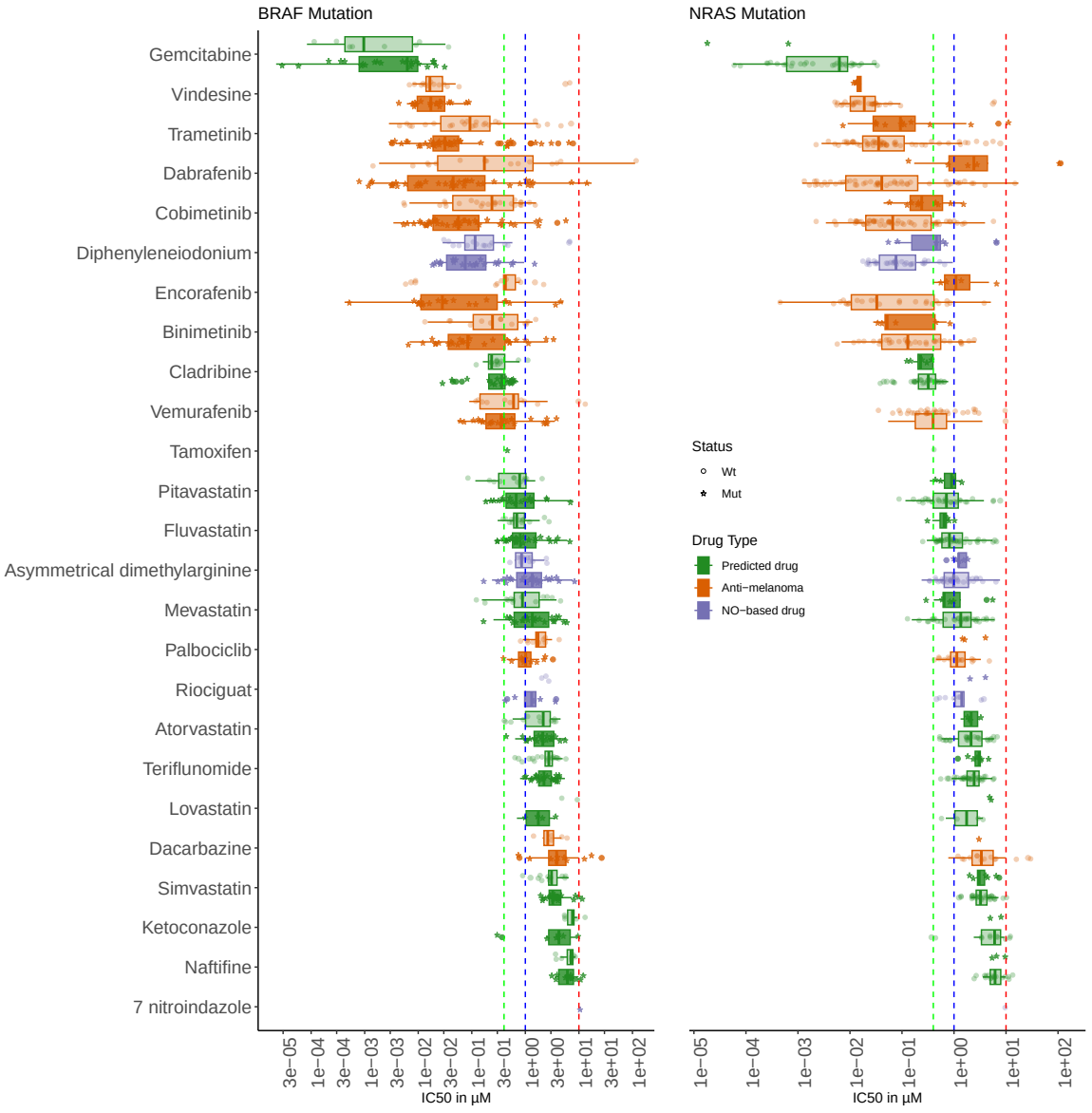

FIGURE 4.7: **The IC_{50} values of cladribine and other predicted drugs, unlike anti-melanoma drugs, are independent of the BRAF or NRAS mutation status.** IC_{50} (Supplementary Figure S 4.6.A) were classified based on the mutation status in BRAF and NRAS genes. Transparent and opaque box plots correspond to wildtype and mutants, respectively.

that tend to be more effective for either BRAF-mutant or NRAS-wildtype cell lines (Supplementary Figure S 4.7), cladribine and other predicted drugs show good efficacy regardless of the mutation status with narrow IC_{50} ranges (see Supplementary File 2 for the IC_{50} values found in the databases and the literature and additional information on clinical trials).

Contributions

T.S., M.P.P., L.S., D.K., S.K. and D.D.Z. performed study concept and design; T.B., M.P.P., T.S., A.K. and M.M.G. performed development of methodology and computational analysis; D.P., C.M., G.D.M., L.D.L. and R.H. performed experimental validation. All authors contributed to the writing, review, and revision of the paper. All authors read and approved the

final paper.

Acknowledgments

This research was funded in part by the Luxembourg National Research Fund (FNR), grant reference [PRIDE15/10675146/CANBIO]. D.D.Z. is supported by the LEO Foundation (LF-OC-19-000004) and the Melanoma Research Alliance young investigator grant (MRA 620385). For open access, the authors have applied a Creative Commons Attribution 4.0 International (CC BY 4.0) licence to any Author Accepted Manuscript version arising from this submission. We acknowledge Aurélien Ginolhac for processing the raw data and generating the FPKM. The computational experiments presented in this paper were carried out using the HPC facilities of the University of Luxembourg [16],(https://hpc.uni.lu).

4.2 Summary and Outlook

In addition to the previous clinical trials, other clinical data collected in the synopsis (see Table 1.3.8) support the efficacy of statins but not the pyrimidine synthesis inhibitor leflunomide.

Statins: Two retrospective studies found concurrent statins with ICIs [17] and statins use [18] improved immune checkpoint inhibitors (ICIs) response and reduced melanoma incidence, respectively.

Leflunomide: Combining leflunomide with vemurafenib[19] failed in a phase I/II clinical trial in BRAF-mutant metastatic melanoma.
A limitation in this work is the absence of the approved ICIs in the HTS databases.

References

[1] S. M. Corsello, J. A. Bittker, Z. Liu, *et al.*, "The Drug Repurposing Hub: A next-generation drug library and information resource," *Nature Medicine*, vol. 23, no. 4, pp. 405–408, Apr. 2017, Publisher: Nature Publishing Group. DOI: 10.1038/NM.4306.

[2] J. Mintz, A. Vedenko, O. Rosete, *et al.*, "Current advances of nitric oxide in cancer and anticancer therapeutics," *Vaccines*, vol. 9, no. 2, pp. 1–39, Feb. 2021, Publisher: MDPI AG. DOI: 10.3390/VACCINES9020094.

[3] J. P. Stasch, P. Pacher, and O. V. Evgenov, "Soluble Guanylate Cyclase as an Emerging Therapeutic Target in Cardiopulmonary Disease," *Circulation*, vol. 123, no. 20, p. 2263, May 2011, Publisher: NIH Public Access. DOI: 10.1161/CIRCULATIONAHA.110.981738.

[4] C. Pacini, J. M. Dempster, I. Boyle, *et al.*, "Integrated cross-study datasets of genetic dependencies in cancer," *Nature Communications*, vol. 12, no. 1, Dec. 2021, Publisher: Nature Research. DOI: 10.1038/S41467-021-21898-7.

[5] S. M. Corsello, R. T. Nagari, R. D. Spangler, *et al.*, "Discovering the anti-cancer potential of non-oncology drugs by systematic viability profiling," *Nature cancer*, vol. 1, no. 2, pp. 235–248, Feb. 2020, Publisher: NLM (Medline). DOI: 10.1038/S43018-019-0018-6.

[6] B. Louveau, M. Resche-Rigon, T. Lesimple, *et al.*, "Phase i–ii open-label multicenter study of palbociclib+ vemurafenib in braf v600mut metastatic melanoma patients: Uncovering chek2 as a major response mechanism," *Clinical Cancer Research*, vol. 27, no. 14, pp. 3876–3883, 2021.

[7] W. Yang, J. Soares, P. Greninger, *et al.*, "Genomics of Drug Sensitivity in Cancer (GDSC): A resource for therapeutic biomarker discovery in cancer cells," *Nucleic Acids Research*, vol. 41, no. D1, pp. D955–D961, Jan. 2013. DOI: 10.1093/nar/gks1111.

[8] P. M. Haverty, E. Lin, J. Tan, *et al.*, "Reproducible pharmacogenomic profiling of cancer cell line panels," *Nature 2016 533:7603*, vol. 533, no. 7603, pp. 333–337, May 2016, Publisher: Nature Publishing Group. DOI: 10.1038/nature17987.

[9] J. R. Beguerie, J. Xingzhong, and R. P. Valdez, "Tamoxifen vs. non-tamoxifen treatment for advanced melanoma: A meta-analysis," *International Journal of Dermatology*, vol. 49, no. 10, pp. 1194–1202, Oct. 2010. DOI: 10.1111/J.1365-4632.2010.04529.X.

[10] A. V. Novik, S. A. Protsenko, I. A. Baldueva, *et al.*, "Melatonin and Metformin Failed to Modify the Effect of Dacarbazine in Melanoma," *Oncologist*, vol. 26, no. 5, 364–e734, May 2021, Publisher: John Wiley and Sons Inc. DOI: 10.1002/ONCO.13761.

[11] K. G. Linden, S. A. Leachman, J. S. Zager, *et al.*, "A randomized, double-blind, placebo-controlled phase II clinical trial of lovastatin for various endpoints of melanoma pathobiology," *Cancer Prevention Research*, vol. 7, no. 5, pp. 496–504, 2014, Publisher: American Association for Cancer Research Inc. DOI: 10.1158/1940-6207.CAPR-13-0189.

[12] W. E. Samlowski, H. Gundacker, J. P. Kuebler, *et al.*, "Evaluation of gemcitabine in patients with recurrent or metastatic squamous cell carcinoma of the head and neck: A Southwest Oncology Group Phase II study," *Investigational New Drugs*, vol. 19, no. 4, pp. 311–315, 2001. DOI: 10.1023/A:1010657609609.

[13] D. J. Kim, J. Kim, K. Spaunhurst, *et al.*, "Open-label, exploratory phase II trial of oral itraconazole for the treatment of basal cell carcinoma," *Journal of Clinical Oncology*, vol. 32, no. 8, pp. 745–751, Mar. 2014, Publisher: American Society of Clinical Oncology. DOI: 10.1200/JCO.2013.49.9525.

[14] E. Pereira, O. Camacho-Vanegas, S. Anand, *et al.*, "Personalized circulating tumor DNA biomarkers dynamically predict treatment response and survival in gynecologic cancers," *PLoS ONE*, vol. 10, no. 12, G. Samimi, Ed., e0145754, Dec. 2015, ISBN: 19326203 (Electronic). DOI: 10.1371/journal.pone.0145754.

[15] R. Benz, K. Arn, M. Andres, *et al.*, "Prospective long-term follow-up after first-line subcutaneous cladribine in hairy cell leukemia: A SAKK trial," *Blood Advances*, vol. 4, no. 15, pp. 3699–3707, Aug. 2020, Publisher: American Society of Hematology. DOI: 10.1182/BLOODADVANCES.2020002160.

[16] S. Varrette, P. Bouvry, H. Cartiaux, and F. Georgatos, "Management of an academic HPC cluster: The UL experience," *Proceedings of the 2014 International Conference on High Performance Computing and Simulation, HPCS 2014*, pp. 959–967, Sep. 2014, ISBN: 9781479953127 Publisher: Institute of Electrical and Electronics Engineers Inc. DOI: 10.1109/HPCSIM.2014.6903792.

[17] A. Cortellini, M. Tucci, V. Adamo, *et al.*, "Integrated analysis of concomitant medications and oncological outcomes from pd-1/pd-l1 checkpoint inhibitors in clinical practice," *Journal for immunotherapy of cancer*, vol. 8, no. 2, 2020.

[18] R. Ghiasvand, L. A. Berge, B. K. Andreassen, *et al.*, "Statin use and risk of cutaneous melanoma: A nationwide nested case–control study," *British Journal of Dermatology*, vol. 188, no. 6, pp. 805–807, 2023.

[19] H. Cortes, O. D. Reyes-Hernandez, S. Alcala-Alcala, *et al.*, "Repurposing of drug candidates for treatment of skin cancer," *Frontiers in oncology*, vol. 10, p. 605 714, 2021.

Chapter 5

Bruceine D Identified as a Drug Candidate against Breast Cancer by a Novel Drug Selection Pipeline and Cell Viability Assay

Claudia Cipriani[1], Maria Pires Pacheco[1], Ali Kishk[1], Maryem Wachich[2], Daniel Abankwa[2], Elisabeth Schaffner-Reckinger[2], and Thomas Sauter[1], *

[1] Department of Life Sciences and Medicine, University of Luxembourg, Belval Campus, 2, avenue de l'Université L-4365 Esch-sur-Alzette, Luxembourg; Claudia.Cipriani1307@gmail.com (C.C.); Maria.Pacheco@uni.lu (M.P.P.); Ali.Kishk@uni.lu (A.K.)

[1] Department of Life Sciences and Medicine, University of Luxembourg, L-4367 Belvaux, Luxembourg

[2] Cancer Cell Biology and Drug Discovery Group, Department of Life Sciences and Medicine, University of Luxembourg, L-4365 Esch-sur-Alzette, Luxembourg; MaryemWachich@gmail.com (M.W.); Daniel.Abankwa@uni.lu (D.A.); Elisabeth.Schaffner@uni.lu (E.S.-R.)

* Correspondence: Thomas.Sauter@uni.lu

This article has been published in:

Pharmaceuticals, Volume 15, 2022, https://doi.org/10.3390/ph15020179\

Introduction to the paper

Natural products have been used for medicinal purposes for centuries, with isolated compounds now comprising half of approved chemotherapies. Despite there being over 30 approved chemotherapies for breast cancer in women, approximately one in eight women will be diagnosed with the disease. This high incidence rate calls for the search for new compounds with anti-breast cancer properties, as well as for compounds with potential preventative effects found in common diets. The chemopreventive properties of many NPs have been studied in retrospective studies. However, the systematic search for chemopreventive NPs compounds faced hurdles due to the focus on whole herbs, the multi-target effect of NPs, and the absence of mechanistic understanding. Nevertheless, recent preclinical compounds-treated expression data provide an unbiased investigation of various NPs. Here, we built genome-scale metabolic models of breast cancer cell lines pre-treated with 101 NPs to rank them for potential anti-breast cancer activity. This ranking includes similarity to approved anti-breast cancer drugs, dissimilarity to the control model, pathway analysis, and drug deletion. Out of the 101 NPS, 23 were predicted as candidate drugs, of them, nine NP were selected and tested in a 2D cell viability assay. Bruceine D, emodin, and scutellarein inhibited MCF-7 and Hs 578T cell proliferation in a dose-dependent manner with IC50 values ranging from 0.7 to 65 M.

Contribution: I carried out the literature review, wrote the manuscript, and prepared the figures.

Abstract

The multi-target effects of natural products allow us to fight complex diseases like cancer on multiple fronts. Unlike docking techniques, network-based approaches such as genome-scale metabolic modeling can capture multi-target effects. However, the incompleteness of natural product target information reduces the prediction accuracy of *in silico* gene knockout strategies. Here, we present a drug selection workflow based on context-specific genome-scale metabolic models, built from the expression data of cancer cells treated with natural products, to predict cell viability. The workflow comprises four steps: first, in silico single-drug and drug combination predictions; second, the assessment of the effects of natural products on cancer metabolism via the computation of a dissimilarity score between the treated and control models; third, the identification of natural products with similar effects to the approved drugs; and fourth, the identification of drugs with the predicted effects in pathways of interest, such

as the androgen and estrogen pathway. Out of the initial 101 natural products, nine candidates were tested in a 2D cell viability assay. Bruceine D, emodin, and scutellarein showed a dose-dependent inhibition of MCF-7 and Hs 578T cell proliferation with IC_{50} values between 0.7 to 65 μM, depending on the drug and cell line. Bruceine D, extracted from *Brucea javanica* seeds, showed the highest potency.

Keywords

natural products; bruceine D; emodin; scutellarein; drug prediction workflow; metabolic modeling

5.1 Introduction

Breast cancer is one of the leading cancers in women, with around 2.26 million cases worldwide in 2020, representing an incidence of 11.7% and a mortality of 6.9% of all diagnosed cancers [1]. Breast cancer is a heterogeneous disease with various molecular features, clinical outcomes, and degrees of chemotherapy resistance. In order to provide a tailored treatment, breast carcinomas can be subdivided into five different molecular subtypes based on the presence of hormone receptors (HR, corresponding to estrogen receptor, ER, and progesterone receptor, PR), human epidermal growth factor receptor 2 (HER2), and the protein Ki-67, which serves as a marker for cellular proliferation: luminal A, normal-like (similar to luminal A, but with a slightly worse prognosis), luminal B, HER2-enriched, and triple-negative, which is also referred to as basal-like [2]. Typically, the luminal A subtype has a better prognosis, whereas the triple-negative subtype has the worst 5-year survival rate [3]. Breast cancer can further be clinically classified as a function of its size, location, and invasiveness. This classification comprises stage 0 (carcinoma *in situ*), and then ranges from stage I to stage IV, with the latter corresponding to invasive cancer that has propagated to distant sites of the body [4]. Besides the inter-tumor heterogeneity between patients, the clonal heterogeneity of a single breast tumor can cause therapies to fail to eradicate the whole tumor; hence, residual tumor cells tend to develop chemoresistance and metastasis [5]. The multi-target and heterogenous pharmacological mechanisms of action of natural products—and thus, their more ubiquitous efficiency—help to counteract cancer heterogeneity and prevent drug resistance [6]. Natural products, extracted from plants or animals, have been used to treat many diseases in various regional traditional medicines [7]. Nowadays, natural products including isolated herbal compounds and botanical

mixtures containing a plethora of plant ingredients, as well as semi-synthetic derivatives and mimics, are being studied extensively for the treatment of different diseases, including cancer. To date, only two botanicals have been reviewed and approved by the FDA (sinecatechins and crofelemer) [8]. On the other hand, more single herbal compounds are used in clinical practice, such as paclitaxel and cabazitaxel for cancer treatment. These single herbal compounds are either extracted from plants or produced at an industrial scale in a semi-synthesis or total synthesis process, such as paclitaxel. Notably, some studies on breast cancer cell lines have shown synergistic effects following combined treatment with natural products and estrogen receptor modulators such as genistein and ormeloxifene [9], or equol and tamoxifen [10]. *in silico* metabolic models allow the simulation of the metabolism of a whole cell or an organism [11], both for different metabolic phenotypes [12] and diseases, such as cancer [13]–[15]. Metabolic models were recently used to speed up the process of identifying possible new applications for existing drugs [15], [16]. In the present study, we present a new drug prediction and analysis pipeline (`https://github.com/sysbiolux/Herbal_drug_prediction` accessed date 14 December 2021) tailored to the complex mode of action of natural products and the lack of the complete knowledge of their targets. The pipeline requires the gene expression data of cells treated with natural products and a genome-scale reconstruction such as Recon3D as an input in order to build context-specific metabolic models via FASTCORMICS or rFASTCORMICS [15], [17]. The models are then used to simulate the effects of the natural products on the metabolism of cancer cells, and to prioritise the natural products based on their predicted efficacy. Here, microarray gene expression data of the MCF-7 breast cancer cell line treated with 101 natural products [18] were used as the input for the pipeline. Out of 101 single natural products, and one mixture of natural products, nine products were identified as promising candidates with anticancer activity, and were subjected to experimental validation via a 2D cell viability test, which is commonly used in the drug discovery process. Among the nine candidates, emodin, scutellarein, and bruceine D caused a decrease in the proliferation of MCF-7 and Hs 578T cells at low IC_{50} values, indicating the good performance of the developed drug prediction pipeline.

5.2 Results

In order to assess the potential effect of natural products on the metabolism of breast cancer cells, and to identify promising drug candidates, a microarray expression dataset composed of the expression data of MCF-7 cells treated with 101 natural products, one mixture of natural products (salvianic acid A sodium, salvianolic acid B, protocatechuic aldehyde and

Table 5.1: Summary of the 103 context-specific models (101 natural products, one mixture of natural products, and one DMSO model) in terms of the median number of reactions, metabolites, and genes.

	Reactions	Metabolites	Genes
Median	1895 ± 87	1593	2169
Min	1593 ± 66	1353	1790
Max	1036 ± 49	908	1128

tanshinone IIA), and the control—dimethyl sulfoxide (DMSO) [18]—was used to reconstruct context-specific metabolic models (102 natural product models and a control model) via the FASTCORMICS workflow [17]. The median, minimal and maximal number of reactions, metabolites, and genes of the models are displayed in Table 5.1. The size of the models varies between 1593 and 2169 reactions, with a median of 1895 reactions. An *in silico* drug prediction and analysis workflow composed of (i) the drug prediction of growth by natural products' target deletion, (ii) the assessment of the dissimilarity of the included reactions compared to the DMSO (control) model reactions, (iii) the assessment of the similarity of the predicted flux ranges carried by the reactions of natural product models and the DMSO model constrained by the approved breast cancer drugs, and (iv) a pathway analysis, which was used on these 103 models to predict 23 potential candidates. The model statistics for all of the 102 conditions (101 natural products + one mixture) are available in Table S1 of Supplementary File S1. However, in order to facilitate the representation of the data, only the data of the predicted 23 drugs are shown in the main text.

5.2.1 *Ferulic Acid, Resveratrol, Capecitabine, and Methotrexate Are Predicted to Reduce the Growth of MCF-7 Cells*

Among these 101 natural products, human targets for only 44 drugs were found in DrugBank V5 [19], PROMISCUOUS 2.0 [20], and NPASS [21]; 35 drugs thereof targeted metabolic genes (see Supplementary File S1, Table S2 for the detailed drug–target interactions, and Supplementary File S2, Table S3 for the summary of the number of interactions). The effect of these 35 natural products on the growth of MCF-7 cells was simulated *in silico* by setting the bounds of all of the target reactions in the control DMSO model to zero. After the knockout of the targets of ferulic acid and resveratrol, the DMSO model could not produce biomass anymore. As a quality control, 26 approved breast cancer drugs (see Supplementary File S1, Table S4 for the list of breast cancer drugs, and Supplementary File S1, Table S5 for the detailed drug–target interactions) were tested using the same approach on the DMSO model. Capecitabine, a precursor of the drug fluorouracil [22], and methotrexate, an antagonist of

folic acid [23], were predicted to stop the growth of cancer cells. The other 24 tested breast cancer drugs had a predicted growth ratio of more than 0.998, suggesting that the other 24 breast cancer drugs have modes of action that do not target the metabolism of cancer cells, or target pathways that are not directly related to growth. In order to assess whether the other 24 breast cancer drugs could have a combined effect with natural products, two different experiments were performed. First, the targets of every combination of natural product and breast cancer drug in the DMSO model were set to zero, in order to assess whether the combination of the two drugs caused a stronger reduction of the growth than each natural product or cancer drug individually. Second, in order to verify that the natural products do not have undescribed targets that might result in synergies when used in combination with breast cancer drugs, the targets of the breast cancer drugs were set to zero in the reconstructed 102 natural product models (101 single drugs and one mixture of four drugs). However, there was no significant reduction of the growth when we compared the cancer drug deletion on the DMSO model and the natural product model. The single-gene deletion was applied to ferulic acid, resveratrol, methotrexate, and capecitabine in order to determine which of these drug targets can decrease the biomass individually. Single-gene deletion did not predict any single essential genes for ferulic acid or resveratrol but identified three single essential genes for methotrexate (Thymidylate synthase (TYMS), Dihydrofolate reductase (DHFR), 5-Aminoimidazole-4-Carboxamide Ribonucleotide Formyltransferase (ATIC)) and one single essential gene (TYMS) for capecitabine.

5.2.2 *Bruceine D, Narciclasine, Hydroxysafflor Yellow A, Ferulic Acid, and Salvianolic Acid B Are Predicted to Show the Strongest Perturbations of the Metabolism of MCF-7 Cells*

As mentioned before, no metabolic target information could be found in DrugBank V5 [19], PROMISCUOUS 2.0 [20], or NPASS [21] for 66 out of the 101 natural products, and the list of targets of the 35 listed drugs is likely to be incomplete, as these drugs have multiple targets. Hence, in order to further identify candidate natural products that might affect the metabolism of MCF-7 cells, the structure of the reconstructed natural product models in terms of the included reactions in the natural product models was compared to the DMSO control model. A dissimilarity score was computed for each natural product model against the DMSO model (using 1-Jaccard Index J, where J is the number of shared reactions between a natural product and the DMSO model divided by the total number of reactions). A dissimilarity score of 1 means that the natural product model does not share any reaction with the DMSO model;

hence, the associated drug has a strong effect on the metabolism of MCF-7 cells. On the other hand, a score of 0 means that the two models are identical; hence, the effect of the natural product drug on the MCF-7 metabolism is negligible in terms of its network structure. The calculated dissimilarity score ranged from 0.19 to 0.44 for ephedrine hydrochloride and narciclasine, respectively. The group of the top five natural product models (narciclasine, bruceine D, hydroxysafflor yellow A, ferulic acid, and salvianolic acid B) with the highest dissimilarity scores in the DMSO model (ranging from 0.44 to 0.40) were retained for further analysis. Figure 5.1 shows the dissimilarity values for the 23 drugs predicted as potential candidates by at least one of the steps of the drug prediction workflow (Table 5.2), and Supplementary Figure S1 contains the complete results. The fifth and sixth top-ranked drugs, salvianolic acid B and nitidine chloride, have dissimilarity scores of 0.40 and 0.37, respectively, which are larger differences compared to the drugs higher ranks (Supplementary Figure S1).

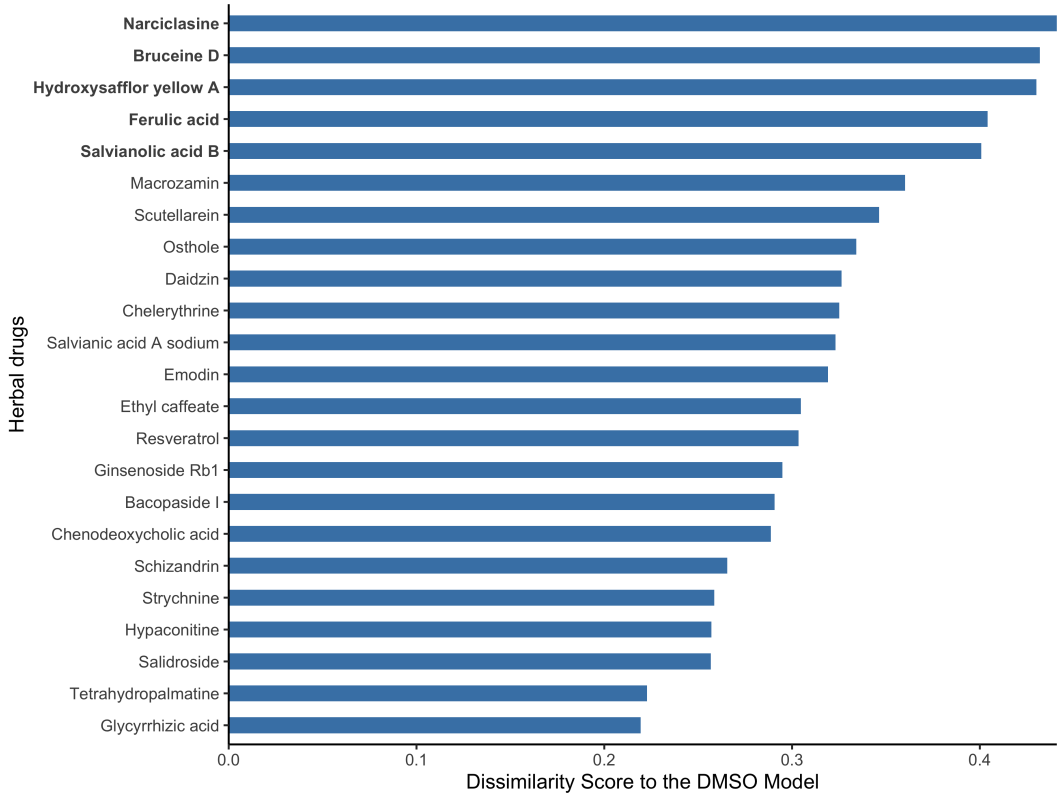

FIGURE 5.1: **Dissimilarity scores between the breast cancer models reconstructed from the expression data of MCF-7 cells treated with natural products and the DMSO model (control model).**

Natural products that alter the metabolism of breast cancer cells to a large extent (in bold) have a high dissimilarity to the control DMSO model. A dissimilarity score (D) was computed based on the Jaccard Similarity index (J, where J is the number of shared reactions between two models divided by the total number of reactions), where D is equal to 1-J. The dissimilarity score represents the fraction of reactions that are different between the two models.

Table 5.2: Summary table of the 23 candidate natural products for potential anticancer action based on four *in silico* analysis steps.

Highlighted in green are the drugs that were predicted in two steps; in blue are the drugs predicted in only one step, but that were additionally supported by data from the Dr. Duke Database and the Drug Repurposing Hub Database. Both sets were submitted for experimental validation. Highlighted in red is the drug strychnine, which was eliminated due to toxicity; highlighted in orange is the drug narciclasine, which was removed due to a large amount of published data. In yellow are the drugs that were predicted by one step and not retained for validation. The background colors correspond to the different NP selection criteria, which are mentioned in the main text as (Table 2, COLOR).

Natural Product	Drug Deletion	Dissimilarity to DMSO model	Similarity to cancer drug models	Pathway analysis	Anticancer activity (Dr. Duke Database)	Mode of action (Drug Repurposing Hub Database)	Clinical Phase
Ferulic Acid	1	1	1			antioxidant	Phase 2
Glycyrrhizic acid			1	1			
Resveratrol	1			1	Antitumor, Antioxidant, Apoptotic, Antiangiogenic	cytochrome P450 inhibitor, SIRT activator	Launched
Scutellarein				1	Antioxidant, Cancer-preventive		
Strychnine				1	Antioxidant	acetylcholine receptor antagonist	Preclinical
Narciclasine		1		1			
Hydroxysafflor yellow A		1	1			anti-tumor agent	Preclinical
Salvianolic Acid B		1	1			EGFR inhibitor, metalloproteinase inhibitor	Phase 2
Daidzin			1		Antioxidant, Cancer-preventive	antioxidant	Phase 1
Macrozamin			1				
Chelerythrine				1	Antimitotic		
Chenodeoxych acid				1		11-ß hydroxysteroid dehydrogenase inhibitor, FXR agonist	Launched
Emodin				1	Antitumor, Immunosuppressant	11-ß hydroxysteroid dehydrogenase inhibitor	Preclinical
Tetrahydropal				1			
Bacopaside I			1				
Ethyl caffeate			1				
Ginsenoside Rb1			1				
Hypaconitine			1				

Salidroside			1			beta-amyloid protein neurotoxicity inhibitor	Preclinical
Salvianic acid A sodium			1			matrix metalloprotease inhibitor	
Schizandrin			1		Antioxidant		
Bruceine D		1				glycine receptor antagonist	Preclinical
Osthole				1		Calcium channel blocker	Preclinical

5.2.3 *13 Natural Products Are Predicted to Affect the Metabolism of MCF-7 Cells Similarly to the Breast Cancer Drugs Capecitabine and Methotrexate*

With a high dissimilarity score for a natural product model compared to the DMSO model does not necessarily imply that the associated natural product is efficient against breast cancer, but rather that the metabolic changes induced by the natural products are different from the ones induced by DMSO. However, selecting natural products that have a similar effect to known breast cancer drugs on the metabolic models increases the likelihood of the identification of efficient drug candidates. As a first step, and in order to quantify the effect of all 26 breast cancer drugs, the dissimilarity score between the DMSO model constrained by the cancer drug targets (cancer drug models) and the unconstrained DMSO model was computed based on flux ranges obtained using Flux Variability Analysis (FVA). Models that included reactions that maintained the same flux range between two models have a dissimilarity score of 0, whereas models that have very different flux ranges will receive a score close to 1. Methotrexate and capecitabine had the highest dissimilarity scores with the DMSO model (Figure 5.2A), which is consistent with the strong effect of these drugs in the growth prediction step above. Then, the similarity score (1, dissimilarity score) between the natural product models and two DMSO models constrained by methotrexate and capecitabine (cancer drug models) were calculated. The combined top-ten natural product models which were similar to methotrexate and capecitabine (resulting in 13 unique natural products) were selected as candidate anticancer drugs. The results for these 13 natural product models are shown in (Figure 5.2B).

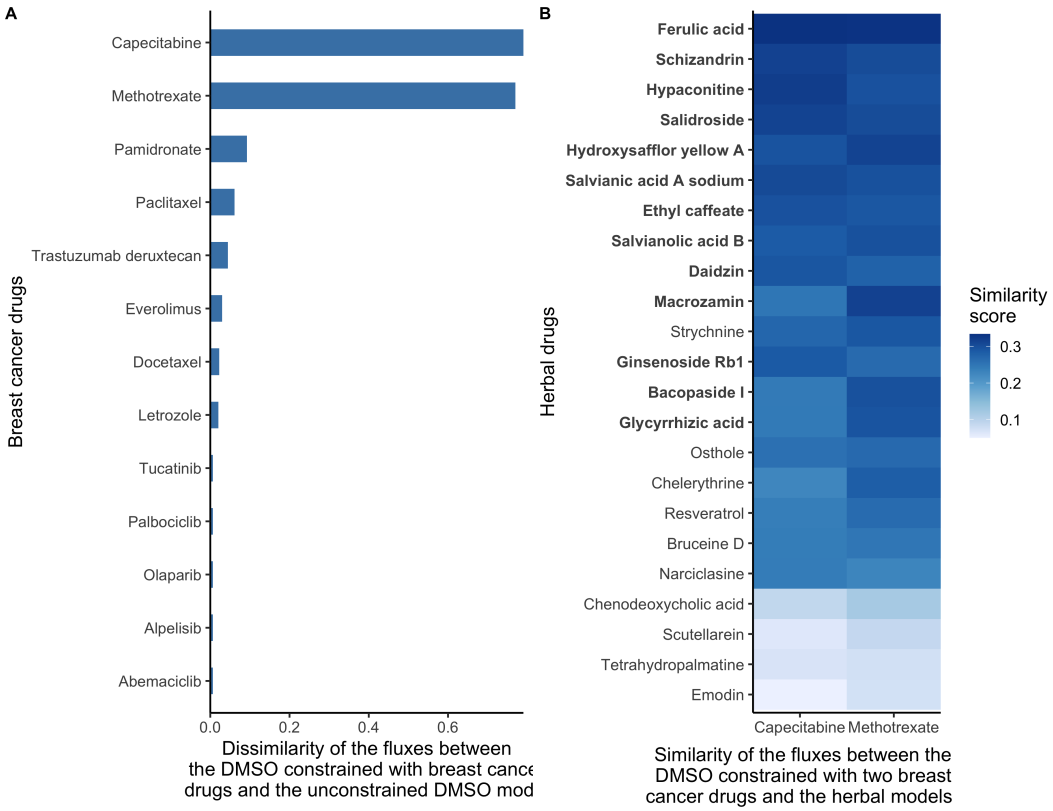

FIGURE 5.2: **Dissimilarity and similarity of the natural products to the control model and the approved drugs' models, respectively.**

(**A**) Dissimilarity of the flux ranges between the DMSO models constrained with breast cancer drugs and the unconstrained DMSO model. Breast cancer drugs that significantly alter the metabolism of MCF-7 cells have a high dissimilarity to the control DMSO model. With low dissimilarity scores suggests that the main targets of some drugs are non-metabolic, that these drugs have indirect effects on growth, or that the drugs cause cancer death by affecting pathways that are unrelated to growth. The dissimilarity score was computed based on the flux ranges of the reactions included in the models. If both models maintain similar ranges, the dissimilarity score is close to 0. (**B**) Similarity scores between the reconstructed natural product models and the DMSO model constrained with capecitabine and methotrexate. The target deletion of these two drugs is predicted to stop the growth of MCF-7 cells. Hence, natural product models with a high similarity with DMSO constrained with these drugs are more likely to have a similar effect on the metabolism. The similarity score was computed based on the flux ranges of the reactions included in the models. If both models maintain similar ranges, then the similarity score tends to 1. The natural products were sorted by the average similarity score to methotrexate and capecitabine, with the ten natural products with the highest similarity to capecitabine and the ten drugs with the highest similarity score to methotrexate are highlighted in bold.

5.2.4 *Narciclasine, Emodin, Scutellarein, Strychnine, Resveratrol, Chenodeoxycholic Acid, Chelerythrine, Tetrahydropalmatine, Osthole, and Glycyrrhizic Acid Are Predicted to Alter the Androgen and Estrogen Synthesis and Metabolism Pathway*

In order to determine which metabolic pathway should be preferably targeted in order to reduce the growth of breast cancer, and which pathways are targeted by natural products, the

drug targets of natural products and breast cancer drugs were mapped to the reaction–gene matrix (*rxnGeneMat* field) of Recon3D [24], the input reconstruction which was used to build the natural product models. The number of breast cancer drugs targeting the same pathway was plotted against the number of natural products (Figure 5.3). Most breast cancer and natural products target eight pathways: androgen and estrogen synthesis and metabolism, arachidonic acid metabolism, drug metabolism, bile acid synthesis, steroid metabolism, cytochrome C metabolism, linoleate metabolism, and extracellular transport pathways. The color code on the plots represents the size of the pathway (the number of reactions under gene control in this pathway, which can therefore be targeted). Larger pathways such as extracellular transport and drug metabolism, which have 332 and 55 associated genes, respectively, are expected to be targeted by a higher number of drugs than smaller pathways. In order to verify whether the metabolism of these pathways was significantly altered by the natural products, the difference in the active reactions (the reactions present in the models) between each natural product model and the DMSO model was computed. Among the eight pathways that are targeted by most approved breast cancer drugs (Figures 5.3 and 5.4), the androgen and estrogen synthesis and metabolism pathway had the lowest rate of reactions that were shared between the natural product models and the DMSO model, i.e., reactions that were active in the DMSO model tended to be inactive in the natural product models, and vice versa. Hence, this suggests that natural product models more strongly impact this pathway. The same analysis was performed on all of the pathways in Recon3D. Among the pathways with the highest rate of altered reactions are pathways with a low overall number of reactions. For pathways, with less than or equal to five reactions, the activation or inactivation of a single reaction will result in a rate of altered reactions that is above or equal to 0.2, whereas for larger pathways the alteration of one reaction would have a more modest effect (see the color code for the size of the pathways). The choice of the androgen and estrogen synthesis and metabolism pathway as the pathway of interest for breast cancer treatment is consistent with three facts. First, the inhibition of Estrogen Receptor α (ERα) by fulvestrant was shown to prevent invasion by MCF-7 cells, which are ER-positive, in a xenograft experiment [25]. Second, genistein, which also targets ERα, inhibits the proliferation of MCF-7 cells and induces apoptosis [26]. Third, estrogen- and androgen-based therapeutics are used for breast cancer treatment [27].

In total, 12 natural products were described to have targets in the androgen and estrogen synthesis and metabolism pathway. However, only ten out of these twelve showed a difference in the fraction of reactions present per pathway when compared to the DMSO model (see Supplementary File S2, Figure S4): narciclasine, emodin, scutellarein, strychnine, resveratrol,

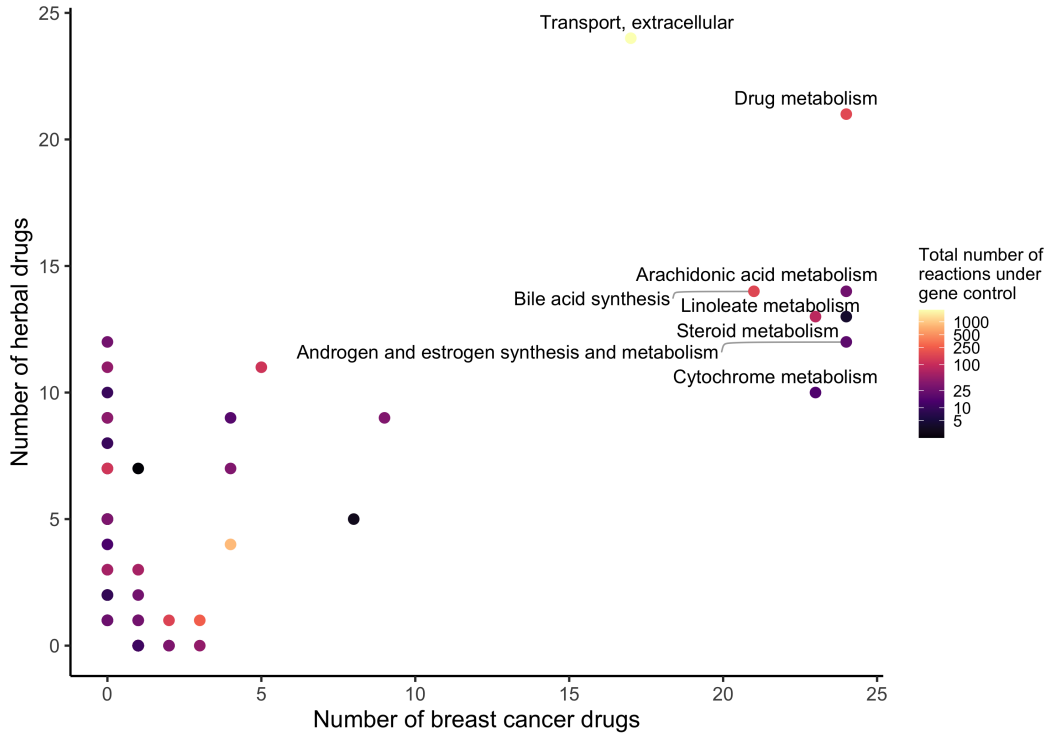

FIGURE 5.3: **Pathway analysis of the dysregulated pathways by natural product and approved cancer models.**
Androgen and estrogen synthesis and metabolism, arachidonic acid metabolism, cytochrome metabolism, drug metabolism, bile acid synthesis, steroid metabolism, linoleate metabolism, and extracellular transport are the most frequently targeted pathways of approved breast cancer drugs and natural products. The x- and y-axes correspond to the number of breast cancer drugs and natural products that target Recon3D. The color map represents the total number of reactions in each pathway under gene control.

chenodeoxycholic acid, chelerythrine, tetrahydropalmatine, osthole, and glycyrrhizic acid.

5.2.5 *23 Natural Products with Potential Anticancer Activity Emerged from the Different Stages of Analysis*

In total, 23 out of the 101 natural products and one drug mixture were predicted as the top candidates in at least one of the four *in silico* analysis steps: (i) the drug deletion prediction by the natural products' targets, (ii) the dissimilarity to the DMSO model, (iii) the similarity to breast cancer drugs, and (iv) pathway analysis. This number was further reduced for the experimental validation by selecting only those natural products that popped up in more than one of the *in silico* steps (Table 5.2, green). Notably, strychnine and narciclasine were removed from the list due to toxicity (Table 5.2, red) [28], and due to the abundance of available experimental data (Table 5.2, orange, see Supplementary File S1, Table S6) on breast cancer cell lines, respectively [29]. Additionally, emodin, salvianic acid A sodium, scutellarein,

and bruceine D (Table 5.2, blue)—which were predicted by only one analysis step—were added to the list of drugs for validation due to previous evidence from two databases (Dr. Duke's Phytochemical and Ethnobotanical Databases (Dr. Duke Database) and the Drug Repurposing Hub Database) [30], [31] and from the literature [32]. This resulted in a final list of nine drugs for experimental validation.

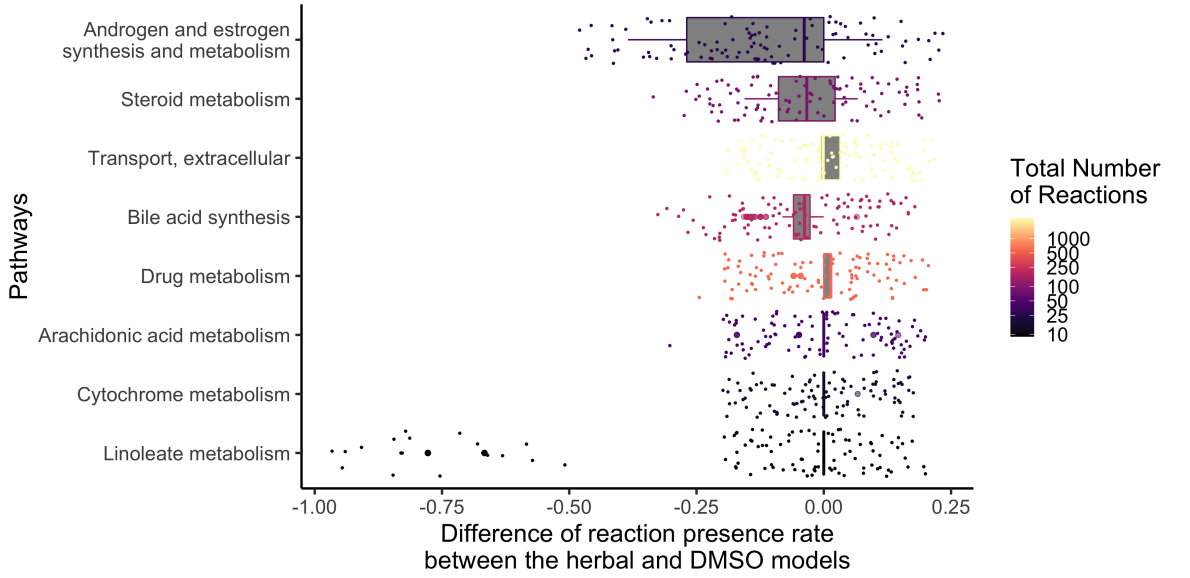

FIGURE 5.4: **Among the pathways that are targeted by most breast cancer drugs, androgen and estrogen synthesis and metabolism had the lowest fraction of shared reactions between the natural product and control models.**
The fraction of reactions present per pathway for the eight most frequently targeted pathways of breast cancer drugs was calculated for each natural product by dividing the number of present reactions in each context model by the total number of reactions in this pathway. Then, the difference in reactions present per pathway between the natural product models and the DMSO model was computed. The pathways were sorted by the interquartile range of the differences in the fraction of present reactions. The color code corresponds to the total number of reactions in each pathway.

5.2.6 *Scutellarein, Emodin, and Bruceine D Decrease the 2D Cell Viability of MCF-7 and Hs 578T Breast Cancer Cells*

In order to experimentally validate the *in silico* predictions, 2D cell viability assays were performed to determine the anticancer activity of the nine selected natural product candidates: scutellarein, emodin, bruceine D, resveratrol, hydroxysafflor yellow A, salvianolic acid B, salvianic acid A sodium, ferulic acid, and glycyrrhizic acid. Ophiobolin A, which is a natural product that covalently inhibits calmodulin and has anticancer stemness properties [33], was chosen as a control compound because of its anti-proliferative effects in different cancer cell lines [34]. Two breast cancer cell lines were used for these assays: the non-invasive MCF-7 cells, which are ER+ breast cancer cells that were also used for the computational analysis,

and the highly invasive Hs 578T cells, which are triple-negative breast cancer cells.
The analysis of the cell viability revealed that scutellarein, emodin, and bruceine D inhibited the cell proliferation of both MCF-7 and Hs 578T cells in a concentration-dependent manner (Figure 5.5A). Notably, lower drug concentrations were used for bruceine D, as this compound showed the highest potency. Figure 5.5B shows the DSS3 values as determined using the DSS pipeline website, BREEZE (`https://breeze.fimm.fi/` last accessed on 14 December 2021). DSS3 values essentially correspond to the normalized area under the curve of dose–response curves [35], with a higher DSS3 value reflecting a higher potency of the drug. The obtained DSS3 values point to a higher potency for bruceine D than for the control compound ophiobolin A in invasive Hs 578T cells, and to a similar potency of bruceine D in MCF-7 cells compared to Hs 578T cells (Figure 5.5B and Supplementary File S2, Figure S5A). Notably, bruceine D showed submicromolar IC_{50} (IC_{50} = 0.71 ± 0.05 μM) in Hs 578T, and low micromolar IC_{50} in MCF-7 cells (IC_{50} = 9.5 ± 7.7 μM) (Supplementary File S2, Table S9), which is in the same range. The other two candidates—scutellarein and emodin—gave IC_{50} values ranging from 28 to 65 μM depending on the compound and the cell line (Supplementary File S2, Table S9). The IC_{50} measured for the three natural products is in the same range for MCF-7 as the one found in the literature (Supplementary File S1, Table S10). No data were found for these three natural products for Hs 578T. On the other hand, treatment with hydroxysafflor yellow A, salvianolic acid B, salvianic acid A sodium, ferulic acid, or glycyrrhizic acid did not confirm the *in silico* predictions (Supplementary File S2, Figure S5B), as these natural products did not induce a dose-dependent decrease of 2D cell viability. Only resveratrol showed a minor dose-dependent effect on Hs 578T cells at high concentrations. Consistently, these six drugs gave very low DSS3 values, and no IC_{50} values could be determined (Supplementary File S2, Table S9). Altogether, our experimental validation indicates that the three natural products emodin, scutellarein, and bruceine D are promising therapeutic candidates for breast cancer treatment, as predicted by the computational model, with bruceine D being the top candidate.

5.2.7 *Targeting the Androgen and Estrogen Synthesis and Metabolism, as well as the Accumulation of ROS, Are the Two Main Modes of Action of Emodin, Bruceine D and Scutellarein*

In order to understand how emodin, bruceine D, and scutellarein affect the metabolism of MCF-7 cells, the difference in the reaction presence rates between the three respective natural product models and the DMSO model was calculated. The androgen and estrogen synthesis and metabolism pathway, as well as the pathways required for the biosynthesis of estrogens

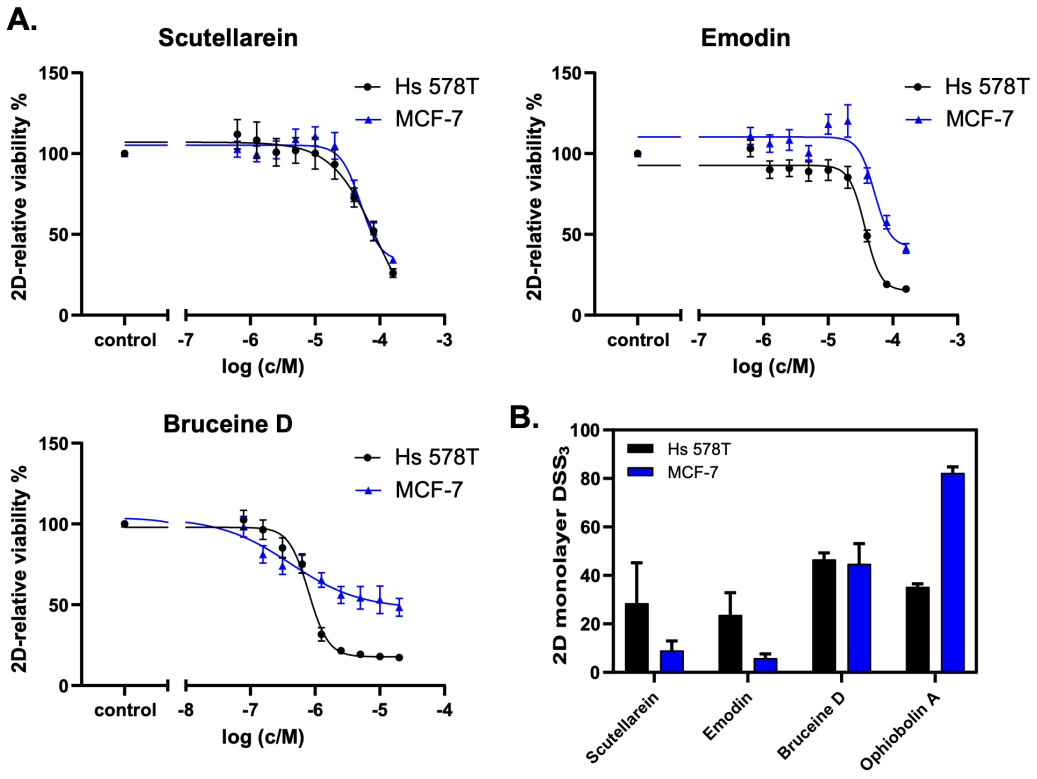

FIGURE 5.5: **Scutellarein, emodin, and bruceine D reduce 2D breast cancer cell viability.**

(A) The natural products scutellarein, emodin, and bruceine D dose-dependently decrease the 2D cell viability of both MCF-7 and Hs 578T breast cancer cell lines after 72 h. The treatment was performed in a 1:2 dilution series ranging from 160 μM to 0.625 μM for scutellarein (n = 4) and emodin (n = 4), and ranging from 20 μM to 0.078 μM for bruceine D (n = 3). (B) The 2D monolayer DSS3 values as a quantification of the anti-proliferative effects of the natural products scutellarein, emodin, and bruceine D, and of the control compound, ophiobolin A. The DSS3 values correspond to the normalized area-under-the-curve values of the dose–response data, as shown under (A). The results are expressed as the mean ± SEM, n $\geq$ 3 for natural products, and n = 2 for ophiobolin A.

such as cholesterol, steroid and squalene, and cholesterol synthesis, had a lower presence rate in the three natural product models, suggesting that estrogen synthesis is downregulated by these three drugs (Figure 5.6; the results for all of the pathways are shown in Supplementary File S2, Figure S6). Furthermore, pathways directly implicated in redox homeostasis—such as Reactive Oxygen Species (ROS) detoxification (bruceine D), Heme degradation, and NAD metabolism—and pathways such as purine and pyrimidine, which are required to replenish the stocks of NAD(P)H, folate metabolism (emodin, scutellarein), and glutathione metabolism (bruceine D and emodin) were also downregulated. Transporters that indirectly reduce stress by transporting compounds that might cause redox stress out of the Golgi and endoplasmic reticulum are also targeted by the three drugs. Vitamins, phenylalanine, and histidine metabolismwhich are pathways known to alleviate redox oxidative stresswere activated, suggesting that these pathways are activated in order to reduce the accumulation of ROS in

MCF-7 cells. The differences in the reactions present per pathway between the natural product and the DMSO models were calculated. Only pathways that have at least an absolute difference of 0.1 in the fraction of present reactions for bruceine D, scutellarein and emodin are displayed. The pathways are ranked in the y-axis by their absolute differences in reactions present per pathway for bruceine D. Supplementary File S2, Figure S6 shows the results for all of the pathways in Recon3D.

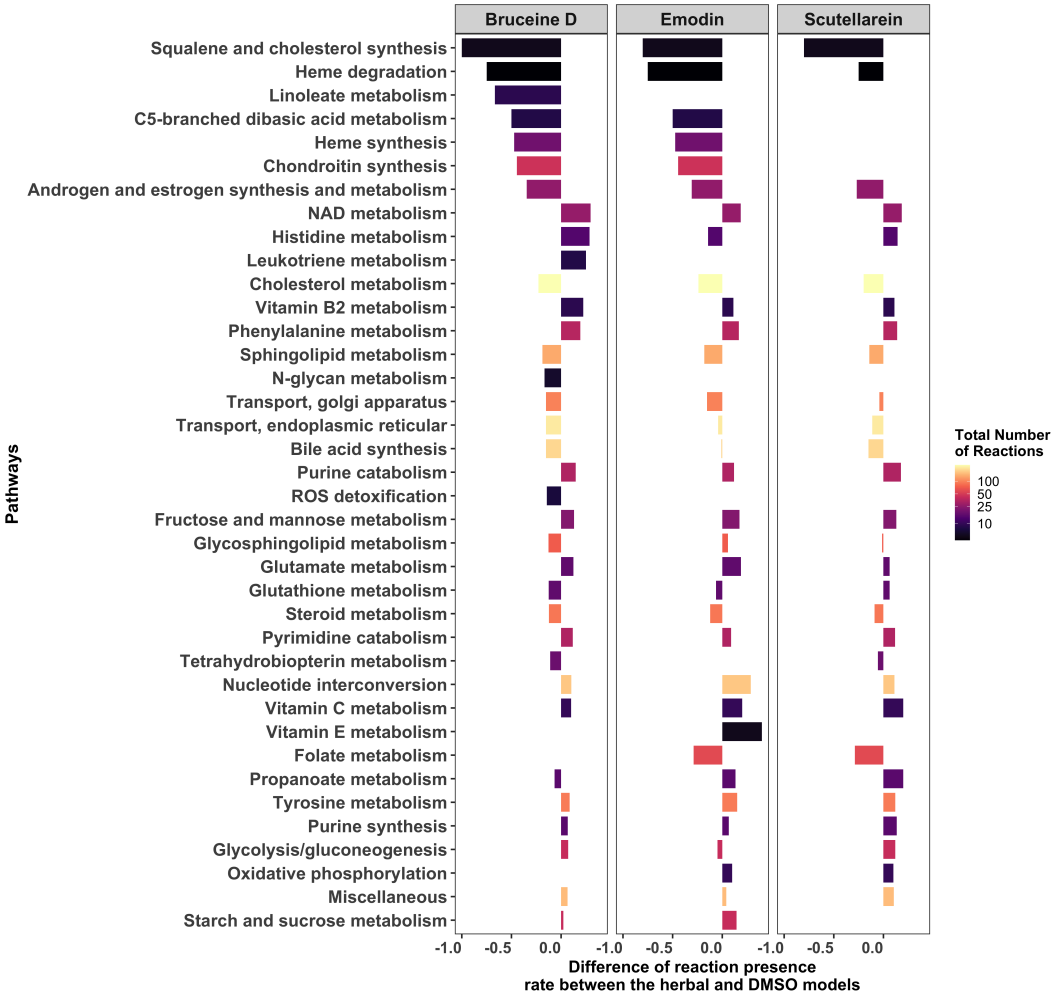

FIGURE 5.6: **Androgen and estrogen synthesis and metabolism, and pathways implicated in the maintenance of redox homeostasis, are the main targets of bruceine D, emodin, and scutellarein.**

In order to ascertain which enzymes are most likely targeted by bruceine D, emodin, and scutellarein, the number of reactions impacted in each pathway was plotted against the known drug targets for each compound. The size of the dots indicates how many cancer drugs target the same gene. Bruceine D has no described targets in DrugBank V5 [19] (version 5.1.8), PROMISCUOUS 2.0 [20], or NPASS [21]. Emodin has 24 metabolic targets — notably CYP3A4, CYP2C9, CYP2C19, CYP2D6-targeting, among others, the androgen and estrogen synthesis and metabolism pathway. These four genes are also targeted by 21, seven, three

and two breast cancer drugs, respectively (Figure 5.7A). Scutellarein has nine metabolic targets, notably CYP1A1 and CYP1B1 in the androgen and estrogen synthesis and metabolism pathway, which are targeted by toremifene, and by paclitaxel and docetaxel, respectively (Figure 5.7B). Furthermore, 17 genes of the androgen and estrogen synthesis and metabolism pathway are targeted by breast cancer drugs. Notably, CYP3A4 is targeted by 21 drugs. The same gene controls reactions in the steroid, linoleate, drug, cytochrome C, bile acid, and arachidonic acid metabolism (Figure 5.7C). The 17 target genes in the androgen and estrogen synthesis and metabolism pathway (including CYP3A4) regulate four reactions that hydrolyse oestrone, testosterone, and pregnenolone into products that have been described to bind estrogen or androgen receptors and induce proliferation in breast cancer cells [36] (Supplementary File S1, Table S11, Supplementary File S2, Figure S8). In the arachidonic pathway and other pathways with the reactions controlled by the CYP proteins targeting breast cancer drugs, none or few reactions were differentially present in the natural product models, suggesting that these pathways were not targeted by natural product models (Supplementary File S2, Figure S8).

Besides the androgen and estrogen synthesis and metabolism pathway, emodin targets 12, 10, nine, six, and five genes in the drug, steroid, vitamin A, linoleic, and arachidonic metabolisms, respectively, whereas scutellarein targets three genes in the starch and sucrose metabolisms (Supplementary File S2, Figure S7).

The 26 cancer drugs mainly target CYP proteins, SLC carriers, ATP transporters, and UDP-glucuronosyltransferases, which are mainly found in the eight following pathways: androgen and estrogen synthesis and metabolism, arachidonic acid metabolism, bile acid synthesis, cytochrome metabolism, drug metabolism, linoleate metabolism, steroid metabolism, transport, and extracellular pathways. Some of these genes and pathways are also targeted by emodin. On the other hand, although scutellarein targets two CYP proteins and one UDP-glucuronosyltransferase, it does not target CYP3A1. Unlike emodin, which shares several targets with the breast cancer drugs, scutellarein has only a few targets in these pathways, suggesting a different model of action for this drug (Figure 5.6, Supplementary File S2, Figure S6).

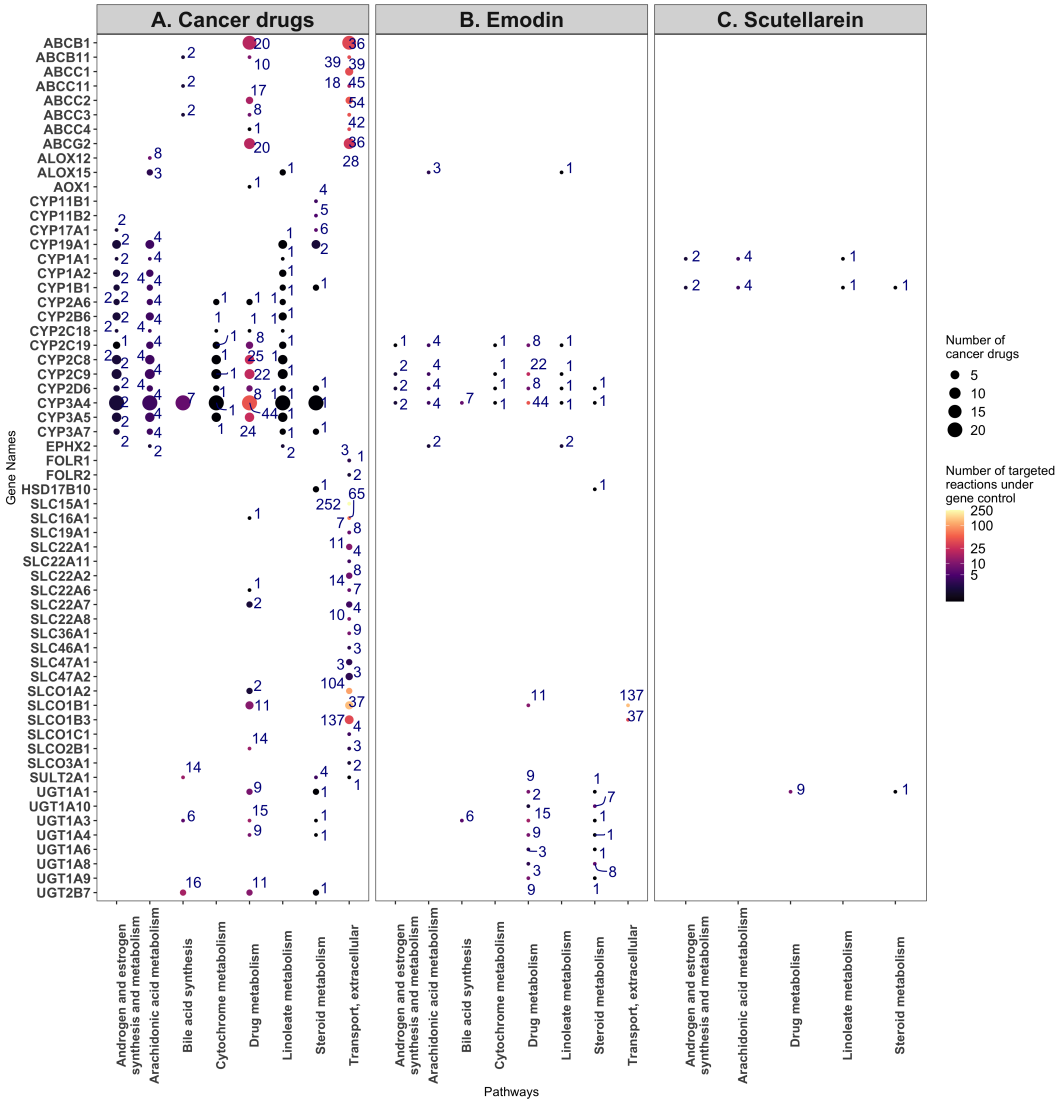

FIGURE 5.7: **Target genes and the number of reactions affected by the breast cancer drugs (A), emodin (B), and scutellarein (C) for the eight most commonly targeted pathways.**

(A) The target genes of the breast cancer drugs were plotted against the eight most commonly targeted pathways, with the size of the dots indicating the number of cancer drugs targeting a gene, and the number near each dot and color map indicating the number of reactions under the control of the gene. (B) The same analysis, but for the targets of emodin. (C) The same analysis, but for the targets of scutellarein.

5.3 Discussion

In the present work, a drug discovery workflow based on FASTCORMICS, Drug deletion, and Flux Variability Analysis was used to predict the best breast cancer drug candidates among 101 natural products, out of which nine were tested in a 2D cell viability assay using MCF-7 and Hs 578T cells. A dose-dependent decrease of cell viability was observed with the three natural products emodin, scutellarein, and bruceine D, with the latter showing a low micromolar IC_{50} in MCF-7 cells (IC_{50} = 9.5 7.7 μM), and a submicromolar IC_{50} in Hs 578T

cells ($IC_{50} = 0.71 \ \ 0.05 \ \mu$M). Metabolic modeling was previously applied, with success, to the prediction of drug candidates and, more specifically, repurposable drugs [15], [16]. However, the information for natural products is scarcer than that for conventional breast cancer drugs. Only 35 of the 101 drugs had target information in DrugBank V5, PROMISCUOUS 2.0, and NPASS (see Supplementary File S2, Table S3). Furthermore, due to the multi-target mode of action of natural products, the list of targets for the natural products present in these databases is probably incomplete. Hence, drug deletion approaches might miss interesting drug candidates as some of their targets might be missing from databases. Finally, some of these drugs that might not have direct metabolic targets could nevertheless have a significant effect on metabolism and cancer cell viability, growth, and migration.

In order to circumvent this issue, we identified natural products that, according to their expression profiles, affect the metabolism of cancer cells differently than the solvent DMSO alone. This approach does not necessarily imply that these products reduce growth, but at least it allows us to eliminate natural products with no or very small effects on the metabolism. We further selected products that have a similar effect to capecitabine and methotrexate on the metabolism of MCF-7 cells. These two breast cancer drugs had the strongest dissimilarity to the flux distribution of DMSO due to the shutdown of all of the reactions that are required for biomass production, suggesting that they have a strong impact on the metabolism. This assumption was further validated by the drug deletion that predicted these two drugs to reduce growth. Methotrexate has three metabolic targets that are predicted to reduce growth upon knockout: TYMS, DHFR, and ATIC. The knockout of TYMS was also predicted to stop growth in the capecitabine-constrained DMSO model. Because it is a rate-limiting enzyme of nucleotide synthesis, the knockdown of TYMS was previously described to reduce the proliferation of breast cancer cells [37]. The inhibition of TYMS by fluoropyrimidine and folate analogues was further shown to induce apoptosis through ROS generation [38]. Methotrexate and other DHFR inhibitors deplete the concentration of folates required for the de novo synthesis of nucleotides and NADP(P)H that regulates oxidative stress by the regeneration of reduced glutathione. Finally, ATIC is an oncogene that suppresses AMPK activation, and hence promotes proliferation via mTOR [39].

The knockout of the metabolic targets of the 24 remaining breast cancer drugs did not affect the growth in the MCF-7 models. Although the cancer drugs had around 82 combined metabolic targets, the targets responsible for the reduction in proliferation or cell death might be non-metabolic. These drug targets might, moreover, have an indirect effect on growth; hence, they would not be captured by constraining the DMSO models by the known targets. Furthermore, the metabolic impact might not be captured by the biomass formulation, i.e., by causing the

accumulation of ROS and the death of the cell by apoptosis. Finally, all of the isozymes described to control a reaction in Recon3D might not be expressed in breast cancer cell lines, or were missing in the target list. Regarding the targets, ABCB1 and ABCG2—which are ATP-dependent drug efflux pumps for the xenobiotic compound, and are known to be linked to multidrug resistance [40]—were targeted by 17 and nine drugs, respectively. More generally, among the 82 combined targets, eight were ABC transporters, 13 were solute carriers, 16 were members of the CYP proteins, and six were members of the SLCO family of organic anion-transporting polypeptides. In Recon3, CYP34A—which is targeted by 21 breast cancer drugs controls sex hormones and metabolizes 50% of cancer drugs. Hence, the overexpression of this CYP protein in cancer tissue might also be linked to multidrug resistance.

Among the natural product models, resveratrol and ferulic acid were predicted to decrease proliferation. However, unlike for methotrexate and capecitabine, the predicted growth reduction is not linked to the knockout of one gene, but to the combined effect of the knockout of multiple targets. In the cell viability assay, nine natural products —scutellarein, emodin, bruceine D, resveratrol, hydroxysafflor yellow A, salvianolic acid B, salvianic acid A sodium, ferulic acid and glycyrrhizic acid— were experimentally assessed for their effect on the 2D cell viability of MCF-7 and Hs 578T cells. Among them, emodin, bruceine D, and scutellarein dose-dependently decreased the 2D cell viability in both cell lines. Although similar assays have previously been performed in ER+ MCF-7 cells [41], this cell line was nevertheless chosen for validation in order to be coherent with the approach taken to build the natural product models, which was based on MCF-7 cells. On the other hand, the Hs 578T cell line was chosen because of its triple-negative status and high invasiveness. To the best of our knowledge, the three drugs had not been tested before in Hs 578T, but they had been tested in other triple-negative cell lines such as MDA-MB-231, MDA-MB-453 or MDA-MB-468 [41]–[45]. Altogether, our results are in good agreement with the previously published studies. In general, we obtained higher DSS3 values and lower IC_{50} values in Hs 578T than in MCF-7 cells (Supplementary File S2, Table S9), indicating a higher potency for the three candidates in the triple-negative cell line compared to the ER+ cell line. In particular, bruceine D showed a submicromolar IC_{50} value in Hs 578T cells (0.71 ∓ 0.05 μM), suggesting that this compound might be a valuable drug for triple-negative breast cancer treatment.

Six of the nine predicted drugs did not show clear effects at the tested concentrations, and their IC_{50} values could not be determined. Resveratrol treatment decreased the Hs 578T cell viability only at a concentration of 160 μM, whereas it showed no effect on MCF-7 cells. This low effect was somewhat surprising, as previous studies have shown a decrease of MCF-7 or MDA-MB-231 survival or proliferation upon resveratrol treatment [46]–[48]. If any effect

could be observed for the other five drugs, it would be a stimulatory rather than an inhibitory effect on cell viability, except for salvianolic acid B and salvianic acid A sodium, both of which decreased MCF-7 viability by 35% at a concentration of 160 μM. Controversial results have been reported regarding the effects of these natural products on breast cancer cells. Whereas glycyrrhizic acid has been shown to induce apoptosis via ROS activation in MDA-MB-231 breast cancer cells [49], both stimulatory [50] and inhibitory effects [51] have been described for MCF-7 cell proliferation. Similarly, contradictory results have been reported regarding ferulic acid. Indeed, ferulic acid was shown to have anti-proliferative and pro-apoptotic activities in MCF-7 cells [52], and to reduce proliferation and reverse EMT in MDA-MB-231 cells [53]. In contrast, in another study, it stimulated the proliferation of MCF-7, MDA-MB-231 and other breast cancer cell lines, with the concomitant upregulation of ERα and HER2 in MCF-7 cells [54]. Hydroxysafflor yellow A has been shown to reduce the proliferation of MCF-7 cells [55]. Finally, Salvianolic acid B showed a similar inhibition of MCF-7 and MDA-MB-231 cell proliferation with a decrease in cyclin B1 levels [56]. Evidence for the anti-tumor activity of salvianolic acid B was also provided by an *in vivo* study, in which the drug decreased the tumor volume and increased the median survival in mice, possibly by enhancing apoptosis [57]. The observed differences between our experimental results and the literature data could be due to different experimental settings, and in a subset of the analyses, they could be due to the differential concentrations used for the treatment. Emodin is an anthraquinone isolated from different Chinese herbs [58], and is commonly accepted as a protein tyrosine kinase inhibitor [59]. Emodin has been shown to exhibit anti-proliferation effects in several cancer types, such as breast, endometrial [60], and renal cancer [61], as well as hepatocarcinoma [62].

Scutellarein is a flavone extracted from the herb *Scutellaria baicalensis*, which induces mitochondria-mediated intrinsic apoptosis selectively on multiple myeloma [63], and inhibits the cell proliferation and EMT of hepatocellular carcinoma. Furthermore, scutellarein has been shown to inhibit the proliferation of MCF-7 and the triple-negative breast cancer cell MDA-MB-468, whereas it had no notable effect on the viability of healthy MCF-10A cells [42]. Bruceine D is a quassinoid compound extracted from the seeds of *Brucea javanica*. Bruceine D was reported to induce autophagy and apoptosis via the generation of ROS in lung cancer cells [64] and pancreatic cancer cells [65]. A bruceine D-dependent decrease in cell viability was also found in the breast cancer cell lines MCF-7 and MDA-MB-231, whereas the proliferation of healthy mammary epithelial cell MCF-10A was not affected [41]. In addition to the cell viability decrease, bruceine D was further shown to reduce the migration and invasion of MDA-MB-231 cells by upregulating the expression of E-cadherin and downregulating vimentin, suggesting

a bruceine D-dependent reversal of EMT in these cells [43]. More recently, evidence was indeed provided that bruceine D treatment led to an upregulation of genes that are negatively correlated with EMT, and to a downregulation of genes that are positively correlated with EMT [66].

Taken together, the targets of emodin, scutellarein, and bruceine D, as well as their exact mode of action, are far from being completely elucidated. However, it is nowadays commonly accepted that these three drugs display anti-proliferative and anti-apoptotic effects across different cancer types, and that they counteract EMT. They induce the accumulation of ROS and regulate several signaling pathways, including PI3K/Akt/NF-B pathways [67], [68]. PI3K/AKT contributes to the regulation of survival, growth, proliferation, and metabolism [69], whereas NF-B is implicated in cell proliferation, apoptosis suppression, angiogenesis, EMT induction, and metabolism regulation [70]. Therefore, although emodin, scutellarein, and bruceine D might not directly target metabolism, they interfere with pathways that regulate metabolism, and pathways that are related to ROS. ROS production is a double-edged sword in cancer. Indeed, depending on the concentrations and context, ROS can either promote tumor initiation and progression or inhibit tumor cell proliferation, induce apoptosis, and prevent multidrug resistance [71], [72]. Cancer cells have developed strategies—such as the antioxidant system, the DNA damage repair pathway, and metabolism reprogramming—to adapt to and alleviate ROS-induced damage. However, if the ROS levels exceed a threshold level, they will overwhelm these strategies and induce oxidative stress, eventually leading to cancer cell death. Many anticancer drugs that increase ROS levels—such as fluorouracil, doxorubicin, rapamycin, and erlotinib—are used in clinics [72].

In order to obtain a deeper insight into the mode of action of bruceine D, scutellarein, and emodin, we had a closer look at their results in the four *in silico* experiments. Among the pathways that were differentially present in the bruceine D, scutellarein and emodin models were the androgen and estrogen synthesis and metabolism pathway, as well as pathways that are required for the synthesis of estrogens, such as cholesterol metabolism, squalene and cholesterol synthesis, and steroid metabolism. Notably, the ROS detoxification pathways (in the bruceine D model) and the pathways responsible for the production of antioxidants—such as folate metabolism (emodin and scutellarein models) and heme degradation (all three models)—were downregulated, which is consistent with the described accumulation of ROS induced by the three natural products [64], [65], [73], [74]. In order to alleviate an increase in ROS due to the lack of antioxidants, pathways that control oxidative stress—such as vitamins, NADH metabolism, and phenylalanine metabolism—were moreover predicted to be upregulated. Taken together, these three drugs show three predicted main metabolic modes of action:

the downregulation of the androgen and estrogen pathway, the accumulation of ROS to initiate programmed cell death, and, to some extent, the induction of the biosynthesis pathways required for proliferation. Increased endogenous levels of androgen and estrogen are associated with a higher risk of prostate and breast cancer development, respectively [75]. Estradiol has been shown to induce the proliferation of breast cancer cells, activate anti-apoptotic pathways, and reduce oxidative stress. Hydroxylated estrogen can further cause mutation in the DNA and induce tumors [75]. However, the effects of estrogen and estradiol vary in the function of the type of ERs at the surface of breast cancer cells. Whereas ERα acts as a tumor accelerator, Estrogen Receptor β (ERβ)—which binds to ERα, and by doing so represses ERα—is generally considered to be a tumor inhibitor. However, it has to be noted that ERβ, which is expressed in all breast cancer molecular subtypes and in the majority of breast cancer stem cells, was recently proposed as a novel therapeutic target to specifically hit stem cells [76].

Androgens have a dual and controversial effect on breast cancer development. At physiological concentrations, androgens can suppress breast cancer cell proliferation. However, at higher concentrations, androgens can promote breast cancer cell proliferation by augmenting free estrogen levels, or by regulating the transcription of genes, such as the mitotic gene Ki-67 [75].

The androgen and estrogen synthesis and metabolism pathway is targeted by 24 out of the 26 breast cancer drugs. These drugs target four reactions of this pathway that are present in the DMSO model and absent in bruceine D, emodin, and scutellarein models. Notably, one of the reactions that causes the oxidation of estrone into 16α-hydroxy-estrone in the reticulum by a monooxygenase is under the control of 13 target genes, and notably of the gene CYP3A4. CYP3A4 is targeted by 21 out of 26 cancer drugs. Hydroxylated forms of estrogen, estradiol, and testosterone were described to be genotoxic, and hence to initiate tumor formation by inducing mutations. In addition, 16α-hydroxy-estrone has a strong affinity for ERs, and the ratio between 2-hydroxy-estrone and 16α-hydroxy-estrone in the urine has, for a long time, been regarded as a biomarker for breast cancer risk, although this assumption is currently under debate [77]. Taken together, breast cancer drugs commonly target CYP3A4 and other genes of the androgen and estrogen synthesis and metabolism pathway. Furthermore, emodin and scutellarein have known targets in this pathway, including CYP3A4 in the case of emodin. CYP3A4 expression has been shown to correlate with poor overall survival in breast cancer [78], [79]. However, CYP3A4 might not only induce breast cancer via hydroxylated forms of estrogen but also by the production of epoxyeicosatrienoic acids through the arachidonic metabolism pathway [79]. Both pathways are under the control of mostly the same CYP proteins that are also targets of the cancer drugs. However, the action of most of the natural products did not strongly affect the arachidonic metabolism (reactions present/absent in the

Table 5.3: Number of replicates for each condition.

Perturbations	Number of Replicates
DMSO	6
A mixture of four natural products (tanshinone IIA, salvianic acid A sodium, protocatechuic aldehyde, salvianolic acid B)	2
101 natural products	2 (except for glycyrrhizic acid that has 4)

DMSO were also present/absent in the natural product model). Furthermore, no difference between bruceine D, emodin, scutellarein, and the DMSO was observed for the reactions involved in the production of epoxyeicosatrienoic acids from arachidonic acid. Finally, the high number of reactions in the steroid and cholesterol pathways present in the natural product models and absent in the DMSO model, suggests that the production of estrogen might be downregulated by a depletion in steroid and cholesterol, rather than through the action of one single enzyme alone.

Taken together, bruceine D, emodin, and scutellarein are predicted to reduce the growth of MCF-7 cells through the activation of ROS with the induction of oxidative stress, and through the downregulation of the androgen and estrogen synthesis and metabolism pathway.

5.4 Methods

5.4.1 *Data Retrieval*

The microarray data published by Lv *et al.* (GEO ID: GSE85871) [18] was retrieved from Gene Expression Omnibus (GEO, `http://www.ncbi.nlm.nih.gov/geo/` accessed date 20 September 2020) [80]. The dataset is a large data collection of a breast cancer cell line (MCF-7) treated with natural products. The 103 perturbations consist of 212 replicates (100 duplicates of single natural products and a duplicate of a mixture of four natural products, i.e., four replicates of glycyrrhizic acid) and six control replicates incubated with only the solvent of the drugs, i.e., DMSO (Table 5.3).

5.4.2 *Building of Context-Specific Metabolic Models via FASTCORMICS*

Gene expression CEL files were read into RStudio (R version 4.0.3) using the *ArrayExpress* package (version 1.50.0) (`https://bioconductor.org/packages/release/bioc/html/`

`ArrayExpress.html` accessed date 3 May 2021) and the *ReadAffy* function from the *Bioconductor* repository. First, the data were log2-transformed and then normalized using the *Frozen Robust Multiarray Analysis* (fRMA) package (version 1.42.0) [81]. The barcode function from the *fRMA* package (version 1.42.0) was further run in order to compare the expression values of the dataset to a vector containing the median and standard variation of the lowest mode for each probe set for a collection of arrays for the same platform, and to compute the z-scores. The probe identifiers were converted to Entrez ID using an in-house pipeline described by [82]. In order to avoid ambiguities, probe IDs matching more than one Entrez ID were removed. The FASTCORMICS algorithm [17] (`https://github.com/sysbiolux/rFASTCORMICS` accessed date 3 May 2021) was used to build the context-specific models using the microarray gene expression data with the human metabolic model Recon3D [24] as inputs. In the Recon3D model, the transcript information is encoded in the model gene identifiers by the addition—i.e., .1, .2, .3—after the Entrez identifiers. As the transcript information cannot unambiguously be matched to the Ensembl identifiers, the suffixes were removed. As Recon3D is already consistent, FASTCC [83] was not run. However, for most of the reconstructions, a consistent model first has to be extracted by removing the blocked reactions identified by FASTCC before running FASTCORMICS. FASTCORMICS optionally allows us to constrain the models using medium information, and to force the inclusion of the biomass reaction or any other reactions required for modeling purposes. As the natural product-treated MCF-7 cell line was cultured in MEM/EBSS medium [18], only the input reactions for metabolites present in this media were allowed (see Supplementary File S1, Table S7 for the medium composition). The medium components were retrieved from the Cytiva website (https://www.cytivalifesciences.com/en/us/shop/cell-culture-and-fermentation/media-and-feeds/classical-media/hyclone-minimal-essential-medium-mem-variations-liquid-p-05698 # related-documents accessed date 1 May 2021), and were converted into the matching metabolites names via Metabolic Atlas (version 1.7) (`https://metabolicatlas.org/` accessed date 1 May 2021) [84]. Additionally, the inclusion of the biomass function in the models was forced by its addition to *optional_ settings.func*.

5.4.3 *Drug Deletion Prediction*

5.4.3.1 Natural Products

In order to predict whether knocking out the natural product targets reduces cell proliferation, the context-specific models were constrained by setting the bounds of the natural product target reactions to zero using a modified version of the *deleteModelGenes* function of the COBRA

Toolbox, which can be downloaded from `https://github.com/sysbiolux/Herbal_Drug_Repurpusing/blob/main/data/constraining_models/DrugDeletionCombination.m` accessed date 20 March 2021. In order to obtain a list of targets for each drug, drug– target interactions information was mined from three databases: DrugBank V5 [19] (version 5.1.8), PROMISCUOUS 2.0 [20], and NPASS [21] (1.0 version). The three databases were downloaded on 12 March 2021. As UniProt IDs are used across the three databases for the target genes, non-human targets were excluded by checking the related Taxon ID (the UniProt database version in bioDBnet was the number 202004, released on 10 September 2020 and updated on 7 November 2020). The UniProt IDs were then converted to Entrez IDs using the *db2db* tool (bioDBnet: `https://biodbnet-abcc.ncifcrf.gov/db/db2db.php` accessed date 20 March 2021), from the biological DataBase network [85] to match the gene IDs in Recon3D. Finally, drugs with metabolic targets that are present in Recon3D were selected. The *deleteModelGenes* function of the COBRA Toolbox V3 [86] was used to set the bounds of the target reactions of natural products of the DMSO model close to zero (most of the growth rate values were around 1 or 0, with no values in between). Drugs with a grRatio of zero (no growth after drug treatment) were retained for further analysis.

5.4.3.2 Breast Cancer Drugs

The drug deletion was repeated with the breast cancer drugs. Therefore, a list of 41 drugs approved for the treatment of breast cancer was retrieved from the NIH (`https://www.cancer.gov/about-cancer/treatment/drugs/breast`) on 16 March 2021 (Supplementary File S1, Table S4). Drug-target information for the breast cancer drugs was retrieved from the three databases for the drugs, and was mapped to Recon3D. As some cancer drugs were only found on the three databases as conjugates (megestrol acetate and sacituzumab govitecan), rather than the parent compound only (megestrol and sacituzumab), conjugates of the 41 cancer drugs were also retrieved from the three target databases (Table S5). In total, 26 cancer drugs could be mapped to the genes included in Recon3D. The drug deletion for the cancer drug was performed as described above, with the bounds of the breast cancer drugs' target reactions being set to zero in the DMSO model. The DMSO model with constraints with the cancer drug targets is referred to as the cancer drug model.

5.4.3.3 Combination of the Natural Product and Breast Cancer Drugs

Two assays were used to assess the potential synergistic effects. First, the control DMSO model was constrained (as mentioned in the Methods—Natural Products subsection) by setting the

targets of each natural product and cancer drug couple to zero. The growths obtained for the drug combinations and the natural product and cancer drug alone were compared, which was performed using the *optimizeCbModel* function of the COBRA toolbox [86]. As some natural product targets might be unknown, the natural product model was constrained with breast cancer drugs as described in Methods—Breast Cancer Drugs.

5.4.3.4 Single-Gene Deletion

An *in silico* single-gene deletion was performed via the *singleGeneDeletion* function from the COBRA Toolbox in order to determine whether the knockout of one of the target genes could explain the biomass reduction, or if the knockout of multiple genes was required to see an effect on growth.

5.4.4 *Dissimilarity of the Natural Product Models to the DMSO Model*

In order to assess the impact of the natural products on the metabolism of breast cancer cells, a dissimilarity score D was computed based on the Jaccard Similarity Index J (D = 1-J). The dissimilarity score is equal to 1 if the number of shared reactions between two models is above the total number of reactions. Using the *dist* function inside the proxy package (version 4.0.3) in Rstudio (version 4.0.3), the Jaccard index was calculated between every natural product and the DMSO model, and then converted into the dissimilarity score. The natural products were then sorted by their dissimilarity to the DMSO model reactions and the top-five natural products were selected, as there was a larger drop of dissimilarity between the fifth and sixth natural product models.

5.4.5 *Similarity between the Natural Product and Breast Cancer Drug Model Fluxes*

In order to identify the natural products that have a similar effect on the MCF-7 metabolism as the breast cancer drugs, a Flux Variability Analysis (FVA) [87] was performed using the fluxVariability function in the COBRA toolbox. A dissimilarity score was computed between the flux range of the cancer drug models and the DMSO model (dissimilarity score = 1 SI, where SI is equal to SI =

$$\text{mean}\left(\frac{\max(0,\min(v_{1\max},v_{2\max})-\max(v_{1\min},v_{2\min})+epsilon)}{\max(v_{1\max},v_{2\max})-\min(v_{1\min},v_{2\min})+epsilon}\right) \tag{5.1}$$

If the reactions in both models have very similar flux ranges (the difference being smaller than epsilon, which is usually set to 1×10^{-4}), then the dissimilarity score is equal to 0. If the reactions shared by both have very different ranges, the dissimilarity score will tend to 1. In case a reaction was not included in one of the two compared models, the bounds were considered to be equal to zero. Based on their dissimilarity scores, two breast cancer drugs were selected: capecitabine and methotrexate (see Figure 5.2. A for cancer drugs with dissimilarity scores $> 1 \times 10^{-4}$). Then, in a second step, the similarity score (SI) was computed between the natural product and the capecitabine and methotrexate models (Figure 5.2B).

5.4.6 *Pathway Analysis*

In order to identify the pathways that are more preferably targeted by breast cancer drugs, the drug targets were identified as described in Methods—Cancer Drugs. These target genes were mapped to the gene identifiers of Recon3D, and the target reactions were obtained using the rxnGeneMat field of Recon3D. These target reactions were then assigned to a pathway using the subSystem field of Recon3D. The number of cancer drugs targeting a pathway was plotted against the number of natural products. In order to take into account the size of the pathways, the number of drugs was normalised based on the number of reactions in the pathway under gene control, and these rates were represented in the color code of the plot. Eight pathways that are targeted by the most approved breast cancer drugs were selected for their potential anticancer action. Among the eight drugs, the drugs that showed the greatest impact on the metabolism of breast cancer were selected by computing the difference of the rate of the reaction presence between the natural product and the cancer models (the rate of the reactions in a pathway that are present in a natural product model and absent in the DMSO model, and vice versa). First, the rate of reactions present per pathway was calculated for each model and each pathway by dividing the number of active reactions in the context-specific models by the total number of reactions in this pathway in Recon3D using the subSystems field. Then, the difference rate of reaction presence was computed between each natural product model and the DMSO model. The pathways were then sorted in the function of the interquartile range. All of the pathways with three reactions or fewer were excluded.

5.4.7 *Drug Selection*

In total, 23 drugs were predicted by at least one of the four previous steps (drug deletion, the dissimilarity to DMSO, the similarity to breast cancer drugs, and the pathway analysis). The

drugs predicted by two or more experiments were in general selected, unless they were toxic or had already been tested in MCF-7 cells (Table 5.2, green). In order to refine the list of drugs for the experimental validation, the drugs that passed one test but which had some preclinical and literature information supporting a potential use in cancer, in general, were also selected. In order to assess whether the drug candidates were already tested for breast cancer or any other cancer type, the Dr. Duke Database [30] (downloaded on 4 November 2020) and the Drug Repurposing Hub [31] (downloaded on 24 May 2021) were downloaded, and clinicalTrials.gov (`https://clinicaltrials.gov` accessed date 1 June 2021) [88] was mined (see Supplementary File S1, Table S8). The 102 Chinese natural products were mapped in the Dr. Duke database. In total, 23 natural products had a phytochemical classification inside the database, and 44 natural products were mapped to 358 unique activities. The Drug Repurposing Hub repository was used to find information, e.g., the mode of action for natural products, and the clinical trials phases were mined to find potential closed or ongoing trials. The preclinical *in vitro* testing data for the 23 drugs were retrieved from different sources; the compiled data, as well as the link to the data source, are found in Supplementary File S1, Table S6. Based on this data mining, two drugs were removed from the list due to high toxicity (strychnine) and due to the abundance of existing experimental treatments on breast cancer cell lines (narciclasine) (Table 5.2, red). However, due to the evidence retrieved from the data mining and literature search, four drugs (bruceine D, emodin, salvianic acid A sodium, and scutellarein) that were predicted by only one step were added to the final list of drugs (Table 5.2, blue). Resveratrol, similar to narciclasine, had already been tested before in more than three breast cancer cell lines, and it is considered to be one of the most promising anticancer natural products. Only resveratrol was kept in the final list of drugs as a positive control, while narciclasine was excluded.

5.4.8 *Experimental Validation*

5.4.8.1 Natural Products and Inhibitors

Salvianic acid A sodium (# SML0679, Merck KGaA, Darmstadt, Germany) was prepared in growth medium and ferulic acid (# HY-N0060), glycyrrhizic acid (# HY-N0184), scutellarein (# HY-N0752), hydroxysafflor yellow A (# HY-N0567), salvianolic acid B (# HY-N1362), emodin (# HY-14393), bruceine D (# HY-N3014) and resveratrol (# HY-16561) (all from MedChemExpress, Monmouth Junction, NJ, USA) were prepared in DMSO at an initial concentration of 100 mM, and then stored in aliquots at -80 $^{\circ}C$. A 10 mM stock solution of

ophiobolin A (# sc-202266, Santa Cruz Biotechnology, Inc., Heidelberg, Germany) was prepared in DMSO, and then stored in aliquots at -20 $°C$. A 100 mM stock solution of benzethonium chloride (# 53751, Merck) was prepared in $H_2O, and then stored in aliquots at -20 °C$.

5.4.8.2 Cell Culture

The MCF-7 (# HTB-22) and Hs 578T (# ACC 781) cells were obtained from American Type Culture Collection (Manassas, VA, USA) and from Leibniz Institute DSMZ-German Collection of Microorganisms and Cell Cultures GmbH (Braunschweig, Germany), respectively. Both cell lines were cultured in Dulbecco's Modified Eagle's Medium (DMEM) (Lonza Group, Basel, Switzerland) supplemented with 10% fetal bovine serum and 2 mM L-glutamine (complete DMEM) (Lonza Group). The cells were routinely passaged and grown at 37 $°C$ in a 5% CO2, H2O-saturated atmosphere.

5.4.8.3 2D Cell Viability Assay (2D Cell Proliferation)

The 2D cell viability was assessed using the alamarBlue^{TM} cell viability reagent (# DAL1100, Thermo Fisher Scientific, Waltham, MA, USA) according to the manufacturer's protocol. Briefly, MCF-7 or Hs 578T cells were seeded at a density of 3000 cells in 100 μL complete DMEM medium per well in 96-well flat-bottom culture plates. After a 24 h incubation at 37 $°C$, the cells were treated with DMSO as a vehicle control, with 200 μM benzethonium chloride (BzCl) as a positive control for cell death, or with natural test products diluted in complete DMEM. The treatment with natural products was performed in a 1:2 dilution series ranging from 160 μM to 0.625 μM, or from 20 μM to 0.078 μM for bruceine D. Ophiobolin A, used here as a control compound for its antiproliferative activities, was used for treatment in a 1:2 dilution series ranging from 20 μM to 0.078 μM. After a 72 h treatment at 37 $°C$, alamarBlueTM cell viability reagent was added to each well to a final concentration of 10%, and the plate reading was performed after a 2.5 h incubation in the dark at 37 $°C$. The fluorescence intensity (excitation at 530 $\pm$ 15 nm and emission at 590 $\pm$ 20 nm) was measured using a CLARIOstar (BMG LABTECH, Ortenberg, Germany) plate reader.

5.4.8.4 Drug Sensitivity Score Determination and Data Analysis

The raw fluorescence intensity values obtained from the cell viability assays were analysed using the DSS pipeline website BREEZE (`https://breeze.fimm.fi` accessed date 14 December 2021) [34], [89]. The absolute IC_{50} and DSS3 values were derived from the data analysis, with

DSS being a more robust parameter to quantitate drug sensitivity than IC_{50}, corresponding essentially to the normalized area under the curve (AUC) of dose–response data [35]. Prism 9.2.0 (GraphPad Software, San Diego, CA, USA) was used to establish the dose–response curves. The results are presented as the mean ± SEM of at least three independent biological replicates, unless otherwise indicated. Each biological replicate was carried out in three technical replicates, out of which at least two were considered for evaluation.

5.4.9 *Post-Experimental Analysis of the Pathways Affected by Bruceine D, Scutellarein, and Emodin*

In order to gain insight into the possible mode of action of bruceine D, scutellarein and emodin, pathway analyses were performed on the three natural product models, which were then compared against the DMSO model, at a pathway level and a reaction level. Furthermore, targeted reactions by emodin and scutellarein were compared with reactions targeted with cancer drugs. First, the differences in the reaction presence rate between the three drugs and the DMSO model were computed. The pathways with absolute differences below 0.1 were not plotted in Figure 5.6 but are shown in Supplementary File S2, Figure S6. Second, the target genes of the 24 cancer drugs, emodin, and scutellarein, were plotted against the eight most commonly targeted pathways of breast cancer drugs (androgen and estrogen synthesis and metabolism, arachidonic acid metabolism, bile acid synthesis, cytochrome metabolism, drug metabolism, linoleate metabolism, steroid metabolism, transport, and extracellular pathways) (see Figure 5.7 and Supplementary File S2, Figure S7). The size of the dots represents the number of drugs targeting the genes, and the numbers correspond to the number of reactions in the pathways under the control of the target gene. Bruceine D was excluded from this analysis because of the lack of target information. Third, the drug targets were plotted against the reactions that were differentially present between each natural product model and the DMSO model for each of the eight most commonly targeted pathways. The reactions present in the natural product models and absent in DMSO are depicted in red, and vice versa in blue (see Supplementary File S2, Figure S8).

5.5 Conclusions

In conclusion, our *in silico* analysis pipeline (`https://github.com/sysbiolux/Herbal_drug_prediction`, accessed on 30 December 2021) enabled us to narrow down a list of 101 single natural products and one mixture of natural products to nine anticancer drug candidates. The

subsequent experimental validation allowed us to confirm the potency of three out of these nine candidates, namely emodin, scutellarein, and bruceine D. Finally, our approach led to the identification of the pathways that are potentially involved in the anticancer activity of the three candidates.

5.6 Summary and Outlook

Further analysis in the synopsis showed one of the predicted NP, narciclasine, exceeded all approved breast cancer drugs in growth reduction in xenografts (see Figure 1.6.C). Moreover, resveratrol intake showed preventive action in reducing breast cancer incidence in a retrospective study [90]. While evaluation of the 23 predicted NPs didn't show differences *in vitro* potency compared to the 78 excluded NPs (see Figure 1.3), highly potent excluded NPs are mostly toxins that induce apoptosis and target epigenetics. Overall, metabolic modeling allowed the ranking of preclinical compounds with potential anti-breast cancer activity on metabolism.

Supplementary Materials

The following supporting information can be downloaded at `https://www.mdpi.com/article/10.3390/ph15020179/s1`. Table S1: Detailed model statistics for the 103 context-specific natural product models; Table S2: Natural product target interactions extracted from DrugBank V5, PROMISCUOUS 2.0 & NPASS; Table S4: List of approved breast cancer from cancer.gov; Table S5: Breast Cancer drug-target interactions extracted from DrugBank V5, PROMISCUOUS 2.0 & NPASS; Table S6: Preclinical *in vitro* evidence for the candidate natural products; Table S7: Medium composition of the MEM medium used for context-specific model building; Table S8: Additional clinical evidence for the candidate natural products; Table S10: Published concentrations and IC_{50} values for bruceine D, scutarellein and emodin; Table S11: List of reactions targeted by emodin, scutellarein, bruceine D and the breast cancer drugs in the androgen and estrogen metabolism and synthesis pathway; Figure S1: Dissimilarity score for the 102 natural product models; Figure S2: Similarity score between the natural product models and methotrexate (blue) and References capecitabine (red); Figure S3: Chondroitin synthesis, folate metabolism, histidine metabolism, and androgen and estrogen synthesis and metabolism are the top four pathways showing the highest difference of reaction presence rate between the natural product and DMSO models (Highest rate of reaction that is present in natural product models and absent in DMSO and

vice versa); Figure S4: Ten out of the 12 natural products that target the androgen and estrogen synthesis and metabolism pathway, have differences in reaction presence rate between the natural product and DMSO models; Figure S5: Resveratrol, hydroxysafflor yellow A, salvianolic acid B, salvianic acid A sodium, ferulic acid, and glycyrrhizic acid do not notably affect 2D breast cancer cell viability; Figure S7: Target genes and number of affected reactions of emodin and scutellarein; Figure S8: Natural product models reactions for bruceine D, emodin and scutellarein that are differently present between the three natural product and DMSO models and that are under the control of breast cancer drugs; Table S3: Number of natural products and cancer drugs with drug-target interaction extracted from three databases;Table S9: DSS3 and IC_{50} values for the control compound ophiobolin A and each natural product tested in Hs 578T or MCF-7 cells (mean ± SEM). ND = Not determined.

Author Contributions

Conceptualization, T.S.; software, C.C., A.K. and M.P.P.; validation, M.W. and E.S.-R.; formal analysis, C.C., M.P.P., A.K. and T.S.; writing—original draft preparation, M.P.P., E.S.-R. and C.C.; writing—review and editing, C.C., M.P.P., A.K., D.A., E.S.-R., M.W. and T.S.; supervision, T.S., M.P.P., A.K., E.S.-R. and D.A.; project administration, T.S. All authors have read and agreed to the published version of the manuscript.

Funding:

This research was funded via an Erasmus+ grant.

Institutional Review Board Statement:

Not applicable.

Informed Consent Statement:

Not applicable.

Data Availability Statement:

Data is contained within the article and supplementary materials.

Acknowledgments:

The authors are grateful to Pelin Kaya for her valuable guidance regarding 2D viability assays and DSS3 determination.

Conflicts of Interest:

The authors declare no conflict of interest.

References

[1] H. Sung, J. Ferlay, R. L. Siegel, *et al.*, "Global Cancer Statistics 2020: GLOBOCAN Estimates of Incidence and Mortality Worldwide for 36 Cancers in 185 Countries," *CA: A Cancer Journal for Clinicians*, vol. 71, no. 3, pp. 209–249, May 2021, Publisher: Wiley. DOI: 10.3322/CAAC.21660.

[2] H. P. Sinn and H. Kreipe, "A brief overview of the WHO classification of breast tumors, 4th edition, focusing on issues and updates from the 3rd edition," *Breast Care*, vol. 8, no. 2, pp. 149–154, 2013, Publisher: S. Karger AG. DOI: 10.1159/000350774.

[3] K. Polyak, "Breast cancer: Origins and evolution," *Journal of Clinical Investigation*, vol. 117, no. 11, pp. 3155–3163, Nov. 2007. DOI: 10.1172/JCI33295.

[4] W. Chen, A. D. Hoffmann, H. Liu, and X. Liu, "Organotropism: New insights into molecular mechanisms of breast cancer metastasis," *npj Precision Oncology*, vol. 2, no. 1, Dec. 2018, Publisher: Nature Publishing Group. DOI: 10.1038/S41698-018-0047-0.

[5] J. Cao, M. Zhang, B. Wang, L. Zhang, M. Fang, and F. Zhou, "Chemoresistance and Metastasis in Breast Cancer Molecular Mechanisms and Novel Clinical Strategies," *Frontiers in Oncology*, vol. 11, Jul. 2021, Publisher: Frontiers Media S.A. DOI: 10.3389/FONC.2021.658552.

[6] F. Qi, L. Zhao, A. Zhou, *et al.*, "The advantages of using traditional Chinese medicine as an adjunctive therapy in the whole course of cancer treatment instead of only terminal stage of cancer," *BioScience Trends*, vol. 9, no. 1, pp. 16–34, 2015, Publisher: International Advancement Center for Medicine and Health Research Co., Ltd. DOI: 10.5582/BST.2015.01019.

[7] Z. G. Wang and J. Ren, "Current status and future direction of Chinese herbal medicine," *Trends in Pharmacological Sciences*, vol. 23, no. 8, pp. 347–348, Aug. 2002, Publisher: Elsevier Ltd. DOI: 10.1016/S0165-6147(02)02051-5.

[8] C. Wu, S. L. Lee, C. Taylor, *et al.*, "Scientific and Regulatory Approach to Botanical Drug Development: A U.S. FDA Perspective," *Journal of Natural Products*, vol. 83, no. 2, pp. 552–562, Feb. 2020, Publisher: American Chemical Society. DOI: 10.1021/ACS.JNATPROD.9B00949.

[9] S. Kaushik, H. Shyam, R. Sharma, and A. Balapure, "Genistein synergizes centchroman action in human breast cancer cells," *Indian Journal of Pharmacology*, vol. 48, no. 6, pp. 637–642, Nov. 2016, Publisher: Medknow Publications. DOI: 10.4103/0253-7613.194852.

[10] C. Charalambous, C. A. Pitta, and A. I. Constantinou, "Equol enhances tamoxifen's anti-tumor activity by induction of caspase-mediated apoptosis in MCF-7 breast cancer cells," *BMC Cancer*, vol. 13, May 2013. DOI: 10.1186/1471-2407-13-238.

[11] S. Shameer, J. G. Vallarino, A. R. Fernie, R. G. Ratcliffe, and L. J. Sweetlove, "Flux balance analysis of metabolism during growth by osmotic cell expansion and its application to tomato fruits," *Plant Journal*, vol. 103, no. 1, pp. 68–82, Jul. 2020, Publisher: Blackwell Publishing Ltd. DOI: 10.1111/TPJ.14707.

[12] C. Y. M. Cheung, T. C. R. Williams, M. G. Poolman, D. A. Fell, R. G. Ratcliffe, and L. J. Sweetlove, "A method for accounting for maintenance costs in flux balance analysis improves the prediction of plant cell metabolic phenotypes under stress conditions," *Plant Journal*, vol. 75, no. 6, pp. 1050–1061, Sep. 2013. DOI: 10.1111/TPJ.12252.

[13] L. Jerby, L. Wolf, C. Denkert, *et al.*, "Metabolic associations of reduced proliferation and oxidative stress in advanced breast cancer," *Cancer Research*, vol. 72, no. 22, pp. 5712–5720, Nov. 2012. DOI: 10.1158/0008-5472.CAN-12-2215.

[14] F. Gatto, H. Miess, A. Schulze, and J. Nielsen, "Flux balance analysis predicts essential genes in clear cell renal cell carcinoma metabolism," *Scientific Reports*, vol. 5, Jun. 2015, Publisher: Nature Publishing Group. DOI: 10.1038/SREP10738.

[15] M. P. Pacheco, T. Bintener, D. Ternes, *et al.*, "Identifying and targeting cancer-specific metabolism with network-based drug target prediction," *EBioMedicine*, vol. 43, pp. 98–106, May 2019, Publisher: Elsevier B.V. DOI: 10.1016/J.EBIOM.2019.04.046.

[16] A. Mardinoglu, R. Agren, C. Kampf, A. Asplund, M. Uhlen, and J. Nielsen, "Genome-scale metabolic modelling of hepatocytes reveals serine deficiency in patients with non-alcoholic fatty liver disease," *Nature Communications*, vol. 5, Jan. 2014, Publisher: Nature Publishing Group. DOI: 10.1038/NCOMMS4083.

[17] M. P. Pacheco, E. John, T. Kaoma, *et al.*, "Integrated metabolic modelling reveals cell-type specific epigenetic control points of the macrophage metabolic network," *BMC Genomics*, vol. 16, no. 1, Oct. 2015, Publisher: BioMed Central Ltd. DOI: 10.1186/S12864-015-1984-4.

[18] C. Lv, X. Wu, X. Wang, *et al.*, "The gene expression profiles in response to 102 traditional Chinese medicine (TCM) components: A general template for research on TCMs," *Scientific Reports*, vol. 7, no. 1, Dec. 2017, Publisher: Nature Publishing Group. DOI: 10.1038/S41598-017-00535-8.

[19] D. S. Wishart, Y. D. Feunang, A. C. Guo, *et al.*, "DrugBank 5.0: A major update to the DrugBank database for 2018," *Nucleic Acids Research*, vol. 46, no. D1, pp. D1074–D1082, Jan. 2018, Publisher: Oxford University Press. DOI: 10.1093/NAR/GKX1037.

[20] K. Gallo, A. Goede, A. Eckert, B. Moahamed, R. Preissner, and B. O. Gohlke, "PROMISCUOUS 2.0: A resource for drug-repositioning," *Nucleic Acids Research*, vol. 49, no. D1, pp. D1373–D1380, Jan. 2021, Publisher: Oxford University Press. DOI: 10.1093/NAR/GKAA1061.

[21] X. Zeng, P. Zhang, W. He, *et al.*, "NPASS: Natural product activity and species source database for natural product research, discovery and tool development," *Nucleic Acids Research*, vol. 46, no. D1, pp. D1217–D1222, Jan. 2018, Publisher: Oxford University Press. DOI: 10.1093/NAR/GKX1026.

[22] G. Aprile, M. Mazzer, S. Moroso, and F. Puglisi, "Pharmacology and therapeutic efficacy of capecitabine: Focus on breast and colorectal cancer," *Anti-Cancer Drugs*, vol. 20, no. 4, pp. 217–229, Apr. 2009. DOI: 10.1097/CAD.0B013E3283293FD4.

[23] M. Hannoodee and M. Mittal, "Methotrexate," in *StatPearls [Internet]*, StatPearls Publishing, 2022.

[24] E. Brunk, S. Sahoo, D. C. Zielinski, *et al.*, "Recon3D enables a three-dimensional view of gene variation in human metabolism," *Nature Biotechnology*, vol. 36, no. 3, pp. 272–281, Mar. 2018, Publisher: Nature Publishing Group. DOI: 10.1038/NBT.4072.

[25] E. R. Nelson, S. E. Wardell, J. S. Jasper, *et al.*, "27-Hydroxycholesterol links hypercholesterolemia and breast cancer pathophysiology," *Science*, vol. 342, no. 6162, pp. 1094–1098, 2013. DOI: 10.1126/SCIENCE.1241908.

[26] E. J. Choi, J. Y. Jung, and G. H. Kim, "Genistein inhibits the proliferation and differentiation of MCF-7 and 3T3-L1 cells via the regulation of ER expression and induction of apoptosis," *Experimental and Therapeutic Medicine*, vol. 8, no. 2, pp. 454–458, 2014, Publisher: Spandidos Publications. DOI: 10.3892/ETM.2014.1771.

[27] K. M. McNamara, N. L. Moore, T. E. Hickey, H. Sasano, and W. D. Tilley, "Complexities of androgen receptor signalling in breast cancer," *Endocrine-Related Cancer*, vol. 21, no. 4, 2014, Publisher: BioScientifica Ltd. DOI: 10.1530/ERC-14-0243.

[28] J. Otter and J. L. D'Orazio, "Strychnine toxicity," in StatPearls Publishing, 2017.

[29] C. Cao, W. Huang, N. Zhang, *et al.*, "Narciclasine induces autophagy-dependent apoptosis in triple-negative breast cancer cells by regulating the AMPK-ULK1 axis," *Cell Proliferation*, vol. 51, no. 6, Dec. 2018, Publisher: Blackwell Publishing Ltd. DOI: 10.1111/CPR.12518.

[30] James A. Duke, *Dr. Duke's Phytochemical and Ethnobotanical Databases*, U.S. Department of Agriculture, Agricultural Research Service., 1992. DOI: http://dx.doi.org/10.15482/USDA.ADC/1239279.

[31] S. M. Corsello, J. A. Bittker, Z. Liu, *et al.*, "The Drug Repurposing Hub: A next-generation drug library and information resource," *Nature Medicine*, vol. 23, no. 4, pp. 405–408, Apr. 2017, Publisher: Nature Publishing Group. DOI: 10.1038/NM.4306.

[32] Z. W. Sin, V. Bhardwaj, A. K. Pandey, and M. Garg, "A brief overview of antitumoral actions of bruceine D," *Exploration of Targeted Anti-tumor Therapy*, vol. 1, no. 4, pp. 200–217, 2020, Publisher: Open Exploration Publishing Inc. DOI: 10.37349/ETAT.2020.00013.

[33] A. K. Najumudeen, A. Jaiswal, B. Lectez, *et al.*, "Cancer stem cell drugs target K-ras signaling in a stemness context," *Oncogene*, vol. 35, no. 40, pp. 5248–5262, Oct. 2016, Publisher: Nature Publishing Group. DOI: 10.1038/ONC.2016.59.

[34] S. Okutachi, G. B. Manoharan, A. Kiriazis, *et al.*, "A Covalent Calmodulin Inhibitor as a Tool to Study Cellular Mechanisms of K-Ras-Driven Stemness," *Frontiers in Cell and Developmental Biology*, vol. 9, Jul. 2021, Publisher: Frontiers Media S.A. DOI: 10.3389/FCELL.2021.665673.

[35] B. Yadav, T. Pemovska, A. Szwajda, *et al.*, "Quantitative scoring of differential drug sensitivity for individually optimized anticancer therapies," *Scientific Reports*, vol. 4, Jun. 2014, Publisher: Nature Publishing Groups. DOI: 10.1038/SREP05193.

[36] M. Zweifel, B. Thürlimann, S. Riniker, *et al.*, "Phase I trial of the androgen receptor modulator CR1447 in breast cancer patients," *Endocrine Connections*, vol. 6, no. 7, pp. 549–556, Oct. 2017, Publisher: BioScientifica Ltd. DOI: 10.1530/EC-17-0174.

[37] S. Song, B. Tian, M. Zhang, *et al.*, "Diagnostic and prognostic value of thymidylate synthase expression in breast cancer," *Clinical and Experimental Pharmacology and Physiology*, vol. 48, no. 2, pp. 279–287, Feb. 2021, Publisher: Blackwell Publishing. DOI: 10.1111/1440-1681.13415.

[38] U. Ozer, K. W. Barbour, S. A. Clinton, and F. G. Berger, "Oxidative stress and response to thymidylate synthase-targeted antimetabolites," *Molecular Pharmacology*, vol. 88, no. 6, pp. 970–981, Dec. 2015, Publisher: American Society for Pharmacology and Experimental Therapy. DOI: 10.1124/MOL.115.099614.

[39] M. Li, C. Jin, M. Xu, L. Zhou, D. Li, and Y. Yin, "Bifunctional enzyme ATIC promotes propagation of hepatocellular carcinoma by regulating AMPK-mTOR-S6 K1 signaling," *Cell Communication and Signaling*, vol. 15, no. 1, Dec. 2017, Publisher: BioMed Central Ltd. DOI: 10.1186/S12964-017-0208-8.

[40] R. W. Robey, K. M. Pluchino, M. D. Hall, A. T. Fojo, S. E. Bates, and M. M. Gottesman, "Revisiting the role of ABC transporters in multidrug-resistant cancer," *Nature Reviews Cancer*, vol. 18, no. 7, pp. 452–464, Jul. 2018, Publisher: Nature Publishing Group. DOI: 10.1038/S41568-018-0005-8.

[41] C. D. Mohan, Y. Y. Liew, Y. Y. Jung, *et al.*, "Brucein D modulates MAPK signaling cascade to exert multi-faceted anti-neoplastic actions against breast cancer cells," *Biochimie*, vol. 182, pp. 140–151, Mar. 2021, Publisher: Elsevier B.V. DOI: 10.1016/J.BIOCHI.2021.01.009.

[42] V. P. Androutsopoulos, K. Ruparelia, R. R. J. Arroo, A. M. Tsatsakis, and D. A. Spandidos, "CYP1-mediated antiproliferative activity of dietary flavonoids in MDA-MB-468 breast cancer cells," *Toxicology*, vol. 264, no. 3, pp. 162–170, Oct. 2009. DOI: 10.1016/J.TOX.2009.07.023.

[43] C. Luo, Y. Wang, C. Wei, Y. Chen, and Z. Ji, "The anti-migration and anti-invasion effects of Bruceine D in human triple-negative breast cancer MDA-MB-231 cells," *Experimental and Therapeutic Medicine*, Nov. 2019, Publisher: Spandidos Publications. DOI: 10.3892/ETM.2019.8187.

[44] Y. Sun, X. Wang, Q. Zhou, *et al.*, "Inhibitory effect of emodin on migration, invasion and metastasis of human breast cancer MDA-MB-231 cells in vitro and in vivo," *Oncology Reports*, vol. 33, no. 1, pp. 338–346, Jan. 2015, Publisher: Spandidos Publications. DOI: 10.3892/OR.2014.3585.

[45] G. Ni, Y. Tang, M. Li, Y. He, and G. Rao, "Synthesis of scutellarein derivatives with a long aliphatic chain and their biological evaluation against human cancer cells," *Molecules*, vol. 23, no. 2, 2018, Publisher: MDPI AG. DOI: 10.3390/MOLECULES23020310.

[46] Y. Li, J. Liu, X. Liu, *et al.*, "Resveratrol-induced cell inhibition of growth and apoptosis in MCF7 human breast cancer cells are associated with modulation of phosphorylated Akt and caspase-9," *Applied Biochemistry and Biotechnology*, vol. 135, no. 3, pp. 181–192, Dec. 2006. DOI: 10.1385/ABAB:135:3:181.

[47] Z. J. Liang, Y. Wan, D. D. Zhu, *et al.*, "Resveratrol Mediates the Apoptosis of Triple Negative Breast Cancer Cells by Reducing POLD1 Expression," *Frontiers in Oncology*, vol. 11, Feb. 2021, Publisher: Frontiers Media S.A. DOI: 10.3389/FONC.2021.569295.

[48] S. Poschner, A. Maier-Salamon, M. Zehl, *et al.*, "Resveratrol inhibits key steps of steroid metabolism in a human estrogen-receptor positive breast cancer model: Impact on cellular proliferation," *Frontiers in Pharmacology*, vol. 9, no. JUL, Jul. 2018, Publisher: Frontiers Media S.A. DOI: 10.3389/FPHAR.2018.00742.

[49] S. C. Lin, P. Y. Chu, W. T. Liao, *et al.*, "Glycyrrhizic acid induces human MDA-MB-231 breast cancer cell death and autophagy via the ROS-mitochondrial pathway," *Oncology Reports*, vol. 39, no. 2, pp. 703–710, Feb. 2018, Publisher: Spandidos Publications. DOI: 10.3892/OR.2017.6123.

[50] S. Dong, A. Inoue, Y. Zhu, M. Tanji, and R. Kiyama, "Activation of rapid signaling pathways and the subsequent transcriptional regulation for the proliferation of breast cancer MCF-7 cells by the treatment with an extract of Glycyrrhiza glabra root," *Food and Chemical Toxicology*, vol. 45, no. 12, pp. 2470–2478, Dec. 2007. DOI: 10.1016/J.FCT.2007.05.031.

[51] Z. Zhang, Y. Feng, Z. Y. Li, and X. Z. Cao, "Antiproliferative and apoptotic activity of glycyrrhizinic acid in MCF-7 human breast cancer cells and evaluation of its effect on cell cycle, cell migration and m-TOR/PI3K/Akt signalling pathway," *Archives of Medical Science*, vol. 15, no. 1, pp. 174–182, 2019, Publisher: Termedia Publishing House Ltd. DOI: 10.5114/AOMS.2018.79429.

[52] M. ElKhazendar, J. Chalak, W. El-Huneidi, A. Vinod, W. M. Abdel-Rahman, and E. Abu-Gharbieh, "Antiproliferative and proapoptotic activities of ferulic acid in breast and liver cancer cell lines," en, *Tropical Journal of Pharmaceutical Research*, vol. 18, no. 12, pp. 2571–2576, 2019, Number: 12. DOI: 10.4314/tjpr.v18i12.

[53] X. Zhang, D. Lin, R. Jiang, H. Li, J. Wan, and H. Li, "Ferulic acid exerts antitumor activity and inhibits metastasis in breast cancer cells by regulating epithelial to mesenchymal transition," *Oncology Reports*, vol. 36, no. 1, pp. 271–278, Jul. 2016, Publisher: Spandidos Publications. DOI: 10.3892/OR.2016.4804.

[54] C. J. Chang, J. H. Chiu, L. M. Tseng, *et al.*, "Modulation of HER2 expression by ferulic acid on human breast cancer MCF7 cells," *European Journal of Clinical Investigation*, vol. 36, no. 8, pp. 588–596, Aug. 2006. DOI: 10.1111/J.1365-2362.2006.01676.X.

[55] Y. Li, Y. Wu, Y. Guan, Z. Wang, and L. Zhang, "Hydroxysafflor yellow A induces apoptosis in MCF-7 cells by blocking NFB/p65 pathway and disrupting mitochondrial transmembrane potential," *RSC Advances*, vol. 4, no. 88, pp. 47 576–47 586, 2014, Publisher: Royal Society of Chemistry. DOI: 10.1039/C4RA07417C.

[56] W. Sha, Y. Zhou, Z. Q. Ling, *et al.*, "Antitumor properties of Salvianolic acid B against triple-negative and hormone receptor-positive breast cancer cells via ceramide-mediated apoptosis," *Oncotarget*, vol. 9, no. 91, pp. 36 331–36 343, Nov. 2018, Publisher: Impact Journals LLC. DOI: 10.18632/ONCOTARGET.26348.

[57] M. A. Katary, R. Abdelsayed, A. Alhashim, M. Abdelhasib, and A. A. Elmarakby, "Salvianolic acid B slows the progression of breast cancer cell growth via enhancement of apoptosis and reduction of oxidative stress, inflammation, and angiogenesis," *International Journal of Molecular Sciences*, vol. 20, no. 22, Nov. 2019, Publisher: MDPI AG. DOI: 10.3390/IJMS20225653.

[58] A. T. Sougiannis, R. T. Enos, B. N. VanderVeen, *et al.*, "Safety of natural anthraquinone emodin: An assessment in mice," *BMC Pharmacology and Toxicology*, vol. 22, no. 1, Dec. 2021, Publisher: BioMed Central Ltd. DOI: 10.1186/S40360-021-00474-1.

[59] H. Jayasuriya, N. M. Koonchanok, R. L. Geahlen, J. L. Mclaughlin, and C. J. Chang, "Emodin, a protein tyrosine kinase inhibitor from polygonum cuspidatum," *Journal of Natural Products*, vol. 55, no. 5, pp. 696–698, May 1992. DOI: 10.1021/NP50083A026.

[60] J. Jiang, N. Zhou, P. Ying, T. Zhang, R. Liang, and X. Jiang, "Emodin promotes apoptosis of human endometrial cancer through regulating the MAPK and PI3K/ AKT pathways," *Open Life Sciences*, vol. 13, no. 1, pp. 489–496, 2018, Publisher: De Gruyter. DOI: 10.1515/BIOL-2018-0058.

[61] K. J. Wang, X. Y. Meng, J. F. Chen, *et al.*, "Emodin Induced Necroptosis and Inhibited Glycolysis in the Renal Cancer Cells by Enhancing ROS," *Oxidative Medicine and Cellular Longevity*, vol. 2021, 2021, Publisher: Hindawi Limited. DOI: 10.1155/2021/8840590.

[62] X. Dong, B. Ni, J. Fu, *et al.*, "Emodin induces apoptosis in human hepatocellular carcinoma HepaRG cells via the mitochondrial caspase-dependent pathway," *Oncology Reports*, vol. 40, no. 4, pp. 1985–1993, Oct. 2018, Publisher: Spandidos Publications. DOI: 10.3892/OR.2018.6620.

[63] L. Shi, Y. Wu, D. l. LV, and L. Feng, "Scutellarein selectively targets multiple myeloma cells by increasing mitochondrial superoxide production and activating intrinsic apoptosis pathway," *Biomedicine and Pharmacotherapy*, vol. 109, pp. 2109–2118, Jan. 2019, Publisher: Elsevier Masson SAS. DOI: 10.1016/J.BIOPHA.2018.09.024.

[64] J. Fan, D. Ren, J. Wang, *et al.*, "Bruceine D induces lung cancer cell apoptosis and autophagy via the ROS/MAPK signaling pathway in vitro and in vivo," *Cell Death and Disease*, vol. 11, no. 2, Feb. 2020, Publisher: Springer Nature. DOI: 10.1038/S41419-020-2317-3.

[65] Z. Q. Lai, S. P. Ip, H. J. Liao, *et al.*, "Brucein D, a naturally occurring tetracyclic triterpene quassinoid, induces apoptosis in pancreatic cancer through ROS-associated PI3K/Akt signaling pathway," *Frontiers in Pharmacology*, vol. 8, no. DEC, Dec. 2017, Publisher: Frontiers Media S.A. DOI: 10.3389/FPHAR.2017.00936.

[66] Y. Park, J. Jeong, S. Seong, and W. Kim, "In silico evaluation of natural compounds for an acidic extracellular environment in human breast cancer," *Cells*, vol. 10, no. 10, Oct. 2021, Publisher: MDPI. DOI: 10.3390/CELLS10102673.

[67] M. Stompor–gorący, "The health benefits of emodin, a natural anthraquinone derived from rhubarb—a summary update," *International Journal of Molecular Sciences*, vol. 22, no. 17, Sep. 2021, Publisher: MDPI. DOI: 10.3390/IJMS22179522.

[68] S. E. Ha, S. M. Kim, P. Vetrivel, *et al.*, "Inhibition of cell proliferation and metastasis by scutellarein regulating PI3K/Akt/NF-B signaling through PTEN activation in hepatocellular carcinoma," *International Journal of Molecular Sciences*, vol. 22, no. 16, Aug. 2021, Publisher: MDPI AG. DOI: 10.3390/IJMS22168841.

[69] G. Hoxhaj and B. D. Manning, "The PI3K–AKT network at the interface of oncogenic signalling and cancer metabolism," *Nature Reviews Cancer*, vol. 20, no. 2, pp. 74–88, Feb. 2020, Publisher: Nature Research. DOI: 10.1038/S41568-019-0216-7.

[70] Y. Xia, S. Shen, and I. M. Verma, "NF-B, an active player in human cancers," *Cancer immunology research*, vol. 2, no. 9, pp. 823–830, Sep. 2014. DOI: 10.1158/2326-6066.CIR-14-0112.

[71] R. Huang, H. Chen, J. Liang, *et al.*, "Dual role of reactive oxygen species and their application in cancer therapy," *Journal of Cancer*, vol. 12, no. 18, pp. 5543–5561, 2021, Publisher: Ivyspring International Publisher. DOI: 10.7150/JCA.54699.

[72] B. Perillo, M. D. Donato, A. Pezone, *et al.*, "ROS in cancer therapy: The bright side of the moon," *Experimental and Molecular Medicine*, vol. 52, no. 2, pp. 192–203, Feb. 2020, Publisher: Springer Nature. DOI: 10.1038/S12276-020-0384-2.

[73] H. Kamei, T. Koide, T. Kojima, Y. Hashimoto, and M. Hasegawa, "Inhibition of cell growth in culture by quinones," *Cancer Biotherapy and Radiopharmaceuticals*, vol. 13, no. 3, pp. 185–188, 1998, Publisher: Mary Ann Liebert Inc. DOI: 10.1089/CBR.1998.13.185.

[74] F. Guo, F. Yang, and Y. H. Zhu, "Scutellarein from Scutellaria barbata induces apoptosis of human colon cancer HCT116 cells through the ROS-mediated mitochondria-dependent pathway," *Natural Product Research*, vol. 33, no. 16, pp. 2372–2375, Aug. 2019, Publisher: Taylor and Francis Ltd. DOI: 10.1080/14786419.2018.1440230.

[75] W. J. Liu, G. Zhao, C. Y. Zhang, *et al.*, "Comparison of the roles of estrogens and androgens in breast cancer and prostate cancer," *Journal of Cellular Biochemistry*, vol. 121, no. 4, pp. 2756–2769, Apr. 2020, Publisher: Wiley-Liss Inc. DOI: 10.1002/JCB.29515.

[76] R. Ma, G. M. Karthik, J. Lovrot, *et al.*, "Estrogen Receptor B as a therapeutic target in breast cancer stem cells," *Journal of the National Cancer Institute*, vol. 109, no. 3, Mar. 2017, Publisher: Oxford University Press. DOI: 10.1093/JNCI/DJW236.

[77] F. Z. Stanczyk, "The 2-/16-Hydroxylated Estrogen Ratio-Breast Cancer Risk Hypothesis: Insufficient Evidence for its Support: Running title: 2-/16-Hydroxyestrone-Breast Cancer Risk Hypothesis," *Journal of Steroid Biochemistry and Molecular Biology*, vol. 201, Jul. 2020, Publisher: Elsevier Ltd. DOI: 10.1016/J.JSBMB.2020.105685.

[78] S. Haas, C. Pierl, V. Harth, *et al.*, "Expression of xenobiotic and steroid hormone metabolizing enzymes in human breast carcinomas," *International Journal of Cancer*, vol. 119, no. 8, pp. 1785–1791, Oct. 2006, Publisher: Wiley-Liss Inc. DOI: 10.1002/IJC.21915.

[79] R. Mitra, Z. Guo, M. Milani, *et al.*, "CYP3A4 mediates growth of estrogen receptor-positive breast cancer cells in part by inducing nuclear translocation of phospho-Stat3 through biosynthesis of (±)-14,15-epoxyeicosatrienoic acid (EET)," *Journal of Biological Chemistry*, vol. 286, no. 20, pp. 17 543–17 559, May 2011. DOI: 10.1074/JBC.M110.198515.

[80] T. Barrett, S. E. Wilhite, P. Ledoux, *et al.*, "NCBI GEO: Archive for functional genomics data sets - Update," *Nucleic Acids Research*, vol. 41, no. D1, Jan. 2013. DOI: 10.1093/NAR/GKS1193.

[81] M. N. McCall, B. M. Bolstad, and R. A. Irizarry, "Frozen robust multiarray analysis (fRMA)," *Biostatistics*, vol. 11, no. 2, pp. 242–253, Apr. 2010. DOI: 10.1093/BIOSTATISTICS/KXP059.

[82] K. Greenhalgh, J. Ramiro-Garcia, A. Heinken, *et al.*, "Integrated In Vitro and In Silico Modeling Delineates the Molecular Effects of a Synbiotic Regimen on Colorectal-Cancer-Derived Cells," *Cell Reports*, vol. 27, no. 5, 1621–1632.e9, Apr. 2019, Publisher: Elsevier B.V. DOI: 10.1016/J.CELREP.2019.04.001.

[83] N. Vlassis, M. P. Pacheco, and T. Sauter, "Fast Reconstruction of Compact Context-Specific Metabolic Network Models," *PLoS Computational Biology*, vol. 10, no. 1, 2014, Publisher: Public Library of Science. DOI: 10.1371/JOURNAL.PCBI.1003424.

[84] J. L. Robinson, P. Kocabaş, H. Wang, *et al.*, "An atlas of human metabolism," *Science Signaling*, vol. 13, no. 624, Mar. 2020, Publisher: American Association for the Advancement of Science. DOI: 10.1126/SCISIGNAL.AAZ1482.

[85] U. Mudunuri, A. Che, M. Yi, and R. M. Stephens, "bioDBnet: The biological database network," *Bioinformatics*, vol. 25, no. 4, pp. 555–556, Feb. 2009. DOI: 10.1093/BIOINFORMATICS/BTN654.

[86] L. Heirendt, S. Arreckx, T. Pfau, *et al.*, "Creation and analysis of biochemical constraint-based models using the COBRA Toolbox v.3.0," *Nature Protocols*, vol. 14, no. 3, pp. 639–702, Mar. 2019, Publisher: Nature Publishing Group. DOI: 10.1038/S41596-018-0098-2.

[87] S. Gudmundsson and I. Thiele, "Computationally efficient flux variability analysis," *BMC Bioinformatics*, vol. 11, Sep. 2010. DOI: 10.1186/1471-2105-11-489.

[88] J. E. Gillen, T. Tse, N. C. Ide, and A. T. McCray, "Design, implementation and management of a web-based data entry system for clinicaltrials. gov," in *MEDINFO 2004*, IOS Press, 2004, pp. 1466–1470.

[89] S. Potdar, A. Ianevski, J. P. Mpindi, *et al.*, "Breeze: An integrated quality control and data analysis application for high-throughput drug screening," *Bioinformatics*, vol. 36, no. 11, pp. 3602–3604, Jun. 2020, Publisher: Oxford University Press. DOI: 10.1093/BIOINFORMATICS/BTAA138.

[90] F. Levi, C. Pasche, F. Lucchini, R. Ghidoni, M. Ferraroni, and C. La Vecchia, "Resveratrol and breast cancer risk," *European journal of cancer prevention*, vol. 14, no. 2, pp. 139–142, 2005.

Chapter 6

DCcov: Repositioning of drugs and drug combinations for SARS-CoV-2 infected lung through constraint-based modeling

Ali Kishk[1], Maria Pires Pacheco[1], and Thomas Sauter[1],*

[1] Department of Life Sciences and Medicine, University of Luxembourg, Belval Campus, 2, avenue de l'Université L-4365 Esch-sur-Alzette, Luxembourg

* Correspondence: Thomas.Sauter@uni.lu

This article has been published in:

iScience, Volume 24 (Issue 11), 2021, https://doi.org/10.1016/j.isci.2021.103331

Introduction to the paper

The 2019 coronavirus disease (COVID-19) is caused by a virus called severe acute respiratory syndrome coronavirus 2 (SARS-CoV-2), leading to a global pandemic with nearly seven million deaths. Despite previous knowledge of other species, the spread of COVID-19 caused global confinement and self-isolation. Due to the presence of only symptomatic treatments for SARS-CoV-2 during the start of the pandemic and high biosafety requirements for drug screening, computational drug repurposing has become essential. In this work, we build genome-scale metabolic models of the SARS-CoV-2-infected lung cell lines to repurpose approved drugs and predict essential genes. We show the consistency of predicted essential genes governing cysteine and glycine synthesis and metabolomics study of serum biomarkers in COVID-19-positive patients.

Contribution: I carried out the literature review, wrote the manuscript, and prepared the figures.

Highlights

- Metabolic modeling of COVID-19 utilized public RNA-Seq of SARS-CoV-2-infected lung
- *In silico* knockout identified 23 human essential genes for SARS-CoV-2 replication
- Drug repositioning predicted single drugs targeting essential gene pairs
- Among others, pyrimidine metabolism and ferroptosis are candidate druggable pathways

Summary

The 2019 coronavirus disease (COVID-19) became a worldwide pandemic with currently no approved effective antiviral drug. Flux balance analysis (FBA) is an efficient method to analyze metabolic networks. Here, FBA was applied on human lung cells infected with severe acute respiratory syndrome coronavirus 2 (SARS-CoV-2) to reposition metabolic drugs and drug combinations against the virus replication within the host tissue. Making use of expression datasets of infected lung tissue, genome-scale COVID-19-specific metabolic models were reconstructed. Then, host-specific essential genes and gene pairs were determined through *in silico* knockouts that permit reducing the viral biomass production without affecting the host biomass. Key pathways that are associated with COVID-19 severity in lung tissue are related to oxidative stress, ferroptosis, and pyrimidine metabolism. By *in silico* screening of Food and Drug Administration (FDA)-approved drugs on the putative disease-specific essential genes and gene pairs, 85 drugs and 52 drug combinations were predicted as promising candidates for COVID-19 (`https://github.com/sysbiolux/DCcov`).

6.1 Introduction

Constraint-based modeling (CBM) approaches have successfully been applied in fundamental research [1]–[3] especially in cancer research [4]–[7], as well as in microbial engineering [8], [9] among other research fields. CBM uses data- and prior knowledge-driven constraints to identify feasible metabolic flux distributions for a given condition [10]. Many communities and collaborative works contributed to reconstructing organism-specific generic metabolic networks, which serve as starting points for CBM. Examples of such generic models are Recon 2 [11], Recon 2.2 [3], Recon3D [12], Human1 [13], and HMR [4]. Other types of metabolic models are context-specific models that are built from tissue- or disease-specific data. Usually, the context-specific models are draft reconstructions built from the expression data of this condition by building algorithms such as FASTCORE [14], rFASTCORMICS [6],

INIT [4], and RegrEX [15]/or manually curated such as for E. coli [16], hepatocyte [17], and Zea mays [18]. These models are often used as scaffolds for the integration of omics data or more interesting to simulate the metabolic phenotypes of organisms, tissues, or cell lines. Within the CBM methods, flux balance analysis (FBA) is a linear programming-based approach that maximizes or minimizes an objective function, often a growth rate, to identify the optimal flux distribution(s) [19], [20]. *In silico* knockout studies are common in FBA through gene or reaction deletion. This deletion may be single, double, or multiple [21]. The goal of single reaction deletion is finding the most critical reactions in respect to the objective function through brute force removal of each reaction individually and calculating the ratio of the objective rates between mutated and wild-type models. Gene deletion studies are taking advantage of Boolean representations of the gene-reaction links known as gene–protein-reaction (GPR) rules [9]. Gene deletion helps in defining essential genes whose deletion impacts the flux through the objective function [19]. Essential genes are often used as targets for drug repositioning.

The 2019 coronavirus disease (COVID-19) is caused by a betacoronavirus strain called severe acute respiratory syndrome coronavirus 2 (SARS-CoV-2). COVID-19 was declared as a global pandemic on 11 March 2020 by WHO [22]. Human-to-human infection can be transmitted by droplets [23] or aerosols [24] by both symptomatic and asymptomatic patients [25]. The virus strain might have originated from the betacoronaviruses in bats and pangolins [26]. SARS-CoV-2 can cause upper and lower respiratory infections, increasing its transmissibility and severity. SARS-CoV-2 utilizes the human protein angiotensin I-converting enzyme 2 (ACE2) for cell entry with its spike protein. ACE2 is expressed on lung epithelial cells and other organs. The role of ACE2 is converting angiotensin II (AT-II) to angiotensin-(1,7) (AT-1,7) to negate the inflammatory effect of AT-II [27]. Thus, SARS-CoV-2 infection decreases the concentration of cellular unbound ACE2 molecules to facilitate the cell entry, causing an increase of AT-II which eventually increases the oxidative stress ion superoxide [28]. People with increased COVID-19 risk are patients with cancer [29], chronic kidney disease [30], obesity [31], type 2 diabetes mellitus [32], immunocompromised [33], cardiac diseases [34], chronic obstructive pulmonary disease (COPD) [34], and sickle cell disease [35].

Acute respiratory distress syndrome (ARDS) is one of the severe symptoms of COVID-19, which may be attributed to alveolar epithelial cell injury [36]. This ARDS may become unresponsive to invasive mechanical ventilation and increase lung injury [37]. Severe COVID-19 courses are also associated with acute injury to heart, kidney, and cerebrovascular diseases [38]. In addition to the previous symptoms, long-term effects for COVID-19 survivors (or long-haulers) have been emerging. These long-term effects include new-onset diabetes, increasing severe complications in pre-existing diabetes [39], fatigue, dyspnea, psychological distress [40], and myocardial inflammation [41]. Metabolic modeling and in particular FBA were often used to understand the effects of microbes on human cells. Notably, a human alveolar model was used to assess the metabolic interaction between the host and Mycobacterium tuberculosis [42]. Lately, a similar approach was applied in the viral genomes to model the impact of the Chikungunya, Dengue, and Zika viruses on the macrophage [43].

Only a few studies employed FBA on COVID-19 so far. Renz *et al.* used the viral genome information available at that time, to generate a SARS-CoV-2 specific viral biomass objective function (VBOF) [44]. This VBOF generation from the genome information consisted of six steps on nucleotide,

and amino acid investment, adenosine triphosphate (ATP) requirements, pyrophosphate liberation, total viral molar mass, and final construction of the VBOF [44]. Then, the VBOF was added to a human alveolar macrophage model (*iAB-AMØ1410*) [42] to build a SARS-CoV-2-infected macrophage model. They identified guanylate kinase (GUK1) as an essential gene through *in silico* knockout that allows decreasing the viral biomass without affecting the human biomass maintenance. Several worldwide collaborative works in computational modeling of COVID-19 were established. Cheng *et al.* built context-specific models for different infected cell lines using multiple expression data [45]. They also predicted drug combinations to remdesivir [45]. Ostaszewski *et al.* built the COVID-19 Disease Map to understand the mechanistic interactions between SARS-CoV-2 and human tissues [46]. In another collaborative study, Gysi *et al.* applied network analysis for drug repositioning using three different ranking approaches: network proximity, diffusion, and deep learning-based [47]. With the rising SARS-CoV-2 variants globally, variant-specific metabolic models were built and found GUK1 as a shared essential target [48]. Previous methods for metabolic modeling of SARS-CoV-2, either focused on generating the VBOF from the viral genome [44] or on multiple cell line modeling and drug combination prediction with remdesivir [45]. To further support the search for an effective treatment for COVID-19, we employ here FBA to find candidate drugs and drug combinations that target viral-specific essential genes in SARS-CoV-2-infected lung cells through context-specific models built from expression data and the VBOF from [44] by the rFASTCORMICS workflow [6] (see Figure 6.1). We also highlight key pathways of these essential genes that might contribute to COVID-19 severity.

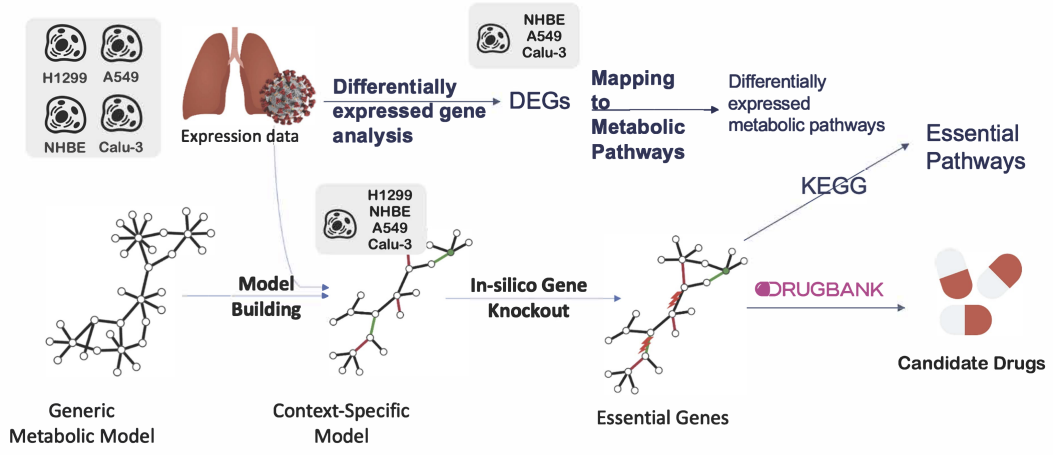

FIGURE 6.1: **Overview of the pipeline of essential gene prediction for SARS-CoV-2-infected lung cells.**
The viral biomass function (VBOF) was added to the generic metabolic models (Recon2.04 and Recon3D_01) (related to STAR Methods 6.6.1.2.1) to build the infected generic models. Consistent versions of both the control and the infected generic models were obtained. Mock and infected lung expression data were used to build the context-specific models using rFASTCORMICS and the consistent control models as input for the mock-specific models and the consistent infected models for infected-specific models, respectively. The objective functions were adjusted (related to STAR Methods 6.6.1.2.2). Then, essential genes and gene pairs were identified by *in silico* gene knockout before mapping to DrugBank V5 for drug repositioning to drugs and drug combinations.

6.2 Results

The main goal of the present study is to understand metabolic changes induced by COVID-19 in several lung cell lines, at various severity of infection, and at different time points after the infection (see Tables 6.1 and 6.2 for the metadata of the two RNA-Seq studies). We then used single and double knockouts to identify vulnerabilities specific to infected cells predicted by our network models to reduce the viral proliferation, while only moderately affecting the growth of host and control cells (see Figure 6.1). To further prioritize essential genes, we considered their essentiality scores across cell lines and in time and the effect of a knockout of these genes in the healthy tissues. The final aim is to identify conserved essential genes across infected models that do not provoke severe side effects when the gene is knocked out in the healthy counterpart model. To further identify vulnerabilities in the networks that could be exploited as drug targets, *in silico* inactivation of reactions was simulated. We further investigated the pathways harboring the predicted essential genes and reactions, to gain insight into how the virus adapts to the metabolism of lung cells. Finally, we proposed drug and drug combinations that target the predicted essential genes and synergistic essential gene pairs.

Table 6.1: Severity study metadata (GEO: GSE147507).

Expression data from three lung cell lines infected with SARS-CoV-2 at three different viral loads and for some samples transfected with a vector expressing ACE2 with their controls.

Condition Name	Cell Line	Multiplicity of Infection	ACE2 Vector	Abbreviation	Number of Samples (Infected/Mock)
Series 1	NHBE	2	No	NHBE_2	3/3
Series 2	A549	0.02	No	A549_0.02	3/3
Series 5	A549	2	No	A549_2	3/3
Series 6	A549	0.2	Yes	A549_0.2_ACE2	3/3
Series 7	Calu-3	2	No	Calu3_2	3/3
Series 16	A549	2	Yes	A549_2_ACE2	3/3

Table 6.2: Time-series study metadata (GEO: GSE148729).

Time series expression data with five time-points (4, 8, 12, 24, and 36 hrs) with infected and mock samples for two lung cell lines.

Condition Name	Cell Line	Time Point (hrs)	Number of Samples (Infected/Mock)
Calu3_4h	Calu-3	4	4/4
Calu3_8h	Calu-3	8	2/0
Calu3_12h	Calu-3	12	4/2
Calu3_24h	Calu-3	24	2/2
H1299_4h	H1299	4	2/2
H1299_12h	H1299	12	2/0
H1299_24h	H1299	24	2/0
H1299_36h	H1299	36	2/2

6.2.1 *Metabolic pathway analysis of differentially expressed genes indicates COVID-19-based rewiring of core metabolism*

Infection by the SARS-CoV-2 virus provokes alterations in the metabolism of the host cells. To elucidate these induced metabolic changes, we took advantage of two available expression datasets (Severity Study; Time-series Study; see STAR Methods for details). Principal component analysis (PCA) of the severity study samples shows a clear cluster separation according to the cell type (see Figure S1). Besides determining the differentially expressed genes (DEGs), we built genome-scale metabolic models applying rFASTCORMICS (related to STAR Methods 6.6.1.2.1). The context-specific model reconstruction process resulted in 50 models (28 infected and 22 mock) with a median of 3646 metabolites (2465-5088) and 2456.5 reactions (1790-3474). To determine the key dysregulated pathways, we mapped the DEGs on the Recon3D_01 model and displayed the pathway alterations in the mostly dysregulated conditions (Figures 6.2 and S2 that shows a representation of all pathways without filtering on the number of reactions, nor the reactions per pathway). A549_0.02 condition didn't show any differentially expressed metabolic genes, thus it was discarded from the DEGs metabolic pathways. Meanwhile, the Normal Human Bronchial Epithelial cell line with MOI of 2 (NHBE_2) condition pathways were filtered (related to STAR Methods 6.6.1.1.2). Among the most down-regulated pathways in the A549 cell lines with transfection (A549_2_ACE2 and A549_0.2_ACE2) in comparison to no ACE2 vector (A549_2) were chondroitin sulfate degradation, phosphatidylinositol phosphate metabolism, and phenylalanine metabolism, whereas glutathione metabolism was upregulated. For the A549 cell line with high viral load (A549_2_ACE2 and A549_2) in comparison to low (A549_0.2_-ACE2), a downregulation of fatty acid synthesis, androgen and estrogen synthesis and metabolism, chondroitin synthesis, and pyruvate metabolism were also detected. Across all conditions, including Calu3_2, we found a moderate downregulation of several pathways (glycerophospholipid metabolism, glycosphingolipid metabolism, sphingolipid metabolism). Other regulated pathways in Calu3_2 are the downregulated chondroitin sulfate degradation, nucleotide interconversion, and the upregulated cholesterol metabolism. The two additional DEG analyses on the ACE2 transfection showed some dysregulated pathways, such as the metabolism of folate, cholesterol, butanoate, arginine, proline, and D-alanine. Only cholesterol metabolism was shared between ACE2 transfection and Calu3_2 pathways (Figure S2).

6.2.2 *In silico single-gene deletion predicts common potential drug targets across infected cell lines with reduced side effects on control cells*

The DEGs and the performed pathway analysis indicate a rewiring of the metabolism induced by SARS-CoV-2. The next step was then to verify if these alterations caused the appearance of infected cell-specific essential genes that could specifically be targeted by repositioned drugs. Therefore, for every condition of both lung studies, *in silico* single-gene deletion was performed on the respective reconstructed metabolic models. Twenty-three unique genes were predicted to be essential in the

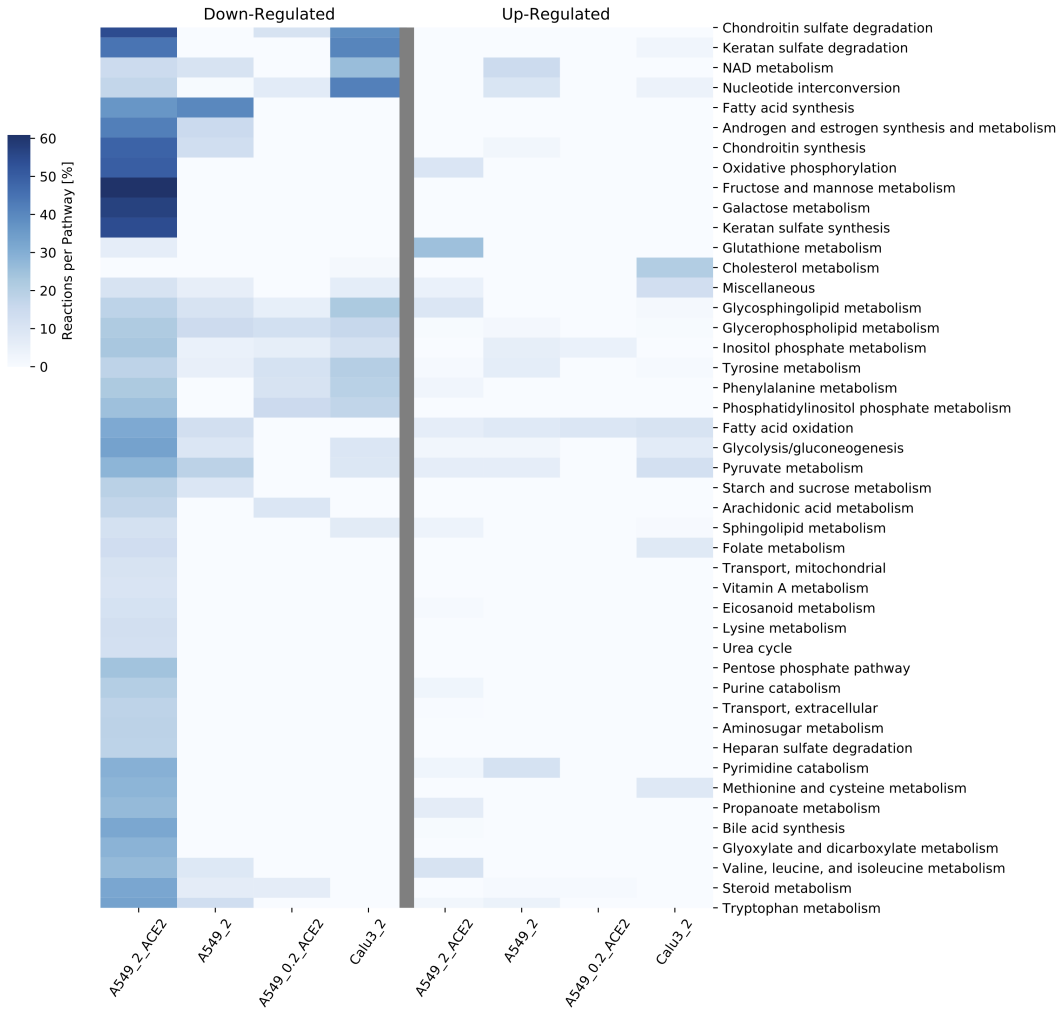

FIGURE 6.2: **Reactions per pathway Heatmap for pathway analysis of differentially expressed genes in the severity study.**
Differentially expressed genes (DEGs) were computed with DESeq2 (absolute log2 fold change >1, adjusted p-value < 0.05). The Down- and up-regulated were mapped to the pathways (*subSystems*) of Recon3D_01. The number of up and down-regulated reactions was then summed up to identify the top altered pathways in the infected lung cell lines in the severity study (related to STAR Methods 6.6.1.1.2). The color code "Reactions per Pathway [%]" represents the number of enriched metabolic reactions in a pathway divided by the overall number of reactions in this pathway. The transfection of ACE2 at an MOI of two in the A549 cell lines caused the downregulation of many pathways, which was not seen when the MOI was decreased by a factor of ten.

infected models (Tables S1 and S4). To assess if a drug targeting the candidate essential gene will kill the infected cell or reduce the viral proliferation, we computed an essentiality score for each essential gene, which sums up the number of models in which this gene is predicted to be essential. Essential genes that are only found in one or a few conditions might be cell line or experiment (e.g., medium) specific and hence might not have general biological relevance. Single-gene deletion of each predicted essential gene was then performed on the counterpart control model (related to STAR Methods 6.6.1.2.2) to predict the effect of the gene knockout on the healthy tissue. This allowed obtaining a safety score and, hence, estimating the potential toxicity of each of the considered drug targets.

The obtained essentiality and safety scores are plotted for visual inspection (see Figure 6.1). Cardiolipin

synthase 1 (CRLS1) and sphingomyelin synthase 1 (SGMS1) scored highest for essentiality, but were among the lowest for safety, thus indicating that targeting any of these genes might be effective against the virus but also reduces the growth of healthy cells, suggesting high toxicity of respective drugs. On the other hand, GUK1 gene showed a moderate essentiality score, but a higher safety score expecting fewer side effects. No gene could be identified that has high efficiency and safety. Also, nine of the 23 essential genes belong to the solute carrier (SLC) transporter gene family. Transporters are known key regulators of metabolic flux [6], [49]; hence, modulating their expression might contribute to diverting metabolic fluxes to pathways for viral survival and proliferation. Of the 23 essential genes, 10 genes were shared between the two investigated lung studies, and many essential gene sets are shared between the investigated conditions (CRLS1, GUK1, SGMS1 in the severity study and CRLS1, ISYNA1, SGMS1, SLC27A4 in the time-series study), suggesting the existence of a consistent metabolic rewiring of the host metabolism rather than random alterations.

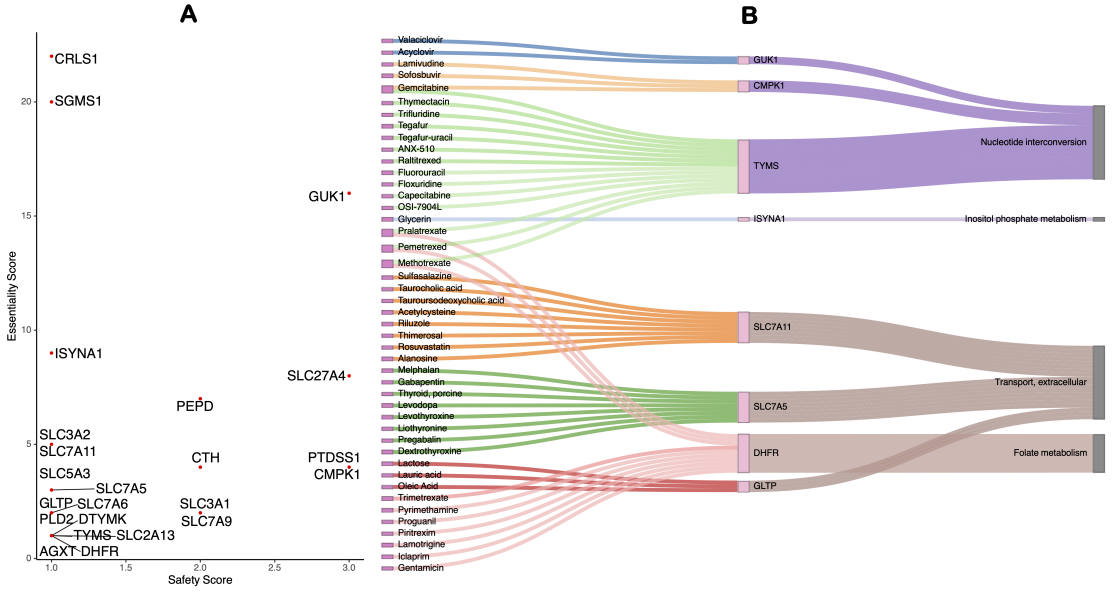

FIGURE 6.3: **Scatterplot and tripartite network of essential genes, and their predicted drugs and pathways, determined by *in silico* single-gene deletions on the infected lung models.**

(A) Scatterplot of essentiality and safety scores of the essential genes. Essentiality and safety scores correspond to the number of infected and healthy models, respectively, in which each gene is predicted to be essential. The y-axis indicates the number of infected cell lines for which the gene is predicted to be essential, whereas the x-axis indicates the number of control cell lines that are predicted to remain unharmed by the silencing of the target genes. (B) Tripartite network of the drug-gene-pathway interactions of the essential genes: A network of the single repositioned drugs and their essential genes, predicted by *in silico* gene deletion, was built. The relationships between the essential genes and their pathways were mapped using Recon3D_01 *subSystem*. Genes, and their connected drugs, that don't have pathways in Recon3D_01 *subSystems* were discarded.

6.2.3 *In silico single-gene deletion predicts potential drug targets for different stages and disease severity levels*

Variability in the metabolism of cell lines, viral load, and time of infection gives rise to the appearance of context-specific essential genes. Core essential genes in infected cells are optimal drug targets as likely to be efficient for a majority of patients. Essential genes that are specific to the time of the disease or severity level are also of interest, as it allows modulating the specific treatment. It might be reasonable to provide drugs with strong adverse effects to more severe cases and to opt for lighter treatments for mild affections. To identify core and context-specific essential genes, we performed *in silico* gene knock-outs on all reconstructed models and compared the sets of essential genes across all the conditions and between the severity and time-series studies. And more specifically, we focused on the effect of the transfection of the ACE2 vector, the viral load in the severity study, and the time after infection in the time-series study. ACE2 is crucial for SARS-CoV-2 cell entry by binding with its spike protein, but ACE2 also has many cellular functions crucial to the host cells, such as in the angiotensin–renin system. By comparing the essential genes in the absence (A549_2) and the presence of the ACE2 vector (A549_2_ACE2 & A549_0.2_ACE2), we could identify one set of genes (ISYNA1, SLC3A2, SLC7A11) that are essential for the virus in the absence of the ACE2 vector. By comparing the essential genes in the A549 cell line in the severity study with a high multiplicity of infection (MOI) (A549_2 & A549_2_ACE2) against low MOI (A549_0.02 & A549_0.2_ACE2), we identified essential genes for high viral load (CMPK1, CTH, PTDSS1, SLC2A13, SLC3A1, SLC5A3, SLC7A9) in A549_2_ACE2 and one essential gene, DTYMK, in A549_2, where the gene set (AGXT, DHFR, SLC27A4, TYMS) were unique for low viral load in A549_0.2_ACE2.

For the time-series study, a list of core essential genes (7–10 genes) was common to every time point and for each cell line (see Table S2). Besides the core essential genes, there were time point-specific essential genes that were essential only at very specific time-points owing to the inactivation of alternative pathways (Table S2). The Calu-3 cell line has eight core essential genes (CRLS1, GUK1, ISYNA1, PEPD, SGMS1, SLC27A4, SLC3A2, SLC7A11) and three-time point-specific genes (see Table S2). Out of the eight core essential genes, five (SLC27A4, CRLS1, GUK1, PEPD, SGMS1) were also in the six essential genes of the Calu3_2 condition in the severity study. Six core essential genes (CRLS1, ISYNA1, PLD2, SGMS1, SLC27A4, SLC7A6) and two time-specific genes were predicted for the H1299 cell line. Jaccard similarity of the essential genes between different conditions shows cell type-specific essential genes in the time-series study (see Figure S4). Clustering of the reconstructed models by core reactions using Jaccard similarity (see Figure S3) shows four clusters by cell type (A549, H1299, NHBE, Calu-3), even for cell lines between the two studies (Calu-3). This cell line-specific clustering is more apparent in Recon 3D than in Recon2. Moreover, the infection state (Mock, infected) forms sub-clusters within each of the four main clusters.

6.2.4 *Essential genes and reactions are predicted to be harbored in 8 unique pathways among which is methionine and cysteine metabolism*

To obtain a comprehensive picture of viral essentiality, we apply pathway analysis for core and context-specific essential genes to identify pathways that are major players in the determination of the severity as well as the stage of the infections. For both studies, the predicted essential genes were enriched in 13 unique pathways, of which eight were shared between both studies (Figure 6.4B) (fatty acid oxidation, glycerophospholipid metabolism, inositol phosphate metabolism, methionine, and cysteine metabolism, nucleotide interconversion, sphingolipid metabolism, starch, and sucrose metabolism, extracellular transport). Glycerophospholipid metabolism was enriched in all conditions across both studies. Nucleotide interconversion and extracellular transport were highly enriched in the severity and in the time-series study, respectively. Also, two pathways were shared with the DEGs pathways (glycerophospholipid metabolism, and sphingolipid metabolism). The essential gene ISYNA1, encoding a synthase in the inositol phosphate metabolism pathway, was specific to cell lines without ACE2 vectors. No unique change in the set of essential genes' pathways was found in the function of the viral load in both conditions (A549_2 & A549_2_ACE2).

To also explore pathways harboring essential genes that are not directly linked to metabolism or that are not captured by the metabolic genes and pathways in Recon3D_01, and Enrichr pathway analysis was performed [50]. Among others, ferroptosis, selenocompound metabolism, cysteine, and methionine metabolism, mTOR signaling pathway, and ether lipid metabolism were enriched for the essential genes (Figure 6.4A). Ferroptosis was the only Enrichr-derived pathway that was associated with non-ACE2 vector samples owing to context-specific essential genes (SLC3A2, SLC7A11). Protein digestion and absorption were also enriched in some conditions with high viral load, whereas glycerophospholipid metabolism was highly enriched in both lung studies. Finally, pyrimidine metabolism was enriched in most severity study conditions; meanwhile, sphingolipid metabolism was enriched in all time-series study conditions. Only folate metabolism was shared between the essential genes' metabolic pathways and the dysregulated pathways of ACE2 transfection (Figure S2).

6.2.5 *Prediction of candidates for repositioning of drugs and drug combinations targeting essential genes and synergetic gene pairs*

Out of the 23 predicted essential genes, eight genes are druggable by 45 unique drugs (Table S3) from DrugBank [51]. Six antiviral drugs (acyclovir, valaciclovir, lamivudine, sofosbuvir, methotrexate, and trifluridine) were identified in these 45 drugs. These drugs cover many modes-of-actions such as immunosuppressive, antiviral, folic acid antagonists, antirheumatic, and hypolipidemic actions besides some known nutraceutical cofactors such as lactose and folic acid (see Figure S5). The mode of actions were downloaded from the Drug Repurposing Hub [52], while side effects were extracted from the MedDRA database (downloaded on 26th May 2020) [53] with selecting only side effects containing

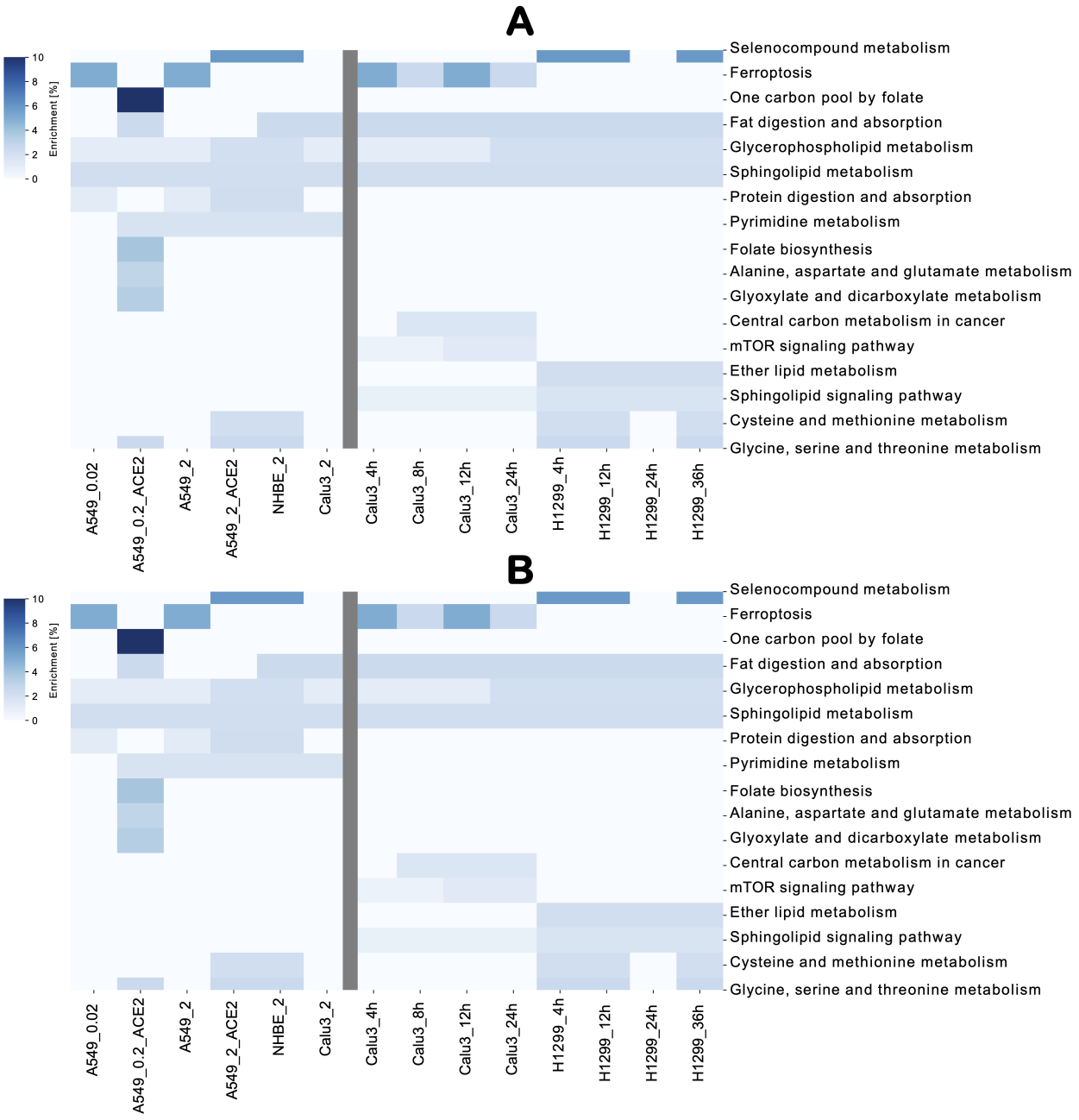

FIGURE 6.4: **Pathway analysis of the essential genes in the two lung studies.** Identification of the pathways harboring the identified essential genes using Enrichr and Recon3D_01 *subSystem*, and hence the most critical pathways for the viral survival and proliferation across cell type, severity level, and time after infection. On the x-axis from the left to the right, are the conditions of both the severity study and the time-series lung studies, respectively (related to STAR Methods). Conditions in the severity study were named as cell line + ACE2 vector (if exists) + MOI. Conditions in the second lung cell line were named as cell line + time point. (A) Enrichr enrichment: The color code in (A) "Enrichment [%]" represents the number of enriched genes in this pathway divided by the overall number of genes in this pathway. (B) Metabolic pathway analysis: The color code in (B) "Reactions per Pathway [%]" represents the number of enriched metabolic reactions in a pathway divided by the overall number of reactions in this pathway.

the pattern "toxic." The tripartite network of individual repositioned drugs (Figure 6.5.B) shows a multi-target effect of four drugs (pralatrexate, pemetrexed, methotrexate, gemcitabine). Gemcitabine affects the nucleotide interconversion pathway through both CPMK1 and TYMS essential genes. Meanwhile, pralatrexate, pemetrexed, and methotrexate affect both nucleotide interconversion and folate metabolism pathways through thymidylate synthetase (TYMS) and dihydrofolate reductase (DHFR) essential genes, respectively.

Double gene deletion produced 598 unique gene pairs across the two lung studies. Out of these 598 gene pairs, 56 gene pairs are druggable by 3411 unique drugs or drug pairs. We found 47 single drugs with two paired targets (Table S4), owing to multiple identified targets per drug. As these 3411 drug pairs could target more than one gene-pair, safety scores and essentiality scores were calculated using the average of these scores. To prioritize among the 3411 drug pairs, we filtered by keeping drug pairs with more than two essentiality scores, and more than one in either the number of gene pairs or safety scores. This reduced drug pair list has 52 drug pairs that consist of 37 individual drugs (Table S5). The top-ranked drug pairs in the number of gene pairs are (azathioprine-pemetrexed and mercaptopurine-pemetrexed) affecting five essential gene pairs, while (imexon–valaciclovir and imexon–acyclovir) are top-ranked in the essentiality score of 10. The pathway analysis of the druggable essential gene pairs (see Figure 6.5) shows that most of the single drugs with two paired, targets the extracellular transport pathway. Meanwhile, the reduced drug pairs cover more diverse pathways. These pathways include new pathways in addition to the single druggable pathways such as purine catabolism, purine synthesis, nucleotide salvage pathway, and NAD metabolism. The aforementioned azathioprine–pemetrexed drug pair targets seven metabolic pathways such as transporter pathway and purine synthesis and catabolism. Also, among the 47 predicted single drugs with two paired targets, four drugs are affecting more than one gene-pair (gemcitabine, trifluridine, mercaptopurine, tegafur–uracil).

6.3 Discussion

In the present study, we analyzed changes in transcriptomic data of lung cell lines infected with COVID-19 at various viral loads and at different time points after infection. The main focus was on the alteration of expression of metabolic genes that could be evidence of a metabolic rewiring induced by the virus. Then, *in silico* single and gene double knockouts were performed to identify potential infected cell-specific essential genes that arise from this metabolic rewiring and that could be used as potential drug targets. To extend the list of targets and identify critical pathways for the growth or survival of the virus, reactions were inactivated *in silico* and the resulting impact on the viral biomass production was estimated. In addition, we explored pathways enriched for predicted essential genes and reactions to obtain a better picture of the occurring metabolic rewiring. Furthermore, we predicted a set of 85 repositionable single drugs (45 drugs on single targets in Table S3 and 47 drugs on gene pairs in Table S4 with 7 drugs shared between the 2 drug lists), and 52 drug combinations that could be explored as

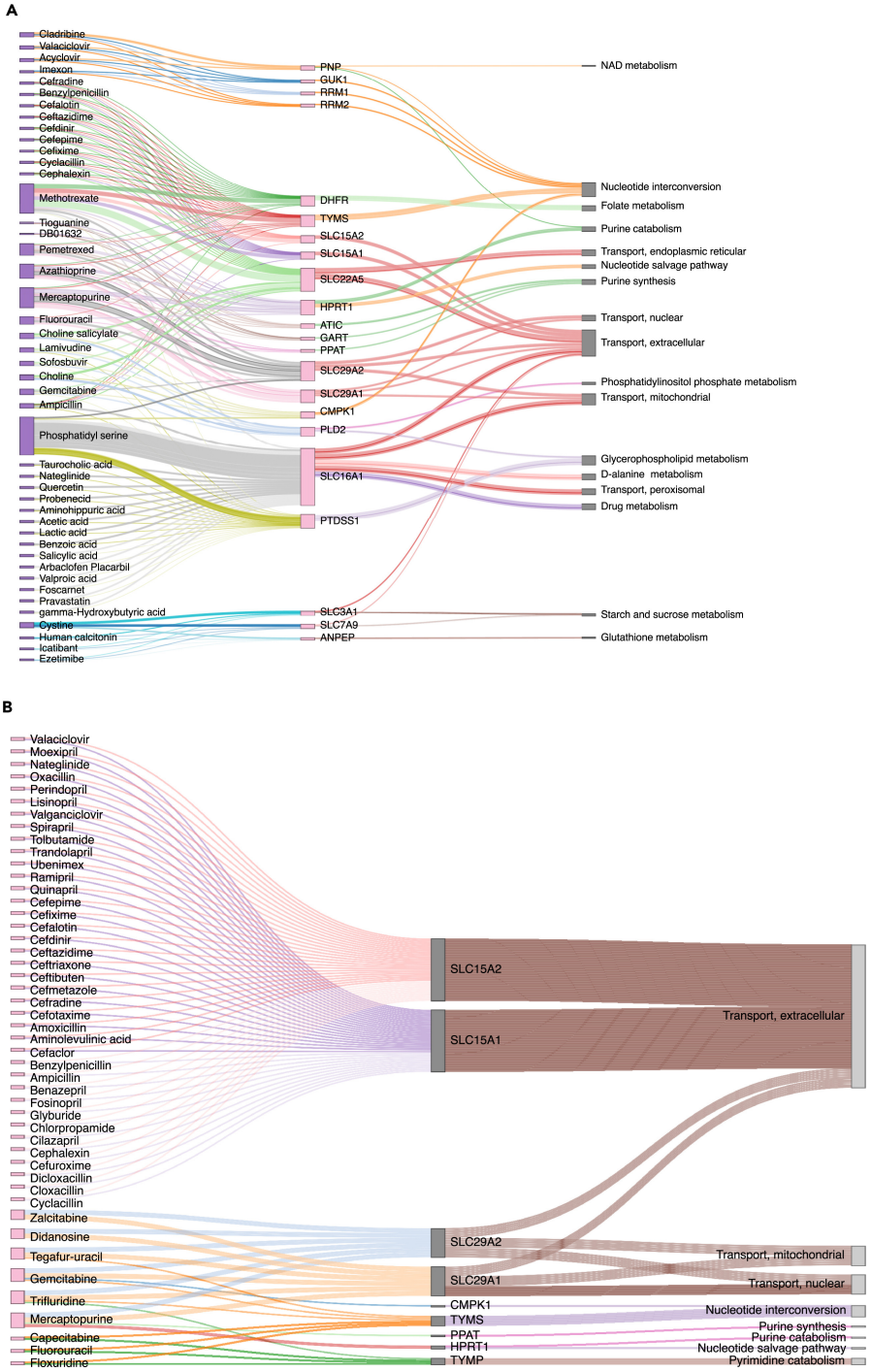

FIGURE 6.5: **Tripartite network of the drug-gene-pathway interactions of the synergistic gene pairs determined by double gene deletion.**

Determination for the individual repositioned drugs for the synergistic gene pairs, and also mapping the relationships of the genes to pathways determined by Recon3D_01 *subSystem*. (A) Tripartite network of the reduced list of double gene deletion drug pairs: Candidate gene pairs causing synergistic lethality were determined by double gene knockout (DKO) (related to STAR Methods 6.6.1.2.3). Gene pairs for which both genes are targeted by the same drug were excluded from the candidate list for drug combinations and added to the list of single drugs. Genes, and their associated drugs, that are not present in Recon3D_01 were discarded. (B) Tripartite network of single drugs targeting two genes that reduce biomass when knocked-out together: The gene pairs were determined by DKO (related to STAR Methods 6.6.1.2.3). Only targets present in Recon3D_01 were included in the analysis.

a treatment against COVID-19. Finally, we compared our results against two recent studies that cover the candidate metabolic pathways' alternation in COVID-19 infection [54], [55].

6.3.1 *COVID-19-induced dysregulated pathways may not be essential*

To unravel the metabolic rewiring induced by COVID-19 on the host lung cell after ACE2 or a mock transfection at different viral loads, we computed the metabolic differentially expressed genes (DEGs) in the severity study. Among the metabolic pathways with a different activation pattern after the transfection with the ACE2 vector, are chondroitin sulfate degradation and synthesis that have a link to oxidative stress. Chondroitin is a glycosaminoglycan (GAG) with antioxidant and neuroprotective effects against oxidative stress through the upregulation of phosphoinositide 3-kinases (PI3K)/Akt signaling and heme oxygenase-1 (HMOX1) [56]. Chondroitin sulfate degradation was downregulated after the transfection with ACE2 vector, while chondroitin synthesis was downregulated with a high viral load. This dysregulation is consistent with the hypothesis of chondroitin accumulation in the infected cells to balance the oxidative stress induced by the virus. The phosphoinositol phosphate pathway, which includes PI3K, was also downregulated after transfection with the ACE2 vector, further supporting the protective role of chondroitin in COVID-19 infection. Although this hypothesis was not tested *in vitro*, in an *in vivo* study on the Vero cell line, chondroitin sulfate showed weak inhibition of SARS-CoV-2 cell entry in comparison to other types of GAGs such as heparin and enoxaparin [57]. Finally, HMOX1 has been found to bind to SARS-CoV-2 open reading frame 3 A (ORF3a) [58]. The ineffectiveness of chondroitin sulfate as an antiviral agent in SARS-CoV-2 was expected owing to its unspecific mode of action. Reducing oxidative stress may alleviate the symptoms but may not kill the virus nor does it reduce its ability to replicate itself. The assessment of ACE2 transfection alone (see Figure S2) didn't show that shared dysregulation after infection with SARS-CoV-2. Meanwhile, ACE2 transfection increased the viral reads to 54% of the total mapped reads [59]. Also, ACE2 transfection decreases the interferons IFN-I and IFN-III through the inactivation of the kinase TBK1 [59].

6.3.2 *Pyrimidine metabolism as a candidate druggable essential pathway*

To be more effective, drug candidates have to target genes, reactions, or pathways that are key and specific to viral metabolism. Hence, *in silico* single and double gene knockouts were performed to identify genes essential to the viral biomass production but whose knockout has little or no effect on the host biomass production. Among the 23 predicted essential genes for viral biomass, two genes of the phospholipid metabolism (CRLS1 and SGMS1) showed the highest essentiality score. GUK1, which was the main essential gene identified in [44], is also among the top predicted targets and displays moderate essentiality and safety score. Also, pyrimidine biosynthesis was among the pathways with consistent flux changes in the metabolic modeling of multiple cell lines [45]. Furthermore, three essential genes (DTYMK, CMPK1, and TYMS) are part of pyrimidine metabolism (through pyrimidine deoxyribonucleotides de novo biosynthesis) that were enriched in all conditions in the severity

study, but for the last time point of the time-series study in the Calu-3 cell line. In two separate *in vivo* studies on the Vero cell line, inhibition of de novo pyrimidine biosynthesis pathway through dihydroorotate dehydrogenase (DHODH) inhibitors, showed broad-spectrum antiviral activity, stopped, or halted SARS-CoV-2 replication, respectively [60], [61]. Although DHODH inhibitor PTC299 showed a little cytotoxic effect on SARS-CoV2, they were proven to have an immunomodulatory effect on IL-6, IL-7A, IL-17F, and VEGF [60]. Alterations in the expression of genes of the pyrimidine metabolism were significantly higher in the A549, suggesting a response that could be specific to this cell line. Additionally, using pyrimidine biosynthesis inhibitors on SARS-CoV-2-infected mouse models, reduced individually viral infectivity, and reduced lung inflammation when used in combinations [62].

6.3.3 *Ferroptosis as a candidate prognostic and target pathway for COVID-19*

To further understand why a gene is essential for viral biomass production, we examined the pathways harboring the essential genes, where eight out of 13 pathways were found between the two lung studies. Pathways harboring essential genes were also enriched for DEGs. Exploring the ferroptosis-specific database FerrDb shows that three out of the 23 essential genes are related to ferroptosis. SLC7A11 and SLC3A2 are classified as suppressors; meanwhile, SLC7A5 is a marker. Also, FerrDb, classified only one of our predicted drugs, sulfasalazine, as an inducer of ferroptosis. Ferroptosis is an iron-dependent programmed cell death that can be inhibited by selenium. In a cross-sectional study, selenium level was found to be higher in tissue samples from COVID-19 survivors in comparison to non-survivors [63]. Similarly, the analysis of blood single-cell expression data found that four genes governing ferroptosis were upregulated in infected patients than recovered [64]. Also in a population retrospective analysis, the selenium concentration in the hair in the population of Chinese cities outside Hubei province was correlated with the COVID-19 cure rate in Chinese cities [65]. Even though the last retrospective study, using city population-level data instead of patient-level data, might be less reliable, these studies suggest a role of ferroptosis in the survival of patients with COVID-19.

6.3.4 *Comparison to a metabolomics study shows altered polyunsaturated fatty acids*

We further compared our enriched pathways from the DEGs and essential genes (Figure 6.2) with a recent metabolomics study [55]. In this study, serum metabolites were compared among SARS-CoV-2 positive and negative patients, also altered IL-6 levels measures as an indication of COVID-19 severity. The study found several altered pathways and dysregulation, notably of nitrogen and tryptophan metabolism associated with increased severity. Also, some metabolite levels were increased in patients with COVID-19 such as kynurenines, methionine sulfoxide, cystine, and free polyunsaturated fatty acids (PUFAs). Up-regulated fatty acid oxidation in DEGs and glycerophospholipid metabolism in essential gene pathways is consistent with the increased levels of PUFAs [55]. The increased PUFAs are biomarkers for ferroptosis, which was predicted in the condition without ACE2 vector. The recent evidence for the role of selenium in COVID-19 and the significant presence of PUFAs as a biomarker

in severe COVID-19 cases might be a further indication of the role of ferroptosis regarding COVID-19 severity. Moreover, the SARS-CoV-2 spike protein was discovered to have a binding pocket for free fatty acids [66]. This seems to allow the PUFA linoleic acid to have a synergistic effect with the antiviral remdesivir against SARS-CoV-2 *in vitro* [66]. The use of 5-aminosalicylate or sulfasalazine, a 5-aminosalicylate prodrug, has recently been shown to increase COVID-19 severity in patients with inflammatory bowel disease (IBD) in a retrospective study (n = 525) [67]. As sulfasalazine was found as a ferroptosis inducer in FerrDb [68], this could strengthen the evidence of a role of ferroptosis in COVID-19 severity. It also illustrates the need for a careful assessment of the toxicity of the predicted drugs in follow-up *in vitro* and *in vivo* studies as well as a patient or group of patient-tailored approaches.

6.3.5 *Methionine, cysteine, and pyrimidine metabolism are enriched in a multi-omics study*

To discover which lung essential pathways might be shared with other infected organs, we also compared our identified pathways with a multi-omics study on three cell types: megakaryocytes, erythroid cells, and plasmablasts [54]. In this longitudinal study of COVID-19 severity, cell-/tissue-specific metabolic models were reconstructed from single-cell/bulk RNA-seq, respectively [54]. The goal of the metabolic reconstruction in this study was to find cell-specific metabolic pathways associated with different disease progression and recovery time points [54]. The essentiality of genes and reactions in these pathways across the three cell types are unknown as single-gene or reaction deletions were not applied. Many identified metabolic pathways in this multi-omics study across megakaryocytes, erythroid cells, and plasmablasts were also shared with our essential pathways on the lung such as pyrimidine metabolism and cysteine and methionine metabolism. Also, our lung essential metabolic pathways such as inositol phosphate metabolism and sphingolipid metabolism have been identified as both erythroid cells- and plasmablasts-specific. Meanwhile, the lung-essential fatty acid oxidation and non-essential pyruvate metabolism have been identified as megakaryocytes-specific. Interestingly, a high upregulation of pyruvate kinase M in PI3K/Akt signaling was found in critical patients in megakaryocytes [54], that participate in the dysregulated chondroitin sulfate metabolism [56]. Furthermore, serum sphingosine-1-phosphate, a metabolite in the lung-essential sphingolipid metabolism, was found to significantly decrease with COVID-19 severity in a small study (n = 111) [69]. Moreover, clofazimine, an inhibitor to the acid sphingomyelinase in the sphingolipid metabolism pathway, was found to have antiviral activity in the golden Syrian hamster model against MERS & SARS-CoV-2 [70]. Taken together, the shared metabolic pathways between the different studies such as pyrimidine metabolism and methionine and cysteine metabolism across different tissues might represent core viral-specific pathways that could harbor efficient drug targets that would eliminate or slow down the virus regardless of the infected tissue.

6.3.6 *Some candidate drugs have antiviral, immunomodulatory, and angiotensin I-converting enzyme inhibitor actions*

To prioritize drug and drug combinations and as many conditions in the time-series study were lacking mock samples, we relied for the present work rather on the essentiality score of each gene identified in terms of reducing the viral proliferation rather than the predicted toxicity on control tissue models (safety score). In total, SARS-COV-2-specific essential genes and gene pairs were predicted by rFASTCORMICS-based lung models that can be targeted by 85 single repositionable drugs and 52 drug combinations. The safety of the drugs was assessed by simulation knockouts on the biomass of the counterpart mock sample. This strategy allows estimating which drugs might be potential candidates for not having too drastic side effects. Although the drug candidates are all FDA-approved drugs, some treatments are associated with severe side effects, and combining two drugs can have additional unexpected side effects. Hence, further tests would be required on other tissues and using other optimization functions as well as *in vitro* and *in vivo* validations before considering any predictions as potential drug candidates. Among the 85 predicted single drugs, five are broad-spectrum antivirals (lamivudine, methotrexate, sofosbuvir, valaciclovir, zalcitabine) [71]. Also, five drugs in the candidate drug combinations have broad-spectrum antivirals (ezetimibe, lamivudine, methotrexate, sofosbuvir, valaciclovir). In a small clinical trial (n = 62), the combination of sofosbuvir-daclatasvir decreased the COVID-19 mortality rate (6%) in comparison to ribavirin (33%) [72]. Of the predicted drugs, two drugs (acyclovir, valaciclovir) target the GUK1 gene, which shows relative essentiality and safety. Acetylcysteine, another predicted drug by our workflow, is mucolytic and antioxidant in high doses through regenerating glutathione. Acetylcysteine alone or with bromelain was able *in vitro* to fragment the recombinant spike and envelope SARS-CoV-2 proteins [73]. Moreover, gemcitabine has been shown to have antiviral activity against SARS-CoV-2 in the Vero-E6 cell line [74]. Methotrexate shows antiviral activity against SARS-CoV-2 in Vero-E and Calu-3 cell lines [75]. This antiviral activity was better than the only authorized antiviral for emergency use for COVID-19 remdesivir. Till 29 July 2021, out of the 85 single drugs, nine drugs are being tested currently in clinical trials (acetylcysteine, liothyronine, melphalan, methotrexate, moexipril, quinapril, ramipril, rosuvastatin, sofosbuvir, trandolapril) according to DrugBank COVID-19 Clinical Trial Summary [51]. Among the single drugs targeting gene pairs, nine were drugs belonging to angiotensin-converting enzyme inhibitors (ACEIs) such as ramipril, affecting the gene-pair SLC15A1-SLC15A2 through targeting the extracellular transport pathway. Interestingly, in a prospective study of COVID-19 (n = 19,486), patients taking ACEIs have a reduced risk of COVID-19, with differences according to ethnicity [76]. Meanwhile, ACEIs did not reduce the risk of receiving ICU care [76]. Furthermore, statins, lipid-lowering drugs that were enriched among the predicted drugs were debated for their efficacy in reducing COVID-19 severity at the onset of the pandemic and their usefulness for COVID-19 is still unclear [77]. Also, a retrospective study (n = 13,981) has shown an association between statins and reduced COVID-19 mortality from 9.4% in patients not taking statins to 5.2% with statins [65]. Owing to the relative number of the different statin recipients, this study couldn't rank the different statin types. But, a recent *in vitro* study of different statins showed an antiviral effect on SARS-CoV-2 [78], where rosuvastatin was ranked

second in the antiviral activity [78]. In the candidate drug combinations, immunomodulators appear such as mercaptopurine, azathioprine, pemetrexed, and methotrexate. Also, three predicted nucleoside analogs (azathioprine, mercaptopurine, gemcitabine), were among 16 nucleoside analogs and 122 drugs validated *in vitro* against Calu-3 [62].

In conclusion, unlike drug repositioning using expression reversal or drug docking that lack targets' identification or genome-scale multi-targeting, respectively, constraint-based metabolic modeling is a powerful *in silico* tool for drug repositioning with genome-scale information and producing known targets. These powerful advantages come from gene essentiality prediction. In this work, context-specific models from expression data from infected lung cell lines were built, then constrained by both viral and host biomass. *In silico* gene deletion identified 23 single essential genes and 598 essential gene pairs. Drug repositioning using approved drugs in DrugBank V5 identified 85 single drugs and 52 drug combinations, of which 47 single drugs are targeting both genes in the gene-pair. Pathway analysis of the essential genes identifies ferroptosis as a candidate biomarker pathway of COVID-19 severity. Gemcitabine was predicted to target two single essential genes in the nucleotide interconversion pathway and three gene pairs in drugs identified by both single and double gene deletion, respectively. Finally, we predicted the GUK1 gene as both relatively safe and essential against SARS-CoV2 as reported by a previous *in silico* modeling.

6.4 Limitations of study

Although this study predicts some interesting drug candidates and drug combinations, the work is limited by the modeled lung cell lines (A549, Calu-3, H1299, NHBE). Another limitation to this work is that the identified drug and drug pairs are based on targets identified by network effects on the host metabolome (as the virus is only modeled through its biomass function) rather than direct docking on the viral proteome. Thus, further *in vitro* single- and double-gene deletion studies are needed to determine the essentiality of the identified single genes and gene pairs. These could, for example, involve some selected drug and drug combinations on the different cell lines at various concentrations in order to obtain drug response curves and landscapes, respectively, to identify IC-50 and synergy scores for the drug combinations. These experiments would be more beneficial for genes with predicted essentiality across different cell lines such as (CRLS1, SGMS1, SLC27A4) which were essential in the four lung cell lines.

6.5 STAR* Methods

Detailed methods are provided in the online version of this paper and include the following:

- Key Resources Table

- Resource Availability
  - Lead contact
  - Materials availability
  - Data and code availability
- METHODS DETAILS
  - A. SARS-CoV-2 essentiality analysis in lung
  - B. Gene enrichment of the potential targets
  - C. Drug repositioning of the essential genes
  - D. Relationship with ferroptosis

Supplemental Information

Supplemental information can be found online at `https://doi.org/10.1016/j.isci.2021.103331`.

Acknowldgements

The experiments presented in this paper were carried out using the HPC facilities of the University of Luxembourg [79].

Author Contributions

A.K. carried out the experiments. M.P.P. and T.S. conceived and planned the experiment. A.K., M.P.P., and T.S. analyzed the data. All the authors wrote, read, and revised the manuscript.

Declarations of Interests

The authors declare no competing interests.

Key Resources Table

Resource Availability

Lead contact

Further information and requests for code or datasets should be directed to and will be fulfilled by the lead contact, Prof. Thomas Sauter (Thomas.Sauter@uni.lu).

Reagent or Resource	Source	Identifier
Deposited data - FPKM for the time-series study (GSE148729)	MDC-berlin	https://filetransfer.mdc-berlin.de/?u=CVXckugR&p=MACT6Xw9
Read counts of the severity study (GSE147507)	NCBI GEO	https://ftp.ncbi.nlm.nih.gov/geo/series/GSE147nnn/GSE147507/suppl/GSE147507_RawReadCounts_Human.tsv.gz
Formulation of the viral biomass function	BioModels	https://www.ebi.ac.uk/biomodels/MODEL2003020001#Files
DrugBank V5	DrugBank	https://go.drugbank.com/releases/latest
Drug Repurposing Hub mode of actions	Clue.io	https://s3.amazonaws.com/data.clue.io/repurposing/downloads/repurposing_drugs_20200324.txt
GHDDI Broad-spectrum antiviral agents	GHDDI	https://ghddiai.oss-cn-zhangjiakou.aliyuncs.com/file/Antivirus_Drug_Profile_k2.csv
Recon 2	VMH	https://www.vmh.life/#downloadview
Recon3D	VMH	https://www.vmh.life/#downloadview
Software and algorithms - rFASTCORMICS	[6]	https://github.com/sysbiolux/rFASTCORMICS
COBRA Toolbox	GitHub	https://github.com/opencobra/cobratoolbox/tree/master/src
IBM CPLEX solver		https://www.ibm.com/products/ilog-cplex-optimization-studio
RStudio		https://www.rstudio.com/
R CRAN (FactoMineR, networkD3, ggplot2 & dependencies)		https://cran.r-project.org/
Bioconductor (edgeR, DESeq2 & dependencies)		https://www.bioconductor.org/

Materials availability

This study did not generate new unique reagents.

Data and code availability

This paper analyses existing, publicly available data. The source of the data is listed in the key resources table. The models and code generated during this study are available at GitHub (https://github.com/sysbiolux/DCcov).

6.6 Methods Details

6.6.1 *SARS-CoV-2 essentiality analysis in lung*

6.6.1.1 *Differentially expressed genes analysis*

6.6.1.1.1 *Data preprocessing.* At the onset of the pandemic, two datasets were available, focusing mainly on the effects of the virus on lung tissues. These two bulk RNA seq datasets GSE147507 [59] and GSE148729 [80] of human cell lines hosting SARS-CoV-2, as well as of mock samples, were downloaded from the NCBI Gene Expression Omnibus (GEO) [81] data repository on April 23, and May 15, 2020,

respectively. The GSE147507 dataset, which focuses on the expression changes at various severity levels of Infection (severity study), contains 36 samples originating from healthy epithelial, A549, and Calu-3 cells infected by SARS-CoV-2 at three different viral loads, as well as control samples with a mock infection. As the level of plasma ACE2 is a potential predictor of COVID-19 severity [82], the comparison between conditions with different levels of ACE2 and viral load would allow identifying essential genes, and hence drug targets for different stages and severity levels of COVID-19. Using drugs associated with severe effects would not be beneficial for milder forms of COVID-19, but could be crucial for the cure of more severe forms. The A549 cell line was found to express ACE2 at a lower level than Calu-3, which doesn't allow the cell entry of SARS-CoV-2 [59]. For this reason, the A549 cell line was transfected with a vector expressing ACE2 (Table 6.1). Conditions with two replicates only or subjected to drug perturbations were not considered for the analysis. Raw counts were converted to the Reads Per Kilobase of transcript (RPKM) using an in-house Python script. For the GSE148729 dataset, which monitors how expression changes at different points after the infection (time-series study), the normalized Fragments Per Kilobase of transcript per Million (FPKM) values of Calu-3 and H1299 cell lines infected by SARS-CoV-2, as well as controls were retrieved from GEO.

6.6.1.1.2 *Differentially expressed genes analysis.* The differential gene expression analysis was only applied to the severity study, as the time-series has either missing mock samples or two samples in some conditions. First, a principal component analysis was first performed using FactoMineR [83] to identify and, if necessary, remove outliers by visual inspection. Then, genes with low expression values were filtered out using edgeR's *filterByExpr* function (Version 3.30.3). This function keeps genes based on a minimum count-per-million in at least k samples, determined by the lowest sample size between all conditions [84]. DESeq2 identifies the significant DEGs using the Wald test and adjusted for multiple testing by Benjamini and Hochberg, yielding adjusted p-values. DESeq2 (Version 1.28.1) [85] via R (Version 4.0.1) was run on the preprocessed data to identify differentially expressed genes (DEG) between the infected and the mock samples applying an adjusted p-value threshold of 0.05, and an absolute log fold change threshold of 1. To assess if the gene expression changes observed after ACE2 transfection were caused by the transfection itself, rather than the overexpression of ACE2, a DEG analysis was performed to compare two conditions (A549_2_ACE2 against A549_2), using first the mock samples only (ACE2_Mock), then only the infected samples (ACE2_Infected). DEGs were mapped to the genes of the generic model Recon3D_01 [12] via the GPR rules to retrieve differentially expressed reactions (DERs) as well as their associated pathways. For each pathway with at least three reactions, the ratio of up-and down-regulated reactions overall reactions was computed. To improve the readability of the plot, only pathways with more than 5% of DERs were depicted.

6.6.1.2 *Essentiality analysis*

6.6.1.2.1 *Condition-specific model building.* To further elucidate the metabolic alteration provoked by the virus, metabolic models for the infected samples and mock samples were built. Therefore, the VBOF from the infected alveolar macrophage model *iAB-AMØ1410_SARS-CoV-2* (BioModels: MODEL2003020001) [44] was added to both the generic reconstructions Recon2.04 [11] and Recon3D_-01 [12] using the *addReaction* function of the COBRA Toolbox v.3.0 [19]. The identifiers of metabolites included in the biomass had first to be modified to match the ones of the generic reconstruction. Then, FASTCC [14] was run to remove blocked reactions. For each condition, the RPKM values and the modified consistent generic reconstruction were used as input for the rFASTCORMICS [6] to get condition-specific models. COBRA Toolbox v.3.0 and FASTCC were used via MATLAB (R2019a).

6.6.1.2.2 *Single gene knockout.* The metabolic models were then used to identify viral-specific vulnerabilities, using a single gene deletion approach on the mock and infected models. For the infected model, to ensure that both host and viral biomass's objective functions can carry simultaneously a flux in the infected models, the objective coefficients were set to 100 and 1, respectively, and the upper bound of the host biomass was fixed to 10% of its maximal flux. This setting constrains the model to guarantee cell homeostasis and protein turnover in the host model while diverting all non-essential resources for viral reproduction.

$$\text{model.c(viral biomass)} = 1$$
$$\text{model.c(host biomass)} = 100$$
$$\text{model.ub(host biomass)} = 10\ \%\ \text{of max flux determined by FBA}$$

In silico single-gene knockouts (SKO) were performed on the infected models using a corrected version of the *singleGeneDeletion* function of the COBRA Toolbox v.3.0 [19] to assess the impact of the knockout of each gene on the viral biomasses. The 0.2 threshold was used as a cutoff for gene growth rate Ratio (grRatio) to identify essential genes.

6.6.1.2.3 *Double gene knockout.* To identify potential targets for drug combinations, double gene knock-outs (DKO) for all gene-pair combinations were simulated using the *doubleGeneDeletion* function on the infected models. From the analysis, we obtained two lists of synergistic gene-pairs: non-essential gene-pairs that allow reducing the growth rate below the specified thresholds when simultaneously knocked out and pairs of essential and non-essential genes that induced a stronger reduction of the growth than the knockout of the essential gene alone. Both non-essential and essential gene-pairs were concatenated as DKO outputs for further drug repositioning.

6.6.1.2.4 *Essentiality and safety scoring.* To test the knockout impact of SARS-CoV-2-infected host-specific predicted essential genes and gene-pairs on the healthy counterpart tissue, SKO, and DKO of these genes were performed on the healthy models. Genes or gene-pairs that cause a reduction of biomass only in the infected models are considered safe, whereas those that cause also a reduction of biomass in the healthy models are regarded as potentially toxic. The essentiality score of an essential gene is the sum of infected models that show this gene as essential. The safety score of an essential gene is the sum of healthy models that show this gene as safe. A healthy model, SKO and DKO of a gene was applied only if the gene is determined as essential in its respective infected model. A scatterplot of essentiality scores against safety scores was plotted (see Figure 6.3).

6.6.2 *Gene enrichment of the potential targets*

The identifiers of the essential genes and synergetic genes were translated into HGNC gene symbols using GSEApy (Version 0.9.17, `https://github.com/zqfang/GSEApy/`) Python package (3.7.4) and then uploaded to Enrichr API [50] to identify enrichment of these genes in KEGG pathways (KEGG2019 human [86] database with 0.05 p-value cutoff). Fisher exact test (default hypothesis test) was performed for calculating the p-value based on the assumption of the binomial distribution of the input gene set. All enrichment results based on only one gene were discarded. Then, the enrichment percentage was calculated (related to STAR Methods 6.6.1.1.2). Metabolic pathway analysis was also applied using the Recon3D_01 *subSystem* as background instead of KEGG pathways on the essential genes (related to STAR Methods 6.6.1.1.2) without further filtering of the pathways. Comparison of pathways of Calu-3 and NHBE cell lines were excluded from the analysis of the effect of viral load and ACE2 vector in the severity study because these cell lines didn't have ACE2 vector conditions.

6.6.3 *Drug repositioning of the essential genes*

To identify drugs targeting the predicted viral-specific essential genes, drug-target interactions were downloaded from DrugBank V5 [51] on April 23, 2020. Drugs that were withdrawn, nutraceutical, or experimental were discarded from the analysis. Drugs that are described as having any effect on the potential targets were selected as candidate drugs (Table S3) and drug combinations (Tables S4 and S5). To determine which drugs, have a multi-target effect, tripartite networks of the drug-gene-pathway interactions were constructed for the single and double knockout drugs using Recon3D_01 *subSystems* as pathways (Figures 6.3.B and 6.5). The tripartite networks were constructed using the *sankeyNetwork* function in networkD3 [87] (version 0.4) package in R.

6.6.4 *Relationship with ferroptosis*

As SKO targets were enriched for many pathways related to ferroptosis, the potential targets and SKO drugs were searched in a curated database (FerrDb) [88] for ferroptosis genes and related drugs. FerrDb classifies genes into driver, suppressor, and marker, while it classifies drugs into inducer and inhibitor. These classes were also used to identify the role of the potential targets and SKO drugs in the ferroptosis pathway.

6.7 Summary and Outlook

In 2023, two years after the publication of this work, many predicted drugs showed improved survival in COVID-19 clinical trials (see Table 1.3.8). Notably, drugs targeting cysteine synthesis but not glycine uptake improved COVID-19 survival. Similarly, predicted essential genes targeting once carbon cycle by folate showed higher dependency than recently approved drugs in a genome-scale CRISPR screen (see Figure 1.6). As new COVID-19 variants keep emerging, as well as current understanding of the multi-organ failure caused by COVID-19, future GEMs could benefit from the whole-body model [89] with organ -instead of cell line- expression data. All in all, using the available cell line datasets in 2020 and no approved drugs, metabolic modeling was able to repurpose approved drugs, of which five improved COVID-19 survival or severity in randomized control trials.

References

[1] M. A. Blätke and A. Bräutigam, "Evolution of C4 photosynthesis predicted by constraint-based modelling," *eLife*, vol. 8, Dec. 2019, Publisher: eLife Sciences Publications Ltd. DOI: 10.7554/ELIFE.49305.

[2] G. Marinos, C. Kaleta, and S. Waschina, "Defining the nutritional input for genome-scale metabolic models: A roadmap," *PLoS ONE*, vol. 15, no. 8, Aug. 2020, Publisher: Public Library of Science. DOI: 10.1371/JOURNAL.PONE.0236890.

[3] N. Swainston, K. Smallbone, H. Hefzi, *et al.*, "Recon 2.2: From reconstruction to model of human metabolism," *Metabolomics*, vol. 12, no. 7, Jul. 2016, Publisher: Springer New York LLC. DOI: 10.1007/S11306-016-1051-4.

[4] R. Agren, S. Bordel, A. Mardinoglu, N. Pornputtapong, I. Nookaew, and J. Nielsen, "Reconstruction of genome-scale active metabolic networks for 69 human cell types and 16 cancer types using INIT," *PLoS Computational Biology*, vol. 8, no. 5, 2012, Publisher: Public Library of Science. DOI: 10.1371/JOURNAL.PCBI.1002518.

[5] I. Larsson, M. Uhlén, C. Zhang, and A. Mardinoglu, "Genome-Scale Metabolic Modeling of Glioblastoma Reveals Promising Targets for Drug Development," *Frontiers in Genetics*, vol. 11, Apr. 2020, Publisher: Frontiers Media S.A. DOI: 10.3389/FGENE.2020.00381.

[6] M. P. Pacheco, T. Bintener, D. Ternes, *et al.*, "Identifying and targeting cancer-specific metabolism with network-based drug target prediction," *EBioMedicine*, vol. 43, pp. 98–106, May 2019, Publisher: Elsevier B.V. DOI: 10.1016/J.EBIOM.2019.04.046.

[7] K. Yizhak, B. Chaneton, E. Gottlieb, and E. Ruppin, "Modeling cancer metabolism on a genome scale," *Molecular Systems Biology*, vol. 11, no. 6, Jun. 2015, Publisher: EMBO. DOI: 10.15252/MSB.20145307.

[8] Y. W. Choon, M. S. Mohamad, S. Deris, *et al.*, "Differential bees flux balance analysis with OptKnock for in silico microbial strains optimization," *PLoS ONE*, vol. 9, no. 7, Jul. 2014, Publisher: Public Library of Science. DOI: 10.1371/JOURNAL.PONE.0102744.

[9] J. L. Reed, T. D. Vo, C. H. Schilling, and B. O. Palsson, "An expanded genome-scale model of Escherichia coli K-12 (iJR904 GSM/GPR)," *Genome Biology*, vol. 4, no. 9, R54, 2003.

[10] J. Schellenberger, R. Que, R. M. T. Fleming, *et al.*, "Quantitative prediction of cellular metabolism with constraint-based models: The COBRA Toolbox v2.0," *Nature Protocols*, vol. 6, no. 9, pp. 1290–1307, Sep. 2011. DOI: 10.1038/NPROT.2011.308.

[11] I. Thiele, N. Swainston, R. M. T. Fleming, *et al.*, "A community-driven global reconstruction of human metabolism," *Nature Biotechnology*, vol. 31, no. 5, pp. 419–425, May 2013. DOI: 10.1038/NBT.2488.

[12] E. Brunk, S. Sahoo, D. C. Zielinski, *et al.*, "Recon3D enables a three-dimensional view of gene variation in human metabolism," *Nature Biotechnology*, vol. 36, no. 3, pp. 272–281, Mar. 2018, Publisher: Nature Publishing Group. DOI: 10.1038/NBT.4072.

[13] J. L. Robinson, P. Kocabaş, H. Wang, *et al.*, "An atlas of human metabolism," *Science Signaling*, vol. 13, no. 624, Mar. 2020, Publisher: American Association for the Advancement of Science. DOI: 10.1126/SCISIGNAL.AAZ1482.

[14] N. Vlassis, M. P. Pacheco, and T. Sauter, "Fast Reconstruction of Compact Context-Specific Metabolic Network Models," *PLoS Computational Biology*, vol. 10, no. 1, 2014, Publisher: Public Library of Science. DOI: 10.1371/JOURNAL.PCBI.1003424.

[15] S. R. Estévez, "Context-specific metabolic predictions : Computational methods and applications," *Max-Planck-Institut für Molekulare Pflanzenphysiologie und Universität Potsdam*, vol. PhD, p. 174, 2017.

[16] J. L. Reed and B. Palsson, "Thirteen years of building constraint-based in silico models of Escherichia coli," *Journal of Bacteriology*, vol. 185, no. 9, pp. 2692–2699, May 2003. DOI: 10.1128/JB.185.9.2692-2699.2003.

[17] C. Gille, C. Bölling, A. Hoppe, *et al.*, "HepatoNet1: A comprehensive metabolic reconstruction of the human hepatocyte for the analysis of liver physiology," *Molecular Systems Biology*, vol. 6, 2010. DOI: 10.1038/MSB.2010.62.

[18] R. Saha, P. F. Suthers, and C. D. Maranas, "Zea mays irs1563: A comprehensive genome-scale metabolic reconstruction of maize metabolism," *PLoS ONE*, vol. 6, no. 7, 2011. DOI: 10.1371/JOURNAL.PONE.0021784.

[19] L. Heirendt, S. Arreckx, T. Pfau, *et al.*, "Creation and analysis of biochemical constraint-based models using the COBRA Toolbox v.3.0," *Nature Protocols*, vol. 14, no. 3, pp. 639–702, Mar. 2019, Publisher: Nature Publishing Group. DOI: 10.1038/S41596-018-0098-2.

[20] J. D. Orth, I. Thiele, and B. O. Palsson, "What is flux balance analysis?" *Nature Biotechnology*, vol. 28, no. 3, pp. 245–248, Mar. 2010. DOI: 10.1038/NBT.1614.

[21] D. Perumal, A. Samal, K. R. Sakharkar, and M. K. Sakharkar, "Targeting multiple targets in Pseudomonas aeruginosa PAO1 using flux balance analysis of a reconstructed genome-scale metabolic network," *Journal of Drug Targeting*, vol. 19, no. 1, pp. 1–13, Jan. 2011. DOI: 10.3109/10611861003649753.

[22] T. Adhanom, *WHO Director-General's opening remarks at the media briefing on COVID-19*, Publication Title: World Health Organization, 2020.

[23] C. Huang, Y. Wang, X. Li, *et al.*, "Clinical features of patients infected with 2019 novel coronavirus in Wuhan, China," *The Lancet*, vol. 395, no. 10223, pp. 497–506, Feb. 2020, Publisher: Lancet Publishing Group. DOI: 10.1016/S0140-6736(20)30183-5.

[24] L. Morawska and J. Cao, "Airborne transmission of SARS-CoV-2: The world should face the reality," *Environment International*, vol. 139, Jun. 2020, Publisher: Elsevier Ltd. DOI: 10.1016/j.envint.2020.105730.

[25] A. Kronbichler, D. Kresse, S. Yoon, K. H. Lee, M. Effenberger, and J. I. Shin, "Asymptomatic patients as a source of COVID-19 infections: A systematic review and meta-analysis," *International Journal of Infectious Diseases*, vol. 98, pp. 180–186, Sep. 2020, Publisher: Elsevier B.V. DOI: 10.1016/j.ijid.2020.06.052.

[26] K. G. Andersen, A. Rambaut, W. I. Lipkin, E. C. Holmes, and R. F. Garry, "The proximal origin of SARS-CoV-2," *Nature Medicine*, vol. 26, no. 4, pp. 450–452, Apr. 2020, Publisher: Nature Research. DOI: 10.1038/S41591-020-0820-9.

[27] M. A. Sparks, S. D. Crowley, S. B. Gurley, M. Mirotsou, and T. M. Coffman, "Classical renin-angiotensin system in kidney physiology," *Comprehensive Physiology*, vol. 4, no. 3, pp. 1201–1228, 2014. DOI: 10.1002/CPHY.C130040.

[28] M. C. Zimmerman, E. Lazartigues, R. V. Sharma, and R. L. Davisson, "Hypertension caused by angiotensin II infusion involves increased superoxide production in the central nervous system," *Circulation Research*, vol. 95, no. 2, pp. 210–216, Jul. 2004. DOI: 10.1161/01.RES.0000135483.12297.E4.

[29] M. Fung and J. M. Babik, "COVID-19 in Immunocompromised Hosts: What We Know so Far," *Clinical Infectious Diseases*, vol. 72, no. 2, pp. 340–350, Jan. 2021, Publisher: Oxford University Press. DOI: 10.1093/CID/CIAA863.

[30] J. S. Hirsch, J. H. Ng, D. W. Ross, *et al.*, "Acute kidney injury in patients hospitalized with COVID-19," *Kidney International*, vol. 98, no. 1, pp. 209–218, Jul. 2020, Publisher: Elsevier B.V. DOI: 10.1016/j.kint.2020.05.006.

[31] C. M. Petrilli, S. A. Jones, J. Yang, *et al.*, "Factors associated with hospital admission and critical illness among 5279 people with coronavirus disease 2019 in new york city: Prospective cohort study," *bmj*, vol. 369, 2020.

[32] G. P. Fadini, M. L. Morieri, E. Longato, and A. Avogaro, "Prevalence and impact of diabetes among people infected with SARS-CoV-2," *Journal of Endocrinological Investigation*, vol. 43, no. 6, pp. 867–869, Jun. 2020, Publisher: Springer. DOI: 10.1007/S40618-020-01236-2.

[33] J. Tschopp, A. G. L'Huillier, M. Mombelli, *et al.*, "First experience of SARS-CoV-2 infections in solid organ transplant recipients in the Swiss Transplant Cohort Study," *American Journal of Transplantation*, vol. 20, no. 10, pp. 2876–2882, Oct. 2020, Publisher: Blackwell Publishing Ltd. DOI: 10.1111/AJT.16062.

[34] J. Yang, Y. Zheng, X. Gou, *et al.*, "Prevalence of comorbidities and its effects in coronavirus disease 2019 patients: A systematic review and meta-analysis," *International Journal of Infectious Diseases*, vol. 94, pp. 91–95, May 2020, Publisher: Elsevier B.V. DOI: 10.1016/J.IJID.2020.03.017.

[35] J. A. Panepintoa, A. Brandow, L. Mucalo, *et al.*, "Coronavirus Disease among Persons with Sickle Cell Disease, United States, March 20-May 21, 2020," *Emerging Infectious Diseases*, vol. 26, no. 10, pp. 2473–2476, Oct. 2020, Publisher: Centers for Disease Control and Prevention (CDC). DOI: 10.3201/EID2610.202792.

[36] X. Li and X. Ma, "Acute respiratory failure in COVID-19: Is it "typical" ARDS?" *Critical Care*, vol. 24, no. 1, May 2020, Publisher: BioMed Central Ltd. DOI: 10.1186/S13054-020-02911-9.

[37] G. McGuinness, C. Zhan, N. Rosenberg, *et al.*, "Increased incidence of barotrauma in patients with COVID-19 on invasive mechanical ventilation," *Radiology*, vol. 297, no. 2, E252–E262, Nov. 2020, Publisher: Radiological Society of North America Inc. DOI: 10.1148/RADIOL.2020202352.

[38] T. Wu, Z. Zuo, S. Kang, *et al.*, "Multi-organ dysfunction in patients with COVID-19: A systematic review and meta-analysis," *Aging and Disease*, vol. 11, no. 4, pp. 874–894, 2020, Publisher: International Society on Aging and Disease. DOI: 10.14336/AD.2020.0520.

[39] F. Rubino, S. A. Amiel, P. Zimmet, *et al.*, "New-Onset Diabetes in Covid-19," *New England Journal of Medicine*, vol. 383, no. 8, pp. 789–790, Aug. 2020, Publisher: Massachusetts Medical Society. DOI: 10.1056/NEJMC2018688.

[40] S. J. Halpin, C. McIvor, G. Whyatt, *et al.*, "Postdischarge symptoms and rehabilitation needs in survivors of COVID-19 infection: A cross-sectional evaluation," *Journal of Medical Virology*, vol. 93, no. 2, pp. 1013–1022, Feb. 2021, Publisher: John Wiley and Sons Inc. DOI: 10.1002/JMV.26368.

[41] V. O. Puntmann, M. L. Carerj, I. Wieters, *et al.*, "Outcomes of Cardiovascular Magnetic Resonance Imaging in Patients Recently Recovered from Coronavirus Disease 2019 (COVID-19)," *JAMA Cardiology*, vol. 5, no. 11, pp. 1265–1273, Nov. 2020, Publisher: American Medical Association. DOI: 10.1001/JAMACARDIO.2020.3557.

[42] A. Bordbar, N. E. Lewis, J. Schellenberger, B. Palsson, and N. Jamshidi, "Insight into human alveolar macrophage and M. tuberculosis interactions via metabolic reconstructions," *Molecular Systems Biology*, vol. 6, 2010. DOI: 10.1038/MSB.2010.68.

[43] S. Aller, A. Scott, M. Sarkar-Tyson, and O. S. Soyer, "Integrated human-virus metabolic stoichiometric modelling predicts host-based antiviral targets against Chikungunya, Dengue and Zika viruses," *Journal of the Royal Society Interface*, vol. 15, no. 146, Sep. 2018, Publisher: Royal Society Publishing. DOI: 10.1098/RSIF.2018.0125.

[44] A. Renz, L. Widerspick, and A. Dräger, "Fba reveals guanylate kinase as a potential target for antiviral therapies against sars-cov-2," *Bioinformatics*, vol. 36, no. Supplement_2, pp. i813–i821, 2020.

[45] K. Cheng, L. Riva, S. Sinha, *et al.*, "Genome-scale metabolic modeling reveals SARS-CoV-2-induced host metabolic reprogramming and identifies metabolic antiviral targets," *bioRxiv*, 2021. DOI: 10.1101/2021.01.27.428543.

[46] M. Ostaszewski, A. Mazein, M. E. Gillespie, *et al.*, "COVID-19 Disease Map, building a computational repository of SARS-CoV-2 virus-host interaction mechanisms," *Scientific Data*, vol. 7, no. 1, Dec. 2020, Publisher: Nature Research. DOI: 10.1038/S41597-020-0477-8.

[47] D. M. Gysi, Í. D. Valle, M. Zitnik, *et al.*, "Network medicine framework for identifying drug-repurposing opportunities for COVID-19," *Proceedings of the National Academy of Sciences of the United States of America*, vol. 118, no. 19, May 2021, Publisher: National Academy of Sciences. DOI: 10.1073/PNAS.2025581118.

[48] A. Renz, L. Widerspick, and A. Dräger, "Genome-scale metabolic model of infection with SARS-CoV-2 mutants confirms guanylate kinase as robust potential antiviral target," *Genes*, vol. 12, no. 6, Jun. 2021, Publisher: MDPI. DOI: 10.3390/GENES12060796.

[49] M. P. Pacheco, E. John, T. Kaoma, *et al.*, "Integrated metabolic modelling reveals cell-type specific epigenetic control points of the macrophage metabolic network," *BMC Genomics*, vol. 16, no. 1, Oct. 2015, Publisher: BioMed Central Ltd. DOI: 10.1186/S12864-015-1984-4.

[50] M. V. Kuleshov, M. R. Jones, A. D. Rouillard, *et al.*, "Enrichr: A comprehensive gene set enrichment analysis web server 2016 update," *Nucleic Acids Research*, vol. 44, no. 1, W90–W97, Jul. 2016, Publisher: Oxford University Press. DOI: 10.1093/NAR/GKW377.

[51] D. S. Wishart, Y. D. Feunang, A. C. Guo, *et al.*, "DrugBank 5.0: A major update to the DrugBank database for 2018," *Nucleic Acids Research*, vol. 46, no. D1, pp. D1074–D1082, Jan. 2018, Publisher: Oxford University Press. DOI: 10.1093/NAR/GKX1037.

[52] S. M. Corsello, J. A. Bittker, Z. Liu, *et al.*, "The Drug Repurposing Hub: A next-generation drug library and information resource," *Nature Medicine*, vol. 23, no. 4, pp. 405–408, Apr. 2017, Publisher: Nature Publishing Group. DOI: 10.1038/NM.4306.

[53] P. Mozzicato, "MedDRA: An overview of the medical dictionary for regulatory activities," *Pharmaceutical Medicine*, vol. 23, no. 2, pp. 65–75, 2009, Publisher: Springer International Publishing. DOI: 10.1007/BF03256752.

[54] J. P. Bernardes, N. Mishra, F. Tran, *et al.*, "Longitudinal multi-omics analysis identifies responses of megakaryocytes, erythroid cells and plasmablasts as hallmarks of severe covid-19 trajectories," *medRxiv*, pp. 2020–09, 2020.

[55] T. Thomas, D. Stefanoni, J. A. Reisz, *et al.*, "COVID-19 infection alters kynurenine and fatty acid metabolism, correlating with IL-6 levels and renal status," *JCI Insight*, vol. 5, no. 14, Jun. 2020, Publisher: American Society for Clinical Investigation. DOI: 10.1172/JCI.INSIGHT.140327.

[56] N. Cañas, T. Valero, M. Villarroya, *et al.*, "Chondroitin sulfate protects SH-SY5Y cells from oxidative stress by inducing heme oxygenase-1 via phosphatidylinositol 3-kinase/Akt," *Journal of Pharmacology and Experimental Therapeutics*, vol. 323, no. 3, pp. 946–953, 2007, Publisher: American Society for Pharmacology and Experimental Therapy. DOI: 10.1124/JPET.107.123505.

[57] R. Tandon, J. S. Sharp, F. Zhang, *et al.*, "Effective inhibition of sars-cov-2 entry by heparin and enoxaparin derivatives," *Journal of Virology*, vol. 95, no. 3, e01987–20, 2021.

[58] D. E. Gordon, G. M. Jang, M. Bouhaddou, *et al.*, "A SARS-CoV-2 protein interaction map reveals targets for drug repurposing," *Nature*, vol. 583, no. 7816, pp. 459–468, Jul. 2020, Publisher: Nature Research. DOI: 10.1038/S41586-020-2286-9.

[59] D. Blanco-Melo, B. E. Nilsson-Payant, W. C. Liu, *et al.*, "Imbalanced Host Response to SARS-CoV-2 Drives Development of COVID-19," *Cell*, vol. 181, no. 5, 1036–1045.e9, May 2020, Publisher: Cell Press. DOI: 10.1016/J.CELL.2020.04.026.

[60] J. Luban, R. A. Sattler, E. Mühlberger, *et al.*, "The dhodh inhibitor ptc299 arrests sars-cov-2 replication and suppresses induction of inflammatory cytokines," *Virus research*, vol. 292, p. 198 246, 2021.

[61] R. Xiong, L. Zhang, S. Li, *et al.*, "Novel and potent inhibitors targeting DHODH are broad-spectrum antivirals against RNA viruses including newly-emerged coronavirus SARS-CoV-2," *Protein and Cell*, vol. 11, no. 10, pp. 723–739, Oct. 2020, Publisher: Higher Education Press Limited Company. DOI: 10.1007/S13238-020-00768-W.

[62] D. C. Schultz, R. M. Johnson, K. Ayyanathan, *et al.*, "Pyrimidine biosynthesis inhibitors synergize with nucleoside analogs to block SARS-CoV-2 infection.," *bioRxiv : the preprint server for biology*, Jun. 2021. DOI: 10.1101/2021.06.24.449811.

[63] A. Moghaddam, R. A. Heller, Q. Sun, *et al.*, "Selenium deficiency is associated with mortality risk from COVID-19," *Nutrients*, vol. 12, no. 7, pp. 1–13, Jul. 2020, Publisher: MDPI AG. DOI: 10.3390/NU12072098.

[64] L. Huang, Y. Shi, B. Gong, *et al.*, "Dynamic blood single-cell immune responses in patients with COVID-19," *Signal Transduction and Targeted Therapy*, vol. 6, no. 1, Dec. 2021, Publisher: Springer Nature. DOI: 10.1038/S41392-021-00526-2.

[65] J. Zhang, E. W. Taylor, K. Bennett, R. Saad, and M. P. Rayman, "Association between regional selenium status and reported outcome of COVID-19 cases in China," *American Journal of Clinical Nutrition*, vol. 111, no. 6, pp. 1297–1299, Jun. 2020, Publisher: Oxford University Press. DOI: 10.1093/AJCN/NQAA095.

[66] C. Toelzer, K. Gupta, S. K. N. Yadav, *et al.*, "Free fatty acid binding pocket in the locked structure of SARS-CoV-2 spike protein," *Science*, vol. 370, no. 6517, pp. 725–730, Nov. 2020, Publisher: American Association for the Advancement of Science. DOI: 10.1126/SCIENCE.ABD3255.

[67] E. J. Brenner, R. C. Ungaro, R. B. Gearry, *et al.*, "Corticosteroids, But Not TNF Antagonists, Are Associated With Adverse COVID-19 Outcomes in Patients With Inflammatory Bowel Diseases: Results From an International Registry," *Gastroenterology*, vol. 159, no. 2, 481–491.e3, Aug. 2020, Publisher: W.B. Saunders. DOI: 10.1053/j.gastro.2020.05.032.

[68] T. Sehm, Z. Fan, A. Ghoochani, *et al.*, "Sulfasalazine impacts on ferroptotic cell death and alleviates the tumor microenvironment and glioma-induced brain edema," *Oncotarget*, vol. 7, no. 24, pp. 36 021–36 033, 2016, Publisher: Impact Journals LLC. DOI: 10.18632/ONCOTARGET.8651.

[69] G. Marfia, S. Navone, L. Guarnaccia, *et al.*, "Serum Sphingosine-1-Phosphate as Novel Prognostic and Predictive Biomarker for COVID-19 Severity and Morbidity and Its Implications in Clinical Management," *SSRN Electronic Journal*, Aug. 2020, Publisher: Elsevier BV. DOI: 10.2139/SSRN.3668364.

[70] S. Yuan, X. Yin, X. Meng, *et al.*, "Clofazimine broadly inhibits coronaviruses including SARS-CoV-2," *Nature*, vol. 593, no. 7859, pp. 418–423, May 2021, Publisher: Nature Research. DOI: 10.1038/S41586-021-03431-4.

[71] *Coronavirus data download - targeting covid-19 portal, 2020.* DOI: https://ghddi-ailab.github.io/Targeting2019-nCoV/CoV_Experiment_Data/#broad-spectrum-antiviral-agents.

[72] G. Eslami, S. Mousaviasl, E. Radmanesh, *et al.*, "The impact of sofosbuvir/daclatasvir or ribavirin in patients with severe COVID-19," *Journal of Antimicrobial Chemotherapy*, vol. 75, no. 11, pp. 3366–3372, Nov. 2020, Publisher: Oxford University Press. DOI: 10.1093/JAC/DKAA331.

[73] J. Akhter, G. Queromes, K. Pillai, *et al.*, "In vitro study of bromac on sars-cov-2 spike and envelope proteins shows synergy and disintegration at modest concentrations," 2020.

[74] Y. N. Zhang, Q. Y. Zhang, X. D. Li, *et al.*, "Gemcitabine, lycorine and oxysophoridine inhibit novel coronavirus (SARS-CoV-2) in cell culture," *Emerging Microbes and Infections*, vol. 9, no. 1, pp. 1170–1173, Jan. 2020, Publisher: Taylor and Francis Ltd. DOI: 10.1080/22221751.2020.1772676.

[75] K. M. Stegmann, A. Dickmanns, S. Gerber, *et al.*, "The folate antagonist methotrexate diminishes replication of the coronavirus sars-cov-2 and enhances the antiviral efficacy of remdesivir in cell culture models," *Virus research*, vol. 302, p. 198 469, 2021.

[76] J. Hippisley-Cox, D. Young, C. Coupland, *et al.*, "Risk of severe COVID-19 disease with ACE inhibitors and angiotensin receptor blockers: Cohort study including 8.3 million people," *Heart*, vol. 106, no. 19, pp. 1503–1511, Oct. 2020, Publisher: BMJ Publishing Group. DOI: 10.1136/HEARTJNL-2020-317393.

[77] R. Subir, M. J. J, and G. K. K, "Pros and cons for use of statins in people with coronavirus disease-19 (COVID-19)," *Diabetes and Metabolic Syndrome: Clinical Research and Reviews*, vol. 14, no. 5, pp. 1225–1229, Sep. 2020, Publisher: Elsevier Ltd. DOI: 10.1016/J.DSX.2020.07.011.

[78] R. Moeller, F. J. Zapatero-Belinchón, L. Lasswitz, *et al.*, "Effect of statins on sars-cov-2 infection," 2020.

[79] S. Varrette, P. Bouvry, H. Cartiaux, and F. Georgatos, "Management of an academic HPC cluster: The UL experience," *Proceedings of the 2014 International Conference on High Performance Computing and Simulation, HPCS 2014*, pp. 959–967, Sep. 2014, ISBN: 9781479953127 Publisher: Institute of Electrical and Electronics Engineers Inc. DOI: 10.1109/HPCSIM.2014.6903792.

[80] E. Wyler, K. Mösbauer, V. Franke, *et al.*, "Transcriptomic profiling of sars-cov-2 infected human cell lines identifies hsp90 as target for covid-19 therapy," *IScience*, vol. 24, no. 3, p. 102 151, 2021.

[81] E. Clough and T. Barrett, "The Gene Expression Omnibus database," *Methods in Molecular Biology*, vol. 1418, pp. 93–110, 2016, Publisher: Humana Press Inc. DOI: 10.1007/978-1-4939-3578-9_5.

[82] T. W. Kragstrup, H. S. Singh, I. Grundberg, *et al.*, "Plasma ACE2 predicts outcome of COVID-19 in hospitalized patients," *PLoS ONE*, vol. 16, no. 6 June 2021, Jun. 2021, Publisher: Public Library of Science. DOI: 10.1371/JOURNAL.PONE.0252799.

[83] S. Lê, J. Josse, and F. Husson, "FactoMineR: An R package for multivariate analysis," *Journal of Statistical Software*, vol. 25, no. 1, pp. 1–18, 2008, Publisher: American Statistical Association. DOI: 10.18637/JSS.V025.I01.

[84] M. D. Robinson, D. J. McCarthy, and G. K. Smyth, "edgeR: A Bioconductor package for differential expression analysis of digital gene expression data," *Bioinformatics*, vol. 26, no. 1, pp. 139–140, Nov. 2009, Publisher: Oxford University Press. DOI: 10.1093/BIOINFORMATICS/BTP616.

[85] M. I. Love, W. Huber, and S. Anders, "Moderated estimation of fold change and dispersion for RNA-seq data with DESeq2," *Genome biology*, vol. 15, no. 12, pp. 1–21, 2014, Publisher: BioMed Central.

[86] M. Kanehisa and S. Goto, "KEGG: Kyoto Encyclopedia of Genes and Genomes," *Nucleic Acids Research*, vol. 28, no. 1, pp. 27–30, Jan. 2000, Publisher: Oxford University Press. DOI: 10.1093/NAR/28.1.27.

[87] J. J. Allaire, C. Gandrud, K. Russell, and C. J. Yetman, "networkD3: D3 JavaScript Network Graphs from R," *R package*, 2017.

[88] N. Zhou and J. Bao, "FerrDb: A manually curated resource for regulators and markers of ferroptosis and ferroptosis-disease associations," *Database*, vol. 2020, 2020, Publisher: Oxford University Press. DOI: 10.1093/DATABASE/BAAA021.

[89] I. Thiele, S. Sahoo, A. Heinken, *et al.*, "Personalized whole-body models integrate metabolism, physiology, and the gut microbiome," *Molecular Systems Biology*, vol. 16, no. 5, May 2020, Publisher: EMBO. DOI: 10.15252/MSB.20198982.

Chapter 7

Supplementary File 1 of Chapter 3

Supplementary File 1: Metabolic models predict fotemustine and the combination of eflornithine/rifamycin and adapalene/ cannabidiol for the treatment of gliomas

Ali Kishk[1], Maria Pires Pacheco[1], Tony Heurtaux[1,2], and Thomas Sauter[1,*]

[1] Department of Life Sciences and Medicine, University of Luxembourg, L-4367 Belvaux, Luxembourg

[2] Luxembourg Center of Neuropathology, L-3555 Dudelange, Luxembourg

* Correspondence: Thomas.Sauter@uni.lu

7.1 Supplementary Methods

To repurpose FDA-approved drugs for the glioma subtypes, building high-quality semi-curated GEMs is crucial. Subtype intra-homogeneity and separability between subtype samples were critical factors assessed before the subtype model building.

7.1.1 Sample stratification based on WHO 2021 glioma subtypes

The 2021 World Health Organization (WHO) classification of the central nervous system (CNS) tumors [1] defined two key molecular markers for glioma subtype classification: IDH mutation status, 1p.19q codeletion. Two RNA-Seq datasets in The Cancer Genome Atlas (TCGA) were selected for model building: TCGA-GBM for glioblastoma (GBM) and TCGA-LGG for lower-grade glioma (LGG) [2]. The metadata for both datasets was downloaded using the R package TCGABiolinks [3], containing three metadata features (IDH mutation status, 1p.19q codeletion, and diagnosis). Both molecular features were used for sample selection and stratification (Figure S7.1). Based on the 2021

WHO classification of CNS tumours [1], IDH-mutant GBM has been moved into IDH-mutant astrocytoma (AST). To ensure intra-homogeneity between subtype samples and constancy to the 2021 WHO classification, IDH-mutant GBM samples were discarded. Moreover, samples with oligoastrocytoma diagnosis ("mixed-glioma") were excluded as they were poorly defined and represented a mixture of AST and oligodendroglioma (ODG) in different proportions between patients. The selected samples for the three glioma subtypes were classified as follows:

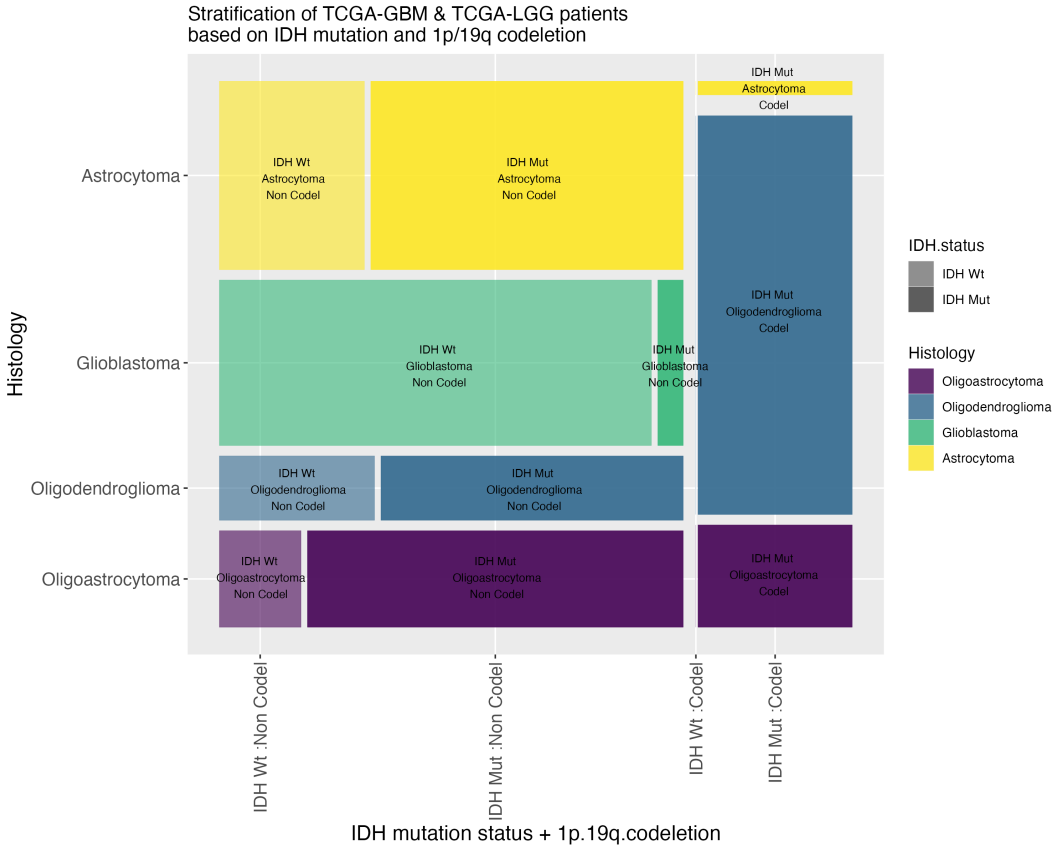

FIGURE 7.1: **TCGA metadata stratification based on 2021 WHO classification of CNS tumors using diagnosis, IDH mutation status, and 1p.19.q co-deletion.**

- iGBM: diagnosis = glioblastoma and IDH mutation = wildtype.
- iAST: diagnosis = astrocytoma, IDH mutation = mutant and 1p.19q codeletion = no codeletion.
- iODG: diagnosis = oligodendroglioma, IDH mutation = mutant and 1p.19q codeletion = codeletion.

7.1.2 Model selection (choosing the optimal combination of preprocessed data, generic model, and curation)

Many factors may affect the contextualization and specificity of the subtype models, such as the choice of generic models, applied curation, the objective function(s), and preprocessed data. Therefore, several settings were tested to find the optimal combination of preprocessed data, generic model, and

medium that ensured the best separation between the sample models. The search included three preprocessed data, generic metabolic models (Recon2 [4], Recon3D [5], or Human1 [6]), and two curation methods (no medium or with cerebrospinal fluid medium (CSF)). The three preprocessed data are Rahman2015 [7], Ceccarelli2016 [8], and TCGABiolinks [3]). These datasets were downloaded in FPKM (Fragments Per Kilobase of transcript per Million mapped reads) format. The CSF medium composition was imported from the Human Metabolome Database [9] like the whole-body metabolic model [10].

7.1.2.1 Separation between the glioma subtypes' sample models

These three factors were used for sample model building using rFASTCORMICS [11]. rFASTCORMICS is a context-specific metabolic model-building algorithm that takes as inputs RNA-Seq data and a consistent generic model with an optional medium composition [11]. The default discretization function in rFASTCORMICS (discretize_FPKM) was used for Ceccarelli2016 and Rahman2015 as their expression distribution peaked at the rightmost side with unexpressed formed leftmost tail (See Figure 7.2). Meanwhile, TCGABiolinks was discretized using another function (discretize_FPKM_skewed) as the expression data had a bimodal distribution with two peaks with comparable heights. In total, 18 combinations were searched, and 358 samples were built for each combination. Biomass production and ATP production were chosen as objective functions. The median number of samples' reactions was computed for each combination, and a hierarchical clustering of the samples was plotted as a metric for separating the three subtypes. After selecting the optimal combination of data, generic model, and curation, three subtype models were built using the abovementioned settings.

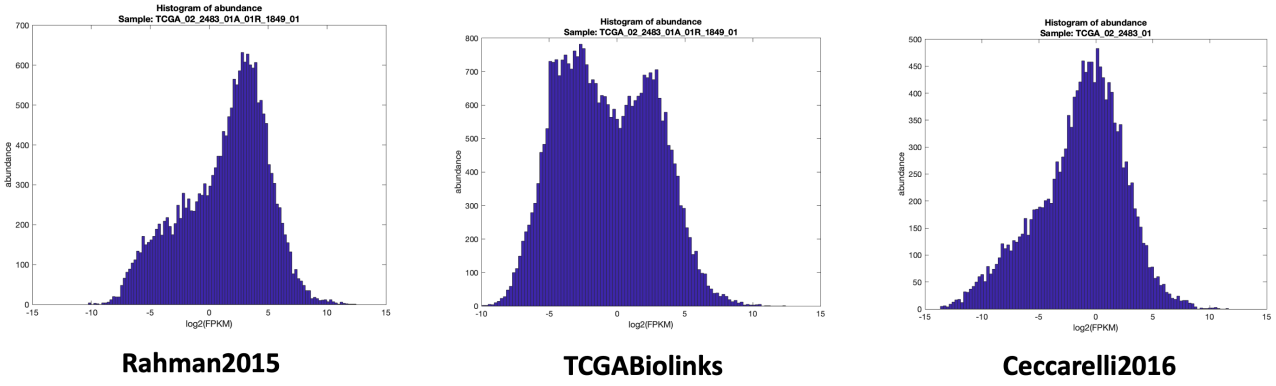

FIGURE 7.2: **Different TCGA RNA-seq data showed different distributions affecting the choice of discretization during model building.**

7.1.2.2 Evaluation to literature-retrieved exchange reactions

In addition to sample model separation, subtype models of the various data-model-curation combinations were evaluated against literature-retrieved metabolic exchanges that are representative of the within subtype variations (Table S 7.2). Flux Variability Analysis (FVA) was applied for the various subtype models exchanges with 100% maximization of the biomass objective function and compared to the literature-retrieved metabolic. Rahman2015 data, Recon3D generic model, and CSF curation showed the best matching to literature-retrieved metabolic exchanges (Figure S 7.5). Similarly, the same setting showed the best sample model separation (Figure S 7.3), suggesting that subtype separation and empirical metabolic exchange matching could improve model selection.

7.1.2.3 Evaluation to cancer common essential genes

To further evaluate if other input reconstruction and prepossessing methods would impact the essential genes prediction. We ran the single gene deletion workflow on all possible data-model-curation combinations and compared the respective essential genes to the list of common genes (defined as genes found to be essential in >90% of cell lines in pan-cancer CRISPR-Cas9 screens) by the Cancer Dependency Map's (DepMap) [12]. All models had accuracy between 0.84-0.90, with Recon3D with and without medium constraints, as well as Human1 having similar accuracy values (above 0.88). However, without medium constraints, Recon2 and Recon3D did predict very few essential genes also captured by the constrained conditions and Human1 is slightly advantaged by the larger number of genes included in the models. Human1 has 3050 genes against 1884 and 1733 for Recon3D and Recon2, inflating so the number of True Negatives. Finally, as we are comparing our predictions to common essential genes (no good quality glioma-specific binary high throughput screens are available), some predicted essential genes corresponding to glioma-specific essential genes might be wrongly identified as False Positives (Figure S 7.6).

7.1.3 Drug prioritization

Different clinical, preclinical, and pharmacokinetics data in brain cancer were collected to rank and filter the predicted single drugs and combinations based on their eligibility for testing (Supplementary File 2, Tables S8-10). The data collected in Supplementary File 2 included clinical trial data (Supplementary File 2, Table S11), *in/ex vivo* xenograft testing (Table S12), *in vitro* potency (Supplementary File 2, Table S13), non-brain cancer cytotoxicity (Supplementary File 2, Table S14), blood-brain barrier (BBB) permeability, CSF bioavailability (Supplementary File 2, Table S15), and possible drug-drug interactions for combinations (Supplementary File 2, Table S16). Other selection criteria included diversity and main mode of action (MOA), proven efficacy in higher clinical evidence, and agreement

Table 7.1: CSF medium constraining reduced sample model sizes by >20% in Recon2 and > 25% in Recon3D.

Sample models were built to determine the optimal combinations of data, generic model, and medium for model separation. The median number of reactions for sample models was computed for each parameter combination. Sample models built with Human1 with CSF medium were missing the objective function (OF) and thus were excluded. The total number of reactions in each generic model is displayed beside the generic model names. Noticeable reduction in model sizes with CSF medium, especially in Recon3D, indicated a separation using a biologically representative medium constraining.

Medium	Generic model	Recon2 (5317)	Recon3D (10600)	Human1 (11887)
`TCGABiolinks`	No medium	2752	5388	6533
`Ceccarelli2016`	No medium	2999	5465	6297
`Rahman2015`	No medium	2701	5183	6279
`TCGABiolinks`	CSF medium	2310	3862	Missing OF
`Ceccarelli2016`	CSF medium	2295	3732	Missing OF
`Rahman2015`	CSF medium	2258	3776	Missing OF

of predicted MOA with literature. Single drugs that showed either *in vitro* increased proliferation, no effect, or substrate drug-target interaction were excluded. Six of the ten excluded single drugs were hormones/co-factors, followed by two antivirals and two psychoactive drugs. The remaining drugs were ranked into selected candidates and weak candidates (see Supplementary File 2, Table S8). The final benchmarking assessed the predicted drugs compared to the approved anti-brain chemotherapies (AntiBCs) using the criteria summarized in Table S 7.7. The final evaluation classified the predicted single and combination drugs into effective, ineffective, and untested drugs across *in vitro*, *in/ex vivo* xenografts, and phase II clinical trials.

7.1.3.1 Clinical trial data

Predicted single and combination drugs were searched on the ClinicalTrials website (beta.clinicaltrials.gov) using ("Brain cancer" OR "Glioma") as the condition. Further clinical trials retrieved by using drug synonyms from Google Scholar were added. Due to the absence of a systematic database of the clinical trials, trials clinical trial identifiers were searched in PubMed to find which had published results. Among the clinical trials with published results, two main survival measures were shared as the primary outcome: overall survival (OS) and progression-free survival (PFS, duration between treatment and symptom worsening). If available, both survival measures were collected for phase I/II or higher clinical trials. The clinical trial data covered 50 phase I/II or higher brain cancers (Supplementary File 2, Table S11), of which seven are two-arm glioma trials where an arm is an approved treatment.

FIGURE 7.3: **The optimal setting using Rahman2015 data, Recon3D generic reconstruction, and CSF curation improved the separation between the sample models.**

Hierarchical clustering was applied for the sample models' reactions of each setting separately to define the best setting in intra- and inter-heterogeneity of the three subtypes. CSF medium constraining showed enhanced separation, but none separated AST and ODG. Only Rahman2015 data, Recon3D generic model, and CSF curation allowed a separation between GBM and LGG (AST and ODG).

7.1.3.2 Potency and pharmacokinetics data

in vitro data for the predicted single and combination drugs were retrieved from high-throughput drug screening (see Table S 7.6) and literature (Supplementary File 2, Table S13). The *in vitro* data in the literature ranged from increased proliferation, no effect, minimum inhibitory concentration, IC_{50}, viability reduction, and apoptosis/autophagy. In literature, if a drug lacks *in vitro* data in brain cancer cell lines, data were collected in non-brain cancer cell lines (Supplementary File 2, Table S14). *in vitro* data from high-throughput drug screening covered only two measure types (viability reduction and IC_{50}). Pharmacokinetics data (CSF bioavailability, BBB permeability, and ABC (ATP Binding Cassette) transporter affinity) were collected from B3DB [13], NCATS Inxight Drugs [14], and the

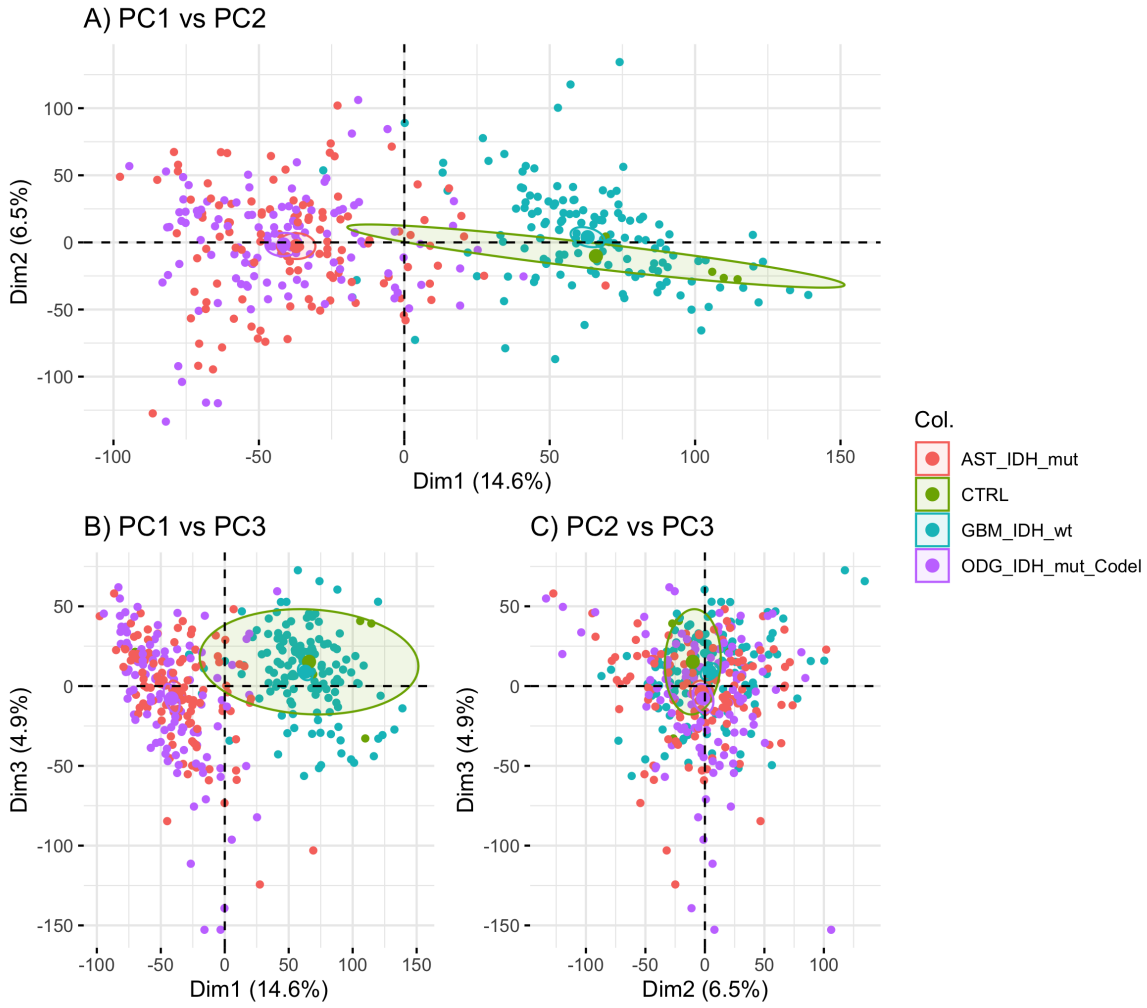

FIGURE 7.4: **Principal component analysis of the TCGA data expression data of Rahman2015 shows a clear separation between GBM and LGG but not between AST and ODG.**

To evaluate the quality of the TCGA expression data, principal component analysis (PCA) was used to examine the separation between the three glioma subtypes based on the 2021 WHO CNS tumors classification. Separation based on IDH mutation was clear but not based on 1a/19q co-deletion, suggesting the closeness between AST and ODG.

literature (Supplementary File 2, Table S15).

TABLE 7.2: **Predicted exchange reactions showed that six out of seven were consistent with previous knowledge.**

Reaction	Prediction	Literature Evidence	Literature Related Subtype	Matching with Literature	Cell Lines /Tissue Samples	Reference
Thymidine uptake	Thymidine uptake has a narrow boundary in GBM alone, with a small influx in AST and ODG	^{18}F-FLT, a radiotracer for thymidine kinase, showed higher uptake in GBM compared to AST and ODG	GBM	Yes	Patient scans	[15], [16]

L-Glutamine uptake	Glutamine uptake has a narrow boundary, and it was higher in GBM, followed by AST with a minute flux in ODG	ODG cell lines are less dependent on glutamine uptake compared to GBM	ODG	Yes	ODG: Hs683; HOG	[17]
L-Phenylalanine uptake	L-phenylalanine flux uptake has a broader range in GBM than in ODG	Metabolomics analysis of tissue samples identified L-phenylalanine as significantly higher in GBM compared to ODG	GBM	Yes	Tissue samples	[18]
Myo-Inositol uptake	Higher myo-inositol uptake was observed in ODG compared to AST and GBM	Metabolomics analysis of tissue samples identified myo-inositol as significantly higher in ODG compared to GBM	ODG	Yes	Tissue samples	[15]
4-Aminobutanoate release	4-Aminobutanoate released only in AST	Tissue biopsies have elevated levels of GABA in AST compared to ODG	AST	Yes	Tissue samples	[19]
L-Glutamate uptake	Glutamate uptake was predicted to be active in ODG but not in AST or GBM	Oligodendrocytes have the highest glutamate uptake among all brain cells	ODG	Yes	Human fetal oligodendrocytes	[20]
(S)-Lactate release	Lactate exchange was predicted to be reversible in AST and ODG but inactive in GBM	AST and ODG MR scans show no lactate production compared to GBM	ODG	No	Patient scans	[21]

TABLE 7.3: **A literature search identified six of the 25 predicted essential genes linked to glioma viability, resistance, or patient survival.**

Gene	**Function**	**Literature Support for Glioma**	**Cell Lines/ Patient Samples**	**Reference**
`TXNRD1`	Thioredoxin reductase	• Selective inhibitors of TXNRD1 induced cell death and decreased proliferation, invasion, and migration of multidrug-resistant glioma cell lines. Additionally, selective inhibitors of TXNRD1 showed synergistic effects with temozolomide (TMZ). • Selective inhibition of thioredoxin reductase was more cytotoxic than TMZ treatment. • TXNRD1 overexpression linked to radio-resistance. Additionally, knockdown (KD) of TXNRD1 reduced radioresistance in GBM. • TXNRD1 is upregulated in $>$ 66% of cases and significantly linked to higher proliferation and poorer prognosis. • Linked to poor diagnosis and higher grade.	• U87, U87-TxR, C6, RC6 (Rat) • GL261 • U87MG, T98G • AST patients • ODG patients	• [22] • [23] • [24] • [25] • [26]
`SLC27A4`	Fatty acid uptake	SLC27A3 knockdown, SLC27A4 isoform, reduced GBM xenograft growth, and its expression was linked to GBM stemness (Human GBM neurosphere lines)	Human GBM neurosphere lines	[27]
`RRM2`	Nucleotide interconversion	Genetic knockdown of RRM2 sensitizes GBM cell lines to TMZ *in vitro* and *in vivo*	U87	[28]

RRM1	Nucleotide interconversion	High-throughput drug screening followed by shRNA of the hit's targets identified RRM1 among nine genes as GBM vulnerabilities	U87, U87vIII, T98G, GL261	[29]
SPTLC1	Sphingolipid synthesis	Knocking down SPLTC genes reduced the viability of GBM cell lines	U87MG	[30]
ANPEP	Glutathione metabolism	ANPEP is highly expressed in GBM and linked to low survival	Not specified	[31]
SLC6A14	L-Arginine uptake	Arginine deprivation reduced cell adhesion and invasiveness of GBM cell lines	U251MG, U87MG	[32]

TABLE 7.4: **Five predicted drugs matched the targeted genes and reactions for their anti-glioma activity in the literature.**

Drug	Evidence from Literature	Glioma Cell Lines	Predicted Targets	Predicted Reactions	Reference
Arsenic-trioxide	Arsenic-trioxide induces cytotoxicity by increasing ROS formation.	C6 and 9L	TXNRD1	Ph[c] + nadph[c] + trdox[c] -> nadp[c] + trdrd[c]	[33]
Acetazolamide and brinzolamide	Both drugs are chemosensitizers for TMZ by reducing extracellular acidosis.	U373, U251, U87MG, GaMG, U87 and GSCs	Carbonic anhydrases	H20 + CO2 <=> H+ + Bicarbonate	[34]
Cannabidiol	Increasing ROS and depletion of glutathione.	U87	ACAT1, CAT, GSR	2 H2O2 -> 2 Water + Oxygen, gthox[c] + h[c] + nadph[c] -> 2.0 gthrd[c] + nadp[c]	[35]
Eflornithine	Eflornithine reduces GBM cell viability by targeting ODC1.	DIPG	ODC1	L-glutamate biosynthesis from 2-oxoglutarate	[36]

TABLE 7.5: **Summary of the high- or medium-drug screening databases used to evaluate the predicted drugs.**
gCSI: Genentech Cell Line Screening Initiative

Database	Type	Tested Concentrations	Number of Cell Lines/ Xenografts	Number of Tested Drugs	Number of Predicted Single Drugs	Number of Predicted Combination Drugs	Reference
Stathias et al., 2018	*in vivo* PDX in mice	1 μM	7 (GBM)	186	10	3	[39]
Bell et al. 2018 Initial screen	*ex vivo* PDX in mice	10 μM	7 (GBM)	520	9	2	[40]
Bell et al. 2018 follow-up screen	Ex vivo PDX in mice	0.1, 1, 10 μM	5 (GBM)	119	8	2	[40]
Primary PRISM	*in vitro* (viability reduction)	2.5-5 μM	25 (GBM), 10 (AST)	4517	31	17	[41]
Nam et al. 2021	*in vitro* (viability reduction)	10 μM	2 (GBM)	975	11	8	[42]
gCSI	*in vitro* (IC_{50})	0.01-20 μM	8 (GBM), 5 (AST), 1 (ODG), 1 (non-glioma)	16	1	0	[43]

GDSC1000	*in vitro* (IC_{50})	3.125e-5 to 15.625 μM	27 (GBM), 9 (AST), 1 (ODG), 4 (non-glioma)	378	1	1	[44]
GDSC2000	*in vitro* (IC_{50})	3.125e-5 to 15.625 μM	28 (GBM), 9 (AST), 1 (ODG), 4 (non-glioma)	286	1	1	[44]
Secondary PRISM	*in vitro* (IC_{50})	6.1e-3 to 10 μM	21 (GBM), 5 (AST), 2 (non-glioma)	1414	14	4	[41]

TABLE 7.6: **Classification criteria of the predicted single and combination drugs into effective, ineffective, and untested compared to the AntiBCs.**

Prediction	Evidence	Effective	Ineffective	Untested
Single Drugs	***in vitro***	• Comparable/improved CSF bioavailability/potency to AntiBCs • more than 50% viability reduction • Induced apoptosis/autophagy	• Induced proliferation • Remaining tested drugs *in vitro*	
Single Drugs	***in/ex vivo***	• >25% growth reduction in GBM xenografts screening databases • Enhanced growth reduction or survival in literature	• Remaining tested drugs *in/ex vivo*	
Single Drugs	**Clinical trial**	• Phase II, two-arms, with improved OS/PFS as monotherapy/in combination against AntiBCs	• Declared non-effective in single-arm phase II trial • Showed antagonism while combined with AntiBCs in phase II trial	• Remaining drugs, including single-arm phase II trials
Combination Drugs	***in vitro***	• In addition to single drugs: • Synergism/additive/ chemosensitizer effect with TMZ	• In addition to single drugs: • Antagonism effect with TMZ	
Combination Drugs	**In/ex vivo**	• In addition to single drugs: • Synergism/additive/ chemosensitizer effect with TMZ • Radio-sensitization	• In addition to single drugs: • Antagonism effect with TMZ	
Combination Drugs	**Clinical trial**	• Same as single drugs		

TABLE 7.7: **Two of three predicted combinations showed synergistic interactions in non-brain cancer cell lines.**

Previous combined testing of each drug in a combination is essential to rank the predicted combinations. PubMed and clinicaltrials.gov were searched for any previous testing of the 17 predicted combinations, including non-cancer, in vitro, and clinical trials. None of the combinations were found to be tested clinically in brain cancer. Only three combinations were tested in vitro in non-brain cancer with synergistic actions, of which two failed in clinical trials. These tests were used to rank the combinations (Supplementary File 2, Table S10).

Predicted combination	**Clinical/ Preclinical**	**Cancer type**	**The rationale for testing this combination**	**Result**	**Side effect (if exists)**	**Reference**
Fluorouracil/ zidovudine	Preclinical	Colon cancer (HT-29)		Synergistic effect		[45]
Fluorouracil/ zidovudine	Clinical (Phase I, $n = 18$)	Various tumors	Preclinical synergistic cytotoxic effect	Terminated, as the plasma concentration of the anticancer activity of zidovudine is above the maximal dose		[46]
Fluorouracil/ celecoxib	Preclinical	Gastric carcinoma cell line	Fluorouracil resistance in gastric cancer is correlated with COX-2 expression	Synergistic effect	Celecoxib did not have additional toxicity to fluorouracil	[47]
Fluorouracil/ celecoxib	Clinical (Phase III, $n = 2526$)	Colon Cancer (Stage III)	Inhibiting COX2 might enhance OS	There is no notable change in OS compared to fluorouracil alone	Tolerated; a slight increase in hypertension	[48]
Fluorouracil/ resveratrol	Preclinical	Colon cancer (HCT116, DLD1)		Resveratrol increased the anti-telomeric and pro-apoptotic actions of fluorouracil		[49]
Fluorouracil/ resveratrol	Preclinical	Normal human keratinocytes (HaCaT)	Resveratrol may avoid fluorouracil-induced side effects	Resveratrol reduced fluorouracil-induced ROS production		[50]

Resources table

Resources	**Version**	**Link**
RNA-Seq of TCGA-GBM and TCGA-LGG		`https://www.ncbi.nlm.nih.gov/geo/query/acc.cgi?acc=GSE62944`
List of common essential genes	DepMap 22Q1	`https://ndownloader.figshare.com/files/34008470`
Stathias et al. 2018 GBM PDX data		`https://data.mendeley.com/datasets/yz8m28gj6r/1`
Bell et al. 2018, initial screen on GBM PDXs		`https://doi.org/10.1158/1541-7786.MCR-17-0397`, Supplementary Table 1
Bell et al. 2018, follow-up screen on GBM PDXs		`https://doi.org/10.1158/1541-7786.MCR-17-0397`, Supplementary Table 2
Primary and secondary PRISM screen	PRISM Repurposing 19Q4	`https://depmap.org/portal/download/all/`

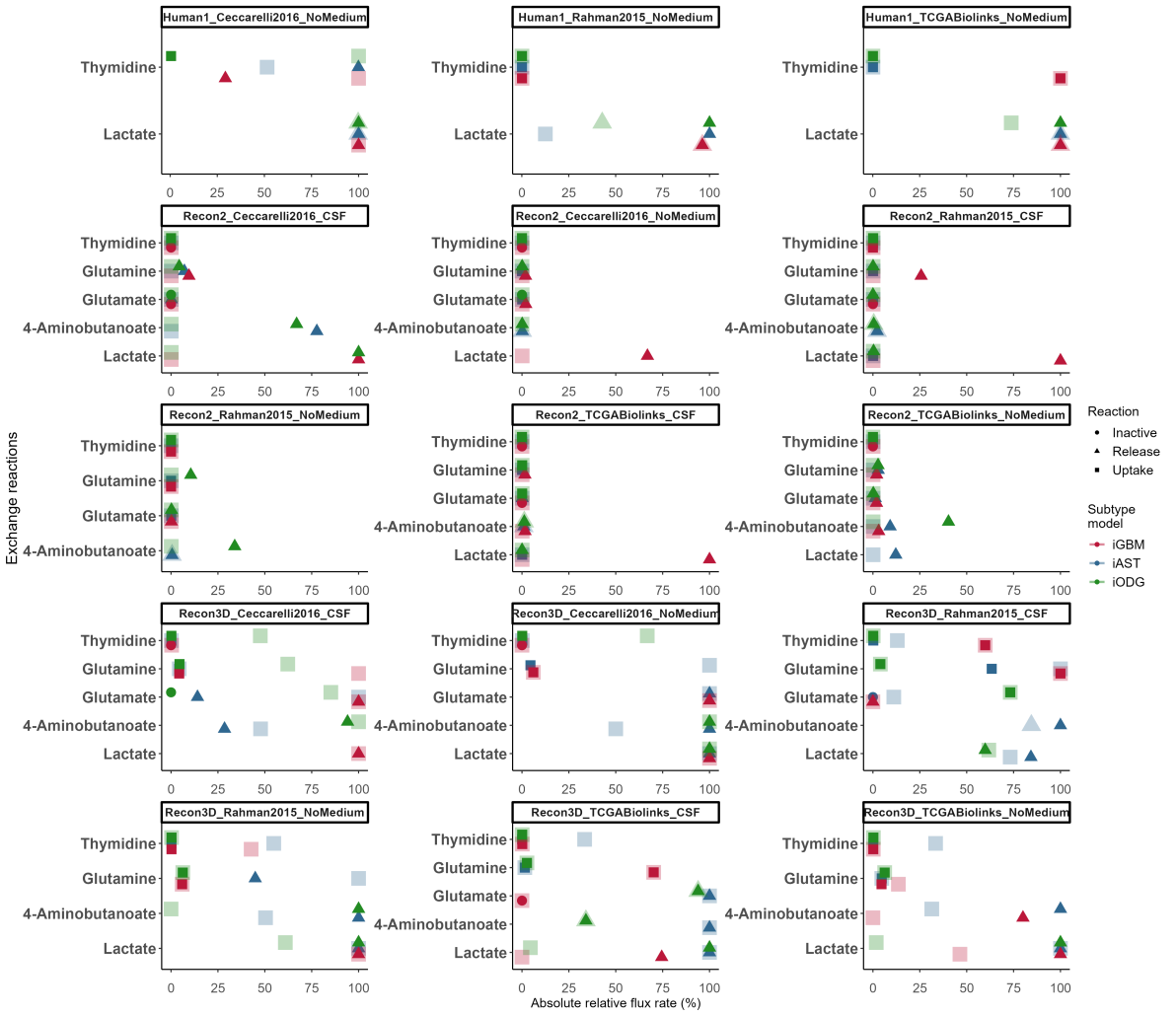

FIGURE 7.5: **Flux variability analysis determined the optimal setting using Rahman2015 data, Recon3D generic model, and CSF curation to better match literature-retrieved metabolic exchanges.**

Flux variability analysis was applied to the various subtype model settings to determine which is the best setting matching literature-retrieved subtype-specific metabolic exchanges (Table S 7.2).

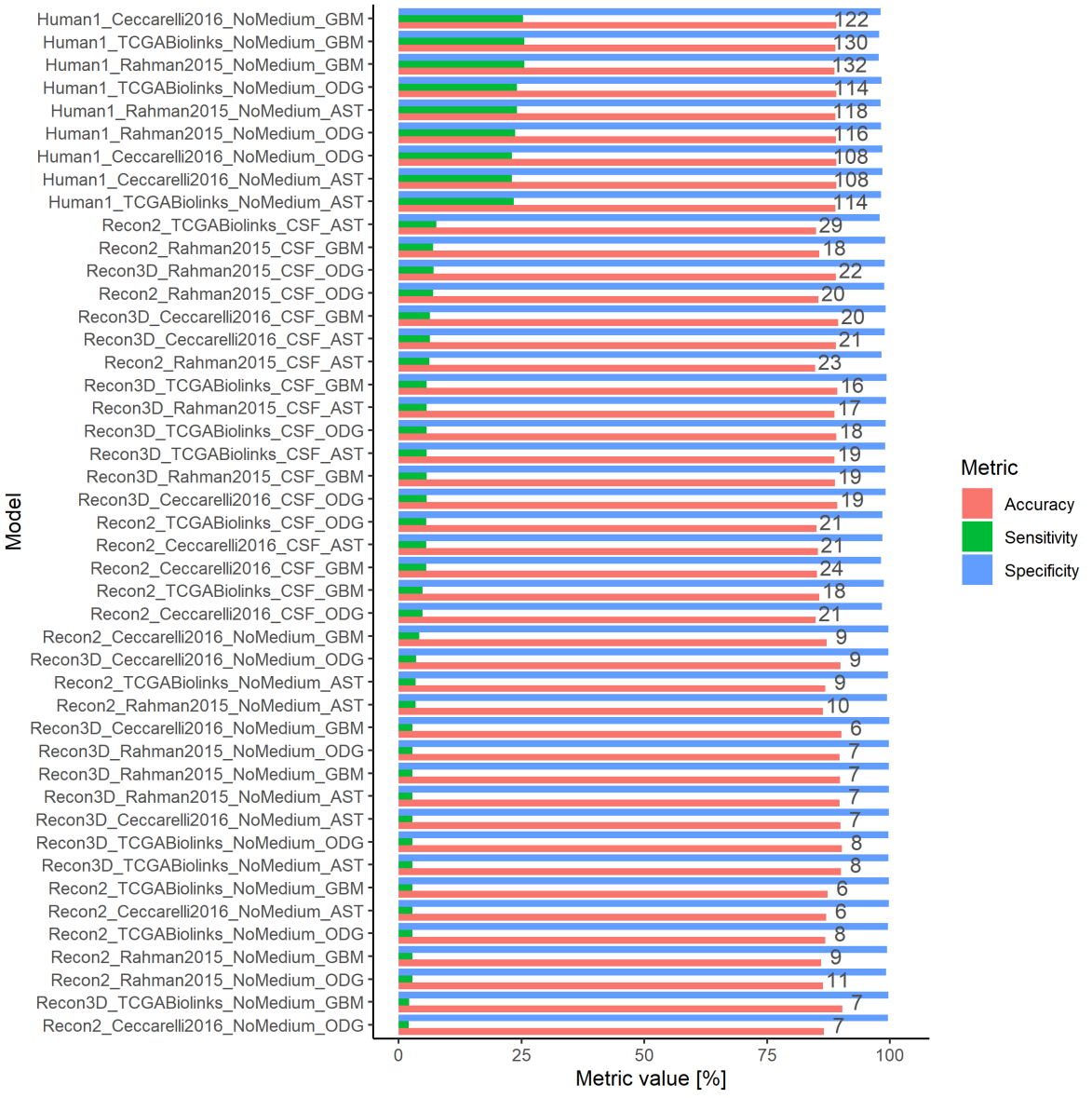

FIGURE 7.6: **The accuracy for all models lies between 0.84 and 0.9 for capturing common essential genes.**

Recon2 and Recon3 models without medium constraint have a lower number of predicted essential genes. Human1 is advantaged by the larger number of metabolic genes included in the model which inflates the number of True Negatives.

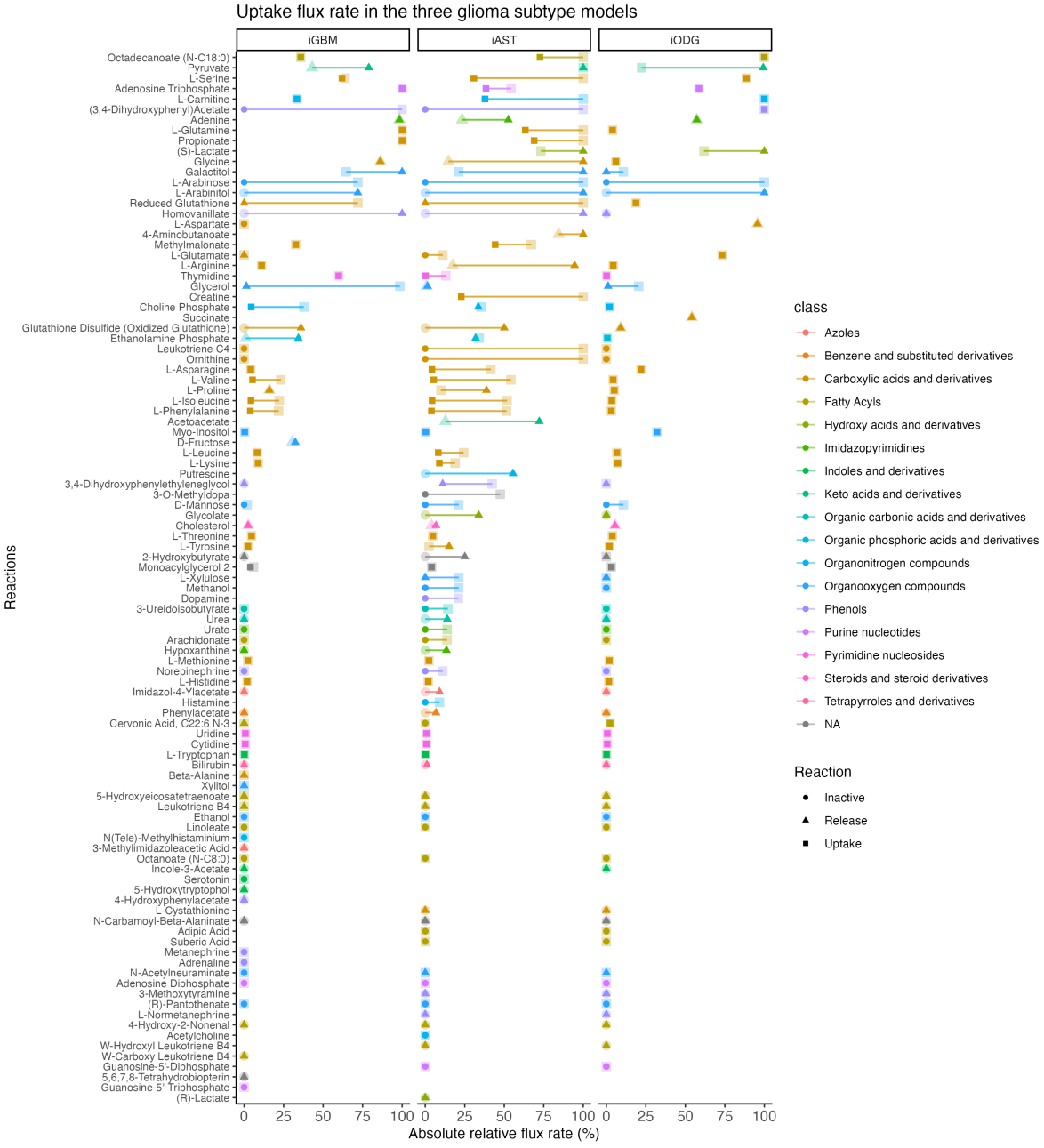

FIGURE 7.7: **Flux variability analysis of the metabolite exchanges identified differential uptake and production between the glioma subtypes.**

As a quality control, the preferred metabolite exchanges were compared to known variations in the literature. The 101 metabolite exchanges shared across the three glioma subtype models were fed to the fluxVariability function from the COBRA Toolbox v3.0 to define reactions with narrow fluxes predicted to influence biomass growth.

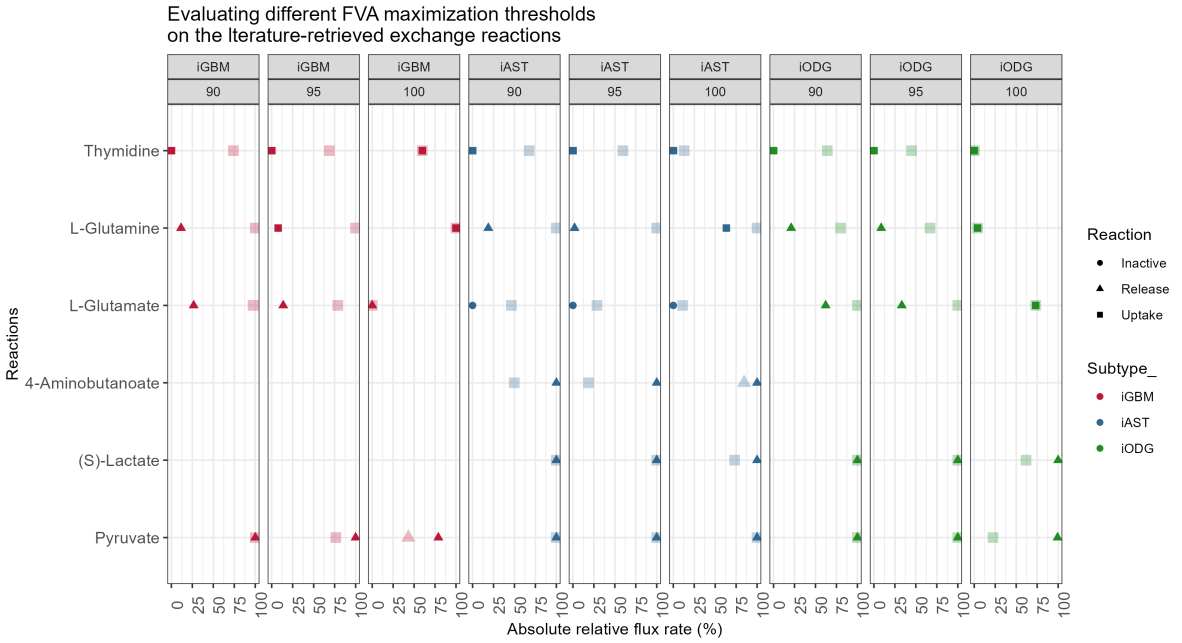

FIGURE 7.8: **A release of the optimization threshold from 100% to 95% and 90% increases the range predicted flux drastically turned some exchange reactions with narrow bounds at 100% to become unbounded.**

To determine the optimal maximization threshold for the Flux Variability Analysis (FVA) matching the literature-retrieved exchange reactions (Table S 7.2), different thresholds (90%, 95%, and 100%) were tested for the three glioma subtype models. Increasing the maximization threshold for the biomass reaction, decreased the range of the metabolic flux and improving their matching to the literature. For example, the known glutamine dependency in GBM and glutamate dependency in ODG were predicted with 100% maximization.

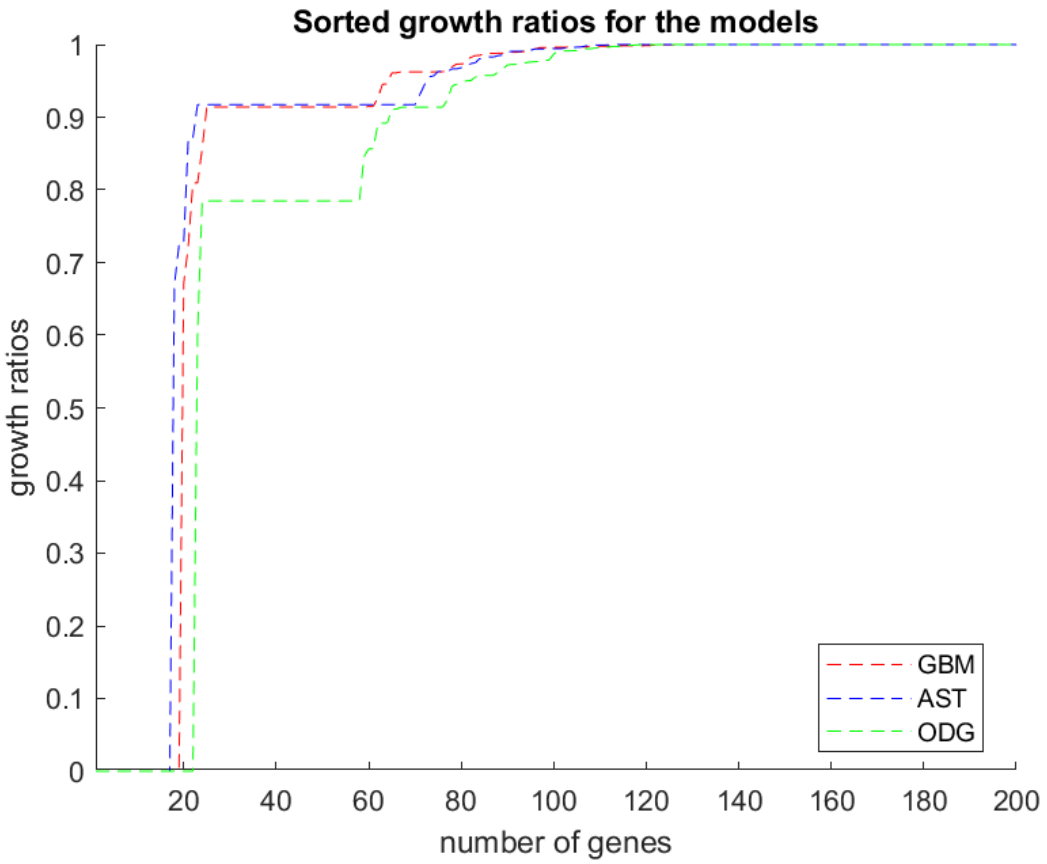

FIGURE 7.9: **The number of predicted essential genes remained constant for growth ratio between 0 and 0.7.**

Above 0.7, the number of essential genes substantially increased but the growth reduction is too modest to consider using these additional genes as cancer targets.

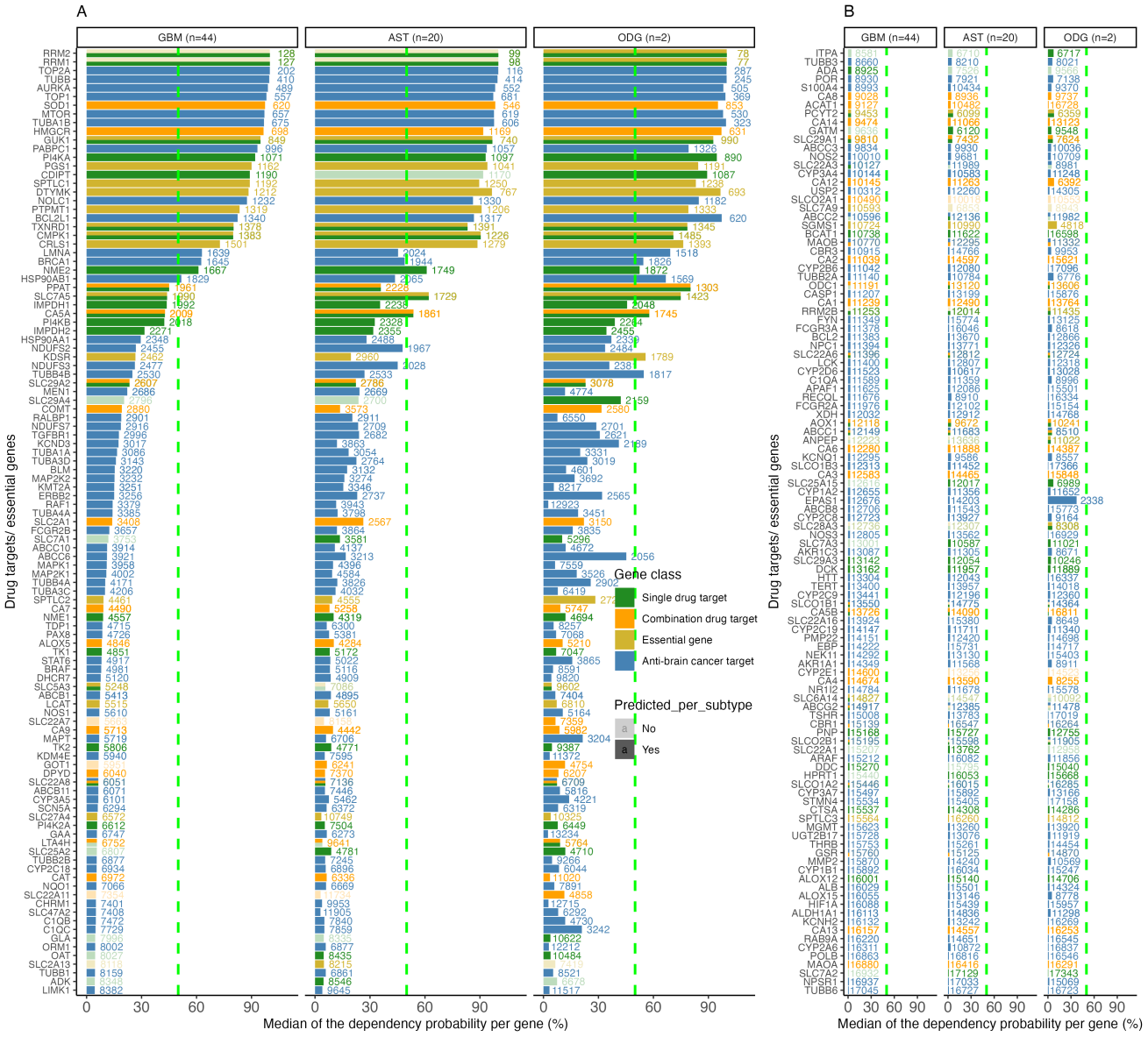

FIGURE 7.10: **Only RRM1 and RRM2 of the predicted essential genes involved in nucleotide biosynthesis showed stronger gene dependency than AntiBCs targets.**

To evaluate predicted drugs against AntiBCs on target essentiality in glioma cell lines, targets of AntiBCs, predicted single and combination drugs and essential genes were ranked according to the dependency probability in the DepMap database. DepMap is the largest database of genome-scale *in vitro* CRISPR-Cas9 KO screening of cancer cell lines, with dependency probability representing the likelihood of cell death upon gene KO. Genes were ranked by median dependency probability in GBM cell lines, and genes not predicted in a subtype were highlighted in transparent color. RRM1 and RMM2 targeted by anti-metabolites exceeded AntiBCs targets, followed by non-alkylating AntiBCs targets (doxorubicin (TOP2A, AURKA, TOP1) and vincristine (TUBB, TUBA1B)).

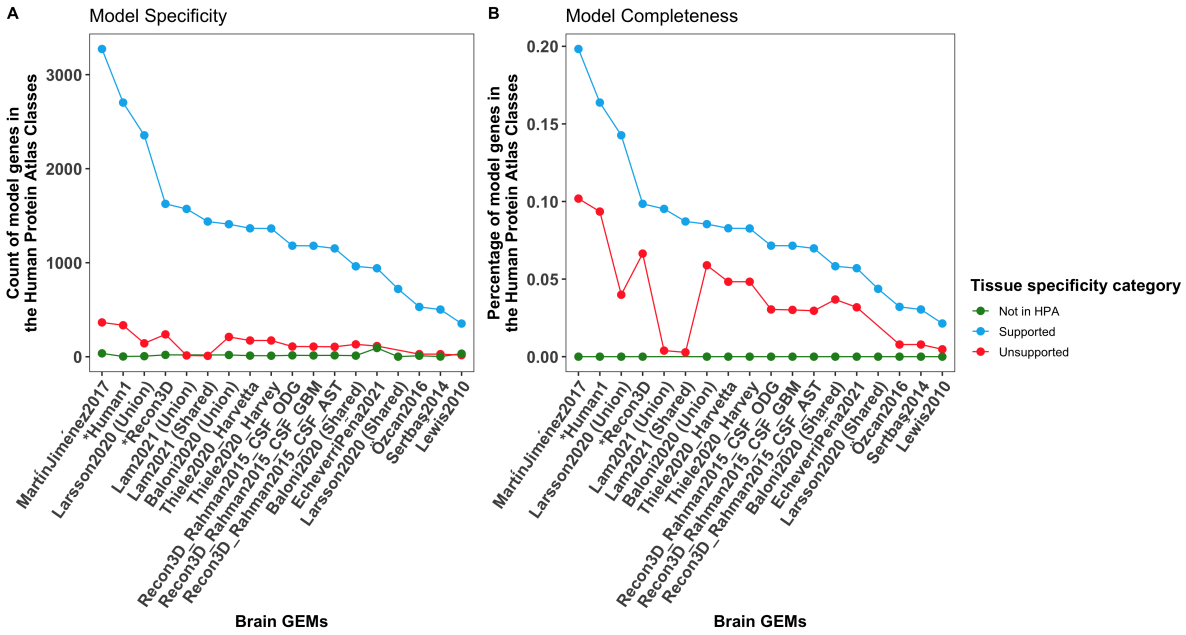

FIGURE 7.11: **Glioma subtype models' genes showed comparable specificity and completeness to curated and semi-curated brain metabolic models according to the Human Protein Atlas brain-specific category.**

The genes of the glioma subtype models were compared to the ones included in the brain metabolic models discussed in our previous review [37] using the Human Protein Atlas [38] (HPA) as reference to determine the quality of each model. HPA gene categories classify genes based on differential tissue expression of the brain, that were combined into "Expressed" in green and Unexpressed" in red. Model specificity (A) was computed as the number of model genes in each category, while model completeness was computed as the ratio of model genes in a category and the total number of genes in that category. Our glioma subtype models showed comparable specificity and completeness compared to the curated and semi-curated models in the brain.

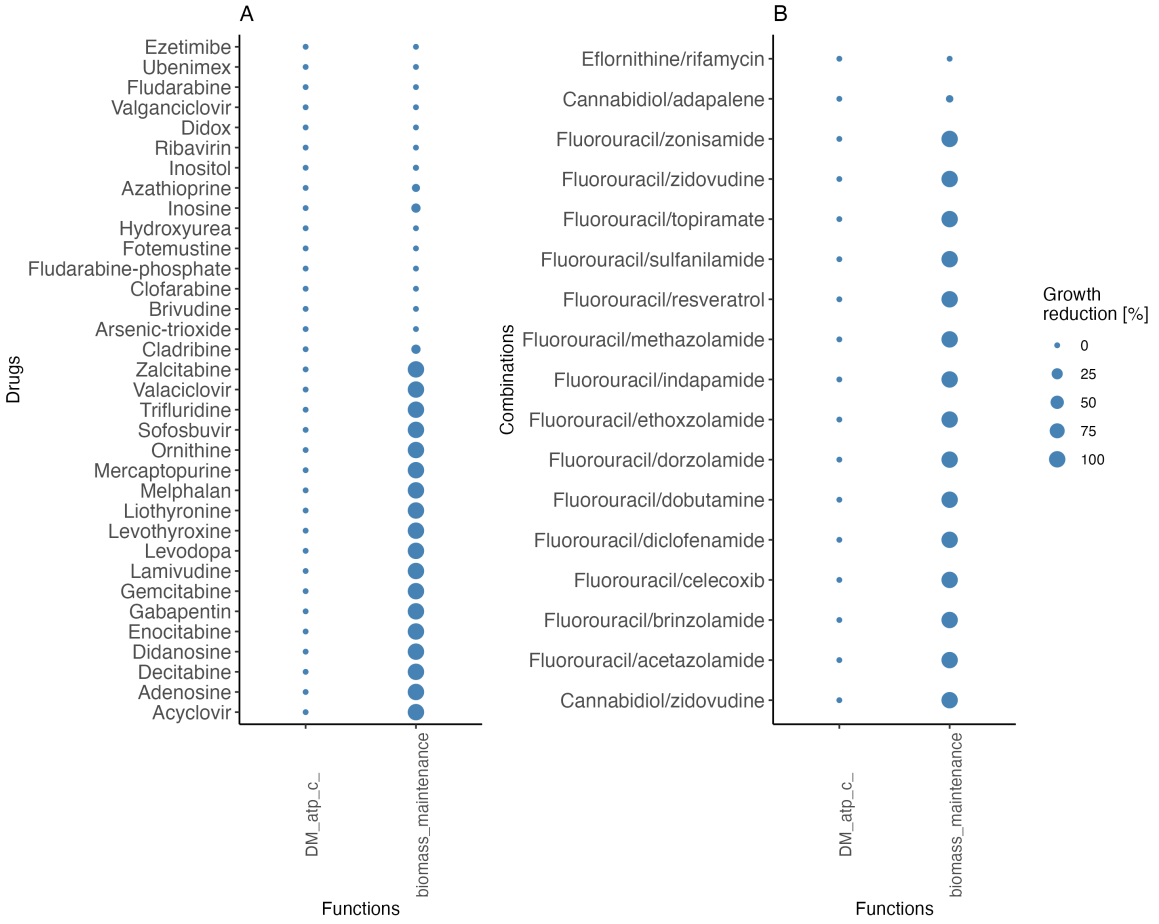

FIGURE 7.12: **Half of the single drugs and two combinations show a minimal effect on the healthy biomass maintenance reaction of the control model.**

To determine which of the predicted single drugs and combinations are potentially toxic to the healthy brain, drug deletion was applied to a control brain GEM built from five healthy samples in TCGA-GBM. Growth reduction (1-grRatio) was used to rank the predicted drugs based on potential safety for two reactions: ATP production (DM_atp_c_) and growth (biomass_maintainance). All predicted drugs were predicted to be safe on ATP production. Of the single drugs, half are predicted to be safe for healthy brain growth, including clinically effective drugs: fotemustine and valganciclovir. Meanwhile, the subtype-specific combinations (eflornithine/rifamycin and cannabidiol/adapalene) are the only safe combinations on the control model growth.

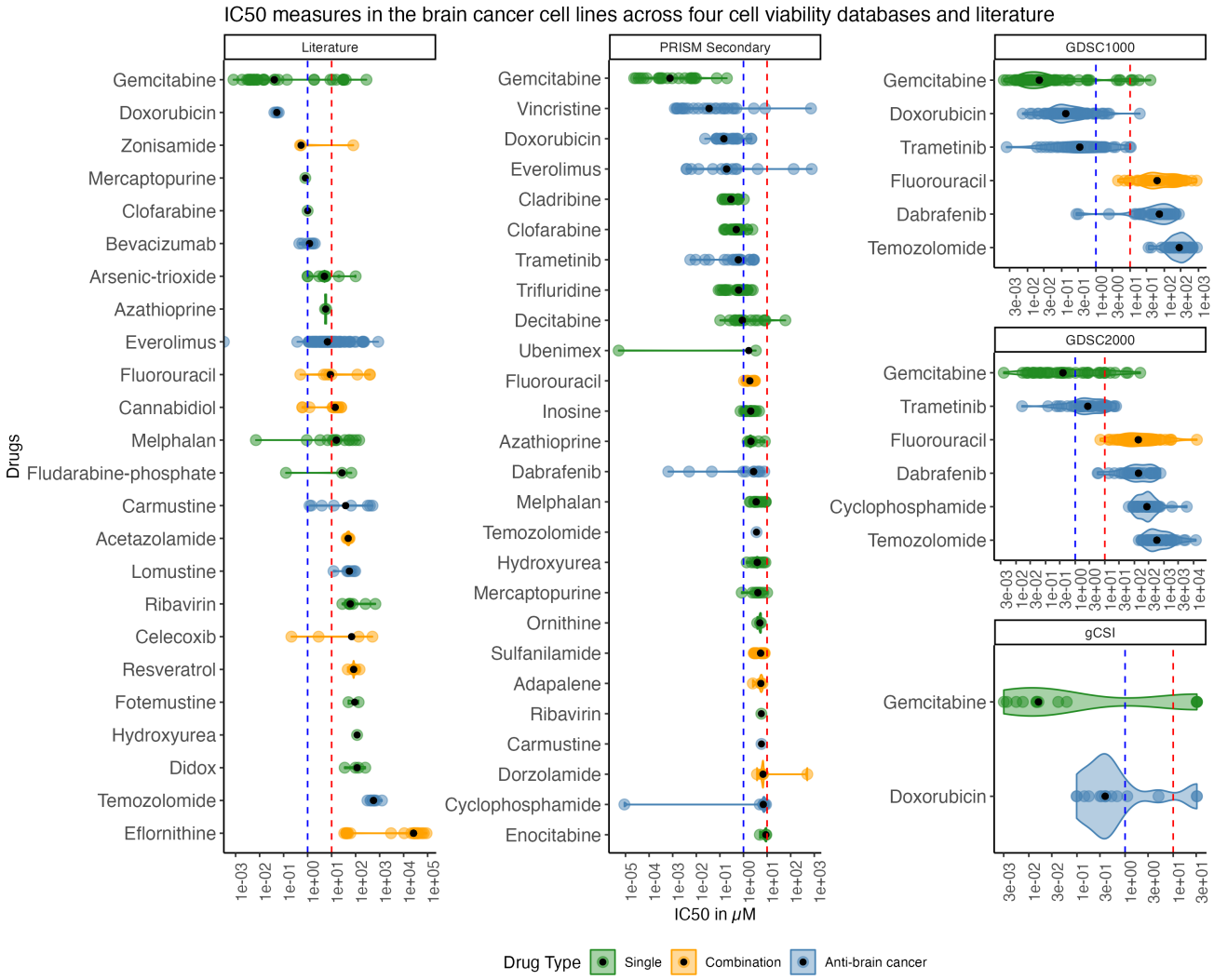

FIGURE 7.13: **Gemcitabine showed superior potency in all IC_{50} databases to approved AntiBCs, while alkylating AntiBCs are commonly used for glioma.**

Drug screening databases with IC_{50} measures and IC_{50} measures collected from the literature (Supplementary File 2, Table S13) were used to rank predicted single, combinations drugs and AntiBCs using median IC_{50} as a potency measure. Alkylating AntiBCs (temozolomide, lomustine, carmustine, and cyclophosphamide) show the lowest potency, with gemcitabine having the highest potency across the five databases. Other combinations of drugs, such as zonisamide and fluorouracil, showed comparable potency to non-alkylating AntiBCs and higher than alkylating AntiBCs.

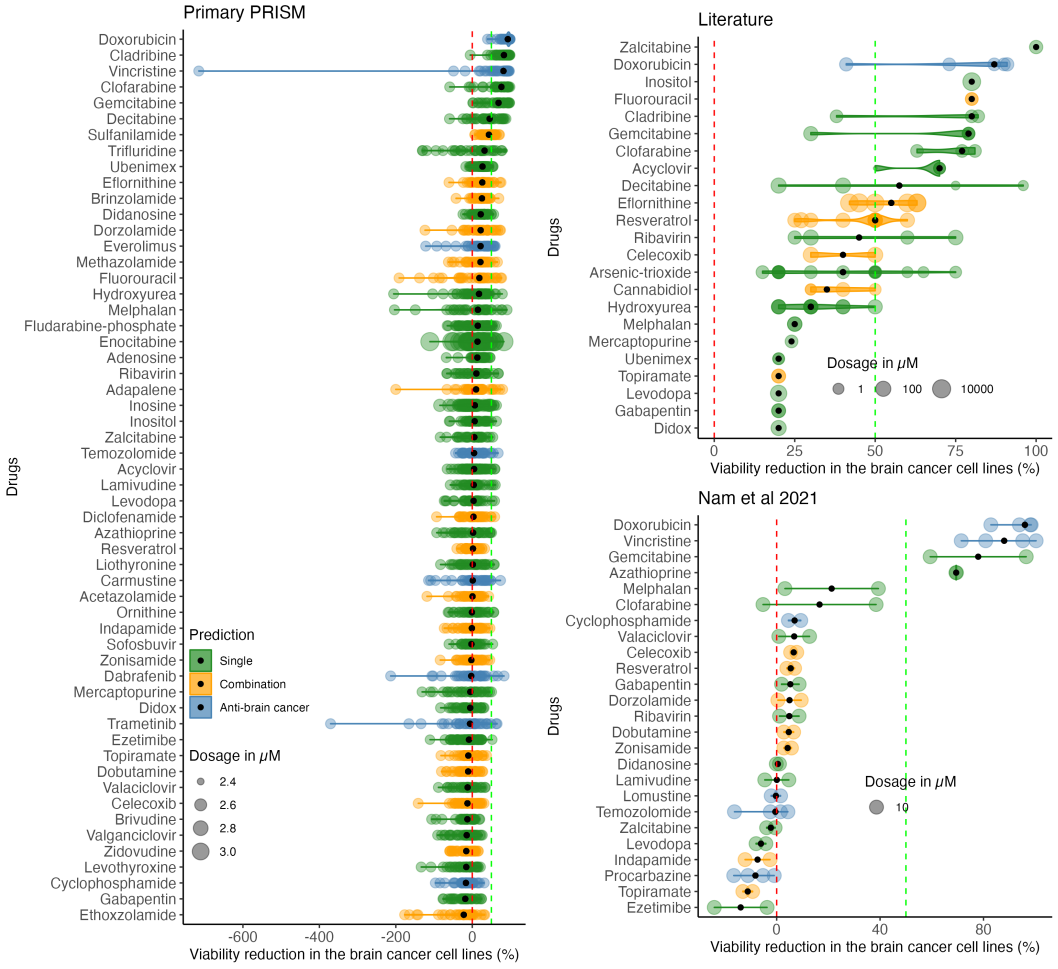

FIGURE 7.14: **Doxorubicin, followed by the anti-metabolites, shows the strongest viability reduction in the cell viability databases and literature.**

Besides the IC_{50} data, other drug screening databases included only viability reduction with a small range of tested concentrations. Viability reduction from two databases and literature (Supplementary File 2, Table S13) was used to compare the single and combination drugs to AntiBCs using the median viability reduction (black dot). Doxorubicin was the only AntiBCs, followed by primarily anti-metabolites of the single drugs to exceed 50% viability reduction.

References

[1] D. N. Louis, A. Perry, P. Wesseling, *et al.*, "The 2021 WHO classification of tumors of the central nervous system: A summary," *Neuro-Oncology*, vol. 23, no. 8, pp. 1231–1251, Aug. 2021, Publisher: Oxford University Press. DOI: 10.1093/NEUONC/NOAB106.

[2] J. N. Weinstein, E. A. Collisson, G. B. Mills, *et al.*, "The cancer genome atlas pan-cancer analysis project," *Nature Genetics*, vol. 45, no. 10, 2013. DOI: 10.1038/ng.2764.

[3] A. Colaprico, T. C. Silva, C. Olsen, *et al.*, "TCGAbiolinks: An R/Bioconductor package for integrative analysis of TCGA data," *Nucleic Acids Research*, vol. 44, no. 8, e71, May 2016, Publisher: Oxford University Press. DOI: 10.1093/NAR/GKV1507.

[4] I. Thiele, N. Swainston, R. M. T. Fleming, *et al.*, "A community-driven global reconstruction of human metabolism," *Nature Biotechnology*, vol. 31, no. 5, pp. 419–425, May 2013. DOI: 10.1038/NBT.2488.

[5] E. Brunk, S. Sahoo, D. C. Zielinski, *et al.*, "Recon3D enables a three-dimensional view of gene variation in human metabolism," *Nature Biotechnology*, vol. 36, no. 3, pp. 272–281, Mar. 2018, Publisher: Nature Publishing Group. DOI: 10.1038/NBT.4072.

[6] J. L. Robinson, P. Kocabaş, H. Wang, *et al.*, "An atlas of human metabolism," *Science Signaling*, vol. 13, no. 624, Mar. 2020, Publisher: American Association for the Advancement of Science. DOI: 10.1126/SCISIGNAL.AAZ1482.

[7] M. Rahman, L. K. Jackson, W. E. Johnson, D. Y. Li, A. H. Bild, and S. R. Piccolo, "Alternative preprocessing of RNA-Sequencing data in the Cancer Genome Atlas leads to improved analysis results," *Bioinformatics*, vol. 31, no. 22, pp. 3666–3672, May 2015, Publisher: Oxford University Press. DOI: 10.1093/BIOINFORMATICS/BTV377.

[8] M. Ceccarelli, F. P. Barthel, T. M. Malta, *et al.*, "Molecular Profiling Reveals Biologically Discrete Subsets and Pathways of Progression in Diffuse Glioma," *Cell*, vol. 164, no. 3, pp. 550–563, Jan. 2016, Publisher: Cell. DOI: 10.1016/J.CELL.2015.12.028.

[9] D. S. Wishart, Y. D. Feunang, A. Marcu, *et al.*, "HMDB 4.0: The human metabolome database for 2018," *Nucleic Acids Research*, vol. 46, no. D1, pp. D608–D617, Jan. 2018, Publisher: Oxford University Press. DOI: 10.1093/NAR/GKX1089.

[10] I. Thiele, S. Sahoo, A. Heinken, *et al.*, "Personalized whole-body models integrate metabolism, physiology, and the gut microbiome," *Molecular Systems Biology*, vol. 16, no. 5, May 2020, Publisher: EMBO. DOI: 10.15252/MSB.20198982.

[11] M. P. Pacheco, T. Bintener, D. Ternes, *et al.*, "Identifying and targeting cancer-specific metabolism with network-based drug target prediction," *EBioMedicine*, vol. 43, pp. 98–106, May 2019, Publisher: Elsevier B.V. DOI: 10.1016/J.EBIOM.2019.04.046.

[12] C. Pacini, J. M. Dempster, I. Boyle, *et al.*, "Integrated cross-study datasets of genetic dependencies in cancer," *Nature Communications*, vol. 12, no. 1, Dec. 2021, Publisher: Nature Research. DOI: 10.1038/S41467-021-21898-7.

[13] F. Meng, Y. Xi, J. Huang, and P. W. Ayers, "A curated diverse molecular database of blood-brain barrier permeability with chemical descriptors," *Scientific Data*, vol. 8, no. 1, 2021. DOI: 10.1038/s41597-021-01069-5.

[14] V. B. Siramshetty, I. Grishagin, D. T. Nguyen, *et al.*, "NCATS Inxight Drugs: A comprehensive and curated portal for translational research," *Nucleic Acids Research*, vol. 50, no. D1, 2022. DOI: 10.1093/nar/gkab918.

[15] A. H. Jacobs, A. Thomas, L. W. Kracht, *et al.*, "18F-Fluoro-l-Thymidine and 11C-Methylmethionine as Markers of Increased Transport and Proliferation in Brain Tumors," *Journal of Nuclear Medicine*, vol. 46, no. 12, 2005.

[16] A. Nikaki, G. Angelidis, R. Efthimiadou, *et al.*, "18F-fluorothymidine PET imaging in gliomas: An update," *Annals of Nuclear Medicine*, vol. 31, no. 7, p. 495, Jun. 2017, Publisher: Springer. DOI: 10.1007/S12149-017-1183-2.

[17] M. Chiu, G. Taurino, M. G. Bianchi, *et al.*, "Oligodendroglioma cells lack glutamine synthetase and are auxotrophic for glutamine, but do not depend on glutamine anaplerosis for growth," *International Journal of Molecular Sciences*, vol. 19, no. 4, Apr. 2018, Publisher: MDPI AG. DOI: 10.3390/IJMS19041099.

[18] L. Mörén, A. T. Bergenheim, S. Ghasimi, T. Brännström, M. Johansson, and H. Antti, "Metabolomic Screening of Tumor Tissue and Serum in Glioma Patients Reveals Diagnostic and Prognostic Information," *Metabolites 2015, Vol. 5, Pages 502-520*, vol. 5, no. 3, pp. 502–520, Sep. 2015, Publisher: Multidisciplinary Digital Publishing Institute. DOI: 10.3390/METABO5030502.

[19] S. K. Ganji, Z. An, V. Tiwari, *et al.*, "In Vivo Detection of 2-Hydroxyglutarate in Brain Tumors by Optimized PRESS at 7T," *Magnetic resonance in medicine*, vol. 77, no. 3, p. 936, Mar. 2017, Publisher: NIH Public Access. DOI: 10.1002/MRM.26190.

[20] D. Pitt, I. E. Nagelmeier, H. C. Wilson, and C. S. Raine, "Glutamate uptake by oligodendrocytes: Implications for excitotoxicity in multiple sclerosis," *Neurology*, vol. 61, no. 8, pp. 1113–1120, Oct. 2003, Publisher: Neurology. DOI: 10.1212/01.WNL.0000090564.88719.37.

[21] M. M. Chaumeil, M. Radoul, C. Najac, *et al.*, "Hyperpolarized 13C MR imaging detects no lactate production in mutant IDH1 gliomas: Implications for diagnosis and response monitoring," *NeuroImage: Clinical*, vol. 12, 2016. DOI: 10.1016/j.nicl.2016.06.018.

[22] M. Jovanović, M. Dragoj, D. Zhukovsky, *et al.*, "Novel TrxR1 Inhibitors Show Potential for Glioma Treatment by Suppressing the Invasion and Sensitizing Glioma Cells to Chemotherapy," *Frontiers in Molecular Biosciences*, vol. 7, Oct. 2020, Publisher: Frontiers Media S.A. DOI: 10.3389/FMOLB.2020.586146.

[23] V. Pires, I. Bramatti, M. Aschner, V. Branco, and C. Carvalho, "Thioredoxin Reductase Inhibitors as Potential Antitumors: Mercury Compounds Efficacy in Glioma Cells," *Frontiers in Molecular Biosciences*, vol. 9, Jun. 2022, Publisher: Frontiers Media SA. DOI: 10.3389/FMOLB.2022.889971.

[24] Y. Zhang, F. Chen, G. Tai, *et al.*, "TIGAR knockdown radiosensitizes TrxR1-overexpressing glioma in vitro and in vivo via inhibiting Trx1 nuclear transport," *Scientific Reports 2017 7:1*, vol. 7, no. 1, pp. 1–13, Mar. 2017, Publisher: Nature Publishing Group. DOI: 10.1038/srep42928.

[25] H. Haapasalo, M. Kyläniemi, N. Paunu, V. L. Kinnula, and Y. Soini, "Expression of Antioxidant Enzymes in Astrocytic Brain Tumors," *Brain Pathology*, vol. 13, no. 2, pp. 155–164, Apr. 2003, Publisher: John Wiley & Sons, Ltd. DOI: 10.1111/J.1750-3639.2003.TB00015.X.

[26] H. Hannu, B. Helena, P. Niina, *et al.*, "Antioxidant enzymes in oligodendroglial brain tumors: Association with proliferation, apoptotic activity and survival," *Journal of Neuro-Oncology*, vol. 77, no. 2, pp. 131–140, 2006, Publisher: Kluwer Academic Publishers. DOI: 10.1007/S11060-005-9030-Z.

[27] P. Sun, S. Xia, B. Lal, *et al.*, "Lipid metabolism enzyme ACSVL3 supports glioblastoma stem cell maintenance and tumorigenicity," *BMC Cancer*, vol. 14, no. 1, Jun. 2014, Publisher: BioMed Central Ltd. DOI: 10.1186/1471-2407-14-401.

[28] J. Teng, S. Hejazi, L. Hiddingh, *et al.*, "Recycling drug screen repurposes hydroxyurea as a sensitizer of glioblastomas to temozolomide targeting de novo DNA synthesis, irrespective of molecular subtype," *Neuro-Oncology*, vol. 20, no. 5, pp. 642–654, Apr. 2018, Publisher: Oxford Academic. DOI: 10.1093/NEUONC/NOX198.

[29] J. Ariey-Bonnet, R. Berges, M.-P. Montero, *et al.*, "Combination drug screen targeting glioblastoma core vulnerabilities reveals pharmacological synergisms," *EBioMedicine*, vol. 95, 2023.

[30] E. Bernhart, S. Damm, A. Wintersperger, *et al.*, "Interference with distinct steps of sphingolipid synthesis and signaling attenuates proliferation of U87MG glioma cells," *Biochemical Pharmacology*, vol. 96, no. 2, pp. 119–130, Jul. 2015, Publisher: Elsevier. DOI: 10.1016/J.BCP.2015.05.007.

[31] A. Chen, W. Zhao, X. Li, *et al.*, "Comprehensive Oncogenic Features of Coronavirus Receptors in Glioblastoma Multiforme," *Frontiers in Immunology*, vol. 13, 2022. DOI: 10.3389/fimmu.2022.840785.

[32] I. Pavlyk, Y. Rzhepetskyy, A. K. Jagielski, *et al.*, "Arginine deprivation affects glioblastoma cell adhesion, invasiveness and actin cytoskeleton organization by impairment of -actin arginylation," *Amino Acids*, vol. 47, no. 1, 2015. DOI: 10.1007/s00726-014-1857-1.

[33] Y. Sun, C. Wang, L. Wang, Z. Dai, and K. Yang, "Arsenic trioxide induces apoptosis and the formation of reactive oxygen species in rat glioma cells," *Cellular and Molecular Biology Letters*, vol. 23, no. 1, pp. 1–10, Mar. 2018, Publisher: Springer International Publishing. DOI: 10.1186/S11658-018-0074-4/FIGURES/5.

[34] H. M. Said, C. Hagemann, F. Carta, *et al.*, "Hypoxia induced CA9 inhibitory targeting by two different sulfonamide derivatives including Acetazolamide in human Glioblastoma," *Bioorganic & Medicinal Chemistry*, vol. 21, no. 13, pp. 3949–3957, Jul. 2013, Publisher: Pergamon. DOI: 10.1016/J.BMC.2013.03.068.

[35] P. Massi, A. Vaccani, S. Bianchessi, B. Costa, P. Macchi, and D. Parolaro, "The non-psychoactive cannabidiol triggers caspase activation and oxidative stress in human glioma cells," *Cellular and Molecular Life Sciences*, vol. 63, no. 17, 2006. DOI: 10.1007/s00018-006-6156-x.

[36] A. Khan, L. D. Gamble, D. H. Upton, *et al.*, "Dual targeting of polyamine synthesis and uptake in diffuse intrinsic pontine gliomas," *Nature Communications*, vol. 12, no. 1, 2021. DOI: 10.1038/s41467-021-20896-z.

[37] A. Kishk, M. P. Pacheco, T. Heurtaux, *et al.*, "Review of Current Human Genome-Scale Metabolic Models for Brain Cancer and Neurodegenerative Diseases," en, *Cells*, vol. 11, no. 16, p. 2486, Jan. 2022, Number: 16 Publisher: Multidisciplinary Digital Publishing Institute. DOI: 10.3390/cells11162486.

[38] E. Sjöstedt, W. Zhong, L. Fagerberg, *et al.*, "An atlas of the protein-coding genes in the human, pig, and mouse brain," *Science*, vol. 367, no. 6482, eaay5947, 2020.

[39] V. Stathias, A. M. Jermakowicz, M. E. Maloof, *et al.*, "Drug and disease signature integration identifies synergistic combinations in glioblastoma," *Nature Communications 2018 9:1*, vol. 9, no. 1, pp. 1–13, Dec. 2018, Publisher: Nature Publishing Group. DOI: 10.1038/s41467-018-07659-z.

[40] J. B. Bell, F. Eckerdt, H. D. Dhruv, *et al.*, "Differential response of glioma stem cells to arsenic trioxide therapy is regulated by MNK1 and mRNA translation," *Molecular Cancer Research*, vol. 16, no. 1, 2018. DOI: 10.1158/1541-7786.MCR-17-0397.

[41] S. M. Corsello, R. T. Nagari, R. D. Spangler, *et al.*, "Discovering the anti-cancer potential of non-oncology drugs by systematic viability profiling," *Nature cancer*, vol. 1, no. 2, pp. 235–248, Feb. 2020, Publisher: NLM (Medline). DOI: 10.1038/S43018-019-0018-6.

[42] H. J. Nam, Y. E. Kim, B. S. Moon, *et al.*, "Azathioprine antagonizes aberrantly elevated lipid metabolism and induces apoptosis in glioblastoma," *iScience*, vol. 24, no. 3, 2021. DOI: 10.1016/j.isci.2021.102238.

[43] C. Klijn, S. Durinck, E. W. Stawiski, *et al.*, "A comprehensive transcriptional portrait of human cancer cell lines," *Nature Biotechnology*, vol. 33, no. 3, 2015. DOI: 10.1038/nbt.3080.

[44] W. Yang, J. Soares, P. Greninger, *et al.*, "Genomics of Drug Sensitivity in Cancer (GDSC): A resource for therapeutic biomarker discovery in cancer cells," *Nucleic Acids Research*, vol. 41, no. D1, pp. D955–D961, Jan. 2013. DOI: 10.1093/nar/gks1111.

[45] G. Weber, S. Ichikawa, M. Nagai, and Y. Natsumeda, "Azidothymidine inhibition of thymidine kinase and synergistic cytotoxicity with methotrexate and 5-fluorouracil in rat hepatoma and human colon cancer cells," *Cancer Communications*, vol. 2, no. 4, 1990. DOI: 10.3727/095535490820874498.

[46] J. G. Beitz, J. W. Damowski, F. J. Cummings, *et al.*, "Phase I trial of high-dose infused zidovudine combined with leucovorin plus fluorouracil," *Cancer Investigation*, vol. 13, no. 5, 1995. DOI: 10.3109/07357909509024908.

[47] S. M. Choi, Y. S. Cho, G. Park, S. K. Lee, and K. S. Chun, "Celecoxib induces apoptosis through Akt inhibition in 5-fluorouracil-resistant gastric cancer cells," *Toxicological Research*, vol. 37, no. 1, 2021. DOI: 10.1007/s43188-020-00044-3.

[48] J. A. Meyerhardt, Q. Shi, C. S. Fuchs, *et al.*, "Effect of Celecoxib vs Placebo Added to Standard Adjuvant Therapy on Disease-Free Survival among Patients with Stage III Colon Cancer: The CALGB/SWOG 80702 (Alliance) Randomized Clinical Trial," *JAMA - Journal of the American Medical Association*, vol. 325, no. 13, 2021. DOI: 10.1001/jama.2021.2454.

[49] S. S. Chung, P. Dutta, D. Austin, P. Wang, A. Awad, and J. V. Vadgama, "Combination of resveratrol and 5-flurouracil enhanced antitelomerase activity and apoptosis by inhibiting STAT3 and Akt signaling pathways in human colorectal cancer cells," *Oncotarget*, vol. 9, no. 68, 2018. DOI: 10.18632/oncotarget.25993.

[50] S. Chen, N. Tamaki, Y. Kudo, *et al.*, "Protective effects of resveratrol against 5-fluorouracil-induced oxidative stress and inflammatory responses in human keratinocytes," *Journal of Clinical Biochemistry and Nutrition*, vol. 69, no. 3, 2021. DOI: 10.3164/jcbn.21-23.

Chapter 8

Conclusions and Perspectives

Metabolic modeling is revolutionizing molecular biology from understanding individual biochemical reactions into the holistic network of reactions in various scales of cells, tissues, and organisms. Among the many applications of metabolic modeling, target identification and predicting new drugs stand out, of which some predicted drugs by metabolic modeling succeeded in clinical trials [41], [42]. Failed clinical trials in cancer cost $50 to $60 billion [162], forcing pharmaceutical companies to reconsider the procedure of conventional drug discovery. Drug repurposing represents a cost-effective complementary to conventional drug discovery by redirecting previously approved drugs to other diseases, starting with phase II trials. Meanwhile, drug repositioning involves redirecting experimental drugs from one disease to another beyond the approved drug arsenal. In this thesis, we showed various applications of metabolic modeling-based drug repurposing and repositioning in cancer and infection diseases with precision in predicted essential genes and drugs. While experimental drug repurposing through HTS has been established for single drugs and easy-to-culture disease models, computational drug repurposing is an unexpandable tool for combination prediction, hard-to-culture disease models, and high-risk infections. Moreover, metabolic modeling sometimes outperforms *in vitro* disease models, such as avoiding predicting statins for glioma, highlighting the importance of metabolic modeling in preclinical studies. In this chapter, we will summarise future steps needed to improve drug repurposing using metabolic modeling.

8.1 Metabolic modeling allows balanced drug repurposing combining interpretation and holistic target identification

Various computational drug repurposing approaches with different underlying hypotheses have been proposed, which can be classified into target-based, signature-based, and network-based. Target-based drug repurposing approaches, such as docking, virtual screening, and pharmacophore search, assume diseases have single targets [23]. Target-based approaches rely on experimental identification

of the disease target and its 3D structure. Signature-based approaches assume diseases to have multifactorial fingerprints represented as transcriptomic signatures, where the candidate drug should be able to reverse this signature [22]. High-throughput pharmacogenomics databases of thousands of drugs in many cancer cell lines, such as LINCS [163] and defining the disease transcriptomic signature, are key in signature-based drug repurposing. Thirdly, network-based approaches utilize experimentally determined or predicted interactions between molecular entities to define chock-points in a disease network that could serve a vulnerability target [164]. Protein-protein interaction networks and metabolic networks are two examples of network-based approaches [165], where metabolic network modeling stands out due to the highly annotated biochemical network employed [166]. While signature-based drug repurposing allows holistic prediction of drug candidates, it lacks interpretation in target identification [22]. Meanwhile, metabolic modeling enables pinpoint target gene(s) whose knock-out would diminish the objective function [22]. The interpretability of metabolic modeling was shown in the predicted metabolic exchanges between the glioma subtypes (see Figure 3.1) and COVID-19 biomarkers that matched the literature. Biofluid *in vivo* medium constraining, curating the generic model, adding disease-specific reactions, and choosing the most disease-representative objective functions can improve the interpretability of the GEMs' predictions.

8.2 Biases in context model building are inherent, but equally, adequate sanity checks could minimize these biases

Despite the predictability and the interpretability of metabolic modeling, prediction biases are common, which could be attributed to the choice of model-building algorithm, generic reconstruction, OF, medium constraining, and expression data. The bias factors of metabolic modeling, extensively discussed in this review [167], could reduce the sensitivity of the context GEMs' predictions of metabolic fluxes, essential genes, and repurposed drugs. To minimize the biases of context GEMs, using separate data for model building and model evaluation is crucial as covered in this review [168]. For example, the binary CSF medium of Thiele *et al.*, 2020 [71] was used during glioma GEMs model building; meanwhile, literature-retrieved medium exchange was used for model evaluation [61]. Similarly, shared predictions across many context GEMs for the same disease could reduce model biases, especially built from different expression data as applied in melanoma models [63]. Finally, most GEMs are unable to predict the KO effect of non-metabolic genes which limits the predicted drugs to the ones with metabolic targets. The absence of the non-metabolic genes in GEMs' predictability, was evident in the NPs GEMs where NPs with the strongest potency target apoptosis and regulation (see Figure 1.3) [62]. Future model-building algorithms integrating regulation with GEMs and their benchmarking would allow drug repurposing beyond metabolism [169].

8.3 Exo-metabolomics, patient radiotracer uptake, and biofluid concentrations could fine-tune model constraining

Previous brain GEMs covered in our review [72] used discrete medium composition from CSF that constrains the exchange reactions and enhances model contextualization. Nonetheless, medium metabolites have different concentrations; thus, differences in uptake dependencies are inevitable. Metabolomics studies measuring biofluid metabolite concentrations can be used to constrain the exchange reactions' boundaries quantitatively instead of the discrete medium. This could allow increased uptake and dependency for high-concentration metabolites. In addition to the discrete biofluid mediums, biofluid mediums are unable to distinguish between metabolites produced by the surrounding tissues and the biofluid composition from diffusion. Exo-metabolomics data, such as NCI-60 [170], measured the production and the uptake rates of 213 metabolites of 60 cancer cell lines [170]. NCI-60 exo-metabolomics data were used to calculate the fluxes using a core cancer reconstruction from Recon2 by (Zielinski *et al.*, 2017 [159]). The recalculated flux rates of Zielinski *et al.*, 2017 [159] could fine-tune cancer GEMs after readjusting the boundaries based on the generic reconstruction. Similarly, radiotracer uptake data, commonly available in radiological cancer diagnosis guidelines and reviews, indicates the parent metabolite uptake [158]. All in all, exo-metabolomics data and radiotracers can help distinguish metabolic exchanges from biofluid composition; meanwhile, metabolite concentration could improve the discrete medium constraining.

8.4 Pan-cancer stratification may improve drug repurposing on cancer with faster translation in basket trials

While using clinical guidelines such as WHO cancer classifications helps define poor-characterized subtypes and the biomarkers needed for stratification, the discovery of new classifications can improve the design of future clinical trials. Pan-cancer analysis and search for new biomarkers are gaining more application in clinical trials, such as RAF/MEK inhibitors in BRAF-mutant patients and arginine deprivation in patients with low ASS1 expression [171]. Both examples have been tested in glioma, melanoma, and other solid tumors, with RAF/MEK inhibitors gaining approval in melanoma [48] and then LGG [49]. Pan-cancer stratification is compatible with basket trials, where patient selection is based on defined biomarkers regardless of cancer type [172]. *De novo* pan-cancer discovery of metabolic biomarkers can be applied by correlating patient survival with metabolic model features (metabolites, reactions, and fluxes) with proper statistical testing. In summary, current trends in approved drugs and patient selection in metabolic deprivation treatment warrant pan-cancer patient stratification rather than modeling specific cancer types.

8.5 Absence of drug-target information, inclusion of non-inhibitors, and ABC transporter affinity weakened drug repurposing

While medium constraining and patient stratification could improve predicted drugs to the designated medium and samples of the target disease, the drug repurposing pipeline could affect the efficiency of the predicted drugs. Three key factors contributed to the inefficacy of some of the predicted drugs: 1) the absence of target-target information, 2) the inclusion of non-inhibitors in the drug library, and 3) drug resistance by ABC transporters. Many of the predicted essential genes were untargeted by the FDA-approved drugs, such as genes in cholesterol esterification, glycine synthesis (AGXT and PEPD), and sphingolipid synthesis/salvage. This comes from the limitation of approved drugs in targeting the whole transcriptome. For example, all drugs targeting cholesterol esterification are still investigational in clinical trials and are yet to be approved [173]. The diversity of the druggable essential genes can be improved by including investigational compounds and approved drugs for drug repurposing. Similarly, preclinical compounds usually lack entries in drug-target databases, such as 56% of the NPs used in the BRC study, even with specialized databases such as NPASS [174]. Nevertheless, less curated drug-target databases such as STRING [175] and Therapeutic target database [176] with literature-extracted interactions might improve the retrieval of candidate preclinical compounds.

Non-inhibitors such as substrates and inducers hinder drug repurposing as metabolic modeling-based drug deletion assumes target KO. While DrugBank has the type of interaction (inducer, inhibitor, or co-factor), many of them are classified as unknown. Predicted drugs in the four studies included many cofactors or hormones with no clinical effect. Restricting the drug library to only drugs with inhibitor interactions would greatly affect the number of predicted drugs but would reduce the number of false positives. To avoid predicting drugs with potential resistance, predicted drugs with substate or inducer affinity to the ABC transporters in the context of GEMs should be excluded. All in all, the inclusion of investigational compounds, the exclusion of non-inhibitors, and the exclusion of ABC transporter substrates or inducers would enhance drug repurposing and avoid drug resistance.

8.6 Single-cell RNA-Seq model building could predict resistance due to intratumoral heterogeneity

In addition to the ABC transporter, intratumoral heterogeneity constitutes a factor in cancer drug resistance. While studies covered in this thesis used bulk RNA-Seq and predicted drugs targeting ABC transporters, intratumoral heterogeneity remains unaddressed using bulk RNA-Seq alone. Single-cell RNA-Seq (scRNA-Seq) allows sequencing of the expression of each individual cell; meanwhile, spatial

RNA-Seq employs advanced localization to detect expression from multiple regions of the target organ [177]. Despite spatial RNA-Seq being a relatively new technique, both techniques provide better resolution to intratumoral heterogeneity, especially with drug-tolerant persister (DTP) cells. DTP cells are cancer subclone cell that survives anticancer treatment by adapting DNA repair and shifting from glycolysis to OXPHOS [178]. Currently, the scFASTCORMICS algorithm allows model building of multi-cell population models using scRNA-Seq [179]; meanwhile, spatial RNA-Seq lacks an established model-building algorithm. GEMs built from scRNA-Seq with scFASTCORMICS could allow the detection of DTP cells and further repurpose drugs targeting them or combinations targeting the various metabolic rewiring of DTP cells and other clones. Similarly, GEMs built from scRNA-Seq of non-cancer diseases could identify cell-cell metabolic interactions such as glial-neuron interactions. Overall, metabolic models built from single-cell RNA-Seq could predict cell-cell interactions and improve predicted drugs against resistant DTP cells.

To this end, we can summarize the steps needed for improving drug repurposing using metabolic modeling as follows:

- Metabolic exchange data of radiotracers in cancer can fine-tune medium constraining or validate model consistency with predicted uptakes and efflux.
- Whole-body metabolic models are crucial for acute diseases that are invasive to multiple organs.
- Adding investigational drugs to FDA-approved drugs during drug repurposing could diversify the drug targets to undruggable genes by approved drugs.
- Curating the generic model with ABC transporters could predict potential drug resistance due to secondary drug metabolite efflux.
- Curating the generic model with drug-metabolizing reactions such as CYP genes from prodrug to active metabolite could improve cancer drug toxicity by selecting prodrugs for cancer-specific metabolizing reactions.
- Exclusion of drugs with inducer and substrate affinity, such as cofactors and hormones, from drug predictions can reduce the number of false positives of predicted drugs.

As George Box said, "All models are wrong, but some are useful". Likewise, all disease models, albeit preclinical or computational, are wrong, but some are useful. Systems Biology has been a cornerstone in understanding the interactions between biological entities in disease modeling, with metabolic modeling at the forefront. Metabolic modeling provides the mathematical formulation of metabolic networks that can predict or validate new hypotheses. Similarly, metabolic modeling has applications using bulk expression data from target identification, repurposing drugs and combinations, and biomarker prediction, which warrant its use for personalized medicine. Drug repurposing using metabolic modeling predicted drugs comparable to the disease-approved drugs in clinical trials, such as fotemustine in glioma and melanoma. Moreover, metabolic modeling predicted new combinations in glioma with predicted target genes matching known vulnerabilities in the respective subtypes. Still, many limitations could drive drug resistance, which could be enhanced by model curation and adjusting the drug prediction pipeline. These results make metabolic modeling an ideal disease model for

translational applications in personalized medicine and rare diseases.

Bibliography

[1] E. Ravina, *The evolution of drug discovery: from traditional medicines to modern drugs*. John Wiley & Sons, 2011.

[2] A. Honkala, S. V. Malhotra, S. Kummar, and M. R. Junttila, "Harnessing the predictive power of preclinical models for oncology drug development," *Nature Reviews Drug Discovery*, vol. 21, no. 2, pp. 99–114, 2022.

[3] P. Pound and M. Ritskes-Hoitinga, "Is it possible to overcome issues of external validity in preclinical animal research? why most animal models are bound to fail," *Journal of translational medicine*, vol. 16, no. 1, pp. 1–8, 2018.

[4] I. Simeonova and E. Huillard, *In vivo models of brain tumors: Roles of genetically engineered mouse models in understanding tumor biology and use in preclinical studies*. ISSN: 14209071 Issue: 20 Publication Title: Cellular and molecular life sciences : CMLS Volume: 71, 2014. DOI: 10.1007/s00018-014-1675-3.

[5] M. Loibner, C. Langner, P. Regitnig, G. Gorkiewicz, and K. Zatloukal, "Biosafety requirements for autopsies of patients with covid-19: Example of a bsl-3 autopsy facility designed for highly pathogenic agents," *Pathobiology*, vol. 88, no. 1, pp. 37–45, 2021.

[6] C. H. Wong, K. W. Siah, and A. W. Lo, "Estimation of clinical trial success rates and related parameters," *Biostatistics*, vol. 20, no. 2, pp. 273–286, 2019.

[7] J. G. Moffat, F. Vincent, J. A. Lee, J. Eder, and M. Prunotto, "Opportunities and challenges in phenotypic drug discovery: An industry perspective," *Nature reviews Drug discovery*, vol. 16, no. 8, pp. 531–543, 2017.

[8] R. R. Ramsay, M. R. Popovic-Nikolic, K. Nikolic, E. Uliassi, and M. L. Bolognesi, "A perspective on multi-target drug discovery and design for complex diseases," *Clinical and translational medicine*, vol. 7, no. 1, pp. 1–14, 2018.

[9] A. Burton, A. Castaño, M. Bruno, *et al.*, "Drug discovery and development in rare diseases: Taking a closer look at the tafamidis story," *Drug Design, Development and Therapy*, pp. 1225–1243, 2021.

[10] A. Mullard, "2010 fda drug approvals," *Nature Reviews Drug Discovery*, vol. 10, no. 2, p. 82, 2011.

[11] Z. Zhang, L. Zhou, N. Xie, *et al.*, "Overcoming cancer therapeutic bottleneck by drug repurposing," *Signal transduction and targeted therapy*, vol. 5, no. 1, p. 113, 2020.

[12] R. Mohi-Ud-Din, A. Chawla, P. Sharma, *et al.*, "Repurposing approved non-oncology drugs for cancer therapy: A comprehensive review of mechanisms, efficacy, and clinical prospects," *European Journal of Medical Research*, vol. 28, no. 1, p. 345, 2023.

[13] F. L. Luan, R. Ding, V. K. Sharma, W. J. Chon, M. Lagman, and M. Suthanthiran, "Rapamycin is an effective inhibitor of human renal cancer metastasis," *Kidney international*, vol. 63, no. 3, pp. 917–926, 2003.

[14] V. Blay, B. Tolani, S. P. Ho, and M. R. Arkin, "High-throughput screening: Today's biochemical and cell-based approaches," *Drug Discovery Today*, vol. 25, no. 10, pp. 1807–1821, 2020.

[15] L. Rasmussen, B. Tigabu, E. L. White, *et al.*, "Adapting high-throughput screening methods and assays for biocontainment laboratories," *Assay and drug development technologies*, vol. 13, no. 1, pp. 44–54, 2015.

[16] K. R. Acharya, E. D. Sturrock, J. F. Riordan, and M. R. Ehlers, "Ace revisited: A new target for structure-based drug design," *Nature Reviews Drug Discovery*, vol. 2, no. 11, pp. 891–902, 2003.

[17] K. Sonehara and Y. Okada, "Genomics-driven drug discovery based on disease-susceptibility genes," *Inflammation and Regeneration*, vol. 41, no. 1, pp. 1–5, 2021.

[18] D. Ochoa, M. Karim, M. Ghoussaini, D. G. Hulcoop, E. M. McDonagh, and I. Dunham, "Human genetics evidence supports two-thirds of the 2021 fda-approved drugs," *Nat Rev Drug Discov*, vol. 21, no. 8, p. 551, 2022.

[19] T. Sauter and M. Albrecht, *Introduction to Systems Biology: Workbook for Flipped-classroom Teaching*. Open Book Publishers, 2023.

[20] C. Nogales, Z. M. Mamdouh, M. List, C. Kiel, A. I. Casas, and H. H. Schmidt, "Network pharmacology: Curing causal mechanisms instead of treating symptoms," *Trends in Pharmacological Sciences*, vol. 43, no. 2, pp. 136–150, 2022.

[21] A. Teumer, Y. Li, S. Ghasemi, *et al.*, "Genome-wide association meta-analyses and fine-mapping elucidate pathways influencing albuminuria," *Nature communications*, vol. 10, no. 1, p. 4130, 2019.

[22] R. Shukla, N. D. Henkel, K. Alganem, *et al.*, "Signature-based approaches for informed drug repurposing: Targeting cns disorders," *Neuropsychopharmacology*, vol. 46, no. 1, pp. 116–130, 2021.

[23] K. Park, "A review of computational drug repurposing," *Translational and clinical pharmacology*, vol. 27, no. 2, pp. 59–63, 2019.

[24] Y. Seif and B. Ø. Palsson, "Path to improving the life cycle and quality of genome-scale models of metabolism," *Cell Systems*, vol. 12, no. 9, pp. 842–859, 2021.

[25] J. D. Orth, I. Thiele, and B. O. Palsson, "What is flux balance analysis?" *Nature Biotechnology*, vol. 28, no. 3, pp. 245–248, Mar. 2010. DOI: 10.1038/NBT.1614.

[26] N. C. Duarte, S. A. Becker, N. Jamshidi, *et al.*, "Global reconstruction of the human metabolic network based on genomic and bibliomic data," *Proceedings of the National Academy of Sciences of the United States of America*, vol. 104, no. 6, pp. 1777–1782, Feb. 2007. DOI: 10.1073/PNAS.0610772104.

[27] M. M. Islam, W. L. Schroeder, and R. Saha, "Kinetic modeling of metabolism: Present and future," *Current Opinion in Systems Biology*, vol. 26, pp. 72–78, 2021.

[28] J. S. Edwards, R. Ramakrishna, and B. O. Palsson, "Characterizing the metabolic phenotype: A phenotype phase plane analysis," *Biotechnology and Bioengineering*, vol. 77, no. 1, pp. 27–36, Jan. 2002, Publisher: John Wiley & Sons, Inc. DOI: 10.1002/bit.10047.

[29] R. Mahadevan and C. H. H. Schilling, "The effects of alternate optimal solutions in constraint-based genome-scale metabolic models," *Metabolic Engineering*, vol. 5, no. 4, pp. 264–276, Oct. 2003, ISBN: 1096-7176 (Print)\r1096-7176 (Linking). DOI: 10.1016/j.ymben.2003.09.002.

[30] M. P. Pacheco, E. John, T. Kaoma, *et al.*, "Integrated metabolic modelling reveals cell-type specific epigenetic control points of the macrophage metabolic network," *BMC Genomics*, vol. 16, no. 1, Oct. 2015, Publisher: BioMed Central Ltd. DOI: 10.1186/S12864-015-1984-4.

[31] M. P. Pacheco, T. Bintener, D. Ternes, *et al.*, "Identifying and targeting cancer-specific metabolism with network-based drug target prediction," *EBioMedicine*, vol. 43, pp. 98–106, May 2019, Publisher: Elsevier B.V. DOI: 10.1016/J.EBIOM.2019.04.046.

[32] N. Vlassis, M. P. Pacheco, and T. Sauter, "Fast Reconstruction of Compact Context-Specific Metabolic Network Models," *PLoS Computational Biology*, vol. 10, no. 1, 2014, Publisher: Public Library of Science. DOI: 10.1371/JOURNAL.PCBI.1003424.

[33] M. P. Pacheco, T. Pfau, and T. Sauter, "Benchmarking Procedures for High-Throughput Context Specific Reconstruction Algorithms," *Frontiers in Physiology*, vol. 6, p. 410, 2016. DOI: 10.3389/fphys.2015.00410.

[34] B. García-Jiménez, J. Torres-Bacete, and J. Nogales, "Metabolic modelling approaches for describing and engineering microbial communities," *Computational and Structural Biotechnology Journal*, vol. 19, pp. 226–246, 2021.

[35] S. Gomez Romero and N. Boyle, "Systems biology and metabolic modeling for cultivated meat: A promising approach for cell culture media optimization and cost reduction," *Comprehensive Reviews in Food Science and Food Safety*, vol. 22, no. 4, pp. 3422–3443, 2023.

[36] M. P. Pacheco, T. Bintener, and T. Sauter, "Towards the network-based prediction of repurposed drugs using patient-specific metabolic models," *EBioMedicine*, vol. 43, pp. 26–27, May 2019. DOI: 10.1016/j.ebiom.2019.04.017.

[37] A. Mardinoglu, R. Agren, C. Kampf, A. Asplund, M. Uhlen, and J. Nielsen, "Genome-scale metabolic modelling of hepatocytes reveals serine deficiency in patients with non-alcoholic fatty liver disease," *Nature Communications*, vol. 5, Jan. 2014, Publisher: Nature Publishing Group. DOI: 10.1038/NCOMMS4083.

[38] A. Heinken, S. El Kouche, R. M. Rodriguez-Guéant, and J.-L. Guéant, "Towards personalized genome-scale modeling of inborn errors of metabolism for systems medicine applications," *Metabolism*, p. 155 738, 2023.

[39] J. Jansma and S. El Aidy, "Understanding the host-microbe interactions using metabolic modeling," *Microbiome*, vol. 9, pp. 1–14, 2021.

[40] L. Heirendt, S. Arreckx, T. Pfau, *et al.*, "Creation and analysis of biochemical constraint-based models using the COBRA Toolbox v.3.0," *Nature Protocols*, vol. 14, no. 3, pp. 639–702, Mar. 2019, Publisher: Nature Publishing Group. DOI: 10.1038/S41596-018-0098-2.

[41] B. Yulug, O. Altay, X. Li, *et al.*, "Combined metabolic activators improve cognitive functions in alzheimer's disease patients: A randomised, double-blinded, placebo-controlled phase-ii trial," *Translational Neurodegeneration*, vol. 12, no. 1, pp. 1–23, 2023.

[42] O. Altay, M. Arif, X. Li, *et al.*, "Combined metabolic activators accelerates recovery in mild-to-moderate covid-19," *Advanced Science*, vol. 8, no. 17, p. 2 101 222, 2021.

[43] S. Explorer, *Seer*explorer: An interactive website for seer cancer statistics [internet]. surveillance research program, national cancer institute; 2023 apr 19. [updated: 2023 jun 8; cited 2023 sep 28]. available from: Https://seer.cancer.gov/statistics-network/explorer/. data source(s): Seer incidence data, november 2022 submission (1975-2020), seer 22 registries (excluding illinois and massachusetts). expected survival life tables by socio-economic standards.*

[44] H.-P. Sinn and H. Kreipe, "A brief overview of the who classification of breast tumors, focusing on issues and updates from the 3rd edition," *Breast care*, vol. 8, no. 2, pp. 149–154, 2013.

[45] V. Di Nunno, L. Gatto, A. Tosoni, S. Bartolini, and E. Franceschi, "Implications of braf v600e mutation in gliomas: Molecular considerations, prognostic value and treatment evolution," *Frontiers in Oncology*, vol. 12, p. 1 067 252, 2023.

[46] L. Dang, D. W. White, S. Gross, *et al.*, "Cancer-associated IDH1 mutations produce 2-hydroxyglutarate," *Nature*, vol. 462, no. 7274, pp. 739–744, Dec. 2009. DOI: 10.1038/nature08617.

[47] M. P. Rausch and K. T. Hastings, "Immune checkpoint inhibitors in the treatment of melanoma: From basic science to clinical application," *Exon Publications*, pp. 121–142, 2017.

[48] G. Long, K. Flaherty, D. Stroyakovskiy, *et al.*, "Dabrafenib plus trametinib versus dabrafenib monotherapy in patients with metastatic braf v600e/k-mutant melanoma: Long-term survival and safety analysis of a phase 3 study," *Annals of Oncology*, vol. 28, no. 7, pp. 1631–1639, 2017.

[49] P. Y. Wen, A. Stein, M. van den Bent, *et al.*, "Dabrafenib plus trametinib in patients with brafv600e-mutant low-grade and high-grade glioma (roar): A multicentre, open-label, single-arm, phase 2, basket trial," *The lancet oncology*, vol. 23, no. 1, pp. 53–64, 2022.

[50] P. Bhave, L. Pallan, G. V. Long, *et al.*, "Melanoma recurrence patterns and management after adjuvant targeted therapy: A multicentre analysis," *British journal of cancer*, vol. 124, no. 3, pp. 574–580, 2021.

[51] Y. Peng, Y. Wang, C. Zhou, W. Mei, and C. Zeng, "Pi3k/akt/mtor pathway and its role in cancer therapeutics: Are we making headway?" *Frontiers in oncology*, vol. 12, p. 819 128, 2022.

[52] R. Bai, Z. Lv, D. Xu, and J. Cui, "Predictive biomarkers for cancer immunotherapy with immune checkpoint inhibitors," *Biomarker research*, vol. 8, pp. 1–17, 2020.

[53] J. J. Mandel, S. Yust-Katz, A. J. Patel, *et al.*, "Inability of positive phase II clinical trials of investigational treatments to subsequently predict positive phase III clinical trials in glioblastoma," *Neuro-Oncology*, vol. 20, no. 1, 2018. DOI: 10.1093/neuonc/nox144.

[54] M. Rudiansyah, S. A. Jasim, Z. G. Mohammad Pour, *et al.*, "Coronavirus disease 2019 (covid-19) update: From metabolic reprogramming to immunometabolism," *Journal of Medical Virology*, vol. 94, no. 10, pp. 4611–4627, 2022.

[55] G. Li, R. Hilgenfeld, R. Whitley, and E. De Clercq, "Therapeutic strategies for covid-19: Progress and lessons learned," *Nature Reviews Drug Discovery*, pp. 1–27, 2023.

[56] P. Chen, M. Wu, Y. He, B. Jiang, and M.-L. He, "Metabolic alterations upon sars-cov-2 infection and potential therapeutic targets against coronavirus infection," *Signal Transduction and Targeted Therapy*, vol. 8, no. 1, p. 237, 2023.

[57] P. Persico, E. Lorenzi, A. Losurdo, *et al.*, "Precision Oncology in Lower-Grade Gliomas: Promises and Pitfalls of Therapeutic Strategies Targeting IDH-Mutations," *Cancers*, vol. 14, no. 5, p. 1125, Mar. 2022, Publisher: Multidisciplinary Digital Publishing Institute (MDPI). DOI: 10.3390/CANCERS14051125.

[58] B. Zagidullin, J. Aldahdooh, S. Zheng, *et al.*, "Drugcomb: An integrative cancer drug combination data portal," *Nucleic acids research*, vol. 47, no. W1, W43–W51, 2019.

[59] G. L. Law, J. Tisoncik-Go, M. J. Korth, and M. G. Katze, "Drug repurposing: A better approach for infectious disease drug discovery?" *Current opinion in immunology*, vol. 25, no. 5, pp. 588–592, 2013.

[60] A. Kishk, M. P. Pacheco, and T. Sauter, "DCcov: Repositioning of drugs and drug combinations for SARS-CoV-2 infected lung through constraint-based modeling," *iScience*, vol. 24, no. 11, p. 103 331, Nov. 2021, Publisher: Elsevier. DOI: 10.1016/J.ISCI.2021.103331.

[61] A. Kishk, M. Pires Pacheco, T. Heurtaux, and T. Sauter, "Metabolic models predict fotemustine and the combination of eflornithine/rifamycin and adapalene/cannabidiol for the treatment of gliomas," *Briefings in Bioinformatics*, vol. 25, no. 3, bbae199, 2024.

[62] C. Cipriani, M. P. Pacheco, A. Kishk, *et al.*, "Bruceine D Identified as a Drug Candidate against Breast Cancer by a Novel Drug Selection Pipeline and Cell Viability Assay," *Pharmaceuticals*, vol. 15, no. 2, Feb. 2022, Publisher: MDPI. DOI: 10.3390/PH15020179/S1.

[63] T. Bintener, M. P. Pacheco, D. Philippidou, *et al.*, "Metabolic modelling-based in silico drug target prediction identifies six novel repurposable drugs for melanoma," *Cell Death & Disease*, vol. 14, no. 7, p. 468, Jul. 2023. DOI: 10.1038/s41419-023-05955-1.

[64] M. Rahman, L. K. Jackson, W. E. Johnson, D. Y. Li, A. H. Bild, and S. R. Piccolo, "Alternative preprocessing of RNA-Sequencing data in the Cancer Genome Atlas leads to improved analysis results," *Bioinformatics*, vol. 31, no. 22, pp. 3666–3672, May 2015, Publisher: Oxford University Press. DOI: 10.1093/BIOINFORMATICS/BTV377.

[65] D. Blanco-Melo, B. E. Nilsson-Payant, W. C. Liu, *et al.*, "Imbalanced Host Response to SARS-CoV-2 Drives Development of COVID-19," *Cell*, vol. 181, no. 5, 1036–1045.e9, May 2020, Publisher: Cell Press. DOI: 10.1016/j.cell.2020.04.026.

[66] E. Wyler, K. Mösbauer, V. Franke, *et al.*, "Transcriptomic profiling of sars-cov-2 infected human cell lines identifies hsp90 as target for covid-19 therapy," *IScience*, vol. 24, no. 3, p. 102 151, 2021.

[67] C. Lv, X. Wu, X. Wang, *et al.*, "The gene expression profiles in response to 102 traditional Chinese medicine (TCM) components: A general template for research on TCMs," *Scientific Reports*, vol. 7, no. 1, Dec. 2017, Publisher: Nature Publishing Group. DOI: 10.1038/S41598-017-00535-8.

[68] E. Brunk, S. Sahoo, D. C. Zielinski, *et al.*, "Recon3D enables a three-dimensional view of gene variation in human metabolism," *Nature Biotechnology*, vol. 36, no. 3, pp. 272–281, Mar. 2018, Publisher: Nature Publishing Group. DOI: 10.1038/NBT.4072.

[69] A. Renz, L. Widerspick, and A. Dräger, "Fba reveals guanylate kinase as a potential target for antiviral therapies against sars-cov-2," *Bioinformatics*, vol. 36, no. Supplement_2, pp. i813–i821, 2020.

[70] D. S. Wishart, Y. D. Feunang, A. Marcu, *et al.*, "HMDB 4.0: The human metabolome database for 2018," *Nucleic Acids Research*, vol. 46, no. D1, pp. D608–D617, Jan. 2018, Publisher: Oxford University Press. DOI: 10.1093/NAR/GKX1089.

[71] I. Thiele, S. Sahoo, A. Heinken, *et al.*, "Personalized whole-body models integrate metabolism, physiology, and the gut microbiome," *Molecular Systems Biology*, vol. 16, no. 5, May 2020, Publisher: EMBO. DOI: 10.15252/MSB.20198982.

[72] A. Kishk, M. P. Pacheco, T. Heurtaux, *et al.*, "Review of Current Human Genome-Scale Metabolic Models for Brain Cancer and Neurodegenerative Diseases," en, *Cells*, vol. 11, no. 16, p. 2486, Jan. 2022, Number: 16 Publisher: Multidisciplinary Digital Publishing Institute. DOI: 10.3390/cells11162486.

[73] J. L. King and S. R. Benhabbour, *Glioblastoma multiforme—a look at the past and a glance at the future*, ISSN: 19994923 Issue: 7 Publication Title: Pharmaceutics Volume: 13, 2021. DOI: 10.3390/pharmaceutics13071053.

[74] R. Bjerkvig, S. Bougnaud, and S. P. Niclou, "Animal models for low-grade gliomas," in *Diffuse Low-Grade Gliomas in Adults: Natural History, Interaction with the Brain, and New Individualized Therapeutic Strategies*, vol. 9781447122135, 2013. DOI: 10.1007/978-1-4471-2213-5_11.

[75] E. Vergani, G. L. Beretta, M. Aloisi, *et al.*, "Targeting of the lipid metabolism impairs resistance to braf kinase inhibitor in melanoma," *Frontiers in Cell and Developmental Biology*, vol. 10, p. 927 118, 2022.

[76] I. Thiele, N. Swainston, R. M. T. Fleming, *et al.*, "A community-driven global reconstruction of human metabolism," *Nature Biotechnology*, vol. 31, no. 5, pp. 419–425, May 2013. DOI: 10.1038/NBT.2488.

[77] S. Dutta, S. Mahalanobish, and P. C. Sil, "Phytoestrogens as novel therapeutic molecules against breast cancer," in *Discovery and Development of Anti-Breast Cancer Agents from Natural Products*, Elsevier, 2021, pp. 197–229.

[78] A. Rayan, J. Raiyn, and M. Falah, "Nature is the best source of anticancer drugs: Indexing natural products for their anticancer bioactivity," *PloS one*, vol. 12, no. 11, e0187925, 2017.

[79] L. Zhongwen, Y. Fucheng, W. Xiaobing, and K. Lingyi, "Progress in approved drugs from natural product resources," *Chinese Journal of Natural Medicines*,

[80] A. C. Codo, G. G. Davanzo, L. de Brito Monteiro, *et al.*, "Elevated glucose levels favor sars-cov-2 infection and monocyte response through a hif-1α/glycolysis-dependent axis," *Cell metabolism*, vol. 32, no. 3, pp. 437–446, 2020.

[81] T. Bintener, M. P. Pacheco, A. Kishk, J. Didier, and T. Sauter, "Drug Target Prediction Using Context-Specific Metabolic Models Reconstructed from rFASTCORMICS," in *Methods in Molecular Biology*, vol. 2535, ISSN: 19406029, 2022. DOI: 10.1007/978-1-0716-2513-2_17.

[82] D. S. Wishart, Y. D. Feunang, A. C. Guo, *et al.*, "DrugBank 5.0: A major update to the DrugBank database for 2018," *Nucleic Acids Research*, vol. 46, no. D1, pp. D1074–D1082, Jan. 2018, Publisher: Oxford University Press. DOI: 10.1093/NAR/GKX1037.

[83] T. Thomas, D. Stefanoni, J. A. Reisz, *et al.*, "COVID-19 infection alters kynurenine and fatty acid metabolism, correlating with IL-6 levels and renal status," *JCI Insight*, vol. 5, no. 14, Jun. 2020, Publisher: American Society for Clinical Investigation. DOI: 10.1172/JCI.INSIGHT.140327.

[84] J. P. Bernardes, N. Mishra, F. Tran, *et al.*, "Longitudinal multi-omics analysis identifies responses of megakaryocytes, erythroid cells and plasmablasts as hallmarks of severe covid-19 trajectories," *medRxiv*, pp. 2020–09, 2020.

[85] H. J. Nam, Y. E. Kim, B. S. Moon, *et al.*, "Azathioprine antagonizes aberrantly elevated lipid metabolism and induces apoptosis in glioblastoma," *iScience*, vol. 24, no. 3, 2021. DOI: 10.1016/j.isci.2021.102238.

[86] S. M. Corsello, R. T. Nagari, R. D. Spangler, *et al.*, "Discovering the anti-cancer potential of non-oncology drugs by systematic viability profiling," *Nature cancer*, vol. 1, no. 2, pp. 235–248, Feb. 2020, Publisher: NLM (Medline). DOI: 10.1038/S43018-019-0018-6.

[87] W. Yang, J. Soares, P. Greninger, *et al.*, "Genomics of Drug Sensitivity in Cancer (GDSC): A resource for therapeutic biomarker discovery in cancer cells," *Nucleic Acids Research*, vol. 41, no. D1, pp. D955–D961, Jan. 2013. DOI: 10.1093/nar/gks1111.

[88] P. Smirnov, I. Smith, Z. Safikhani, *et al.*, "Evaluation of statistical approaches for association testing in noisy drug screening data," *BMC bioinformatics*, vol. 23, no. 1, p. 188, 2022.

[89] C. Pacini, J. M. Dempster, I. Boyle, *et al.*, "Integrated cross-study datasets of genetic dependencies in cancer," *Nature Communications*, vol. 12, no. 1, Dec. 2021, Publisher: Nature Research. DOI: 10.1038/S41467-021-21898-7.

[90] J. B. Bell, F. Eckerdt, H. D. Dhruv, *et al.*, "Differential response of glioma stem cells to arsenic trioxide therapy is regulated by MNK1 and mRNA translation," *Molecular Cancer Research*, vol. 16, no. 1, 2018. DOI: 10.1158/1541-7786.MCR-17-0397.

[91] V. Stathias, A. M. Jermakowicz, M. E. Maloof, *et al.*, "Drug and disease signature integration identifies synergistic combinations in glioblastoma," *Nature Communications 2018 9:1*, vol. 9, no. 1, pp. 1–13, Dec. 2018, Publisher: Nature Publishing Group. DOI: 10.1038/s41467-018-07659-z.

[92] R. J. Williams, H. D. Dobbins, T. Tse, *et al.*, "Approach for reporting master protocol study designs on clinicaltrials. gov: Qualitative analysis," *bmj*, vol. 377, 2022.

[93] C. Collaboration, "The cochrane library," *Database available on disk and CDROM. Oxford, UK, Update Software*, 2002.

[94] P. Smirnov, Z. Safikhani, N. El-Hachem, *et al.*, "Pharmacogx: An r package for analysis of large pharmacogenomic datasets," *Bioinformatics*, vol. 32, no. 8, pp. 1244–1246, 2016.

[95] R. H. Shoemaker, "The nci60 human tumour cell line anticancer drug screen," *Nature Reviews Cancer*, vol. 6, no. 10, pp. 813–823, 2006.

[96] J. Barretina, G. Caponigro, N. Stransky, *et al.*, "The Cancer Cell Line Encyclopedia enables predictive modelling of anticancer drug sensitivity," *Nature*, vol. 483, no. 7391, pp. 307–603, Mar. 2012, ISBN: 1476-4687 (Electronic)\r0028-0836 (Linking) Publisher: Nature Research. DOI: 10.1038/nature11003.

[97] B. Seashore-Ludlow, M. G. Rees, J. H. Cheah, *et al.*, "Harnessing Connectivity in a Large-Scale Small-Molecule Sensitivity Dataset," *Cancer Discovery*, vol. 5, no. 11, pp. 1210–1223, Nov. 2015. DOI: 10.1158/2159-8290.CD-15-0235.

[98] M. J. Garnett, E. J. Edelman, S. J. Heidorn, *et al.*, "Systematic identification of genomic markers of drug sensitivity in cancer cells.," *Nature*, vol. 483, no. 7391, pp. 570–575, 2012, ISBN: 1476-4687 (Electronic)\n0028-0836 (Linking) Publisher: Nature Publishing Group. DOI: 10.1038/nature11005.

[99] F. Iorio, T. A. Knijnenburg, D. J. Vis, *et al.*, "A landscape of pharmacogenomic interactions in cancer," *Cell*, vol. 166, no. 3, pp. 740–754, 2016.

[100] A. Bruna, O. M. Rueda, W. Greenwood, *et al.*, "A biobank of breast cancer explants with preserved intra-tumor heterogeneity to screen anticancer compounds," *Cell*, vol. 167, no. 1, pp. 260–274, 2016.

[101] M. Hafner, L. M. Heiser, E. H. Williams, *et al.*, "Quantification of sensitivity and resistance of breast cancer cell lines to anti-cancer drugs using gr metrics," *Scientific data*, vol. 4, no. 1, pp. 1–9, 2017.

[102] J. P. Mpindi, B. Yadav, P. Östling, *et al.*, "Consistency in drug response profiling," *Nature*, vol. 540, no. 7631, E5–E6, 2016.

[103] A. Mammoliti, P. Smirnov, Z. Safikhani, W. Ba-Alawi, and B. Haibe-Kains, "Creating reproducible pharmacogenomic analysis pipelines," *Scientific data*, vol. 6, no. 1, p. 166, 2019.

[104] P. J. Tomezsko, C. W. Phillipson, and M. E. Walsh, "Lessons learned from limited overlap of 15 in vitro covid-19 drug repurposing screens," *Health security*, 2023.

[105] T. Xu, W. Zheng, and R. Huang, "High-throughput screening assays for sars-cov-2 drug development: Current status and future directions," *Drug discovery today*, vol. 26, no. 10, pp. 2439–2444, 2021.

[106] G. A. Pires De Souza, M. Le Bideau, C. Boschi, *et al.*, "Choosing a cellular model to study sars-cov-2," *Frontiers in Cellular and Infection Microbiology*, vol. 12, p. 1 003 608, 2022.

[107] B. Ellinger, D. Bojkova, A. Zaliani, *et al.*, "A sars-cov-2 cytopathicity dataset generated by high-content screening of a large drug repurposing collection," *Scientific data*, vol. 8, no. 1, p. 70, 2021.

[108] K. Chan, A. G. Farias, H. Lee, *et al.*, "Survival-based crispr genetic screens across a panel of permissive cell lines identify common and cell-specific sars-cov-2 host factors," *Heliyon*, vol. 9, no. 1, 2023.

[109] L. Kohtamäki, M. Arjama, S. Mäkelä, *et al.*, "High-throughput ex vivo drug testing identifies potential drugs and drug combinations for nras-positive malignant melanoma," *Translational oncology*, vol. 15, no. 1, p. 101 290, 2022.

[110] R. T. Powell, A. Redwood, X. Liu, *et al.*, "Pharmacologic profiling of patient-derived xenograft models of primary treatment-naıve triple-negative breast cancer," *Scientific reports*, vol. 10, no. 1, p. 17 899, 2020.

[111] S. Wang, W. Yan, L. Kong, *et al.*, "Oncolytic viruses engineered to enforce cholesterol efflux restore tumor-associated macrophage phagocytosis and anti-tumor immunity in glioblastoma," *Nature Communications*, vol. 14, no. 1, p. 4367, 2023.

[112] X. Guo, S. Zhou, Z. Yang, *et al.*, "Cholesterol metabolism and its implication in glioblastoma therapy," *Journal of Cancer*, vol. 13, no. 6, p. 1745, 2022.

[113] Y. Zhang, R. Guo, S. H. Kim, *et al.*, "Sars-cov-2 hijacks folate and one-carbon metabolism for viral replication," *Nature communications*, vol. 12, no. 1, p. 1676, 2021.

[114] S. K. McBrayer, J. R. Mayers, G. J. DiNatale, *et al.*, "Transaminase Inhibition by 2-Hydroxyglutarate Impairs Glutamate Biosynthesis and Redox Homeostasis in Glioma," *Cell*, vol. 175, no. 1, 2018. DOI: 10.1016/j.cell.2018.08.038.

[115] A. H. Jacobs, A. Thomas, L. W. Kracht, *et al.*, "18F-Fluoro-l-Thymidine and 11C-Methylmethionine as Markers of Increased Transport and Proliferation in Brain Tumors," *Journal of Nuclear Medicine*, vol. 46, no. 12, 2005.

[116] A. Nikaki, G. Angelidis, R. Efthimiadou, *et al.*, "18F-fluorothymidine PET imaging in gliomas: An update," *Annals of Nuclear Medicine*, vol. 31, no. 7, p. 495, Jun. 2017, Publisher: Springer. DOI: 10.1007/S12149-017-1183-2.

[117] A. Moghaddam, R. A. Heller, Q. Sun, *et al.*, "Selenium deficiency is associated with mortality risk from COVID-19," *Nutrients*, vol. 12, no. 7, pp. 1–13, Jul. 2020, Publisher: MDPI AG. DOI: 10.3390/NU12072098.

[118] N. R. Roldán-Bretón, A. G. Capuchino-Suárez, M. E. Mejía-León, C. Olvera-Sandoval, and D. N. Lima-Sánchez, "Selenium serum levels in patients with sars-cov-2 infection: A systematic review and meta-analysis," *Journal of Nutritional Science*, vol. 12, e86, 2023.

[119] J. I. Traylor, M. N. Pernik, A. C. Sternisha, S. K. McBrayer, and K. G. Abdullah, *Molecular and metabolic mechanisms underlying selective 5-aminolevulinic acid-induced fluorescence in gliomas*, ISSN: 20726694 Issue: 3 Publication Title: Cancers Volume: 13, 2021. DOI: 10.3390/cancers13030580.

[120] E. R. Nelson, S. E. Wardell, J. S. Jasper, *et al.*, "27-Hydroxycholesterol links hypercholesterolemia and breast cancer pathophysiology," *Science*, vol. 342, no. 6162, pp. 1094–1098, 2013. DOI: 10.1126/SCIENCE.1241908.

[121] L.-J. Deng, Y. Li, M. Qi, *et al.*, "Molecular mechanisms of bufadienolides and their novel strategies for cancer treatment," *European journal of pharmacology*, vol. 887, p. 173 379, 2020.

[122] Y. Hirasaki, A. Okabe, M. Fukuyo, *et al.*, "Cinobufagin inhibits proliferation of acute myeloid leukaemia cells by repressing c-myc pathway-associated genes," *Chemico-biological interactions*, vol. 360, p. 109 936, 2022.

[123] G. Stragliotto, M. R. Pantalone, A. Rahbar, J. Bartek, and C. Soderberg-Naucler, "Valganciclovir as Add-on to Standard Therapy in Glioblastoma Patients," *Clinical Cancer Research*, vol. 26, no. 15, 2020. DOI: 10.1158/1078-0432.CCR-20-0369.

[124] M. R. Pantalone, A. Rahbar, C. Söderberg-Naucler, and G. Stragliotto, "Valganciclovir as Add-on to Second-Line Therapy in Patients with Recurrent Glioblastoma," *Cancers*, vol. 14, no. 8, 2022. DOI: 10.3390/cancers14081958.

[125] G. Stragliotto, A. Rahbar, N. W. Solberg, *et al.*, "Effects of valganciclovir as an add-on therapy in patients with cytomegalovirus-positive glioblastoma: A randomized, double-blind, hypothesis-generating study," *International Journal of Cancer*, vol. 133, no. 5, 2013. DOI: 10.1002/ijc.28111.

[126] V. A. Levin, S. E. Ictech, and K. R. Hess, "Clinical importance of eflornithine (-difluoromethylornithine) for the treatment of malignant gliomas," *CNS oncology*, vol. 7, no. 2, 2018. DOI: 10.2217/cns-2017-0031.

[127] C. McBain, T. A. Lawrie, E. Rogozińska, A. Kernohan, T. Robinson, and S. Jefferies, *Treatment options for progression or recurrence of glioblastoma: A network meta-analysis*, ISSN: 14651858 Issue: 12 Publication Title: Cochrane Database of Systematic Reviews Volume: 2020, 2021. DOI: 10.1002/14651858.CD013579.pub2.

[128] C. Garbe, "Ipilimumab with fotemustine in metastatic melanoma," *The Lancet Oncology*, vol. 13, no. 9, pp. 851–852, Sep. 2012. DOI: 10.1016/S1470-2045(12)70341-8.

[129] R. Ghiasvand, L. A. Berge, B. K. Andreassen, *et al.*, "Statin use and risk of cutaneous melanoma: A nationwide nested case–control study," *British Journal of Dermatology*, vol. 188, no. 6, pp. 805–807, 2023.

[130] A. Cortellini, M. Tucci, V. Adamo, *et al.*, "Integrated analysis of concomitant medications and oncological outcomes from pd-1/pd-l1 checkpoint inhibitors in clinical practice," *Journal for immunotherapy of cancer*, vol. 8, no. 2, 2020.

[131] J. R. Beguerie, J. Xingzhong, and R. P. Valdez, "Tamoxifen vs. non-tamoxifen treatment for advanced melanoma: A meta-analysis," *International Journal of Dermatology*, vol. 49, no. 10, pp. 1194–1202, Oct. 2010. DOI: 10.1111/J.1365-4632.2010.04529.X.

[132] S. Z. Gertler, D. MacDonald, M. Goodyear, *et al.*, "NCIC-CTG phase II study of gemcitabine in patients with malignant glioma (IND.94)," *Annals of Oncology*, vol. 11, no. 3, 2000. DOI: 10.1023/A:1008336607135.

[133] S. V. Rajkumar, P. A. Burch, S. Nair, *et al.*, "Phase II North Central Cancer Treatment Group study of 2- chlorodeoxyadenosine in patients with recurrent glioma," *American Journal of Clinical Oncology: Cancer Clinical Trials*, vol. 22, no. 2, 1999. DOI: 10.1097/00000421-199904000-00012.

[134] E. C. Halperin, J. Herndon, S. C. Schold, *et al.*, "A phase III randomized prospective trial of external beam radiotherapy, mitomycin C, carmustine, and 6-mercaptopurine for the treatment of adults with anaplastic glioma of the brain," *International Journal of Radiation Oncology*Biology*Physics*, vol. 34, no. 4, pp. 793–802, Mar. 1996, Publisher: Elsevier. DOI: 10.1016/0360-3016(95)02025-X.

[135] W. R. Shapiro, S. B. Green, P. C. Burger, *et al.*, "A randomized comparison of intra-arterial versus intravenous BCNU, with or without intravenous 5-fluorouracil, for newly diagnosed patients with malignant glioma," *Journal of Neurosurgery*, vol. 76, no. 5, 1992. DOI: 10.3171/jns.1992.76.5.0772.

[136] M. C. Chamberlain, M. D. Prados, P. Silver, and V. A. Levin, "A phase II trial of oral melphalan in recurrent primary brain tumors," *American Journal of Clinical Oncology: Cancer Clinical Trials*, vol. 11, no. 1, 1988. DOI: 10.1097/00000421-198802000-00011.

[137] W. E. Samlowski, H. Gundacker, J. P. Kuebler, *et al.*, "Evaluation of gemcitabine in patients with recurrent or metastatic squamous cell carcinoma of the head and neck: A Southwest Oncology Group Phase II study," *Investigational New Drugs*, vol. 19, no. 4, pp. 311–315, 2001. DOI: 10.1023/A:1010657609609.

[138] A. A. Brandes, G. Finocchiaro, V. Zagonel, *et al.*, "AVAREG: A phase II, randomized, noncomparative study of fotemustine or bevacizumab for patients with recurrent glioblastoma," *Neuro-Oncology*, vol. 18, no. 9, 2016. DOI: 10.1093/neuonc/now035.

[139] M. Penas-Prado, o. b. o. t. M. A. C. C. O. Program, t. B. T. T. Collaborative, *et al.*, "Randomized phase II adjuvant factorial study of dose-dense temozolomide alone and in combination with isotretinoin, celecoxib, and/or thalidomide for glioblastoma," *Neuro-Oncology*, vol. 17, no. 2, pp. 266–273, Feb. 2015, Publisher: Oxford Academic. DOI: 10.1093/NEUONC/NOU155.

[140] D. J. Kim, J. Kim, K. Spaunhurst, *et al.*, "Open-label, exploratory phase II trial of oral itraconazole for the treatment of basal cell carcinoma," *Journal of Clinical Oncology*, vol. 32, no. 8, pp. 745–751, Mar. 2014, Publisher: American Society of Clinical Oncology. DOI: 10.1200/JCO.2013.49.9525.

[141] R. P. Pereira, S. J. Azevedo, J. Cé Coelho, *et al.*, *Neoadjuvant itraconazole (i) in patients (pts) with resectable basal cell carcinoma (bcc): A phase ii multistage study.* 2020.

[142] H. Cortes, O. D. Reyes-Hernandez, S. Alcala-Alcala, *et al.*, "Repurposing of drug candidates for treatment of skin cancer," *Frontiers in oncology*, vol. 10, p. 605 714, 2021.

[143] F. Levi, C. Pasche, F. Lucchini, R. Ghidoni, M. Ferraroni, and C. La Vecchia, "Resveratrol and breast cancer risk," *European journal of cancer prevention*, vol. 14, no. 2, pp. 139–142, 2005.

[144] C.-K. Hsu, C.-Y. Chen, W.-C. Chen, C.-C. Lai, S.-H. Hung, and W.-T. Lin, "Effect of sofosbuvir-based treatment on clinical outcomes of patients with covid-19: A systematic review and meta-analysis of randomised controlled trials," *International journal of antimicrobial agents*, vol. 59, no. 3, p. 106 545, 2022.

[145] M. S. Alam, M. N. Hasan, Z. Maowa, F. Khatun, K. N. H. Nazir, and M. Z. Alam, "N-acetylcysteine reduces severity and mortality in covid-19 patients: A systematic review and meta-analysis," *Journal of Advanced Veterinary and Animal Research*, vol. 10, no. 2, p. 157, 2023.

[146] P. Malchair, J. Giol, V. García, *et al.*, "Three-day icatibant on top of standard care in patients with coronavirus disease 2019 pneumonia: A randomized, open-label, phase 2, proof-of-concept trial," *Clinical Infectious Diseases*, vol. 76, no. 10, pp. 1784–1792, 2023.

[147] F. Di Pierro, A. Khan, S. Iqtadar, *et al.*, "Quercetin as a possible complementary agent for early-stage covid-19: Concluding results of a randomized clinical trial," *Frontiers in pharmacology*, vol. 13, p. 1 096 853, 2023.

[148] D. E. Martin, N. Pandey, P. Chavda, *et al.*, "Oral probenecid for nonhospitalized adults with symptomatic mild-to-moderate covid-19," *Viruses*, vol. 15, no. 7, p. 1508, 2023.

[149] M. F. Konig, K. M. Grzes, P. C. Robinson, and E. J. Pearce, "Sulfasalazine: A risk factor for severe covid-19?" *The Lancet Rheumatology*, vol. 4, no. 6, e388–e389, 2022.

[150] H. S. Sandhu, J. Lambert, Z. Steckler, *et al.*, "Outpatient medications associated with protection from covid-19 hospitalization," *PLoS One*, vol. 18, no. 3, e0282961, 2023.

[151] S. Florescu, D. Stanciu, M. Zaharia, *et al.*, "Effect of angiotensin-converting enzyme inhibitor and angiotensin receptor blocker initiation on organ support–free days in patients hospitalized with covid-19: A randomized clinical trial," *JAMA*, vol. 329, no. 14, pp. 1183–1196, 2023.

[152] L. Arslanbaeva, G. Tosi, M. Ravazzolo, *et al.*, "Ubiad1 and coq10 protect melanoma cells from lipid peroxidation-mediated cell death," *Redox Biology*, vol. 51, p. 102 272, 2022.

[153] M. Jaganjac, M. Cindrić, A. Jakovčević, K. Žarković, and N. Žarković, *Lipid peroxidation in brain tumors*, ISSN: 18729754 Publication Title: Neurochemistry International Volume: 149, 2021. DOI: 10.1016/j.neuint.2021.105118.

[154] M. C. d. Gooijer, E. M. Kemper, L. C. M. Buil, *et al.*, "ATP-binding cassette transporters restrict drug delivery and efficacy against brain tumors even when blood-brain barrier integrity is lost," *Cell Reports Medicine*, vol. 2, no. 1, 2021. DOI: 10.1016/j.xcrm.2020.100184.

[155] Y. Xie, Q. Lu, C. Lenahan, S. Yang, D. Zhou, and X. Qi, "Whether statin use improves the survival of patients with glioblastoma?: A meta-analysis," *Medicine*, vol. 99, no. 9, 2020.

[156] A. Altwairgi, F. Alnajjar, H. Alhussain, *et al.*, "Phase ii study of atorvastatin in combination with radiotherapy and temozolomide in patients with glioblastoma (art): Final analysis report," *Annals of Oncology*, vol. 30, p. ix20, 2019.

[157] S. L. Holbeck, R. Camalier, J. A. Crowell, *et al.*, "The national cancer institute almanac: A comprehensive screening resource for the detection of anticancer drug pairs with enhanced therapeutic activity," *Cancer research*, vol. 77, no. 13, pp. 3564–3576, 2017.

[158] J. Trotter, A. R. Pantel, B.-K. K. Teo, *et al.*, "Pet/ct imaging in radiation therapy treatment planning: A review of pet imaging tracers and methods to incorporate pet/ct," *Advances in Radiation Oncology*, p. 101 212, 2023.

[159] D. C. Zielinski, N. Jamshidi, A. J. Corbett, A. Bordbar, A. Thomas, and B. O. Palsson, "Systems biology analysis of drivers underlying hallmarks of cancer cell metabolism," *Scientific Reports*, vol. 7, p. 41 241, Jan. 2017, Publisher: Nature Publishing Group. DOI: 10.1038/srep41241.

[160] B. Goldacre and J. Gray, "Opentrials: Towards a collaborative open database of all available information on all clinical trials," *Trials*, vol. 17, no. 1, p. 164, 2016.

[161] C. W. Jones, L. Handler, K. E. Crowell, L. G. Keil, M. A. Weaver, and T. F. Platts-Mills, "Non-publication of large randomized clinical trials: Cross sectional analysis," *Bmj*, vol. 347, 2013.

[162] V. Jentzsch, L. Osipenko, J. W. Scannell, and J. A. Hickman, "Costs and causes of oncology drug attrition with the example of insulin-like growth factor-1 receptor inhibitors," *JAMA Network Open*, vol. 6, no. 7, e2324977–e2324977, 2023.

[163] Z. Wang, N. R. Clark, and A. Ma'ayan, "Drug-induced adverse events prediction with the LINCS L1000 data," *Bioinformatics*, vol. 32, no. 15, pp. 2338–2345, 2016, ISBN: 1367-4803. DOI: 10.1093/bioinformatics/btw168.

[164] F. Cheng, R. J. Desai, D. E. Handy, *et al.*, "Network-based approach to prediction and population-based validation of in silico drug repurposing," *Nature communications*, vol. 9, no. 1, p. 2691, 2018.

[165] D. Gamermann, J. Triana-Dopico, and R. Jaime, "A comprehensive statistical study of metabolic and protein–protein interaction network properties," *Physica A: Statistical Mechanics and its Applications*, vol. 534, p. 122 204, 2019.

[166] M. Moškon and T. Režen, "Context-Specific Genome-Scale Metabolic Modelling and Its Application to the Analysis of COVID-19 Metabolic Signatures," *Metabolites*, vol. 13, no. 1, Jan. 2023, Publisher: MDPI. DOI: 10.3390/METABO13010126.

[167] D. B. Bernstein, S. Sulheim, E. Almaas, and D. Segrè, "Addressing uncertainty in genome-scale metabolic model reconstruction and analysis," *Genome Biology*, vol. 22, pp. 1–22, 2021.

[168] J. A. Kaste and Y. Shachar-Hill, "Model validation and selection in metabolic flux analysis and flux balance analysis," *Biotechnology Progress*, vol. 40, no. 1, e3413, 2024.

[169] C. H. Chung, D.-W. Lin, A. Eames, and S. Chandrasekaran, "Next-generation genome-scale metabolic modeling through integration of regulatory mechanisms," *Metabolites*, vol. 11, no. 9, p. 606, 2021.

[170] M. Jain, R. Nilsson, S. Sharma, *et al.*, "Metabolite Profiling Identifies a Key Role for Glycine in Rapid Cancer Cell Proliferation," *Science*, vol. 336, no. 6084, pp. 1040–1044, May 2012. DOI: 10.1126/science.1218595.

[171] G. C. Field, I. Pavlyk, and P. W. Szlosarek, "Bench-to-bedside studies of arginine deprivation in cancer," *Molecules*, vol. 28, no. 5, p. 2150, 2023.

[172] J. J. Park, E. Siden, M. J. Zoratti, *et al.*, "Systematic review of basket trials, umbrella trials, and platform trials: A landscape analysis of master protocols," *Trials*, vol. 20, no. 1, pp. 1–10, 2019.

[173] A. Websdale, Y. Kiew, P. Chalmers, *et al.*, "Pharmacologic and genetic inhibition of cholesterol esterification enzymes reduces tumour burden: A systematic review and meta-analysis of preclinical models," *Biochemical pharmacology*, vol. 196, p. 114 731, 2022.

[174] X. Zeng, P. Zhang, W. He, *et al.*, "NPASS: Natural product activity and species source database for natural product research, discovery and tool development," *Nucleic Acids Research*, vol. 46, no. D1, pp. D1217–D1222, Jan. 2018, Publisher: Oxford University Press. DOI: 10.1093/NAR/GKX1026.

[175] D. Szklarczyk, A. L. Gable, K. C. Nastou, *et al.*, "The string database in 2021: Customizable protein–protein networks, and functional characterization of user-uploaded gene/measurement sets," *Nucleic acids research*, vol. 49, no. D1, pp. D605–D612, 2021.

[176] Y. Zhou, Y. Zhang, X. Lian, *et al.*, "Therapeutic target database update 2022: Facilitating drug discovery with enriched comparative data of targeted agents," *Nucleic Acids Research*, vol. 50, no. D1, pp. D1398–D1407, 2022.

[177] X. Li and C.-Y. Wang, "From bulk, single-cell to spatial rna sequencing," *International Journal of Oral Science*, vol. 13, no. 1, p. 36, 2021.

[178] M. Mikubo, Y. Inoue, G. Liu, and M.-S. Tsao, "Mechanism of drug tolerant persister cancer cells: The landscape and clinical implication for therapy," *Journal of Thoracic Oncology*, vol. 16, no. 11, pp. 1798–1809, 2021.

[179] M. P. Pacheco, J. Ji, T. Prohaska, M. M. García, and T. Sauter, "Scfastcormics: A contextualization algorithm to reconstruct metabolic multi-cell population models from single-cell rnaseq data," *Metabolites*, vol. 12, no. 12, p. 1211, 2022.